UNIVERSITY OF LEEDS

FLUORESCENCE GUIDED SURGERY:

INTRA-OPERATIVE FLUORESCENT IMAGING IN LAPAROSCOPIC COLONIC TUMOUR RESECTION AND LAPAROSCOPIC CHOLECYSTECTOMY SURGERY

Candidate: Gemma Armstrong

University Reference: 201073014

Leeds Institute of Medical Research

Faculty of Medicine and Health

Primary Supervisor: Mr Andrew Smith

Co-Supervisors: Professor David Jayne and Professor Giles Toogood

Submitted in accordance with the requirements for the degree of Doctor of Philosophy (PhD) by Research

The University of Leeds School of Medicine & Health

Submitted for Examination Date: 12th April 2021

Word count: 40, 478 (excluding refences)

Pages: 238

Intellectual Property and Publication Statements

I, Gemma Armstrong, confirm that the work submitted is my own and that appropriate credit has been given where reference has been made to the work of others.

Copyright Statement

This copy has been supplied on the understanding that it is copyright material and that no quotation from the thesis may be published without proper acknowledgement.

The right of Gemma Armstrong to be identified as Author of this work has been asserted by Gemma Armstrong in accordance with the Copyright, Designs and Patents Act 1988.

The candidate confirms that the work submitted is her own, except where work which has formed part of jointly authored publications has been included. The contribution of the candidate and the other authors to this work has been explicitly indicated below. The candidate confirms that appropriate credit has been given within the thesis where reference has been made to the work of others.

Chapter 1 & 2

Armstrong G.R, Smith A.M & Toogood G (2017). An Overview of Near Infrared Fluorescent Cholangiography with Indocyanine Green during Cholecystectomy. *J Surg Transplant Sci* 5(2): 1051. ISSN 2379-0911

My involvement: conception, literature search, analysis, and manuscript author. Involvement of others: guidance, manuscript corrections.

Presentations:

Association of Upper Gastrointestinal Surgeon of Great Britain and Ireland (AUGIS) 20th Annual Scientific Meeting, Cork 2017. Abstract publication: *BJS* 2017; 104 (S7): 5–68.

Surgical Research Society (SRS) Annual Meeting, Dublin (virtual) October 2020

Chapter 3 & 5

Gemma Armstrong, Mohammed Ibrahim Khot, Christophe Portal, Jim P. Tiernan, Nick P. West, Sarah L. Perry, Tom Maisey, Thomas A. Hughes, Damian J. Tolan and David G. Jayne (2021) A novel fluorescent c-Met targeted imaging agent for intra-operative colonic tumour mapping: translation from the laboratory into a clinical trial. *Submitted to Surgical Oncology September 2021 – decision awaited*.

My involvement: conception, experimental design and data collection, literature search and manuscript author. Involvement of others: experimental support, trial oversight and manuscript preparation.

Presentations: Surgical Research Society (SRS) Annual Meeting Dublin (virtual) October 2020

Chapter 4

Gemma Armstrong, Mohammed Ibrahim Khot, Jim P. Tiernan, Nick P. West, Sarah L. Perry, Tom Maisey, Thomas A. Hughes and David G. Jayne (2021). The utility of c-Met as a diagnostic tissue biomarker in primary colorectal cancer. *Int J Exp Pathol. DOI: 10.1111/(ISSN)1365-2613*

My involvement: conception, experimental design and data collection, literature search and manuscript author. Involvement of others: Manuscript preparation and corrections.

Acknowledgements

I would like to acknowledge my PhD supervisors Professors D Jayne, Smith and Toogood for their enduring support and guidance throughout this process. From the start, they have provided their expertise and knowledge whilst allowing me the academic freedom needed to develop as a clinical scientist and trialist. I am grateful to Cath Moriarty and all of the team in the surgical research office, their help with trial management and participant recruitment has been invaluable. I would like to thank T Maisey, S Perry, and T Hughes for their assistance designing and running experiments and for their patience and expertise in helping me to acquire new skills in the laboratory. A special thank you to my lab-bench-buddy Ibrahim Khot for brightening long days of failed western blots.

I am extremely grateful to my friends and family for their unwavering support.

ABSTRACT

Introduction: Fluorescence-guided surgery could improve the operative decision-making process. Near Infrared Cholangiography (NIR-FC) with Indocyanine Green (ICG) in laparoscopic cholecystectomy (LC) may aid visualisation of bile duct anatomy. The c-met transmembrane protein is over-expressed in colorectal cancer (CRC). EMI-137 is a c-Met specific peptide coupled to fluorophore.

Methods: Twenty-two participants requiring LC were allocated to four dosing subgroups and received a single intravenous (I.V) dose of ICG before surgery. Biliary anatomy was assessed with NIR-FC and surgeon satisfaction was evaluated.

c-Met transcription in HT-29 CRC cells was silenced with targeted SiRNA to demonstrate specificity of EMI-137. A HT-29 xenograft model was developed in female BALB/C mice. EMI-137 (0.18mg/kg) was injected into tail veins and biodistribution analysed by fluorescent imaging. c-Met immunopositivity was graded in matched normal and CRC tissue TMA samples obtained from the MRC CLASICC trial.

Nine participants with colon cancer, received IV EMI-137 1-3 hours before laparoscopic tumour resection surgery. Tumour and lymph node (LN) fluorescence were assessed with a fluorescent laparoscope. Immunohistochemistry analysed c-Met expression.

Results: A prolonged ICG dosing interval consistently increased structure identification at LC and was preferred by the operating surgeon.

c-Met was consistently overexpressed in CRC relative to normal tissue and could be visualised with EMI-137, comparable to indirect c-Met identification methods. EMI-137 uptake in tumour xenografts was observed for 6 hours post-administration

At clinical trial, no serious adverse events related to EMI-137 were reported. Marked background fluorescence was observed in all participants; 4/9 showed mild increase in tumour fluorescence over background; 5/9 had histological LN metastases; no fluorescent LN were

detected intraoperatively. All primary tumours (8/8) and malignant LN (15) exhibited moderate-high c-Met protein expression.

Conclusion: Prolonged ICG dosing improves visualisation of structures with NIR-FC at LC. EMI-137, binds specifically to the human c-Met protein, is safe but its intra-operative utility is limited by insufficient tumour-to-background ratios.

TABLE OF CONTENTS

Acknowledgements 3

ABSTRACT **4**

LIST OF TABLES **9**

LIST OF FIGURES **12**

1. CHAPTER ONE **21**

INTRODUCTION **22**

1.1 The Principles of Fluorescence 22

1.2 Laparoscopic Cholecystectomy and Indocyanine Green 24

1.3 Laparoscopic Colon Cancer Resection and EMI-137 49

2 **CHAPTER TWO** **67**

2.1 AIMS AND OBJECTIVES 68

2.2 MATERIALS AND METHODS 69

2.2.1 Trial Design **70**

2.2.2 Trial Intervention **76**

2.3 RESULTS 82

2.4 DISCUSSION 106

3. **CHAPTER THREE** **110**

3.2 AIMS AND OBJECTIVES 111

3.3 MATERIALS AND METHODS 112

3.3.1 *In Vitro* 2D Model of Colorectal Cancer **112**

3.3.2 3D Animal Model of Colorectal Cancer 122

3.4 *IN-VITRO* RESULTS 126

3.4.1 Spectral properties of EMI-137 ..... **126**

3.4.2 C-Met Protein Expression Quantification by Western Blot **127**

3.4.3 c-Met Silencing with Short Interfering RNA **129**

3.4.4 EMI-137 Specificity for c-Met **132**

3.5 ANIMAL MODEL RESULTS 134

3.6 DISCUSSION 138

4. **CHAPTER FOUR** **142**

4.1 AIMS & OBJECTIVES 143

4.2 METHODS 143

4.2.1 Immunohistochemistry **146**

4.2.2 c-Met Expression Scoring **148**

4.3 RESULTS 150

4.4 DISCUSSION 162

5 **CHAPTER FIVE** **167**

5.1 AIMS AND OBJECTIVES 168

5.2 CLINICAL TRIAL METHODS 169

5.2.1 Trial Design **169**

5.2.2 Eligibility Criteria **172**

5.2.3 Trial Intervention **174**

5.2.4 Radiology Assessment **178**

5.2.5 Histopathology Assessment **178**

5.3 CLINICAL TRIAL RESULTS 182

5.3.1 Participants **182**

5.3.2 Intra-Operative Results **186**

5.3.3 Histopathology Results **191**

5.4 DISCUSSION 201

6 CHAPTER SIX 204

6.1 CONCLUSION 204

REFERENCES 208

APPENDIX 234

LIST OF TABLES

Table 1: Summary of NIR-FC with ICG cholecystectomy clinical trials. Abbreviations: Minute (m), hour (h) 48

Table 2: Eligibility criteria for Clinical Feasibility study of Near Infrared Fluorescence Cholangiography in Laparoscopic Cholecystectomy trial. 74

Table 3: Summary of NIR-FC feasibility study participant demographics by dosing sub-group 84

Table 4: NIR-FC clinical trial intraoperative biliary structure results by individual participant. 91

Table 5: Time to assessment by dosing regimen subgroup. 92

Table 6: Participating surgeon NIR-FC laparoscopic cholecystectomy operative feedback results. Number of “strongly agree” or “agree” responses given to each question and as percentage of total. 101

Table 7: Western Blot equipment and reagents 117

Table 8: Western Blot Antibodies. Abbreviations: RT - room temperature. HRP - Horseradish peroxidase 117

Table 9: Composition of Dharmacon siGENOME Human MET (4233) SiRNA SMARTpool 5 nmol (Dharmacon Inc., Lafayette, CO, USA). Cat No: M-003156-02-0005) 119

Table 10: Western Blot Protein Quantification with BSA Standard 127

Table 11: Key clinical and pathological features of CLASICC patient cohort. Adapted from Jayne et al (2007) and Guillou et al (2005) (152,153) 153

Table 12: Median tumour sample c-Met immunohistochemistry expression score of CLASICC TMA by final pathological Tumour (pT) and Nodal (pN) stage (TNM v5.0) with percentage of total, standard deviation and interquartile range shown, 255/280 TMA tumour samples were suitable for assessment and had TNM stage data available for correlation. 158

Table 13: Final tumour (pT) pathological stage (TNM v5.0) and Spearman correlation with Median c-Met immunohistochemistry expression score of CLASICC TMA with difference between tumour and normal tissue expression score. N = 255 pairs. 159

Table 14: Final lymph node (pN) pathological stage (TNM v5.0) and Spearman correlation with Median c-Met immunohistochemistry expression score of CLASICC TMA with difference between tumour and normal tissue expression score. 159

Table 15: Eligibility Criteria for Intraoperative Imaging of Colon Cancer using a Fluorescent peptide (EMI-137) against the c-Met receptor feasibility study 173

Table 16: Summary of participant baseline demographics 184

Table 17: Key characteristics of trial participants. Abbreviations: pT pathological Tumour stage; pN pathological node stage; M male; F Female; m^2 metre^2: y years; ASA American Society of Anesthesiologists Grade. 185

Table 18: Summary of intraoperative results. (Abbreviations: hh: mm Hour: minute) 186

Table 19: Summary of adverse events reported 188

Table 20: Protocol deviations reported during trial active phase. 189

Table 21: Comparison of pre-operative radiological (CT) TNM v8.0 staging and final pathological grade for each subject. 189

Table 22: Spearman correlation of intraoperative tumour fluorescent signal versus participant peri-operative characteristics, p value not significant. 191

Table 23: Summary of subject histology results. Abbreviations: S.D standard deviation. * in accordance with TNM v8.0..... 192

LIST OF EQUATIONS

Equation 1: Equation to calculate total c-Met expression scores of TMA specimens……149

LIST OF FIGURES

Figure 1: Simplified Jablonski diagram of energy transfer in fluorescence adapted from Davidson et al (2017)(5)..... 23

Figure 2: The Near Infrared optical window. It is useful for in vivo imaging because of minimal light absorption by haemoglobin (<650 nm) and water (>900 nm) Adapted from Weissleder et al (2001)(6). 23

Figure 3: Structure of Indocyanine Green adapted from National Center for Biotechnology Information (2017)(7) 24

Figure 4: Spectral properties of ICG in human whole blood in 100µL cell at excitation wavelength 765nm. Adapted from Benson (1978)(28) 27

Figure 5: The critical view of safety (CVS). Adapted from Strasberg (1995)(91). 40

Figure 6: Anatomical distribution of primary colorectal cancer by percentage. Adapted from Cancer Research UK (2016)(140). 49

Figure 7: Structural formula of EMI-137 salt free. Adapted from Edinburgh Molecular Imaging Ltd. (2017)(220) 64

Figure 8: Schematic representation of EMI-137 targeting the c-Met receptor. Adapted from Esfahani et al (2016)(221)..... 64

Figure 9: a-c colonic lesions easily visible in white light (left) and showing enhanced fluorescence with EMI-137 (right); e-f colonic lesions difficult to detect with white light (left) but easily visible with EMI-137 during fluorescent colonoscopy. Adapted from Burggraaf et al (2015)(218). 65

Figure 10: Clinical feasibility study of Near Infrared Fluorescence Cholangiography in Laparoscopic Cholecystectomy trial schema. 71

Figure 11: NIR-FC in laparoscopic cholecystectomy trial consort diagram 82

Figure 12: Number of extrahepatic biliary structures (CD, CHD and CBD) graded as clearly identifiable at each assessment point by participant. One-way ANOVA p = 0.007 N = 22 ... 93

Figure 13: Average number of structures clearly delineated at each assessment point for all dosing intervals combined. Standard error bars shown. One-way ANOVA p = <0.0001 (N = 22) 93

Figure 14: NIR-FC compared to OTC. Number of biliary structures reported as “clearly identifiable” at each assessment point (structures assessed CD, CBD, CHD, LHD and RHD (N = 10)..... 95

Figure 15: linear regression of participant factors and an average number of extrahepatic biliary structures visualised with NIR-FC. N = 22 for BMI, ICG dose and serum Albumin pre-operatively, N = 7 for pre-operative CRP value. All p values not significant..... 96

Figure 16: Secondary review by assessment point on individual participant level. The number of structures classified as “easily identifiable” (CD, CBD, and CHD). One-way ANOVA analysis of variance performed. N = 21..... 99

Figure 17: the average total number of extrahepatic biliary structures visible at the first and third assessment point for participants allocated to each of the dosing interval subgroups with standard deviation error bars. One Way ANOVA p = 0.02. N = 22. 104

Figure 18: EMI-137 peak absorbance at variable concentrations (20,000nm to 1,000nm) and DPBS control. Left to right; top row DPBS and 1000 NM. Middle row 2000nM and 5000nM. Bottom row 10,000nM and 20,000nM. 126

Figure 19: Western Blot BSA Standard Curve..... 128

Figure 20: Western Blot –detection of c-Met protein expression with a mouse monoclonal anti C-Met antibody (1:1000) at 190-220kDa and alpha tubulin loading control..... 128

Figure 21: Relative quantification of c-Met protein band density relative to matched loading control. 128

Figure 22: HT-29 cells at variable concentrations of SiRNA. A) Targeted to c-Met SiRNA and B) pooled matched untargeted SiRNA. Imaged at x63 magnification using the Zeiss Axioimager fluorescent microscope. Top row shows DAPI nuclear staining. Middle row shows membrane staining with 1:200 monoclonal rabbit recombinant anti c-Met as primary antibody and 1:300 Goat anti-Mouse IgG (H+L) Cross-Adsorbed Secondary Antibody - Alexa Fluor 488 in the FITC channel. Bottom row shows the merged composite image of DAPI nuclear staining and FITC membrane staining. 130

Figure 23: HT-29 incubated with variable concentrations of EMI-137 for 1 hour. Imaged at x40 magnification on the EVOS inverted fluorescent microscope with standardised image acquisition settings. Merged DAPI and Cy5 filter images. 131

Figure 24: HT-29 incubated with 25nm of pooled c-Met targeted SiRNA and untargeted SiRNA. C-Met protein located with a) 1:200 monoclonal c-Met antibody and 1:300 Alexa Fluor 488 fluorescent secondary antibody. Zeiss fluorescent microscope at x40 magnification. b) HT-29 incubated with 500nM EMI-137 and imaged using the EVOS inverted fluorescent microscope at x40 magnification. 132

Figure 25: Dissected organs from each mouse. PBS control versus treated with 0.18mg/kg EMI-137 at each time point. Clockwise from top left A) One-hour post administration B) Four hours post administration and C) Six hours post administration. d) Organ lay-out index map. Imaged using the IVIS Spectrum In-Vivo Imaging System. 136

Figure 26: HT-29 colorectal cancer xenograft from BALB/C nude mice imaged at various time points post IV administration of 0.18mg/kg EMI-137. Imaged with Nikon Eclipse Ti inverted

microscope mounted on Nikon A1R Confocal Laser Scanning Microscope at x60 magnification 137

Figure 27: IHC optimisation results. Fresh frozen colorectal malignant, normal and polyp tissue from two donor patients. Immunohistochemistry analysis of c-Met protein expression (antibody concentration 1;250) relative to matched negative control tissue. Imaged at x20 magnification with Nikon Eclipse MicroscopyU E1000 automated microscope. 152

Figure 28: Representative examples of TMA c-Met immunohistochemical chromogenic visualisation. 155

Figure 29: Example of high c-Met expression in normal and colorectal cancer tissue at x13 and x40 magnification. 155

Figure 30: Summary of statistical analysis of TMA c-Met expression by IHC tumour versus normal tissue. CLASICC TMA c-Met expression median score and interquartile range. Median difference Tumour – normal tissue 2.33 (95%C.I 1.0 to 3.5). 156

Figure 31: Spearman correlation of c-Met expression. Intensity of tumour tissue plotted as function of matched normal tissue from CLASICC trial participants. N = 241 pairs. 157

Figure 32: Box and whisker plot of CLASICC TMA median tumour c-Met IHC expression score by tumour (pT) and node (pN) stage with IQR and range shown. 158

Figure 33: Spearman rank correlation of p stage (ranked from pT1 to pT4) and difference between tumour and normal c-Met IHC expression score in CLASICC TMA cohort samples. Correlation coefficient R -0.14 (p = 0.03). N = 255 pairs. 159

Figure 34: Receiver Operating Characteristic (ROC) curve and Area under Curve (AUC) for c-Met. Sensitivity plotted as function of specificity at various decision thresholds for c-Met as a diagnostic biomarker in colorectal cancer detection. 161

Figure 35: Karl Storz® D -Light Fluorescent laparoscopic system (left) and the prototype detachable camera head filter supplied by Karl Storz® Research & Innovation department (right). 175

Figure 36: Modified Japanese colorectal lymph node staging subgroups diagram - Pericolic, D1 lymph nodes (red); Intermediate D2 lymph nodes (blue); Main, D3, lymph nodes (yellow). Adapted from GLiSten trial protocol(172) with N.P West and D.J Tolan. 180

Figure 37: EMI-137 in laparoscopic colonic resections consort diagram..... 182

Figure 38: fluorescent assessment operative still image from each participant..... 187

Figure 39: Medicines and Healthcare Products Regulatory Agency (MHRA) Acceptance of Amendment Letter 29th August 2017..... 235

Figure 40: Medicines and Healthcare Products Regulatory Agency (MHRA) Acceptance of Amendment Letter 15th March 2018..... 236

Figure 41: Health Research Authority (HRA) Letter of Approval for trial IRAS ID 212190 Intraoperative imaging of colon cancer using a fluorescent peptide (EMI-137) against c-met receptor. Issued 07th November 2017. 237

Figure 42: Health Research Authority (HRA) approval for substantial amendment to trial IRAS ID 212190 Intraoperative imaging of colon cancer using a fluorescent peptide (EMI-137) against c-met receptor. Issued 05th January 2018. 238

LIST OF ABBREVIATIONS

Abbreviation/ Acronym	Definition
^{99m}**Tc**	Technetium-99m
5-ALA	5-aminolevulinic acid
AE	Adverse Event
AL	Anastomotic Leak
AR	Adverse Reaction
BDI	Bile Duct Injury
CBD	Common Bile Duct
CD	Cystic Duct
CEA	Carcinoembryonic Antigen
CHD	Common Hepatic Duct
C.I	Confidence Interval
CLASICC	Conventional versus Laparoscopic-Assisted Surgery in Colorectal Cancer
CME	Complete Mesocolic Excision
CRC	Colorectal Cancer
CRF	Case Report Form
CRLM	Colorectal Cancer Liver Metastases
CRM	Circumferential Resection Margin
CRP	C-Reactive Protein
CT	Computerised Tomography
CTRU	Clinical Trials Research Unit
CVS	Critical View of Safety
DFS	Disease Free Survival

DLC	Delayed Laparoscopic Cholecystectomy
EAES	European Association of Endoscopic Surgery
EM Imaging Ltd	Edinburgh Molecular Imaging Ltd
FDA	Food and Drug Administration
FFT	Fresh Frozen Tissue
FIT	Faecal Immunochemical Test
FL	Fluorescent Light
FNA	Fine Needle Aspiration
FOBT	Faecal Occult Blood Test
FOxTROT	Fluoropyrimidine, Oxaliplatin and Targeted-Receptor pre-Operative Therapy for patients with high-risk, operable colon cancer
GP	General Practitioner
GCP	Good Clinical Practice
GLiSten	Next Generation intraoperative Lymph node staging for Stratified colon cancer surgery - Developmental phase
HGF	Hepatocyte Growth Factor
HGFR	Hepatocyte Growth Factor Receptor
HR	Hazard Ratio
HRP	Horseradish Peroxidase
IALC	Index Admission Laparoscopic Cholecystectomy
ICG	Indocyanine Green
IQR	Interquartile Range
LFTs	Liver Function Tests
LHD	Left Hepatic Duct
LFTs	Liver Function Tests

LTHT	Leeds Teaching Hospitals Trust
MDT	Multi-Disciplinary Team
MET	Mesenchymal-Epithelial Transition Factor
MRC	Medical Research Council
MRI	Magnetic Resonance Imaging
NHS	National Health Service
NIR	Near Infrared
NIR-FA	Near Infrared Fluorescent Angiography
NIR-FC	Near Infrared Fluorescent Cholangiography
nM	nanometre
OD	Optical Density
OR	Odds Ratio
PIS	Participant Information Sheet
PpIX	Protoporphyrin IX
REC	Research and Ethics Committee
RHD	Right Hepatic Duct
ROC curve	Receiver Operating Characteristic curve
RR	Relative Risk
RT	Room temperature
SAE	Serious Adverse Event
SAR	Serious Adverse Reaction
S.D	Standard Deviation
S.E	Standard Error
SF	Scatter Factor
SiRNA	Short interfering Ribonucleic Acid

SLN	Sentinel Lymph Node
SLNB	Sentinel Lymph Node Biopsy
SOP	Standard Operating Procedure
TME	Total Mesorectal Excision
U&E	Urea and Electrolytes
USS	Ultrasound Scan
WL	White Light

1. CHAPTER ONE

FLUORESCENCE GUIDED SURGERY: INTRA-OPERATIVE FLUORESCENT IMAGING IN LAPAROSCOPIC COLONIC TUMOUR RESECTION AND LAPAROSCOPIC CHOLECYSTECTOMY SURGERY

Name: Gemma Armstrong
Student No: 201073014

INTRODUCTION

1.1 The Principles of Fluorescence

A fluorophore is defined as a molecule capable of absorbing and emitting light energy. Fluorophores exist in a lower energy unexcited “ground state”, or S0 state, until excited by light of an appropriate wavelength. Fluorescence is a three-step process, excitation, excitation state lifespan, and emission. During excitation the fluorophore absorbs a photon of light energy and undergoes a conformational change to exist in a higher, unstable energy state. This unstable state only lasts around one picosecond (10^{-12} seconds) before the fluorophore quickly starts to dissipate the absorbed the photon of light energy. As it returns to a more stable, lower energy state (S1), it releases energy as kinetic energy or transfers the energy to other electrons, a process sometimes known as vibrational relaxation and internal conversion respectively. The time taken to dissipate energy to reach a lower energy state varies slightly between different fluorophores and is referred to as the excited state lifespan. Once at the lower energy S1 state, the fluorophore can then slowly emit the photon light energy absorbed as light to return to its low energy ground state, S0. The process of energy dissipation means the fluorophore is already at a lower energy state when it enters the emission phase of fluorescence (S1 to S0). The efficiency of this light conversion process is dependent on the fluorescent quantum yield (Φ_f); defined as *“number of fluorescence photons emitted per excitation photon absorbed”*(1–3).

This unique photo-physical property of fluorophores means the emitted light energy is of a longer wavelength - the colour of the light emitted differs from the colour absorbed. The difference between the excitation and emission wavelength is known as the Stoke shift value. Unless a fluorophore is *“photobleached”,* when irreversible structural damage from high intensity light excitation occurs, it can be repeatedly excited or *“re-radiated”* for sustained detection. It is these essential properties of fluorophores that allows differentiation between absorbed and emitted light and facilitates their multiple diagnostic utilities, including perfusion assessment and tumour localisation. Jablonski first describe fluorescence in pictorial form in

the 1930s and these graphs are commonly referred to as *"Jablonski diagrams"*(1,4) (*Figure 1*).

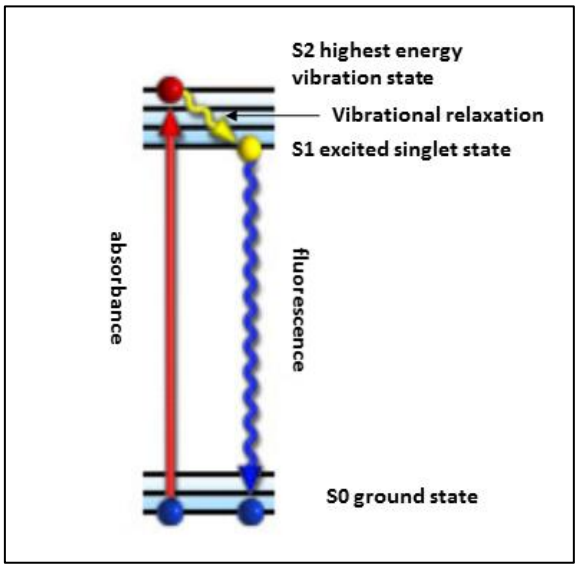

Figure 1: Simplified Jablonski diagram of energy transfer in fluorescence adapted from Davidson et al (2017)(5)*.*

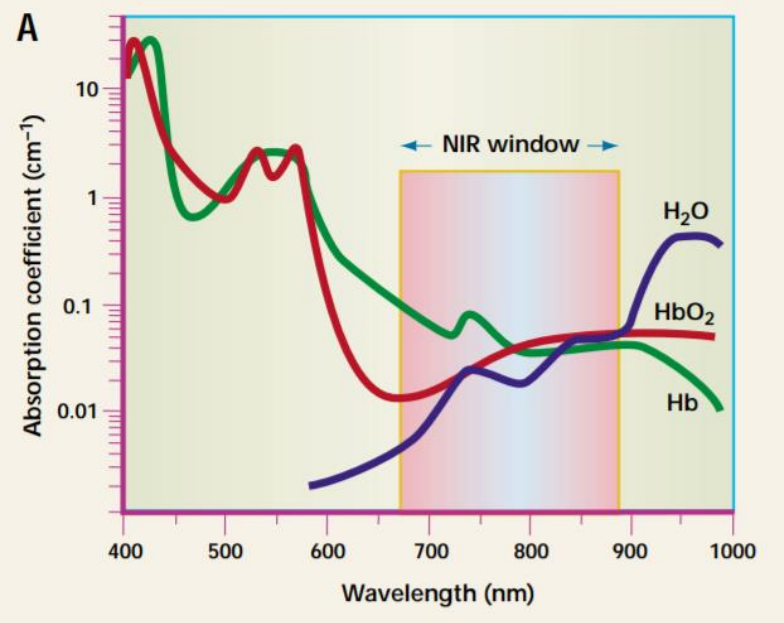

Figure 2: The Near Infrared optical window. It is useful for in vivo imaging because of minimal light absorption by haemoglobin (<650 nm) and water (>900 nm) Adapted from Weissleder et al (2001)(6)*.*

1.2 Laparoscopic Cholecystectomy and Indocyanine Green

Indocyanine Green (ICG)

Background and Pharmacology

Indocyanine Green (ICG) is a tricarbocyanine dye ($C_{43}H_{47}N_2NaO_6S_2$) with fluorescent properties. It is supplied as a sterile lyophilised powder with no more than 5% sodium iodide content(7). ICG was developed by Eastman Kodak® as a sensitising agent in photographic processing in the early 1950s. The Mayo Clinic started investigating the medical applications of ICG in 1956 and it gained US Food and Drug Authority (FDA) approval soon after(8). The chemical formula of ICG is 2,2'-indo6,7,6',7', dibenzocarbocyanine sodium. It has a complex structure *(Figure 3*) with a molecular weight of 774.96 g/mol and pH 6.5 in aqueous solution(7). ICG is considered as amphiphilic – it demonstrates both hydrophilic and lipophilic properties(9,10).

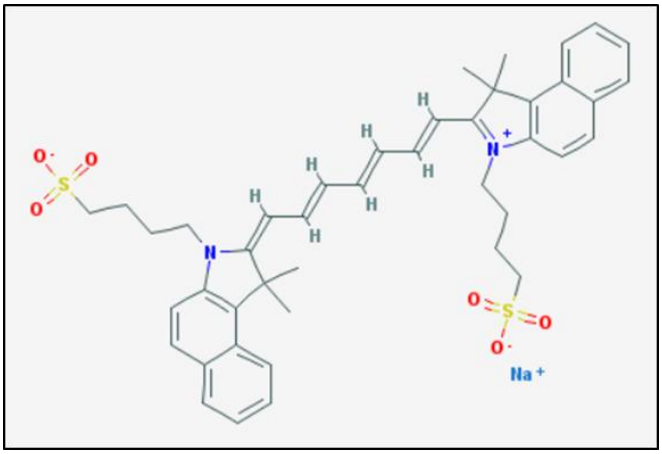

Figure 3: Structure of Indocyanine Green adapted from National Center for Biotechnology Information (2017)(7)

Excretion and Pharmacokinetics

ICG should be reconstituted with sterile water immediately prior to injection(11). Once injected intravenously, it rapidly and fully binds to serum lipoprotein complexes and plasma proteins, favouring α1 lipoproteins, especially High Density Lipoprotein (HDL)(12,13). Reconstituted ICG is rapidly degraded by exposure to light, but if bound to intravascular plasma proteins photo-degradation can be slowed for up to several days.

ICG is exclusively excreted in bile and does not undergo any forms of intrahepatic conjugation, metabolism or enterohepatic circulation(10,14). ICG excretion is a continuous biphasic process(15). ICG extraction and biliary excretion is reliant on energy depend transmembrane carrier proteins. The first stage is uptake across the basolateral sinusoidal plasma membrane of hepatocytes by ATPase dependent carrier proteins(10,16) and extraction by hepatic enzymes including glutathione S-transferase(17).

The second stage is transport through the cell and excretion at the apical membrane into bile fluid. This is the ATPase dependent rate limiting step of ICG clearance. The plateau seen in linear graphs of plasma disappearance and hepatic uptake following injection of ICG is explained by saturation of these carrier proteins. ATPase dependent Multi-drug resistant P-glycoprotein (Mdr2) phospholipid translocator is vitally important and facilitates the formation of biliary phospholipid vesicles containing ICG and excretion of the unaltered ICG into bile. This explains the biphasic elimination profile of ICG. The first t½ is only around 3 to 4 minutes whilst the second t½ is highly variable and dose dependent(18).

The accepted pharmacokinetics of ICG is based, in part, upon the early animal studies of *Wheeler et al* and *Ketterer et al* and relates only to healthy tissue. They report peak biliary excretion two to three hours after administration and almost complete drug recovery in bile within five hours in anaesthetised dogs(19,20). *Cherrick et al*'s human studies from the same era validated this observation(14). After intravenous injection, ICG was first detected in bile within 15 minutes, concentration peaked at two hours, but levels remained high at trial

termination at seven hours post administration, indicating a possible longer elimination profile in humans. ICG shows almost complete intravascular confinement in healthy tissue, but delayed washout of up to 72 hours in diseased and malignant tissue(21). *Alacam et al* proposed disruption to the basement membrane and therefore leaky capillaries in cancerous tumours to explain extravascular retention of ICG in mammillary adenocarcinoma in *in vivo* studies(22).

Several factors adversely affect the clearance of ICG. Bilirubin is a competitive inhibitor of ICG uptake by hepatocytes, as is hypo-perfusion and altered hepatic microcirculation. In clinical practice, severe liver disease with severely reduced hepatocyte function, raised serum bilirubin and low albumin states and hypotension all adversely affect ICG and clearance rates. The expression of the canicular transporter protein, Mdr-2, is moderately decreased in human livers with alcoholic cirrhosis(23). Calorific restriction, as often seen in sepsis and pre-operative fasting regimens, also increases ICG hepatic clearance(24).

Spectral Properties

ICG demonstrates an anomaly in its spectral properties, whereby there is variation in its absorption and emission depending on the *"nature of the solvent medium"* it is reconstituted in and the concentration achieved(25,26). ICG has a very broad optical window, overlapping the edge of the visible light and Near-Infra Red (NIR) region of the electromagnetic spectrum. The peak absorption wavelength is 780nm in water and shifts to 800nm in albumin(25,27), whilst the peak emission wavelength for ICG is 820nm in water and 830nm in whole blood(28). ICG monomers peak at a lower wavelength than ICG oligomers and protein bound ICG. ICG does not obey *Beer-Lambert Law* linear relation between concentration and fluorescence in solution due to its tendency to form aggregates and oligomers(9,29). Owing to dye-protein interactions, the maximum fluorescence intensity in blood is observed at 80 mg/ml. Above this,

self-quenching occurs and the fluorescent intensity of ICG decreases in a non-linear fashion(15).

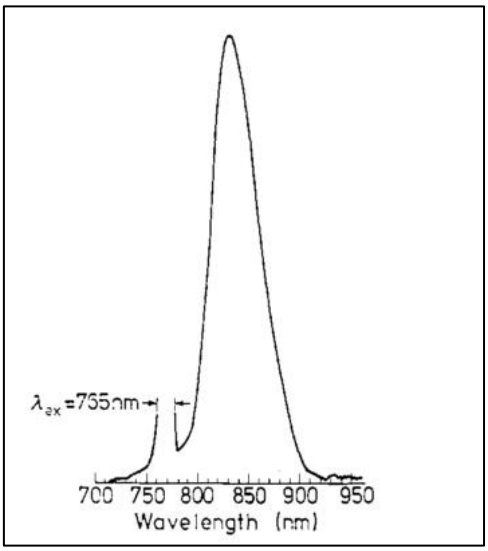

Figure 4: Spectral properties of ICG in human whole blood in 100µL cell at excitation wavelength 765nm. Adapted from Benson (1978)(28)

Safety

ICG is safe, with very few adverse reactions reported. The manufacturers of medicinal ICG quote the risk of anaphylaxis as less than 1 in 10,000 and using case report data estimate the risk of death from an anaphylactic reaction as less than 1 in 330,000(11). The risk is increased in patients with severe renal insufficiency, previously documented iodine allergy, and when ICG is reconstituted with any solvent other than the recommended sterile water(11,17,30)**.** *Rudolf et al,* confirmed the safety of ICG in pregnancy; by simultaneously measuring levels of ICG in maternal and foetal cord blood they confirmed ICG does not cross the placenta(31).

Clinical Applications of ICG

Since the discovery of ICG, it has been used for a myriad of clinical applications. The majority have focused on the intravascular administration of ICG as part of angiographic studies. ICG lends itself well to angiography because of its spectral and intravascular confinement

properties. At the 800nm wavelength, ICG shows peak absorption and this wavelength conveniently overlaps with the exact point whereby the optical density of oxygenated haemoglobin is comparable to that of deoxygenated haemoglobin, facilitating methods of NIR imaging in all three fluid mediums, bloods, plasma and serum(32). ICG is also favoured for fluorescence-guided surgery because the depth of tissue penetrance possible increases with this longer wavelength of light. *Stolik et al ex vivo* tissue study characterised the average depth of detectable fluorescent light penetrance in liver tissue (post-mortem tissue) was 2.9mm (S.D±0.3mm) at emission wavelength 780nm and 3.68mm (±0.35mm) at 835nm. Whilst this was considerably shorter for whole serum blood with the same emission wavelengths applied, the distance was only at 0.42mm (±0.02mm) and 0.51mm (±0.02mm) respectively(33).

Another accepted application of ICG is retention testing (ICGR-15) as part of functional hepatocyte assessment prior to hepatic major resection surgery. Liver resection surgery is a fine balancing act between resecting the underlying pathology and retaining enough functional liver parenchyma; overly extensive resection can lead to the catastrophic complication of post-operative liver failure. The pharmacokinetic and biexponential decay curve of ICG make it an ideal marker for hepatocyte reserve assessment(34). The serum concentration of ICG 15 minutes after intravenous administration can act as an accurate surrogate marker of both hepatocyte volume, function, and blood flow. An ICGR-15 score over 14% (healthy adults 8-14%) is highly predictive of poor post-operative outcomes, including mortality in patients undergoing major liver resection surgery(35,36).

Laparoscopic Surgery

The term laparoscopic originates from the Latin *laparo* - *"wall of the abdomen"* and scope, to visualise or explore. The first documented laparoscopic surgical procedure on a human subject was performed in 1910 by the Swedish physician *Jacobaeus*. He recognised the immense diagnostic and therapeutic potential of laparoscopic surgery, but also the risk of

bowel injury with introduction of the trocar in the abdominal cavity(37). The technique and equipment required for laparoscopy was explored and refined over the ensuing decades. It was not until 1981 that *Semm et al* performed the first laparoscopic appendicectomy(38). *Mühe et al* then performed the first laparoscopic cholecystectomy four years after(39). Thereafter, several pioneers and early adopters around the world started to regularly use the technique and apply it to a myriad of surgical procedures, traditionally performed via an open approach. Today, laparoscopic surgery has become the standard approach for many procedures and significant technological advances have been made. Laparoscopic surgery requires the introduction of a light source into the abdominal or pelvic cavity. A natural progression has been the development of fluorescence enabled laparoscopic technology. The addition of a fluorescent light source and detector coupled with administration of a dedicated fluorophore can improve structure visualisation and surgical accuracy.

Intraoperative Applications of ICG

Tumour Localisation with ICG

Recently, ICG with NIR technology has moved into the operating theatre and has been applied as a dynamic imaging modality for begin and malignant pathologies in both open and laparoscopic surgery. The intraoperative applications of ICG can broadly be divided into angiographic perfusion and lesion localisation studies.

Of interest, is ICG guided navigation in laparoscopic liver resection surgery. The hope is it will compensate, at least in part, for the lack of tactile feedback available in minimally invasive surgery. First trialled by *Ishizara et al and* explored by his colleagues *Kudo et al* and *Morita et al*, ICG has proved highly valuable in Hepatocellular Carcinoma (HCC) resection, in part because of its convenient dosing regimen. HCC localisation can utilise the residual ICG from preoperative ICGR-15 functional reserve assessments and possibly the leaky basement membrane of tumour capillaries. By administering ICG between 3 and 28 days prior to surgery

the three groups were able to delineate all tumours within 5mm of the liver capsule and visualise multiple tumours invisible on white light inspection alone(40–43). ICG had a HCC localisation sensitivity of 96%(42), produced uniform fluorescence in all lesions, and was felt to aide intraoperative decision-making(41). From their early phase assessments, the optimal dosing interval has not yet been established.

Liver metastases are common in the natural history of many cancers, especially colorectal cancer, and must be resected if any attempt at long-term survival is to be made. Therefore, the natural progression for ICG guided NIRF was the field of liver metastases resection. HCC tumours show a characteristic uniform fluorescence with ICG, whereas colorectal liver metastases show ring enhancement with retention of the fluorophore in the tumour stromal and normal liver tissue junction(44). *Handgraaf et al,* found NIRF helped surgeons to identify significantly more CRLM intra-operatively (25% vs 13%, $p = 0.04$) ($n = 86$ NIRF arm vs. $n = 87$ control arm). Many of the additional lesions were small at less than 5mm, subcapsular and only detectable with NIRF. In the 21 (21/86) patients with additional CRLM identified with NIRF, 52% did not have any evidence of liver recurrence at 3-year follow-up(45). The overall sensitivity and specificity of NIRF detection of malignant liver lesions is limited by the depth of penetration achieved with deeper parenchymal lesions(41). *Kudo et al's* trial of NIRF guided resection of HCC lesions yielded a sensitivity of 69% (detecting 11 out of 16 lesions)(41). Whereas, *Handgraaf et al's* subgroup analysis of the sensitivity of NIRF imaging in CRLM yielded an overall sensitivity for all lesions of 83%, but for superficial lesions (<8 mm subcapsular location) it was highly sensitive and yielded a detection rate of 100%(45).

Sentinel Lymph Node Biopsy (SLNB)

In the last two decades, biopsy of the Sentinel Lymph Node (SLN) in multiple forms of cancer with a propensity with early lymph node metastasis has been incorporated into surgical routine practice. Accurately staging the lymph node burden allows risk stratification and

individualisation of surgery and postoperative adjuvant therapies. Identification of high-risk patients who are likely to benefit from extended regional lymph node clearance spares those with low risk localised and/or node negative disease the associated surgical morbidity.

Localisation of the SLN in the axilla and confirmation of its cancer status is vital to breast cancer management. Axillary node clearance with lumpectomy in early breast cancer has a greater postoperative morbidity, but does not offer any survival advantage over the less invasive procedure of lumpectomy and SLN dissection(46,47). The gold standard technique for SLN identification intraoperatively is subcuticular and intraparenchymal injection of the radioisotope Technetium-99m (^{99m}Tc) before surgery and/or with a blue colloid dye such as Isosulfan blue(48). The combination of ^{99m}Tc and blue dye lymphoscintigraphy yields a SNL detection rate and false negative rate of 94.4%(49) and respectively 7%, whilst blue dye as the sole agent has a false negative of 9.9%(50). ^{99m}Tc is costly to manufacture and requires comprehensive radiation safety precautions to safeguard clinical staff from the risks associated with cumulative radiation exposure. Isosulfan blue dye can interfere with intraoperative pulse oximetry readings(51), carries a risk of serious allergic reaction in the region of 1 - 3%(52), and can cause permanent blue skin tattooing or skin necrosis at the injection site(53).

ICG has been investigated as a potential superior alternative to these agents because of its favourable dosing regimen, safety profile, and lower financial cost. Proof-of-principle and efficacy of ICG guided SLNB was confirmed by *Motomura et al* using a prototype NIR device two decades ago(54). *Guo et al's* prospective trial of SNLB with subdermal peri-areolar infiltration of ICG had a diagnostic yield of 97%(55). *Wishart et al* compared detection rates between SLN mapping modalities. ICG was superior to ^{99m}Tc and isosulfan blue used in isolation and even when used as a combined imaging modality. ICG detected all 201 SLN (yield 100%)(56).

In a similar way to breast cancer surgery, dissection of the SLN has also been applied to gynaecology oncology surgery. In the UK, there is disagreement on the merits of routine SLN

biopsy during laparoscopic hysterectomy and bilateral salingo-oophrectomy in the treatment of the most common form of gynaecological cancer - endometrial adenocarcinoma(57). Although lymph node status is important for prognosis prediction, the vast majority of cancers present as early stage I or II and therefore the likelihood of a positive SLN is slim. The Royal College of Obstetricians and Gynaecologists recommends ^{99m}Tc and/or a blue dye to detect the SLN in high grade aggressive endometrial cancers only. There is considerable variability in the techniques and doses used, but the French SENTI-ENDO prospective trial of superficial infiltration of ^{99m}Tc and isosulfan blue dye in early endometrial cancer described an overall SLN detection rate of 80%(58). Whereas, ICG guided NIR laparoscopic surgery yielded an overall and bilateral SLN detection rate of 96% and 88% respectively(59).

Near Infrared Fluorescent Angiography (NIR-FA) Anastomosis Perfusion Assessment

In the field of gastrointestinal surgery, and especially colorectal surgery, NIR-FA with ICG has been widely applied to anastomosis perfusion assessment. Anastomotic leak (AL) defined as "*a leak of luminal contents from a surgical join between two hollow viscera*"(60) is a catastrophic complication of gastrointestinal resectional surgery. The underlying aetiology of AL is multifactorial, with a complex interplay between patient and surgical factors determining healing of the surgical join. However, perfusion of the anastomotic joint is one of the few modifiable operative factors within the control of the operating surgeon.

Jafari et al published the PILLAR II clinical trial results in 2015 reporting an astonishingly low leak rate of only 1.4% in patients undergoing left sided and anterior resection surgery with a mean anastomosis 10 ±4cm from the anal verge(61). Their multicentre prospective trial of 147 patients undergoing surgery with primary anastomosis assessed with NIR-FA included different clinical indications, including malignancy, diverticular disease, and inflammatory bowel disease. Intravenous administration of ICG rapidly and predictably mapped the perfusion of the bowel in 99% of patients. The addition of NIRFA lead to a change in operative strategy in 8% *(n = 11)*. Of these patients, none experienced a clinical or radiological anastomotic leak. *Jafari et al* successfully showed that NIRFA was a feasible and useful adjuvant to colorectal anastomosis construction. However, with such a small and highly variable cohort of patients, and a lack of pre-operative randomisation, it is difficult to argue NIRFA can produce a five to ten-fold reduction in anastomotic leak rate without further robust clinical research(61).

The PILLAR III trial (ClinicalTrials.gov registry identifier NCT02205307) was a randomised controlled trial of NIR-FA in low anterior resection surgery (anastomosis ≤10 cm from the anal verge) versus a white light control arm, in the United States that closed early due to poor recruitment and biased surgeon equipoise. The trial recruited only 347 of the planned 550-900 patients. The preliminary modified intent-to-treat data found no difference in AL rate at 8 weeks

post-operatively between low anterior resection with NIR-FA and white light standard care (10/175 (5.7%) versus 7/168 (4.7%) respectively). However, interpretation of the efficacy of NIR-FA in anterior resection for the prevention of AL is severely limited with these results. The PILLAR III trial is statistically underpowered to draw any meaningful conclusions(62). Despite this, NIR-FA appears remarkably popular and well-received by US colorectal surgeons, but currently lacks a body of high-quality evidence of its efficacy or robust data to support the claims proposed by early adopters of the technology.

Biliary Pathology, Cholecystectomy and NIR-FC

Cholelithiasis, the formation of choleliths (gallstones) in the gallbladder or biliary tree is very common. It is estimated that 15% of adults in the Western World have gallstones(63). The majority of patients with gallstones are asymptomatic, but between 1 to 4% will develop a complication associated with gallstones every year(64), with men more likely to be symptomatic(65). Most (>75%) choleliths are cholesterol stones formed of cholesterol monohydrate crystals. Less commonly they are composed of bilirubin polymers or calcium bilirubinate and these are referred to as brown and black pigment stones respectively(66). The primary metabolic pathophysiological step in biliary calculous disease is supersaturation of the bile with cholesterol or bilirubin pigments. This is often accompanied by impaired bile salts recycling and gallbladder dysmotility, reduced production of solubilising substances, and increased mucus production. Bacterial infection of the static bile also contributes to gallstone formation in some cases(67,68). The gallbladder and ducts become filled with a saturated mucin-rich “biliary sludge”. Nucleation of the saturated bile forms crystals and these aggregate in to choleliths(69).

Several complications of cholelithiasis can arise and require treatment by excision of the gallbladder, a procedure called cholecystectomy. The majority of symptomatic patients complain of biliary colic; episodic postprandial upper abdominal pain with or without

vomiting(70). Biliary colic results from gallbladder spasm in response to transient Cystic Duct (CD) obstruction by a gallstone or intrinsic gallbladder irritation(70,71). Prolonged obstruction of the gallbladder can lead to acute calculous cholecystitis. The gallbladder becomes inflamed, the wall of the gallbladder thickens, and an exudate of pericholecystic fluid can develop. Secondary bacterial infection with anaerobic colonisers of the gastrointestinal tract often follows(65). These patients typically present with constant abdominal pain and signs of a systemic inflammatory response. Other life-threatening complications of cholelithiasis also include gallstone pancreatitis and ascending cholangitis(71). These diagnoses can overlap.

Laparoscopic Cholecystectomy

In 2014, 66,660 cholecystectomy surgeries were performed in the United Kingdom, with the vast majority (92%) completed via a laparoscopic "*keyhole*" surgical approach(63). Laparoscopic cholecystectomy is the gold standard for the treatment of acute and elective biliary pathology, having replaced open surgery in the majority of cases(63,72–74).

Laparoscopic cholecystectomy was adopted into standard surgical practice in the early 1990s(39,72). Initially, laparoscopic cholecystectomy surgery took on average 3 hours to complete and had a conversion to open rate in the region of 15%(75,76). Until relatively recently, acute cholecystitis and gallstone-induced pancreatitis were a contra-indication to early laparoscopic excision of the gallbladder. Early adopters of emergency laparoscopic cholecystectomy in acute cholecystitis reported the procedure feasible but with high rates of morbidity, namely high intra-operative blood loss and bile duct injury with an unacceptable incidence in excess of 5%(72). Many centres, therefore, continued to endorse open cholecystectomy or delayed laparoscopic cholecystectomy (DLC) for this subgroup of patients.

Emergency or "*index admission*" laparoscopic cholecystectomy (IALC) for acute cholecystitis is now the gold-standard treatment. NICE (National Institute for Healthcare Clinical

Excellence) recommends hospital trusts *"offer early laparoscopic cholecystectomy (to be carried out within 1 week of diagnosis) to people with acute cholecystitis"*(63). Multiple comparative studies have confirmed IALC to be cost-efficient, costing £4,570 compared to £4,720 for DLC(77) and dismissed early concerns around higher rates of bile duct injury and open conversion(78,79).

Importantly, there is marked patient morbidity in the delayed group with almost 20% of patients waiting for a DLC representing in the interim. Of those who re-present, 30% will have biliary obstruction or gallstone pancreatitis(77,80). Despite this, only 54.8% of patients presenting with acute cholecystitis to UK hospitals receive an IALC. The varies between UK hospitals (26% to 52.7%)(81,82). The rate of IALC variables considerably crossed the developed world. In Singapore, around 67% of patients receive surgery within 7 days of presentation(83), whereas in Australia rates of IALC are as high as 89.9% in large urban centres(84).

Bile Duct Injury (BDI) during Laparoscopic Cholecystectomy

Bile Duct Injury

The most feared complication of laparoscopic or open cholecystectomy is a bile duct injury (BDI). The implications can be catastrophic, with a significant mortality and morbidity for the patient and medico-legal ramifications for the surgeon and hospital trust involved(85–89). Many years after the bile duct injury, patients can continue to suffer physical and psychological complications. These often have a severely negative impact on their overall quality of life(90).

Prior to the introduction of laparoscopic cholecystectomy surgery into standard care in the early 1990s, the overall bile duct injury rate for open cholecystectomy surgery was low at 0.2% to 0.32%(91,92). Thereafter, the incidence of iatrogenic bile duct injury reported in the literature has varied greatly. Earlier case series encompassing the "*learning curve*" period, quote higher rates than more recent series from experienced hepatobiliary centres. The largest early US series, retrospectively analysing 1,570,361 laparoscopic cholecystectomies

performed between 1992 and 1999, found an overall incidence of bile duct injury of 0.5%(87). *Strasberg et al's* review of bile duct injury during laparoscopic cholecystectomy published in 1995 also estimates the incidence at 0.52%(91) and *Deziel et al* from 1993 quotes a similar figure of 0.6%(93).

In the early years of laparoscopic cholecystectomy associated bile duct injury, 26% of patients who sustained an injury died within one year of the event, compared to only 6.6% of the uncomplicated group. Even when considering independent risk factors, the adjusted hazard ratio (HR) for mortality was 2.8 for the bile duct injury cohort(85). Large European studies from the same period report similar rates of bile duct injury; Italy 0.42%(94), Sweden 0.40%(95), Switzerland 0.3%(96) and *Buanes et al's* Norwegian national review of cholecystectomies performed in the early 1990s reported a higher bile duct injury incidence of 0.8%(97).

Iatrogenic bile duct injury should be considered preventable. Multiple mechanisms and errors contribute to its occurrence. It remains debatable to what extent lack of technical skill, perception error, or combinations of these factors are the key underlying cause of bile duct injury. Misidentification of the CD is a recurring theme in retrospective analyses(91). *Way et al* estimate that just 3% of bile duct injury are due to a true lack of technical ability(98). They analysed 252 bile duct injury cases, regardless of the extent and grade of bile duct injury sustained and found the underlying cause in most cases was the surgeon mistaking an extrahepatic duct for the CD. The surgeon persistently continued to interpret the operative image to fit with their perception of the anatomy and disregarded any information that contradicted their perception. However, previous studies attribute far more blame to the technical skill of the surgeon. *Nuzzo et al,* attributed *"improper use of monopolar coagulation"* and an inability to achieve early haemostasis as the primary mechanism of bile duct injury in nearly 20% of reported cases(94).

The argument for lack of technical skill as a primary cause of bile duct injury is validated by the trend of bile duct injuries rates being higher in surgeons inexperienced in laparoscopic cholecystectomy surgery, in junior surgeons, and in centres with low volume case-load(99).

Sarli et al compared 200 patients from a single centre who underwent laparoscopic cholecystectomy early on the learning curve in 1991 to 1992 to a matched cohort from 1995 to 1996 and reported an overall reduction in all operative complications including bile duct injury from 9% to 2.5% *(p<0.01).* The Relative Risk (RR) of complications was also far higher with open compared to laparoscopic cholecystectomy (RR 5.4; *p=0.0007*)(100). In recent years, the procedure of single-incision cholecystectomy has emerged and gained momentum. Performed relatively infrequency, and mostly by surgeons relatively early on the learning curve with this new technique, it carries a worryingly high rate of bile duct injury of 0.72%(101). This adds further support to the "*learning curve*" theory of bile duct injury in any form of minimally invasive hepatobiliary surgery.

The safety of laparoscopic cholecystectomy surgery has dramatically improved since the early days of minimally invasive surgery. UK centres that limit laparoscopic cholecystectomy surgery to surgeons who have a declared interest in upper gastrointestinal surgery and/or minimally invasive hepatobiliary surgery report extremely low rates of open conversion and bile duct injury; 3.0-3.8% and 0.1% respectively(81,102,103). High-volume American centres also report a bile duct injury incidence of around 0.08% in their most recent published data(104).

Medico-Legal Implications of Iatrogenic Bile Duct Injuries

Aside from the mortality and morbidity associated with bile duct injury there is also a significant medico-legal burden for the surgeon and hospital trust. In our litigious society, patients are more likely to bring successful legal cases against a trust when they are the victim of any perceived avoidable compilation or medical negligence. Surgeons are most at risk of litigation when performing laparoscopic cholecystectomy compared to any other general surgical procedure(88). In the UK, all legal cases of alleged clinical negligence are processed via the NHS Litigation Authority (NHSLA). Between 1995 and 2009, 418 cases of alleged medical

negligence emanating from laparoscopic cholecystectomy in the NHS were considered, with 303 cases settled, and 179 of cases related to bile duct injury. Cases of bile duct injury had the highest success rate (77.9%) of all laparoscopic cholecystectomy litigation cases, and commanded one of the highest average payments at £114,324 per case(86). In the United States, average settlements for clinical negligence relating to laparoscopic cholecystectomy can be four times higher than in the UK(89).

The management of bile duct injury is also vitally important to the likelihood of ligation being brought against a surgeon and the case being upheld. *Roy et al's* review of bile duct injury cases brought to the NHSLA between 2000 and 2005 found *"only half of claims for injuries that had been recognised promptly were successful",* compared to 90% of cases where the bile duct injury was recognised late(88,89). A late diagnosis of bile duct injury also resulted in a higher average financial settlement. In the Netherlands, patients diagnosed with bile duct injury more than seven days after initial surgery received on average 2.4 times higher pay-out from their ligation case than those diagnosed within one week(85). In the UK, the difference in financial settlement between early and late diagnosis is roughly 3.6 times(88).

Critical View of Safety and Protocol Directed Laparoscopic Cholecystectomy Surgery

Strasberg proposed the *"critical view of safety"* (CVS) in laparoscopic cholecystectomy in 1995(91) *(Figure 5).* Since 2006, the Dutch Society of Surgery has demanded all teaching hospitals in the Netherlands produce an institution-specific laparoscopic cholecystectomy protocol in accordance with their best practice guidelines. This mandates the CVS must be recorded photographically prior to transection of the CD and CA(105). Over 97% of Dutch surgeons self-report establishing and confirming the CVS as their usual and preferred method of performing laparoscopic cholecystectomy(106).

The consensus report from the European Association of Endoscopic Surgery (EAES) also recommends a modified surgical technique very similar to *Strasberg's* CVS. An EAES expert panel recommend using an oblique 30° or 45° angled laparoscope to allow full 360° rotational viewing of the Common Bile Duct (CBD). They emphasise firm lateral retraction of the gallbladder to open up the hepatocystic triangle, cautious electrocautery near to the bile ducts, establishment of the CVS with only two tubular structures entering the gallbladder - the CD and Cystic Artery (CA)(107). Along with many expert sources, EAES recommends surgeons maintain a low threshold for open conversion should they be unable to safety obtain the CVS or encounter indeterminate anatomy that cannot be safety identified prior to ductal division.

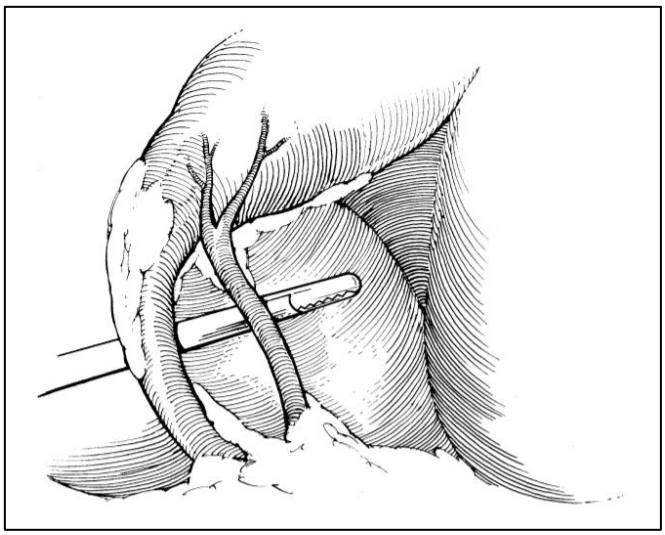

Figure 5: The critical view of safety (CVS). Adapted from Strasberg (1995)(91).

The triangle of Calot (hepatocystic triangle) dissected free of all tissue except for the CD and artery with the base of the liver bed is exposed. The surgeon can safely assume the only two structures entering the gallbladder are the CD and CA.

On-Table Cholangiogram

Since the introduction of laparoscopic cholecystectomy, multiple strategies to reduce bile duct injury have been proposed and intraoperative cholangiography, often referred to as an on-table cholangiogram (OTC), is one of the most accepted. The advantage of OTC is that it can

visualise both the intra and extrahepatic biliary anatomy, the presence of any ductal choleliths, and the flow of contrast into the duodenum. The most common reason for conducting an OTC is to exclude choledocholithiasis. A meta-analysis by *Jamal et al* found OTC yielded a pooled sensitivity and specificity of 87% and 98% for identification of choledocholithiasis(108). However, OTC can be problematic and time-consuming to perform, increasing operative length by around 16 to 24 minutes per case(109,110). The catheterisation process risks injury to the bile ducts and introduction of infection into the biliary system. The intervention also carries a radiation dose, both to the patient and the operating theatre staff, and utilises additional resources.

Proponents of OTC argue it improves outcomes, reduces bile duct injury, and aids intraoperative decision making; a viewpoint not held by all laparoscopic and hepatobiliary surgeons. *Flum et al's* retrospective review of over one and a half million laparoscopic cholecystectomies performed during 1992 and 1999 concluded that, regardless of patient and surgeon factors, the relative risk of bile duct injury was higher (RR 1.71) when OTC was omitted(111). *Fletcher et al's* review of bile duct injury in Western Australia, from introduction up until 1994, demonstrated the greatest protective effect of OTC in complex biliary pathology, reducing the incidence of bile duct injury from 16.9 to 2.2 per 1000 for both open and laparoscopic cholecystectomy(112). *Waage et al* concluded that OTC reduced the incidence of bile duct injury by 34% (OR, 0.66; 95% CI, 0.54-0.79) in Sweden between 1987 and 2001(95). This early period of laparoscopic cholecystectomy was largely experimental without consensus on timing or indication for surgery. It is noteworthy that many centres viewed complex and acute biliary disease as a contraindication to minimally invasive surgery, limiting access to emergency laparoscopic cholecystectomy at that time.

Iatrogenic extrahepatic bile duct injuries are often missed by the operating surgeon. Only 18% - 54%(85,99,113,114) of bile duct injuries are recognised intra-operatively, and a high proportion are not diagnosed until after discharge from hospitall(85). There is a wealth of evidence that outcomes are better when the repair is performed by an experienced

hepatobiliary surgeon not involved in the primary surgery(114). This was first reported by *Stewart et al* in 1995 who noted only 17% (11 of 64) of repairs performed by the primary surgeon were successful, and not requiring any further radiological or surgical re-intervention(98). *Flum et al* report that mortality was 11% higher when repair surgery was performed by the original operating surgeon(87).

The most recent data available found that 24% of laparoscopic surgeons in the UK and about a third in the United States perform routine OTC with every laparoscopic cholecystectomy(115,116). In the Netherlands, where surgeons adhere to a laparoscopic cholecystectomy protocol incorporating the critical view of safety described by *Strasberg*(91), only 2.6% perform routine OTC(117). Preoperative deranged liver function tests and the clinical presentation of cholangitis are independent risk factors for choledocholithiesis(118). Therefore, many surgeons use selective OTC when laboratory, radiological or intraoperative findings raise suspicion of intraductal pathology.

It is argued that OTC only increases intraoperative detection of bile duct injurie but does not reduce the actual incidence. *Ludwig et al* reported that routine OTC reduced the incidence of, and increased the rate of intra-operative bile duct injury identification, from 0.43% to 0.21% and from 44.5% to 87% respectively when compared to selective OTC(113). On preliminary analysis, *Sheffield et al* concurred with *Ludwig et al* and reported a reduction in bile duct injury with OTC from 0.36% to 0.21% between 2000 and 2009(99,113). However, after adjustment for unmeasurable cofounders, and subjecting the data to more rigorous statistical analysis, the difference in outcomes when using routine OTC was not statistically significant *(p=0.31).* Other retrospective analyses support this conclusion(116). Good quality data from large prospective randomised controlled trials of the protective effect of OTC during cholecystectomy is lacking. Systematic review of four small trials found that failure to perform OTC did not increase the risk of bile duct injury in the elective cholecystectomy population (OR: 0.36; 95% CI: 0.01–8.92; *p=0.53*)(110).

Other authorities argue that OTC is not cost effective and does not reduce intraoperative complications. This often ignores late re-presentation with complications from missed ductal stones or stenosis. *Khan et al* disclosed four patients allocated to the control (no OTC) arm of their RCT presenting within one year of surgery with deranged LFTs and pain in their study(119). Without intraoperative imaging, the presumption was of retained ductal stones, which required extensive investigation that might have been avoided had OTC been performed. It is clear OTC has an important role in biliary anatomy mapping, identification of luminal cholelithiasis, and intraoperative identification of bile duct injury. However, there is not a clear consensus to recommend OTC in straightforward laparoscopic cholecystectomy owing to its increased financial cost, prolongation of operative duration, and radiation dose. A sensible recommendation is for OTC to be employed liberally in any complex case, where there is ambiguity of the anatomy, suspicion of ductal stones, stricture, or potential bile duct injury. OTC if often more challenging to perform in difficult and complex laparoscopic cholecystectomy surgery and it is these cases that are more likely to sustain bile duct injury or have missed ductal cholelithiasis.

Near Infrared Fluorescent Cholangiography (NIR-FC)

The technical difficulties associated with performing OTC, combined with the quest to reduce rates of bile duct injury, with its associated morbidity and financial ramifications, makes alternative strategies, such as Near Infrared Fluorescent Cholangiography (NIR-FC) with ICG, attractive as potential adjuvants to laparoscopic cholecystectomy. The potential to delineate the extrahepatic biliary anatomy with NIR-FC may aid surgeons in the accurate identification of biliary structures and potentially reduce the incidence of bile duct injuries. Some proponents of this new technology believe it may even negate the need for traditional intra-operative cholangiogram in certain settings. The technique is simple; patients receive a preoperative dose of ICG, and the fluorescent biliary anatomy is viewed with a NIR laparoscope, allowing dynamic real-time bile duct mapping.

Various teams have performed standard laparoscopic, single incision and robotic cholecystectomy with NIR-FC and ICG *(Table 1).* However, there is no consensus on dose, timing of administration, or clinical endpoints. The small sample sizes, and differing methods, mean there is a lack of comparative data. *Figueiredo et al* explored NIR-FC in a mouse model and concluded the peak intraoperative signal to noise ratio was achieved 25 minutes after intravenous administration(120). The first human application of ICG guided laparoscopic cholecystectomy was reported by *Ishizawa et al* in 2009 using a prototype NIR device(121,122). They deemed the administration of a single intravenous dose of 2.5mg ICG two hours prior to surgery a success and reported ease of visualisation of the CD and the Common Hepatic Duct (CHD).

A small number of non-randomised, prospective NIR-FC trials have followed. A single pre-operative intravenous bolus of 2.5mg ICG is the most popular. *Zarrinpar et al* attempted to define the optimal dose and timing interval and refuted the consensus view that a 2.5mg dose is optimal in hepatobiliary surgery(123). Although small, involving 37 patients in total, and including cholecystectomies and partial hepatectomies, there was a clear improvement in the visualisation of important extrahepatic biliary structures with higher doses of ICG administered at a longer pre-operative interval. Using a semi-quantitative scoring system, they suggested *"a dose of 0.25mg/kg administered at least 45 minutes prior to visualisation facilitates intraoperative anatomical identification".* This is well within the safe adult total daily dose limit of 5mg/kg of ICG(32).

The exact timing of administration of ICG is also contentious and must take into consideration the noise to signal ratio created by background liver fluorescence. Previous studies were guided by the elimination properties of ICG and administered a dose prior to induction of anaesthesia, however this ranged from 15 minutes to more than 3 hours prior to the start of surgery. *Verbeek* attempted to define the optimal dosing regimen in open hepatic surgery prior to application in laparoscopic cholecystectomy(124). Pushing the limits of ICG detectable fluorescence, they proposed 10mg administered 24 hours prior to cholecystectomy as the

optimal dose. They reported far lower liver background signal and therefore greater contrast between the liver and the CBD and favourable navigation for the operating surgeon with prolonged dosing. However, in a surgical setting, where most laparoscopic cholecystectomies are performed on a day-case basis, the feasibility of administering intravenous ICG the day before surgery is questionable. *Zarrinpar et al* observed improved contrast between the liver, bile ducts, and fat with prolonged dosing (3 hours), but compromised to a more achievable 45 minutes with the addition of a higher ICG dose to compensate(123).

A major drawback of NIR-FC is its limited depth of tissue penetration, somewhere in the region of 5 to 10mm. In the UK in 2019, 67% of men and 60% of woman in the England were considered overweight or obese(125). This figure continues to rise and is higher than when laparoscopic cholecystectomy was first introduced into NHS surgical practice. Operating on patients with a high Body Mass Index (BMI), and therefore large volumes of intraabdominal adipose tissue, is now a common occurrence and poses its own challenges. Japanese and American teams piloting NIR-FC have attempted to explore the effect of obesity on extrahepatic ductal visualisation. *Osayi et al* used a single ICG dose of 2.5mg in total in their USA based study – they only visualise the CBD in 64% of patients with a BMI over 35kg/m^2 and in one super morbidly obese patient with a BMI of 63kg/m^2 the CD was the only structure detected with NIR-FC(126).

Other teams reported similar difficulties with NIR-FC in the overweight or obese patient, including the need for extensive dissection in Calot's triangle to achieve any visualisation and a longer operative time(127,128). *Kono et al* contradicts this view, stating *"BMI had no predictive value for detection"* of the CD and CBD confluence(127), although the median BMI was only 23.5kg/m^2 in *Kono et al's* study, as compared to a mean 31.49kg/m^2 in *Osayi et al's* later USA based publication(126). In other fields of NIRF surgery using ICG as the fluorophore, high BMI was found to adversely affected structure visualisation. *Jewel et al* found the median BMI of patients with unmapped SLN in endometrial cancer was 41.2kg/m^2 versus only 30.1kg/m^2 *(p = 0.01)* in the mapped group(129). The inflammatory process underling

cholecystitis and gallstone pancreatitis further compounds the difficulties of using NIR-FC in a population with endemic levels of obesity. The characteristic pathological processes of pericholecystic and peri-hilar inflammation and tissue oedema leads to thickening of the gallbladder wall and inflammatory exudate in the surrounding tissues, which all increase the tissue density and depth between fluorescent structures and the laparoscopic camera, reducing the diagnostic yield of NIR-FC.

Author	Country	Year	Number of patients receiving ICG	Procedure	Dose (mg)	Pre-operative ICG dosing interval (1. as per methodology and 2. Actual dosing interval)	Mode of admission
Zroback(130)	Canada	2016	12	Laparoscopic cholecystectomy (LC)	3.75	1. "pre-operatively" 2. n/a	Elective
Buchs(131)	Switzerland	2013	23	Robotic single site cholecystectomy	2.5	1. "30-45min" pre-op. 2. n/a	Elective
Osayi(126)	USA	2015	82	LC	2.5	1. n/a 2. Mean 73.8±26.4m to incision	Elective
Tagaya(128)	Japan	2010	12	LC (8) Open (4)	2.5	1. 1-2 h pre-op 2. n/a	Elective
Boni(132)	Italy	2015	52	LC	0.4mg/kg	1. n/a 2. 15m prior to incision (range14±9m)	Acute & elective
Schols(133)	Netherlands	2013	15	LC	2.5	1. n/a 2. Mean 33m (range 19-67m) To 1st visualisation	Elective
Daskalaki(134)	USA	2014	184	Robotic LC (112 multiport & 72 single port)	2.5	1. 45m 2. n/a	Elective & acute
Spinoglio(135)	Italy	2013	45	Robotic single port	2.5	1. 45m 2. n/a	Elective
Igami(136)	Japan	2016	21	Single incision LC	2.5	1. n/a 2. 39m±4 (to 1st incision)	Elective
Ishizawa(137)	Japan	2011	7	Single incision LC	2.5	1. 2. 35 – 75m prior (to 1st visualisation)	Elective
Ishizawa(40)	Japan	2009	1	LC	2.5	1. 2 h "pre-operatively"	Elective

						2. n/a	
Kono(127)	Japan	2015	108	LC	2.5	1. n/a 2. Median 90m (range 15 -165m)	Elective & Acute
Ishizawa(138)	Japan	2010	52	LC	2.5	1. n/a 2. 110m mean (range 35 -165m) to 1st incision	Elective
Zarrinpar(123)	USA	2016	37	LC (13) open cholecystectomy (1) laparoscopic bile duct exploration (2) laparoscopic partial liver resection (6) open partial liver resection (11)	0.02 to 0.25mg/kg range	1. n/a 2. 3 groups a) 10m±3m, b) 45m±15m c) 3h±1h	Elective & acute

Table 1: Summary of NIR-FC with ICG cholecystectomy clinical trials. Abbreviations: Minute (m), hour (h)

1.3 Laparoscopic Colon Cancer Resection and EMI-137

Colorectal Cancer

Colorectal cancer (CRC) is the fourth most common cancer in the UK, with 42,000 new cases diagnosed in each year between 2014 and 2016(139). The incidence of CRC is strongly related to age, with 44% of cases diagnosed in those aged 75 and over(139). CRC continues to be the second highest cause of cancer related mortality in the UK. It accounts for 10% of all cancer related deaths - over 16000 UK deaths were attributed to CRC in 2016. This figure is greater in the most deprived social groups. CRC mortality is 30% higher in males from the poorest areas than in their age-standardised counterparts from the least deprived areas. CRC poses a significant disease burden, with the NHS continuing to see a year on year rise in cases, often in an older population with significant co-morbidities(139).

The anatomical distribution of CRC varies slightly between genders and with age. However, more than 65% of tumours are in the colon. There is a left-sided predominance, with over 30% of CRC seen in the rectum/rectosigmoid junction and a further quarter in the sigmoid colon up to the splenic flexure(140).

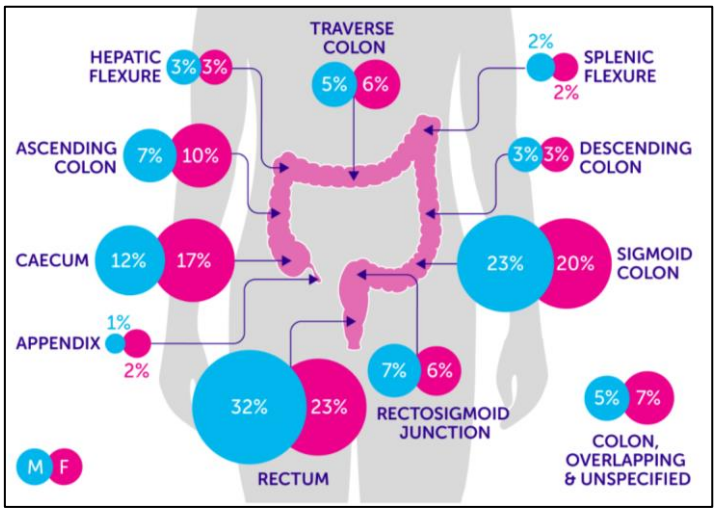

Figure 6: Anatomical distribution of primary colorectal cancer by percentage. Adapted from Cancer Research UK (2016)(140).

Average calculated from yearly total between 2012 and 2014 inclusive. Average total number of patients analysed 23,282 male and 18,317 female.

Survival rates in CRC are strongly correlated to the stage of disease at diagnosis. One-year survival data from 2012 shows 98% of patients presenting with stage I disease were alive after one year compared to only 46% with stage IV disease(141). Long-term survival can usually only be achieved with curative resection. This involves segmental colectomy and *en-bloc* resection of the draining lymph node field. Currently, there is significant variance of opinion regarding the necessary radicality of resection and, in particular, the extent of lymphadenectomy(142). Despite oncological advancements, locoregional recurrence remains a significant problem in colon cancer; the incidence of local recurrence at 5 years is reported to range between 6.1 and 11.5%(143,144).

National Screening

In 2006, the National Bowel Cancer Screening Program was introduced into the NHS in England(145). In England, all patients aged 60 to 74 years are invited to undertake screening every two years. The original system used Faecal Occult Blood Test (FOBT) home screening kits, but this was changed to the more sensitive Faecal Immunochemical Test (FIT) system in 2018(146). Those with a positive FOBT or FIT result are offered further investigation. In 2017, one-off flexible sigmoidoscopy screening for adults aged 55 was also rolled out in England to further aid detection of early cancer and pre-cancerous colorectal polyps(146,147). Since the introduction of national screening more than 25000 cases of bowel cancer have been diagnosed.

Ten-year longitudinal data from Scotland and Wales, where FOBT screening was introduced in 2003 for 50 to 74 years old, shows a statically significant change in both detection rates and the stage at presentation. FOBT screening detected 18% of CRCs and reduced emergency presentations from 20 to 13%(145). Importantly, the introduction of screening has led to an

increase in the early detection of CRC. The percentage total of stage I CRC detected rose from 17% in the pre-screening to 28% in the post-screening era(63,145,148).

Evidence for the introduction of sigmoidoscopy comes from the long term follow-up data from *Atkin et al's* randomised controlled trial of flexible sigmoidoscopy screening for UK adults aged 55 to 64(147). With a median follow-up of 17 years, the incidence of colorectal cancer was reduced by 26% (Hazard Ratio (HR) 0·74 [95% CI 0·70–0·80]; *p = <0·0001*) and the cancer-specific mortality was reduced by 30% (0·70 [0·62–0·79]; *p = <0·0001*) in the intervention group versus the control group respectively with screening.

Surgical Resection Strategies

To maximise the chances of oncological clearance and therefore long-term disease-free survival, the colon cancer needs to be removed with clear surgical margins and along with the draining lymphatic basin. The lymph nodes are divided into three tiers: tier I nodes are next to the bowel lumen (D1), tier II are contained within the mesentery along the supplying segmental artery (D2), and tier III are in close proximity the origin of the segmental vessels (D3). *Resection of twelve or more lymph nodes is recommended for accurate histological assessment and staging*(149).

Loco-regional recurrence following cancer surgery occurs due to residual cancer cells left behind at surgery, either due to inadequate resection or intraperitoneal dissemination. Although distant metastases is the more common pattern of disease recurrence in colon cancer, locoregional recurrence remains a significant problem. The incidence of local recurrence at 5 years is reported to range between 6.1 -11.5%(143,144). Despite this, it has not been the focus of research in the same way as in rectal cancer. *Liska et al* found the median time interval to locoregional recurrence in colon cancer was 21 months post-surgery and, half of cases occurred in the presence of distant metastases(150). For patients with stage III disease at diagnosis, 8.6% developed locoregional recurrence (HR10.8, [95% CI 2.6–

45.8]). The ability to accurately determine pre-operative stage and achieve adequate oncological resection is vitally important to long-term survival.

Laparoscopic Colectomy Surgery

Laparoscopic colectomy for colonic cancer was first trialed in the early 1990s(151). Thorough evaluation of the technique followed; trials such as the Medical Research Council (MRC) CLASICC (Conventional versus Laparoscopic-Assisted Surgery in Colorectal Cancer; Clinical Trial Number ISRCTN 74883561) dismissed concerns regarding increased rates of port-site recurrence and inferior lymph node yields(152,153). Today, laparoscopic colectomy is the preferred elective approach for colorectal cancer resections in most centres(152,154,155). There are several advantages of laparoscopic as compared to open surgery, including quicker patient recovery, fewer complications, and shorter hospital stay(155,156). Initially, operation length was around a third longer with laparoscopic surgery. However, as colorectal surgeons have become more experienced in laparoscopic surgery this difference has been reduced.

Complete Mesocolic Excision (CME)

Whilst survival rates in rectal cancer have significantly improved in recent years, the rates for colon cancer have been less marked. The improved survival seen in rectal cancer is attributed to the introduction of a standardised approach for low and middle rectal cancers, referred to as Total Mesorectal Excision (TME), along with more sophisticated preoperative imaging, (chemo)radiotherapy and better histopathological assessment. TME requires meticulous dissection of the mesorectum along the mesorectal fascial plane to remove the cancer in its contained embryological fascial envelope(157,158).

The same logic is being applied to colonic cancer in an attempt to improve survival(159), with the concept of Complete Mesocolic Excision (CME) and D3 lymphadenectomy. CME can be

performed open or laparoscopically and involves dissection of the mesocolon as an intact “package”. D3 lymphadenectomy refers to central ligation of the feeding vessels at their origin and adequate segmental colectomy to maximise lymph node clearance, both in the vertical and longitudinal direction(142,160,161). Several case series have shown CME with D3 lymphadenectomy to produce higher lymph node yields with a reduction in locoregional recurrence rates. In a recent Danish non-randomised population study, the cumulative 4-year disease-free survival for stages I-III was 85·8% after CME as compared to 73·4% after non-CME surgery (*log-rank p=0·001*). Specifically, for the stage III cohort, the difference in survival was 73·5% compared to 67·5% (HR 0·64 [CI 0·42–1·00])(161). This compliments the low local recurrence rate of 3.6% described by *Hohenberger et al* in their 2009 prospective study of CME(142).

CME with D3 lymphadenectomy may be beneficial in patients with lymph node involvement, however this patient cohort is the minority. In 2017, 24% of CRC cases in patients aged 60-74, and therefore eligible for screening, were diagnosed via the National Bowel Cancer Screening Programme(162). The majority of these were early cancers, with 78.7% of cases being lymph node negative (N0 status) at diagnosis(148). CME with D3 lymphadenectomy carries the risk of greater morbidity, meaning that patients without lymph node disease will be subjected to increased surgical risk without proven benefit. A selective approach is therefore required whereby patients with lymph node disease are offered radical CME with D3 lymphadenectomy, accepting a potential increased morbidity, whilst patients without lymph node disease undergo a less radical CME with D2 resection, with no compromise to their oncological outcome. This requires a means of accurately identifying lymph node status either preoperatively or intraoperatively. Currently, preoperative radiological staging in colon cancer is imprecise.

Colorimetric Dye

A drawback of laparoscopic surgery is the lack of tactile feedback from the laparoscopic instruments, which can make accurate localisation of the site of a colon cancer difficult. To aid intra-operative identification of a colonic tumour, it is standard practice to preoperatively mark the site with a colorimetric dye (India ink) at colonoscopy. Although luminal tattooing is inexpensive and quick to perform at colonoscopy, it is operator dependent and often imprecise.

Several studies have assessed the efficacy and safety of luminal tattooing. The most common complication is transmural inoculation and intraperitoneal spillage. A meta-analysis by *Acuna et al* found luminal tattooing at colonoscopy still had a localisation error rate of 9.5%(163). Free India ink staining of the peritoneal cavity and adjacent viscera negates the diagnostic yield and can cause localised inflammation. This can obscure the plane of dissection and cause adhesions. Conversely, if the inoculation is too superficial it might not be visible at laparoscopy, necessitating further intra-operative colonoscopy. There is also a small risk of serious complications, in particular, abscess formation and bowel perforation with localised peritonitis with colonoscopy and luminal tattooing(163–165). The need for accurate intra-operative identification of colonic cancers, and the limitations of colorimetric tattooing, has driven the search for a real-time intraoperative method for cancer localisation.

Lymph Node Staging in Colon Cancer

Although Computed Tomography (CT) scanning is used for preoperative staging and operative planning, it lacks the required sensitivity and specificity in colonic cancer to inform accurate planning of the radicality of surgery. Whilst MRI is now commonly used in the pre-operative staging of rectal cancer, movement artefact prohibits its application in colonic cancer staging. The FOxTROT pilot study (clinical trial number ISRCTN number 87163246), led by the University of Birmingham, found that CT only accurately discriminated tumour stage, T3

from T4 cancers in 47% of cases. CT lacks the required specificity and overestimates disease spread. Only 56% of cases classified as radiologically node-positive were confirmed node-positive on pathological assessment, whilst only 48% were correctly identified as having extramural vascular invasion on both CT scan and at final pathology assessment(166). There is no validated method for determining if a lymph node contains cancer on pre-operative CT. The clinical experience of the radiologist and several imaging characteristics are used to assess the probability of lymph node metastasis, but there remains a subjective element to this assessment.

Rollvén et al found common criteria such as node size greater than 5mm, when examined in isolation, had a specificity of 31% and positive predictive value of 39% *(p = 0.002)* in predicting stage 3 colon cancer(167). More definitive CT characteristics, such as internal node heterogeneity (specificity 84%; positive predictive value 74% and OR 20.0 $p = <0.001$) and irregular node boarder (specificity 81%; positive predictive value 61% and OR 6.23 $p = <0.001$), were more useful, but were present in relative few of the patients analysed and still did not show complete concordance with final pathological stage.

Sentinel Lymph Node Mapping in Colon Cancer Surgery

Sentinel lymph node (SLN) mapping has become part of standard care in the treatment and staging of many solid organ tumours. Breast cancer, for example, often behaves in a predictable progressive manner. Micro-metastases spread in a logical stepwise sequence to the nearest draining lymph node chain. In resection of breast cancer, if the closest draining lymph node is free of cancer, then it can be safely assumed the patient is node negative and avoid the morbidity associated with radial *en-bloc* lymph node dissection. However, trials of colon cancer SLN mapping have not produced the same level of accuracy and improved clinical outcomes. *Bertagnolli et al* found that for *“patients with node-positive colon cancer sentinel lymph node examination failed to predict nodal status in 54% of cases”*(168). This

high false negative rate was reproduced in other similar studies in colon cancer(169). This relates to the unpredictable metastatic pattern of colon cancer. *Tan et al* identified the first metastatic lymph node directly below the tumour in only 52% of colon cancer cases analysed(170). For 18% of cases, the pattern of metastasis was highly unpredictable and skipped the pericolic nodes entirely; the first metastatic node was detected more than 5cm away from the primary tumour site. No predictive factors for site of lymph node micro-metastases were identified(170).

The unpredictable behaviour of colon cancer lymph node metastases, and the propensity to skip the adjacent draining lymph node basin, limits the adoption of SLN mapping techniques. SLN mapping in its current form would under-stage a high proportion of patients, resulting in undertreatment of the cancer. An alternative method of identifying metastatic lymph nodes within the regional lymphatic basin is required.

Fluorescence Guided Colorectal Tumour and Lymph Node Mapping Intra-Operatively

Laparoscopic surgery is now the standard approach for the resection of many gastrointestinal and intra-abdominal malignancies. This minimally invasive approach involves the introduction of a narrow rigid laparoscope, with a built-in light, into the abdominal cavity. Pneumoperitoneum is established with the insufflation of carbon dioxide gas and the necessary operative instruments are introduced via strategically sited ports in the abdominal wall.

Laparoscopic surgery naturally lends itself to the concept of integrated fluorescence guided surgery. The standard white light laparoscope and light source used can be adapted to emit narrow specific wavelengths of light and used to excite and detect small molecule fluorophores during surgery. This combination creates a myriad of potential opportunities for using fluorescence to improve tumour localisation, lymph node mapping, and perfusion assessment.

Although in its infancy, fluorescence guided surgery could utilise many untargeted fluorophores and will no doubt drive the development of more sophisticated molecules including novel targeted fluorophores. The ability to couple a cancer specific targeted peptide to a safe fluorophore has the potential to increase the accuracy of resectional surgery and facilitate patient individualised surgery where radicality is tailored to the cancer location and biology.

Fluorescence Guided Tumour Detection

The GLiStEN (Next Generation intraoperative Lymph node staging for Stratified colon cancer surgery - Developmental phase; Clinical Trial Number ISRCTN79949827)(171,172) clinical trial led by Professor D. Jayne at the University of Leeds, used the oral administration of 5-aminolevulinic acid (5-ALA) to map metastatic lymph nodes in patients with stage III colon cancer.

Protoporphyrin IX (PpIX) is a naturally occurring protein found in nearly all human cells. The delta amino acid 5-ALA is taken up by mitochondria and converted to the intermediate Protoporphyrin IX (PpIX). It is then chelated with iron by the enzyme ferrochelatase to form heme in the heme synthesis pathway. Aminolevulinic acid is a pro-drug to the photosensitive protein PpIX. Light in the blue-violet bandwidth (wavelength 405nm) excites PpIX and it emits a red fluorescent signal (wavelength 630 to 700 nm)(171–173). Tumour cells of epithelial or mesenchymal origin preferentially uptake exogenous 5-ALA and convert it to the fluorescent PpIX. This can be detected with intraoperative fluorescent imaging devices and creates a marked signal to noise gradient in malignant and normal tissue.

Multiple studies have shown 5-ALA to be beneficial in the resection of primary and recurrent high-grade glioma brain tumours. The positive predictive value of intra-operative 5-ALA guided fluorescence in pathological areas of known recurrent glioma is reported at over 97% and for fluorescence in non-pathological areas up to 80%. The Food and Drug Administration (FDA)

in the USA approved 5-ALA for the intraoperative mapping of high grade gliomas in 2017(174,175). However, the GLiStEN trial failed to show similar results in colon cancer. Participants suffered photosensitive skin rashes post-operatively and the high false negative rate led to early termination of the trial(176).

Peptide Targeted Intra-Operative Fluorescent Imaging

Previous studies of fluorescent guided cancer surgery, such as GLiStEN and those using ICG, have all used untargeted fluorophores for intraoperative imaging. Advances in molecular chemistry have introduced the possibility to conjugate a fluorescent tag to a cancer specific targeted molecule. An interesting example of this evolving technology was published by *Hoogstins et al* in 2016(177). They explored a compound called OTL38, a folate receptor alpha (FRa) ligand coupled to a NIR fluorescent dye (excitation at 776 nm, emission at 796 nm), in a small randomised controlled trial of 12 patients undergoing open cytoreductive surgery in ovarian cancer. The administration of OTL38 increased the yield of true positive metastatic lesions by 29%; 18 of the 62 lesions were invisible in white light assessment. This exploratory work demonstrates the value of these new fluorescent agents and the potential for individualised fluorescent-guided abdominal cancer resection surgery.

Hepatocyte Growth Factor and c-Met

Hepatocyte Growth Factor (HGF)

The remarkable properties of the liver to regenerate after injury, and its ability to facilitate live-donor transplantation, has been of great interest for decades, but the exact mechanism remained elusive until relatively recently. *Nakamara et al* extracted a powerful hepatrophic stimulator of rat liver regeneration from platelets in the 1980s and termed it Hepatocyte Growth Factor (HGF)(178,179). Soon after, HGF was purified from the serum of patients with fulminant liver failure(180) and those who had undergone partial hepatectomy(181,182)**.** It was quickly

established that HGF was indistinguishable to *"Scatter Factor"* (SF); a potent stimulator of epithelial cell motility extracted from normal human embryo fibroblasts described by *Stoker et al. In vitro* studies showed SF to be a potent driver of immature epithelial cell motility and conversion to a more motile phenotype in the absence of a chemotactic agent(183–185). *Weidner et al* quickly discredited *Stoker et al's* observation of *"no scatter factor is released from cancer cell lines…nor are such lines responsive to the factor*"(186). They showed SF to be a significant stimulator of tumour cell line invasiveness and therefore metastasis. The HGF/SF protein increased cell motility and could scatter a sheet of continuous cells, hence the name Scatter Factor. It was quickly established that HGF/SF played an important role in a diverse range of cell-to-cell interactions(183,184,187).

HGF is the only known endogenous ligand of the c-Met transmembrane receptor. HGF is secreted as an inactive polypeptide and cleaved to its active form by serum protein kinases. The gene for human HGF is encoded by chromosome 7q21. Active HGF is a large heterodimer molecule consisting of a 69kDa alpha-subunit bound to a 34kDa beta-subunit(188). The free amine group *N* terminus of the alpha subunit contains the c-Met binding domain and the beta subunit directly actives the c-Met protein with associated downstream tyrosine kinase activation cascade(189). The HGF protein is produced by cells of mesenchymal origin and acts in a paracrine fashion. HGF was the first distinct member of the plasminogen-related growth factor family to be identified(190). Although its domain structure and mechanism of activation resemble those of the blood protease plasminogen, it lacks protease activity(191).

c-Met

The cellular mesenchymal-epithelial transition (c-Met) receptor is the only known target for the endogenous HGF ligand. In 1984, *Cooper et al* discovered the epithelial cell line transforming properties of carcinogen treated human osteosarcoma cells and mapped the Met proto-oncogene locus, but were unable to establish it's activating protein(192). It was the work of

Bottaro et al that linked HGF to the c-Met receptor in 1991(193). Encoded by the 21 exon MET gene on chromosome 7q21 -31, the c-Met receptor consists of a 50kD extracellular alpha unit with three functional domains linked to a large 145kD beta unit with both extracellular, transmembrane and intracellular domains with tyrosine kinase phosphorylation activity via a disulphide bridge(193–195). HGF has a high affinity for the c-Met receptor, but only binding of the β unit of the HGF ligand can activate cellular pathways. Dimerisation of the c-Met receptor leads to autophosphorylation of the tyrosine residues Tyr1349 and Try1356(191,194). The conformational change at the multi-function docking site leads to recruitment of several adapter and intermediate molecules. Activation of Gab1 and Grb2 via tyrosine phosphorylation is crucial to downstream kinetic pathway activation and recruitment including phosphoinositide 3-kinases *PI3K*, rat sarcoma (*Ras*), and extracellular signal regulated kinas (ERK) activation, promoting the mitogenic and morphogenic properties of c-Met-HGF complex coupling(191).

A wealth of evidence has developed around the multitude of biological applications of the HGF/c-Met pathway in recent years. HGF is vital to embryogenesis and for cell development and migration in adult life. HGF is a potent mitogen and morphogen. The importance of functioning HGF and receptor c-Met in organogenesis has been demonstrated mainly by knock-out studies. In embryogenesis, complete knock-out is always fatal. Homozygous HGF null mutated mice embryos show severely restricted hepatic development, in part because the anti-apoptotic function of HGF/c-Met is lost[195]. There is also poor trophoblast migration into the placenta and vascularisation. The migration stimulating properties are also vital for limb bud and central nervous system development. The homozygous state of HGF/c-Met mutation is always incompatible with life(196,197).

HGF/c-Met function is not just a regulator of organogenesis, with HGF/c-met pathways being vital for adult tissue regeneration and proliferation. Acquired c-Met/HGF dysfunction impairs epithelialisation and therefore wound healing and allows sustained, unregulated proliferation of cells to occur. The overexpression and/or upregulation of the c-met receptor protein has been demonstrated in the stroma of several malignancies. The complex tumour and metastatic

microenvironment is composed of multiple cellular and acellular components. The abundant Cancer Associated Fibroblasts (CAFs) in the tumour microenvironment, secretes several soluble factors and activates the HGF/c-Met pathway through the direct release of HGF or by the indirect stimulation of resident cancer cells to secrete HGF via the release of intermediately pro-inflammatory cytokines and interleukins, such as IL-6, prostaglandins or Platelet Derived Growth Factor (PDGF-β). This upregulation promotes infiltration of immune cells and *de novo* angiogenesis(198,199). There is both autocrine and paracrine activation of the pathway. Dysregulation of the c-met pathway is seen as a crucial step in angiogenesis and proliferation in colorectal and other cancers(182,188,200,201). In addition, tumour hypoxia induces increased c-Met RNA transcription and overexpression of c-Met protein. This adaptive response gives malignant cells a survival benefit in the hypoxic tumour microenvironment. It may also produce resistance to anti-cancer therapies, especially those that rely on the generation of reactive oxygen species for their therapeutic effect(202).

c-Met in Colorectal Cancer

Expression of the c-Met receptor by colorectal cancer is known to correlate with adverse tumour characteristics and invasiveness(203–205). Levels of c-Met protein, c-Met rRNA, and its ligand HGF are often elevated in metastatic colorectal cancer(205) Experimental suppression of c-Met transcription attenuates the migratory and invasive properties of parent and invasive CRC cell lines in culture(206). Meta-analysis by *Liu et al* confirmed that high c-Met expression in colorectal tumours was linked to worse overall survival (HR 1.41 [95% CI 1.08-1.74])(207). *Takeuchi et al,* found that the level of c-Met expressed in CRC specimens directly correlated with tumour T stage *(p =0.0005)* and lymph node status *(p=0.06)*(208), whilst *Zeng et al* was able to correlate c-Met expression with vascular invasion status *(p =0.04)*(204).

Mutations of the c-Met protein do not act in insolation; they interact with other well-described steps in the adenoma-adenocarcinoma mutation pathogenic sequence(209) and alter the tumour microenvironment. Mutated *p53* is observed in a significant proportion of colorectal cancers. Normal function of this gene and its protein is vital for tumour suppression; *p53* regulates DNA repair, cell cycle arrest and apoptosis. Genomic instability in the *p53* gene leads to unregulated cellular proliferation and uninhibited maturation of abnormal cells(210,211).

The tumorigenic effects of c-Met are amplified in the presence of inactivated *p53* tumour suppressor function. *Muller et al* have demonstrated increased intracellular phosphorylation of c-Met and increased sensitivity to HGF stimulation in the presence of *p53* mutation(212). Increased downstream signaling leads to enhanced cell migration and invasiveness. This research confirms that c-Met activation in CRC can act in an autocrine manner and in synergic amplification with other known tumorigenic pathways(210). c-Met amplification drives tumour development and resistance to biologic therapies via crosstalk with other tyrosine kinase pathways. C-Met amplification confers resistance to Epidermal Growth Factor Receptor (EGFR) agents in metastatic CRC and reduced disease-free survival(213,214).

The evolving knowledge of c-Met and its role in neoplastic growth and metastases makes it an exciting diagnostic and therapeutic target in gastrointestinal cancer, including colorectal cancer. The small molecule monoclonal antibody to HGF, Rilotumumab, has been explored in early phase clinical trials*. Iveson et al* assessed Rilotumumab in unresectable gastric and oesophageal junction cancer (Clinical Trials Number NCT00719550). The early phase IIa study of Rilotumumab with conventional chemotherapy marginally increased the progression free survival interval with an acceptable adverse event profile compared to the placebo arm(215). However, the follow-up phase III ROLIMET-1 trial in the same patient population screened for c-Met tumour status (Clinical Trial Number NCT01697072) was halted early. Mortality was significantly higher in the treatment arm and futility criteria were met at early review. Rolitumumab was considered *“of no benefit to patients with gastro-eosophageal*

cancer". The study found median overall survival was shorter in the Rilotumumab group than the placebo group (8·8 months vs 10·7 months; HR 1·34 [95% CI 1·10–1·63]). Time to disease progression was shorter and the objective response rate to therapy was also lower in the treatment arm(216).

A possible alternative approach to therapeutic c-Met targeting has been trialed in advanced metastatic colorectal cancer. The human immunoglobulin G2 antibody called Samsung Advance Institute of Technology-301 *(SAIT301)* binds and inhibits c-Met transmembrane protein function. In their small unblinded dose escalation trial, *Lee et al* were able to induce partial response or maintain stable disease in patients with metastatic colorectal cancer, for whom all conventional treatment had failed(217). Further research is needed.

EMI-137

EMI-137, developed by GE Healthcare Technologies Ltd and Edinburgh Molecular Imaging (EM Imaging) Ltd, has been shown to be safe and effective in human and animal studies(218,219). The molecular formula of EMI-137 is C156H213N34O52S8 *(Figure 7).* It is supplied as a blue powder, has a molecular weight of 3653.2u (unified atomic mass units), is high soluble in water with a pH between 4 and 7. EMI-137 consists of a fluorescent cyanine dye coupled to a propriety 26 L-amino acid cyclic peptide targeted to the c-Met receptor. When reconstituted with water, EMI-137 possesses photo-stability in white light, with peak florescence at excitation wavelength 653nm and emission at 675nm. EMI-137 is highly selective and has a high affinity for the extra-cellular domain of the human c-Met receptor owing to its low nanomolar dissociation constant (~2 nM). It binds completely without activation to the c-Met receptor complex. It is renally excreted and shows low affinity for human plasma proteins(218,220,221).

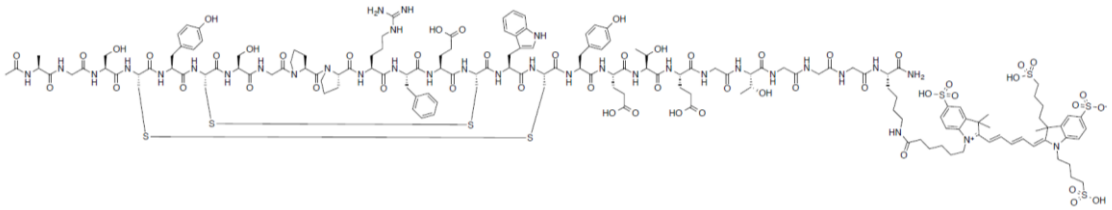

Figure 7: Structural formula of EMI-137 salt free. Adapted from Edinburgh Molecular Imaging Ltd. (2017)(220)

EMI-137 as an Optical Imaging Agent

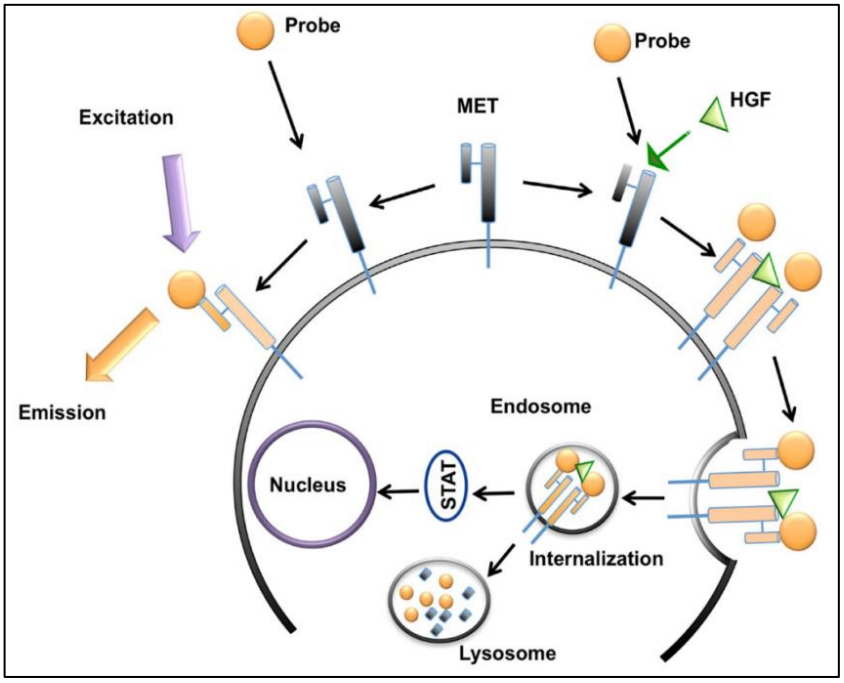

Figure 8: Schematic representation of EMI-137 targeting the c-Met receptor. Adapted from Esfahani et al (2016)(221)

The optical imaging agent binds to the extracellular domain of the c-Met receptor without activation leading to detectable membrane fluorescence. EMI-137 is internalised when it binds to the receptor in the presence of HGF yielding detectable cytoplasmic and membranous fluorescence.

To date, c-Met targeting has failed to demonstrate clear beneficial therapeutic anti-cancer properties in small early phase clinical trials. However, c-Met targeting with an inert fluorescent

probe could be a potential novel solution to the difficulties of intra-operative visualisation of colon cancers and lymph nodes metastases.

Burggraaf et al have demonstrated the safety and efficacy of EMI-137 for the visualisation of colonic polyps at colonoscopy. Their single centre study from Leiden, Netherlands, used healthy volunteers and patients deemed at high risk of colorectal cancer to establish the optimal dose and timing of administration in an early phase clinical trial. This was found to be 0.13mg/kg of EMI-137 given intravenously 3 hours prior to colonoscopy. Higher doses (0.18mg/kg), although safe, created excessive background (noise) fluorescence and reduced fluorescent visualisation of the target tissue. Importantly, no serious adverse reactions related to the administration of EMI-137 were reported(218).

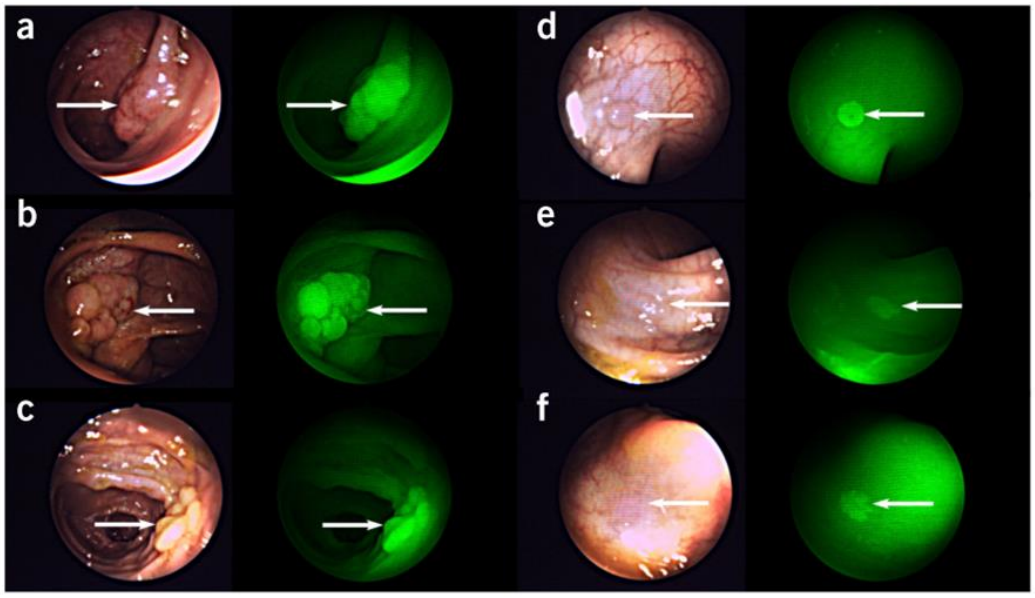

Figure 9: a-c colonic lesions easily visible in white light (left) and showing enhanced fluorescence with EMI-137 (right); e-f colonic lesions difficult to detect with white light (left) but easily visible with EMI-137 during fluorescent colonoscopy. Adapted from Burggraaf et al (2015)(218)*.*

Administration of EMI-137 to 15 patients at high risk of colonic neoplasms led to the visualisation of an additional 22 polyps, of which 17 colonic polyps were only visible with fluorescent light as compared to white light colonoscopy. These were mostly non-polypoidal

and small lesions. Histopathological examination of the resected polyps showed a clear relationship between the degree of fluorescence and the histological dysplasia grade of the polyp. This was mirrored in the immunohistochemical examination of the resected polyps with dysplastic polyps and adenomas showing greater c-Met expression as compared to normal tissue. All the adenomas identified with white light colonoscopy also showed increased fluorescence with EMI-137.

With the problems associated with accurately staging colon cancer and planning the radicality of surgery on an individual patient basis, EMI-137 may offer a novel solution. The potential to apply a safe and targeted imaging agent to intraoperatively map the tumour and any metastatic lymph nodes could aid the decision-making process and allow surgery to be tailored to the individual characteristics of the tumour and the patient.

2 CHAPTER TWO

CLINICAL FEASIBILITY STUDY OF NEAR INFRARED FLUORESCENCE CHOLANGIOGRAPHY IN LAPAROSCOPIC CHOLECYSTECTOMY SURGERY

Name: Gemma Armstrong
Student No: 201073014

2.1 AIMS AND OBJECTIVES

Trial Overview

The need for a dynamic, safe, and cost-effective method of intraoperatively assessing biliary anatomy during laparoscopic cholecystectomy has been a priority for surgeons for some time. The persistently stubborn rate of bile duct injury, even in experienced hands and long after the "*learning curve"* in laparoscopic surgery has plateaued, combined with the catastrophic physical, psychological and fiscal consequences make any method to improve extrahepatic ductal identification and reduced the bile duct injury rate of high clinical importance. The stability and favourable safety profile of ICG, and the increasing number of high quality and relatively inexpensive NIR laparoscopic systems, makes this an exciting and highly applicable technology. Small international studies have explored applications of ICG in laparoscopic and robotic-assisted cholecystectomy, but there have not been any published randomised controlled trials and there is no consensus on dose, timing interval or study end points.

Aims

I aimed to explore and investigate the potential applications of NIR-FC with ICG within a tertiary referral NHS hepatobiliary surgery unit. My aims included:

i) To appraise the safety and efficacy of NIR-FC with ICG as an intraoperative imaging modality in laparoscopic cholecystectomy surgery with a phase IIa clinical trial.

ii) To explore the applications and limitations of ICG aided NIR-FC during laparoscopic cholecystectomy surgery performed by skilled consultant Hepatic and Pancreatico-Biliary surgeons highly competent in the management of complex hepatobiliary disease.

iii) To explore participant and operative factors that adversely affected extra-hepatic biliary structure identification with NIR-FC.

iv) To explore and evaluate ICG dosing regimens, in particular to explore delayed dosing intervals and the possible benefit of ICG accumulation in bile and increased fluorescent biliary structure visualisation.

v) To investigate surgical team satisfaction with the technology and explore likely enthusiasm for adoption of NIR-FC.

2.2 MATERIALS AND METHODS

The trial endpoints as defined in the study protocol:

Primary Endpoints:

1. Successful identification of biliary structures; Cystic Duct (CD), Common Bile Duct (CBD) Common Hepatic Duct (CHD) Left Hepatic Duct (LHD), Right Hepatic Duct (RHD) and Cystic Artery (CA).
2. Dose optimisation of ICG in laparoscopic cholecystectomy. Investigation of the optimal dose and timing of ICG for visualisation of biliary anatomy using NIR-FC.

Secondary Endpoints:

1. Rates of bile duct injury
2. Rates of vascular injury
3. Rate of intraoperative conversion to open cholecystectomy procedure
4. Length of procedure
5. Operating surgeon satisfaction with technique

2.2.1 Trial Design

This trial was designed as a single-centre, prospective, non-randomised, open label, early phase cohort study. The trial explored the feasibility and effectiveness of fluorescence guided bile duct mapping during laparoscopic cholecystectomy surgery at St James' University Hospital, Leeds, between 22nd July 2016 and 27th November 2018. Allocation to dose sub-groups was systematic and dependent on recruitment to trial date. Progression between dosing interval phases was sequential and was dictated by the outcome of regular interim review of trial progress and data. The overall trial schema is outlined in *Figure 10*.

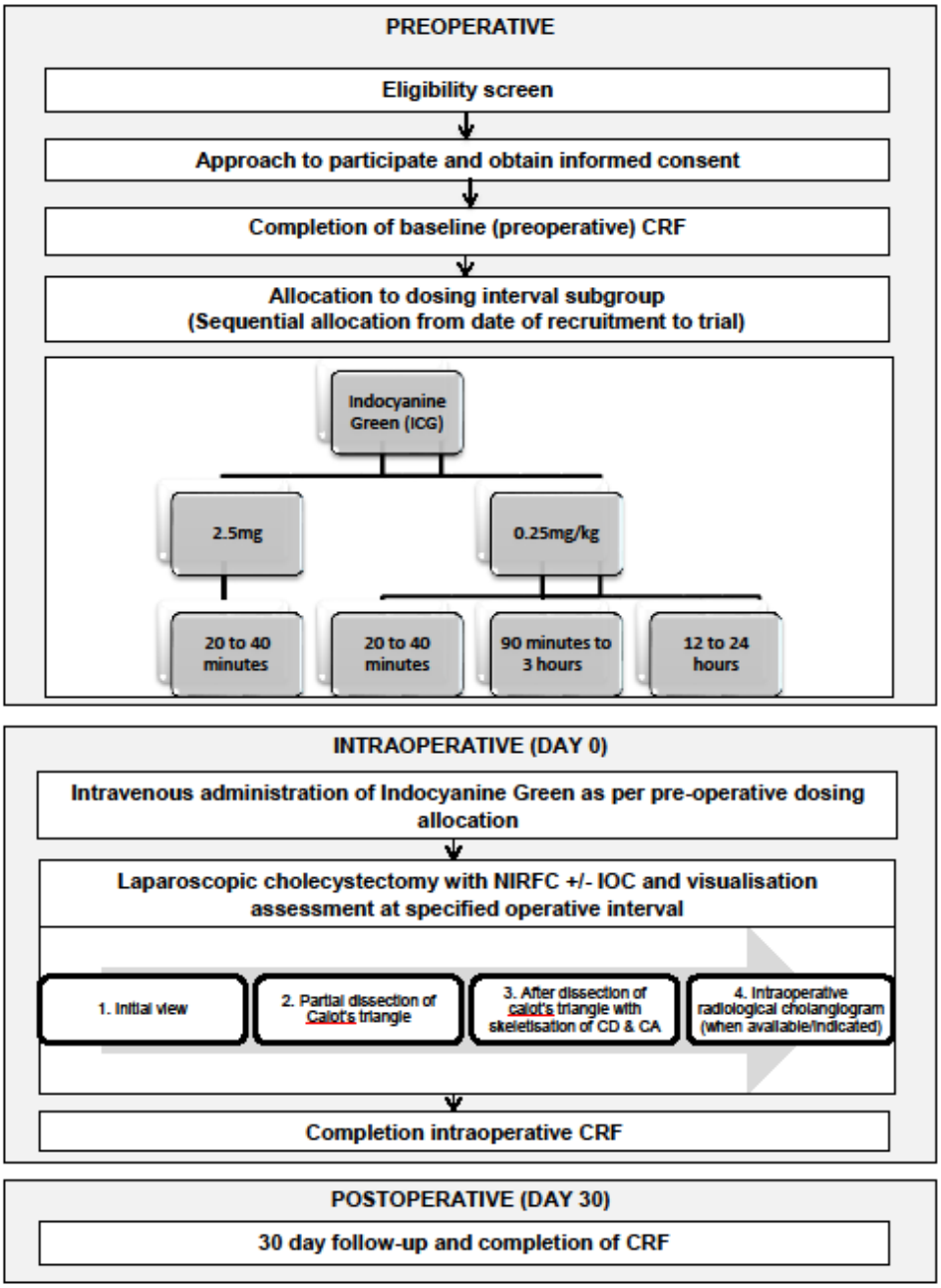

Figure 10: Clinical feasibility study of Near Infrared Fluorescence Cholangiography in Laparoscopic Cholecystectomy trial schema.

Regulatory Approval

Ethical approval for the trial was granted by the North East - Newcastle & North Tyneside 2 Research Ethics Committee on 8th June 2015 (Ref: 15/NE/0131) - approval letter in *Appendix.* Local approval from Leeds Teaching Hospitals NHS Trust (LTHT) was obtained prior to commencing recruitment and participant data collection. The trial was conducted in accordance with all quality assurance and ethical best practice guidelines and there were robust systems in place for reporting of any protocol breaches or adverse events to the trial sponsor, the University of Leeds, and the regulatory authorities as appropriate. LTHT Surgical Clinical Trials Unit (CTU) supported the trial and were actively involved in participant screening, recruitment, and data collection for the duration of the trial. The use of Indocyanine Green as the fluorophore was considered a non-CTIMP (Clinical Trial Investigational Medical Product) clinical trial by the regulatory authorities and therefore Medicines and Healthcare products Regulatory Agency (MHRA) approval was not required.

Substantial Amendments

A substantial amendment to the protocol was approved by the REC on 8th February 2017. The amendment extended the dosing interval for the participant subgroups and allowed a cohort of patients to receive 0.25mg/kg of ICG the day before their surgical procedure. Defining the optimum dosing interval as a trial endpoint definition was also added for clarity.

Training

The operating surgeons, Research Fellow (GRA), and key members of the theatre clinical team received thorough training from an Elemental Healthcare™ representative on behalf of Stryker/Novadaq® Ltd. on how to use the Novadaq PinPoint® Endoscopic Fluorescence Imaging System (Stryker/Novadaq Endoscopy HQ, San Jose, CA, USA) prior to recruitment

of the first patient. An equipment manual was always available, and the local company representative could be contacted during office hours for technical advice. To assist with training, and to familiarise the trial team and theatre staff with the equipment, a training case was performed once regulatory authority approval was in place and prior to commencement of the trial. The participant was screened for eligibility as per trial design and full informed consent was obtained using the approved trial documents.

With the Elemental Healthcare™ representative present in theatre, a laparoscopic cholecystectomy procedure was performed with the PinPoint® Endoscopic Fluorescence Imaging System. This was beneficial to all members of staff and aimed to curtail any early "learning curve" experienced with new technology. During this training procedure, the Case Reporting Forms (CRF) were appraised and their suitability for data collection confirmed.

Study Population

Male and female patients over the age of 18 years with a diagnosis of biliary pathology (including but not limited to, cholelithiasis, cholecystitis, gallstone pancreatitis, biliary dyskinesia or gallbladder polyps) awaiting laparoscopic cholecystectomy at LTHT under the care of one of the five participating consultant HPB surgeons were eligible to participate. The participating consultant surgeons were Mr. A.M Smith, Mr. G Toogood, Mr. C Macutkiewicz, Mr. R.A Adair, and Mr. A Al-Douri.

Eligibility

The eligibility criteria for the trial are defined in *Table 2*.

Inclusion criteria	Exclusion criteria
• Able to give informed consent and be willing to follow trial protocol • Aged over 18 • Fit for laparoscopic surgery • American Society of Anaesthesiologists (ASA) classification ≤ 3 • Normal renal function on most recent blood tests (to be within 30 days prior to surgery). For the purposes of the trial normal renal function can be defined as GFR ≥ 40 mls/min/1.73m^2 or Creatinine within 10% of upper value for normal institutional limits. • Patients with symptomatic biliary disease (chronic cholecystitis, cholelithiasis, biliary dyskinesia, acute cholecystitis, gallstone pancreatitis and cholangitis) eligible for laparoscopic cholecystectomy	• History of hypersensitivity reactions or known allergy to ICG, iodine or iodine dyes • Pregnant (positive pregnancy test) or breast-feeding ICG has unknown teratogenic and abortifacient effects. • In women of childbearing potential (defined as any female who has experienced menarche and who is not postmenopausal or permanently sterilised (e.g. tubal occlusion, hysterectomy, bilateral salpingectomy). A pregnancy test will be performed and evidence of a negative result will be required prior to entry into the study. • Patients with hyperthyroidism, patients with autonomic thyroid adenomas • Poorly controlled or serious medical or psychiatric illness that, in the Investigator's opinion, is likely to interfere with participation and/or compliance in this clinical trial. • Patients taking cyclopropane, probenecid, or rifamycin, which can increase the absorption of ICG

Table 2: Eligibility criteria for Clinical Feasibility study of Near Infrared Fluorescence Cholangiography in Laparoscopic Cholecystectomy trial.

Screening and Recruitment

Potential participants were identified thorough the LTHT inpatient registry, the LTHT theatre booking platform, or during outpatient clinic appointments. All participant eligibility screening and recruitment was performed by the clinical research fellow (GRA), the participating consultant surgeons, or by medically trained members of LTHT Surgical Clinical Trials Unit (CTU).

Screened participants deemed to meet all the eligibility criteria were approached to participate either in face-to-face interactions or over the telephone. All participants were provided with written information in the form of a Participant Information Sheet (PIS) and given verbal information about the trial at least 24 hours prior to involvement. All potential participants were given the opportunity to ask questions and provided with the name and contact details of a delegated member of the research team if they wished to discuss their involvement further at a later date. All members of the research team were experienced in gaining consent for a clinical trial and had valid GCP training. It was stressed to all potential participants that their involvement was voluntary, they could withdraw at any time, and refusal to participate would not adversely affect the care they received in any way. No incentives were offered to participate.

Patients wishing to participate were asked to sign a trial specific patient consent form prior to receiving ICG and undergoing NIR-FC guided LC surgery. Their usual General Practitioner (GP) was also informed of their trial involvement. Patients were assigned a unique trial participant number and baseline preoperative demographics were collected including age, gender, Body Mass Index (BMI), pre-operative blood test results, imaging results, co-morbidities and previous surgical history via a paper preoperative Case Report Form (CRF).

2.2.2 Trial Intervention

Indocyanine Green

The ICG was supplied by the LTHT clinical trials pharmacy department. The ICG (Verdye®, Diagnostic Green GmbH, Aschheim-Dornach, Germany) was supplied as a green dry powder 25mg/5ml preparation. It was reconstituted with 5mL of sterile water immediately prior to intravenous administration as per manufacturer's instructions. All dose calculations, preparation, and administration of the ICG, and prescribing of the trial agent were the responsibility of the clinical research fellow. To adhere to safe prescribing and drug administration best practices, the prepared drug and dose calculations were verified with another clinically trained member of staff prior to administration of the fluorophore. The ICG was administered as single intravenous (I.V) bolus via a peripherally sited cannula device. This was immediately followed by a flush of 10mL of 0.9% saline solution. The sterile water for reconstitution and 0.9% normal saline flush were also supplied to the research team as a standard pharmacy stock supply item by LTHT pharmacy department.

The four possible dosing groups in the trial are listed in the flow chart (*Figure 10)*. Participants received a single intravenous bolus of ICG pre-operatively as per protocol allocation. They were monitored for adverse events and provided with information relating to the possible adverse reactions for which they needed to seek urgent medical attention. The dosing interval allocation was disclosed to all involved parties.

Surgical Procedure

All peri-operative care was as per standard LTHT practice. Participation in the trial did not involve any deviation from routine care or from standard surgical technique. The trial intervention assessed the intraoperative identification of extrahepatic biliary anatomy using NIR-FC at specific points during the cholecystectomy procedure. This was achieved by intravenous administration of ICG and utilisation of a licensed and CE marked NIR

laparoscopic system in place of the standard white light system available within the trust. The Stryker®/Novadaq® PinPoint® Endoscopic Fluorescence Imaging System (Stryker UK Ltd, Newbury, Berkshire, UK) was used to perform all NIR-FC during laparoscopic cholecystectomy.

Laparoscopic cholecystectomy was performed as per surgeon's preference. Participation in the clinical trial did not require any change to operative plan or technique. The anaesthetised patient was transferred to the operating theatre and all safe surgery precautions, including the World Health Organisation (WHO) surgical safety checklist and confirmation of instrument sterility, were completed. Surgery commenced with introduction of the laparoscopic ports and establishment of a pneumoperitoneum with carbon dioxide insufflation. Then, the gallbladder was located and retracted to gain an initial view. Any adhesions prohibiting visualisation were divided. Surgery was always initiated in white light (WL) mode. Once the initial view was obtained, the Novadaq® PinPoint® Endoscopic Fluorescence Imaging System was switched to fluorescent light (FL) mode to assess the extrahepatic biliary anatomy with NIR-FC.

The assessment could be performed in any of the fluorescent modes available on the NIR laparoscopic system. The assessment was the subjective opinion of the most senior operating surgeon in theatre. The assessment was recorded using a semi-quantifiably scale. The assessment was made relative to background liver fluorescence. The overall assessment was a culmination of either a single mode or a combination of modes that together provided the greatest overall diagnostic yield of extrahepatic biliary structures in the opinion of the operating surgeon.

The three modes available on the Novadaq® PinPoint® Endoscopic Fluorescence Imaging System were a pure fluorescence black and white mode called "SPY Fluorescence"; a High Definition (HD) colour mode with fluorescent green overlay called "PINPOINT fluorescence"; or the proprietary colour substitution mode referred to as Color Segmented Fluorescence Mode (CSF). CSF mode artificially overlays a colour on to the screen image depending on the amount of fluorescence detected as a form of semi-quantification of fluorescence. Essentially,

this consists of a colour graduated system artificially colourising areas of maximal fluorescence brown to red, moderate fluorescence purple and minimal fluorescence blue. Assessment of visible structures could be made using a single or combination of modes and appraisal of demarcation was made on the best imaging obtained. Assessment of crucial biliary anatomy, the Cystic Duct (CD), Common Hepatic Duct (CHD), Common Bile Duct (CBD), Cystic Artery (CA), Left and Right Hepatic Duct (LHD) and (RHD) was made using a semi quantifiable scale consisting of: easily identifiable; partially identifiable; equivocal; not seen at three specified points. The results were captured on an intraoperative CRF *(appendix – trial documents).* The three points of assessment were:

1) Initial view

After introduction of the laparoscopic ports and establishment of pneumoperitoneum, the liver was retracted, and the gallbladder extended to facilitate a view prior to any dissection or opening the peritoneum.

2) Partial dissection

A second assessment was made after partial dissection in the hepatocystic triangle, after opening of the anterior peritoneum but prior to skeletisation of the CD or CA.

3) Critical View

A third assessment was made after complete dissection in the hepatocystic triangle and after obtaining the critical view of safety. The CD and CA were skeletonised and identified as the only structures entering the gallbladder. This assessment made was prior to division of any presumed ductal structures.

4) On-Table Cholangiography (OTC)

An OTC was performed when clinically indicated and at the surgeon's discretion. The cystic duct was cannulated with a cholangiogram catheter and a bolus of radio-opaque contrast media injected. A portable C-arm was positioned, and fluoroscopy screening

performed to visualise the intra and extrahepatic bile ducts and observe the flow of contrast into the duodenum. The same semi-quantifiable scale was used to record the identifiable biliary structures as in the NIR-FC assessment, excluding the CA which is not visible via OTC assessment. The remainder of the surgical procedure could be performed in either the standard WL, or any of the FL modes available, or a combination of these modes as per surgeon's preference.

Once the first phase of the trial with a standardised dose and dosing regimen was completed and analysed during interim analysis, a dose optimisation amendment was incorporated into the trial design. A further three subgroups were added (*Figure 10*) to explore optimal dose and dosing interval and the efficacy of each regimen in the clinical setting.

Surgeon Satisfaction

The operating surgeon completed a questionnaire at the end of each NIR-FC case. A Likert scale design provided a semi-quantifiable method allowing surgeons to rate their satisfaction with the equipment, the image obtained, and express an opinion on the usefulness of NIR-FC. A free-text box also allowed for further elaboration. Selection of *"strongly agree"* or *"agree"* was considered a positive response.

Follow-up

Patients received standard post-operative care. As is routine practice in uncomplicated cholecystectomy, patients were not recalled for clinic follow-up after discharge from hospital. Subjects received a trial specific follow-up telephone call 30 days after the date of surgery. If a patient was uncontactable via telephone multiple attempts were made for one week after the expected follow-up date. Alternative means to contact the patient were also sought, this

included review of LTHT electronic medical records to exclude readmission to hospital and contacting a participant's GP to seek an alternative telephone number. During the telephone consultation a postoperative CRF was completed. At this point, trial involvement ceased, and no further data was collected.

Secondary Review and Interim Analysis

When 21 participants had been recruited to the trial, with a minimum of four participants per subgroup, an interim analysis with secondary review of the operative videos was conducted. Two consultant hepatobiliary surgeons from LTHT reviewed all the anonymised NIR-FC videos and OTC for each trial participant. They used the same semi-quantifiable scale used intraoperatively to describe the number of extrahepatic biliary structures identified. The surgeons were also encouraged to provide further free text feedback for analysis.

Data Management

All trial data was captured on trial specific Case Report Forms (CRF) and entered into a Microsoft Excel spreadsheet saved on a secure, recoverable Leeds Teaching Hospitals Trust (LTHT) clinical trial network drive. The intraoperative NIR-FC assessment was recorded on to the hard drive of the Pinpoint fluorescent imaging system and transferred to the LTHT network drive for secure storage. The videos were edited and still images were captured by the trial research fellow. Confidentially was maintained throughout and in accordance with the Data Protection Act and the General Data Protection Regulation. The data collected will be stored securely for 15 years after completion of the clinical trial in accordance with LTHT research governance.

Statistical Analysis

Microsoft Excel and GraphPad Prism 7 (GraphPad V7.04 Software, Inc., California, USA) was used for statistical analysis. One-way ANOVA was used to test the statistical significance of the number of structures identifiable at each time point. A paired student t- test was used to compare the average number of structures identified at the third assessment point and the radiological OTC.

Trial Closure

Following interim analysis, a further patient was recruited to the delayed dosing interval group (0.25mg/kg 12 – 24 hours prior to surgery) in November 2018. The operative video was reviewed by two consultant hepatobiliary surgeons with the research fellow in January 2019. All parties agreed the results supported the outcome summary from the interim analysis and further recruitment to the trial would not advance the technique or provide additional useful data. The end of trial was the last visit of the last subject (LVLS) as per protocol. An end of trial notification was submitted to Newcastle & North Tyneside 2 Research Ethics Committee in February 2019 and trial closure proceeded as per protocol and in accordance with local Standard Operating Procedure (SOP. An end of trial report was submitted to the REC within 12 months of trial closure.

2.3 RESULTS

Primary Phase of Trial

Recruitment & Screening

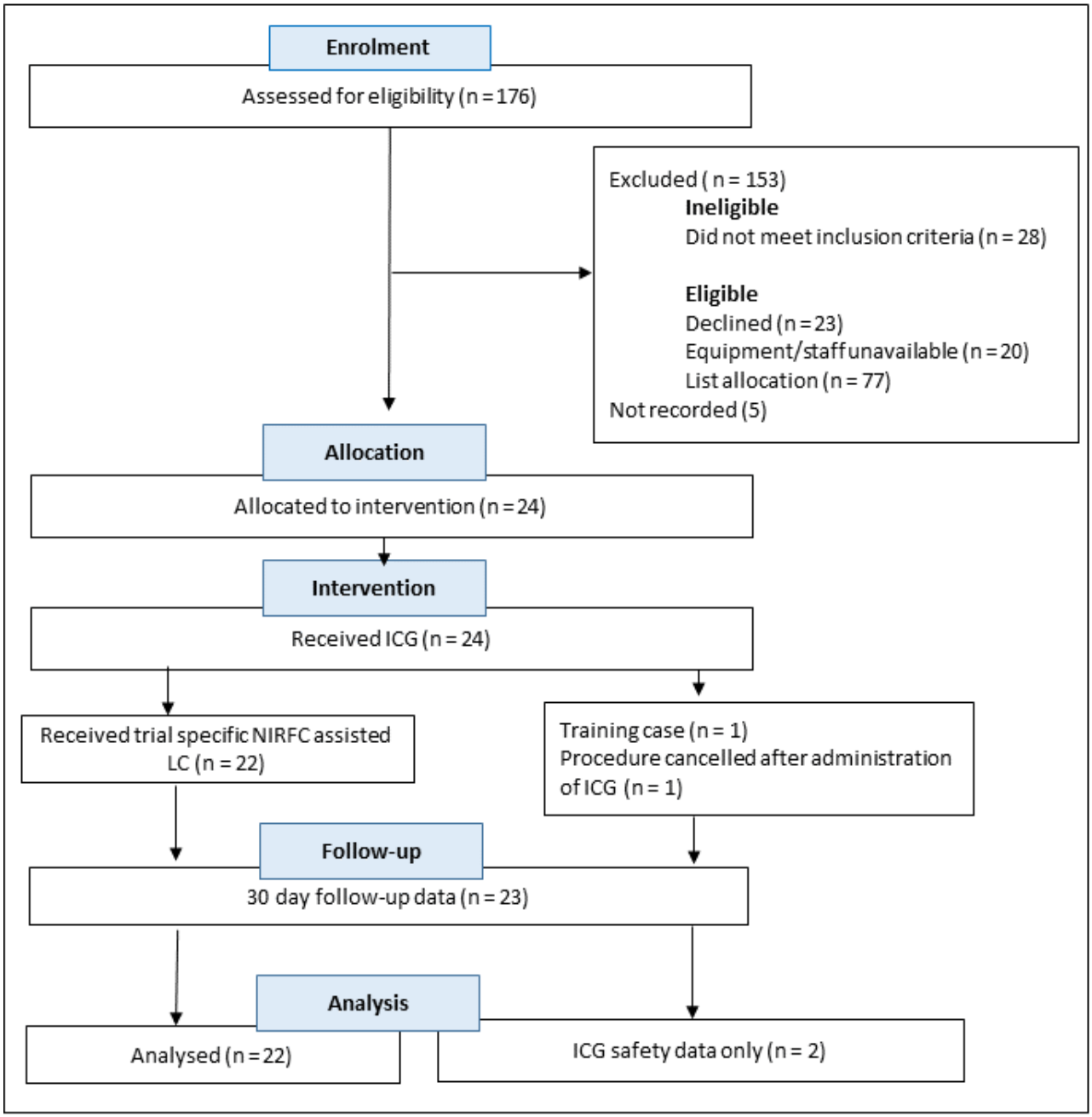

Figure 11: NIR-FC in laparoscopic cholecystectomy trial consort diagram

The first participant enrolled into the trial underwent surgery on 22nd July 2016. A consort diagram of participant recruitment into the first phase of the trial is shown in

Figure 11. Two participants received ICG but did not undergo trial-specific NIR-FC laparoscopic cholecystectomy: one training case was conducted to reduce any learning curve effect at the start of the trial and one participant allocated to the prolonged dosing interval group (administration of ICG ≥12 hours before surgery) received ICG but the procedure was cancelled due to theatre staffing issues on morning of surgery. Both participants received 30-day follow-up as per protocol for purposes of safety reporting and feasibility assessment but were not included in the primary endpoint analysis.

Patient Demographics

A total of twenty-two participants recruited to the trial underwent NIR-FC laparoscopic cholecystectomy as per protocol. The participant demographics are described in *Table 3.*

Dose of ICG	**2.5mg**	**0.25mg/kg**		
Target interval	**20-40min**	**20 - 40min**	**90min – 180min**	**12 – 36 hours**
N = 22	8	4	5	5
Age (years) (±S.D)	44 (±10.2)	53 (±11.2)	57 (±17.6)	48±14)
Gender M: F	0:7	2:2	0:5	1:4
BMI (kg/m^2) (±S.D)	29.1 (±4)	29.7 (±0.5)	27.3 (±3.6)	26.8 (±3.6)
Pre-operative Albumin g/L (±S.D)	36.1 (±5.8)	36.2 (±4.8)	37(±4.8)	40.6 (±3.9)
Indication for surgery				
Biliary colic	3	1	2	2
Gallstone pancreatitis	2	0	2	1
Acute cholecystitis	2	3	1	2
Biliary dyskinesia	1	0	0	0
Acute: Elective Admission	3: 5	1: 3	1: 4	1: 4

Table 3: Summary of NIR-FC feasibility study participant demographics by dosing sub-group

Primary Endpoint Assessment

Individual Participant Results

Demographics	1st assessment	2nd assessment	3rd assessment	OTC
2.5mg 20 to 40 minutes				
Participant 1 50y Female BMI 32.5kg/m^2 DLC gallstone pancreatitis Dose: 2.5mg	No video captured	No video captured	No video captured	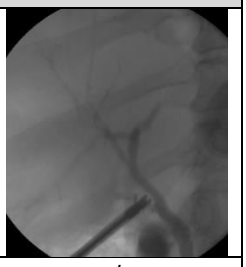
Time Interval	0:35	0:43	0:44	n/a
CD	Easily identifiable	Easily identifiable	Easily identifiable	Easily identifiable
CHD	Easily identifiable	Easily identifiable	Easily identifiable	Easily identifiable
CBD	Partially identifiable	Easily identifiable	Easily identifiable	Easily identifiable
LHD	Partially identifiable	Partially seen	Partially identifiable	Easily identifiable
RHD	Not seen	Not seen	Not seen	Easily identifiable
CA	Not seen	Easily identifiable	Easily identifiable	Easily identifiable
Participant 2 57y Female BMI 22.5 kg/m^2 DLC Gallstone pancreatitis Dose: 2.5mg	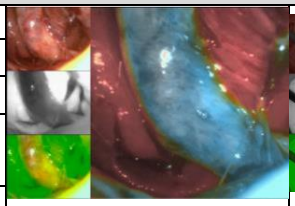	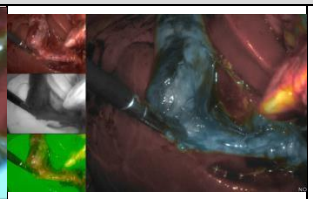	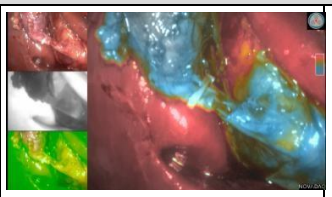	
Time interval	0:27	0:40	0:48	n/a
CD	Not seen	Easily identifiable	Easily identifiable	Easily identifiable
CHD	Easily identifiable	Easily identifiable	Easily identifiable	Easily identifiable
CBD	Easily identifiable	Easily identifiable	Easily identifiable	Easily identifiable
LHD	Easily identifiable	Easily identifiable	Easily identifiable	Easily identifiable
RHD	Easily identifiable	Easily identifiable	Easily identifiable	Easily identifiable
CA	Not seen	Not seen	Easily identifiable	n/a
Participant 3 52y Female BMI 29.4 kg/m^2 Indication biliary colic Dose: 2.5mg	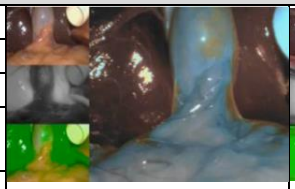	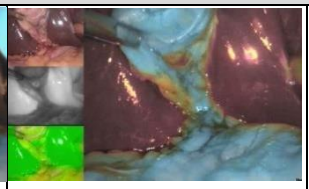	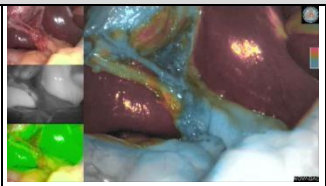	n/a
Time interval	1:05	1:10	1:32	n/a
CD	Not seen	Easily identifiable	Easily identifiable	n/a
CHD	Not seen	Easily identifiable	Easily identifiable	
CBD	Not seen	Partially identifiable	Easily identifiable	
LHD	Easily identifiable	Easily identifiable	Easily identifiable	
RHD	Partially identifiable	Easily identifiable	Easily identifiable	
CA	Not seen	Not seen	Easily identifiable	
Participant 4 50y Female BMI 26.3 kg/m^2				

Indication: Biliary colic 2.5mg	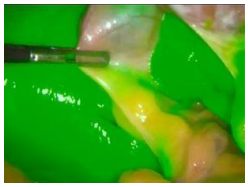		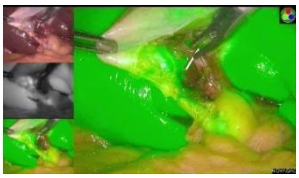	
Time interval	0:34	0:40	0:41	n/a
CD	Easily identifiable	Easily identifiable	Easily identifiable	Easily identifiable
CHD	Easily identifiable	Easily identifiable	Easily identifiable	Easily identifiable
CBD	Easily identifiable	Easily identifiable	Easily identifiable	Easily identifiable
LHD	Not seen	Not seen	Not seen	Easily identifiable
RHD	Not seen	Not seen	Not seen	Easily identifiable
CA	Not seen	Easily identifiable	Easily identifiable	Not seen

Participant 5 36y Female BMI: 36.5 kg/m^2 Indication: acute cholecystitis Dose: 2.5mg	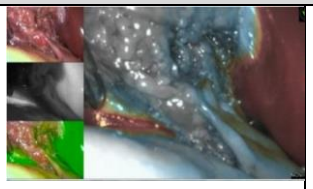	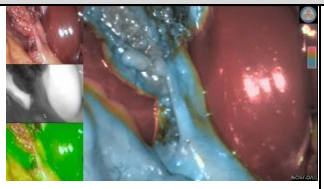	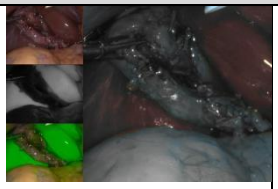	
Time interval	0:52	1:34	1:56	n/a
CD	Not seen	Not seen	Easily identifiable	Easily identifiable
CHD	Partially seen	Partially seen	Equivocal	Easily identifiable
CBD	Partially seen	Easily identifiable	Equivocal	Easily identifiable
LHD	Not seen	Equivocal	Not seen	Easily identifiable
RHA	Not seen	Equivocal	Not seen	Easily identifiable
CA	Not seen	Equivocal	Not seen	n/a
Participant 6 39y Female BMI 29.3 kg/m^2 Indication acute cholecystitis Dose: 2.5mg	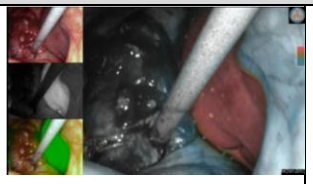	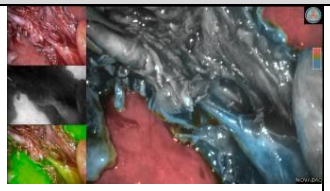	Not performed	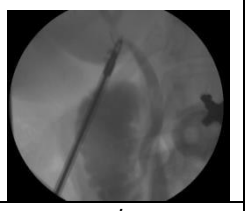
Time Interval	0:40	0:48	Not performed	n/a
CD	Not seen	Not seen	Not performed	Easily identifiable
CHD	Not seen	Not seen	Not performed	Easily identifiable
CBD	Not seen	Not seen	Not performed	Easily identifiable
LHD	Not seen	Not seen	Not performed	Easily identifiable
RHD	Not seen	Not seen	Not performed	Easily identifiable
CA	Not seen	Not seen	Not performed	n/a
Participant 7 46y Female BMI 31.0 kg/m^2 Indication: biliary colic Dose: 2.5mg		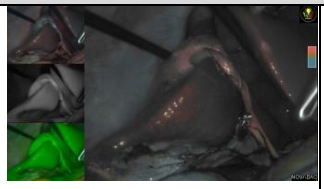	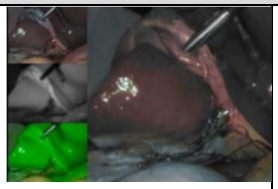	n/a
Time interval	0:33	0:46	0:52	n/a
CD	Easily identifiable	Easily identifiable	Easily identifiable	n/a
CHD	Partially seen	Easily identifiable	Easily identifiable	
CBD	Partially seen	Easily identifiable	Easily identifiable	
LHD	Not seen	Not seen	Not seen	
RHD	Not seen	Partially seen	Partially identifiable	

CA	Not seen	Easily identifiable	Easily identifiable	
Participant 8 23y female BMI 25.7 kg/m^2 Biliary dyskinesia Dose: 2.5mg	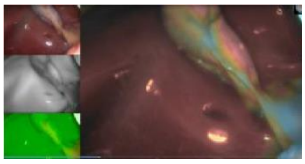	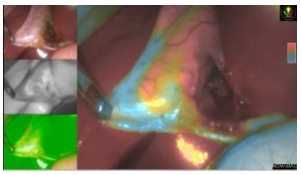	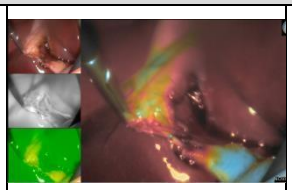	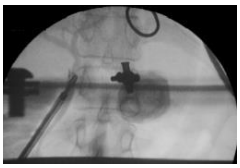
Time interval	0:34	0:40	0:52	
CD	Easily identifiable	Easily identifiable	Easily identifiable	Easily identifiable
CHD	Easily identifiable	Easily identifiable	Not seen	Easily identifiable
CBD	Easily identifiable	Easily identifiable	Easily identifiable	Easily identifiable
LHD	Not seen	Not seen	Not seen	Easily identifiable
RHD	Not seen	Not seen	Not seen	Easily identifiable
CA	Easily identifiable	Easily identifiable	Easily identifiable	n/a

Participant 9 48y Female BMI 33.1 kg/m^2 Biliary colic 18mg	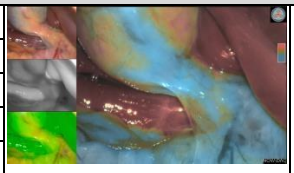	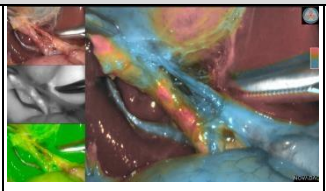	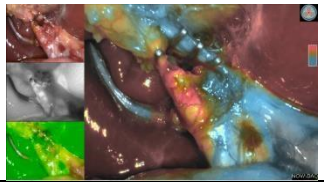	n/a
Time interval	2:32	2:37	2:38	n/a
CD	Easily identifiable	Easily identifiable	Easily identifiable	n/a
CHD	Not seen	Easily identifiable	Easily identifiable	
CBD	Not seen	Easily identifiable	Easily identifiable	
LHD	Not seen	Not seen	Not seen	
RHD	Not seen	Not seen	Not seen	
CA	Not seen	Easily identifiable	Easily identifiable	
Participant 10 60y Female BMI 24.7 kg/m^2 Biliary colic 15mg	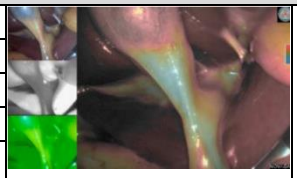	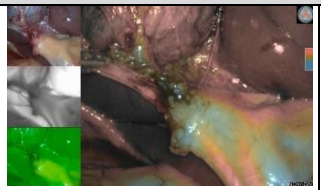	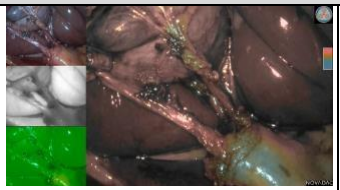	n/a
Time interval	2:28	2:34	2:43	n/a
CD	Easily identifiable	Easily identifiable	Easily identifiable	n/a
CHD	Easily identifiable	Easily identifiable	Easily identifiable	
CBD	Easily identifiable	Easily identifiable	Easily identifiable	
LHD	Easily identifiable	Easily identifiable	Easily identifiable	
RHD	Easily identifiable	Easily identifiable	Easily identifiable	
CA	Not seen	Easily identifiable	Easily identifiable	
Participant 11 79y Female BMI 23.6 kg/m^2 DLC Gallstone pancreatitis 13.75mg	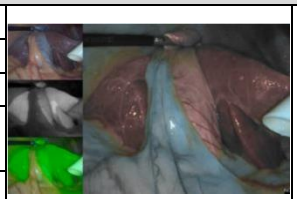		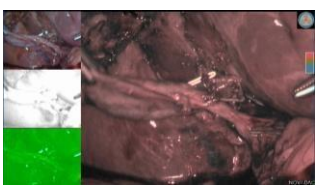	
Time interval	3:11	3:29	3:53	
CD	Not seen	Not seen	Not seen	Easily identifiable
CHD	Easily identifiable	Not seen	Not seen	Easily identifiable

CBD	Equivocal	Not seen	Not seen	Easily identifiable
LHD	Not seen	Not seen	Not seen	Easily identifiable
RHD	Not seen	Not seen	Not seen	Easily identifiable
CA	Not seen	Not seen	Not seen	n/a
Participant 12 28y Female BMI 30.0 kg/m^2 cholecystitis 23.5mg	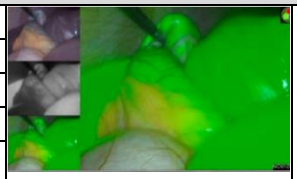	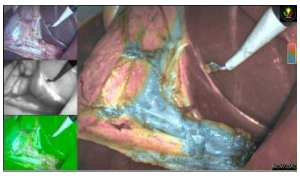	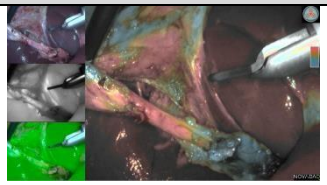	n/a
Time interval	4:07	4:13	4:15	n/a
CD	Not seen	Easily identifiable	Easily identifiable	n/a
CHD	Not seen	Partially seen	Easily identifiable	
CBD	Not seen	Easily identifiable	Easily identifiable	
LHD	Not seen	Easily identifiable	Easily identifiable	
RHD	Not seen	Easily identifiable	Easily identifiable	
CA	Not seen	Easily identifiable	Easily identifiable	

Participant 13 69y Female BMI 25.2 kg/m^2 Gallstone pancreatitis 18mg	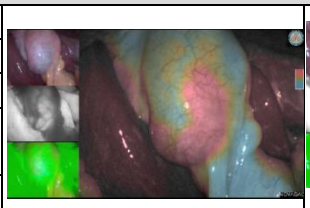	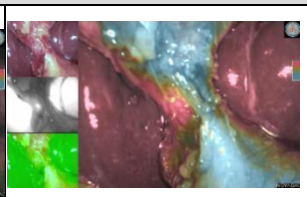	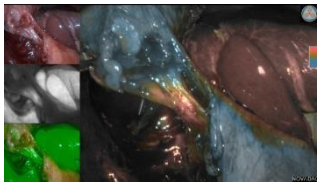	
Time interval	2:47	2:59	3:14	n/a
CD	Not seen	Easily identifiable	Easily identifiable	Easily identifiable
CHD	Not seen	Not seen	Not seen	Easily identifiable
CBD	Not seen	Not seen	Not seen	Easily identifiable
LHD	Not seen	Not seen	Not seen	Easily identifiable
RHD	Not seen	Not seen	Not seen	Easily identifiable
CA	Not seen	Easily identifiable	Easily identifiable	n/a
Participant 14 69y Male BMI 29.3 kg/m^2 DLC for cholecystitis 23.2mg	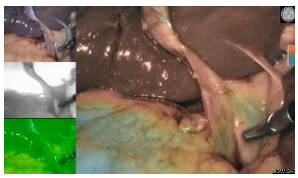	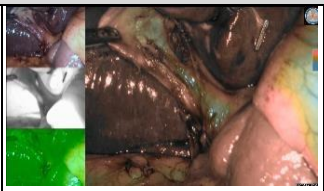	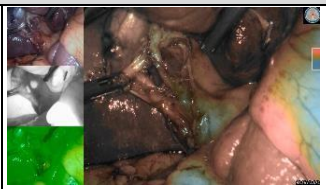	n/a
Time interval	0:33	0:49	0:55	n/a
CD	Partially seen	Easily identifiable	Easily identifiable	n/a
CHD	Not seen	Equivocal	Easily identifiable	
CBD	Equivocal	Easily identifiable	Easily identifiable	
LHD	Not seen	Not seen	Not seen	
RHD	Not seen	Not seen	Not seen	
CA	Not seen	Easily identifiable	Easily identifiable	
Participant 15 57y Female BMI30.4 kg/m^2 Biliary colic				n/a

20.2mg	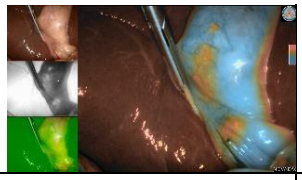	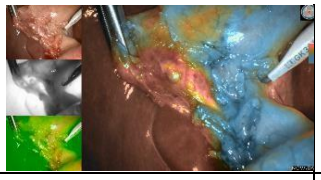	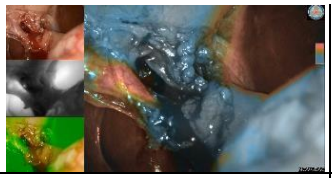	
Time interval	0:29	0:31	0:34	n/a
CD	Not seen	Easily identifiable	Easily identifiable	n/a
CHD	Not seen	Not seen	Not seen	
CBD	Not seen	Not seen	Not seen	
LHD	Not seen	Not seen	Not seen	
RHD	Not seen	Easily identifiable	Easily identifiable	
CA	Not seen	Easily identifiable	Easily identifiable	
Participant 16	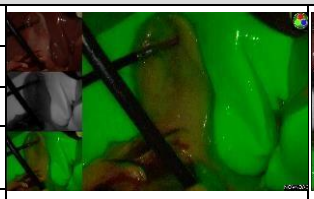	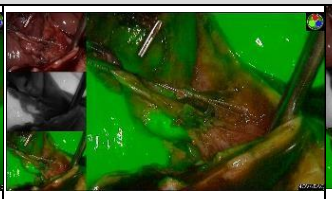		
47y Male				
BMI 30.1 kg/m^2				
Acute cholecystitis				
20.1mg				
Time interval	0:42	0:56	1:03	
CD	Not seen	Not seen	Easily identifiable	Easily identifiable
CHD	Not seen	Not seen	Not seen	Easily identifiable
CBD	Not seen	Not seen	Not seen	Easily identifiable
LHD	Not seen	Not seen	Not seen	Easily identifiable
RHD	Not seen	Not seen	Not seen	Easily identifiable
CA	Not seen	Not seen	Not seen	n/a

Participant 17				n/a
39y Female	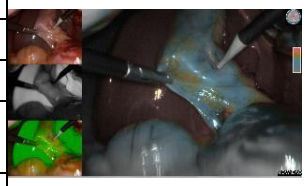		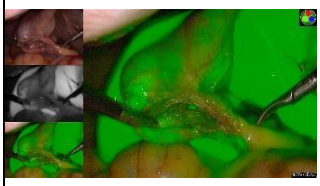	
BMI 29.0 kg/m^2				
Acute cholecystitis				
20.1mg				
Time interval	0:27	0:37	0:41	n/a
CD	Not seen	Equivocal	Partially seen	n/a
CHD	Not seen	Not seen	Not seen	
CBD	Not seen	Not seen	Not seen	
LHD	Not seen	Not seen	Not seen	
RHD	Not seen	Not seen	Not seen	
CA	Partially seen	Partially seen	Easily identifiable	
Participant 18	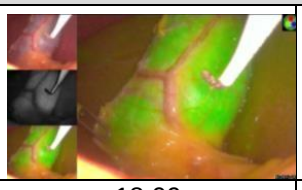	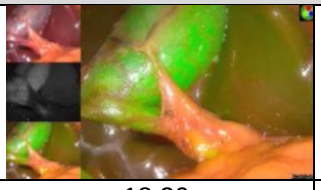	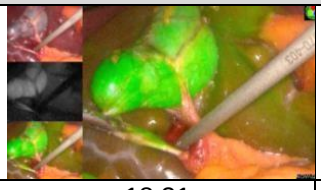	
37y Male				
BMI 30.8 kg/m^2				
Biliary colic				
23.75mg				
Time interval	18:09	18:20	18:31	n/a
CD	Easily identifiable	Easily identifiable	Easily identifiable	

CHD	Easily identifiable	Not seen	Not seen	
CBD	Easily identifiable	Easily identifiable	Partially seen	
LHD	Easily identifiable	Not seen	Not seen	
RHD	Easily identifiable	Not seen	Not seen	
CA	Not seen	Easily identifiable	Easily identifiable	
Participant 19				
67y female	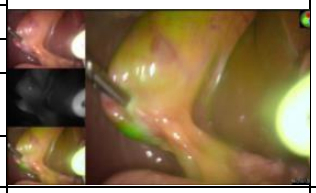	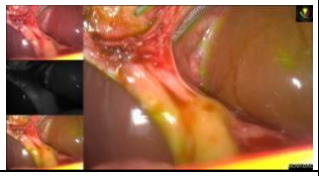		n/a
BMI 22 kg/m^2				
acute cholecystitis				
16.5mg				
Time interval	20:49	21:03	21:14	n/a
CD	Easily identifiable	Easily identifiable	Easily identifiable	
CHD	Equivocal	Partially identifiable	Not seen	
CBD	Easily identifiable	Easily identifiable	Easily identifiable	n/a
LHD	Not seen	Not seen	Not seen	
RHD	Not seen	Not seen	Not seen	
CA	Easily identifiable	Easily identifiable	Not seen	
Participant 20		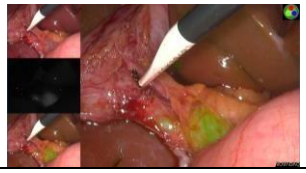	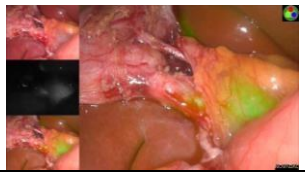	n/a
61y Female				
30.8 kg/m^2				
Biliary colic				
20.0mg				
Time interval	17:00	17:13	17:21	n/a
CD	Easily identifiable	Easily identifiable	Easily identifiable	
CHD	Not seen	Easily identifiable	Easily identifiable	
CBD	Not seen	Easily identifiable	Easily identifiable	n/a
LHD	Not seen	Not seen	Not seen	
RHD	Not seen	Not seen	Not seen	
CA	Not seen	Not seen	Not seen	

Participant 21 29y Female 26.3 kg/m^2 Biliary colic 17.2mg		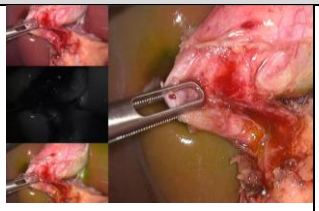		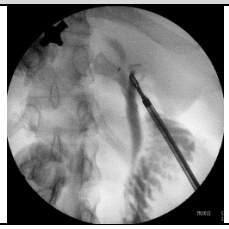
Time interval	22:52	23:06	23:24	**OTC**
CD	Partially identifiable	Not seen	Partially identifiable	Easily identifiable
CHD	equivocal	Not seen	Equivocal	Easily identifiable
CBD	Easily identifiable	Not seen	Easily identifiable	Easily identifiable
LHD	Not seen	Not seen	Not seen	Easily identifiable
RHD	Not seen	Not seen	Not seen	Easily identifiable
CA	Not seen	Not seen	Not seen	n/a
Participant 22 47y Female 24.0 kg/m^2 Gallstone pancreatitis 15.0mg	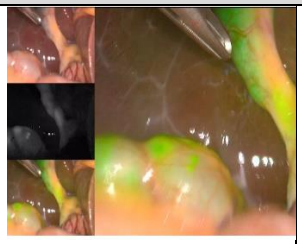	n/a	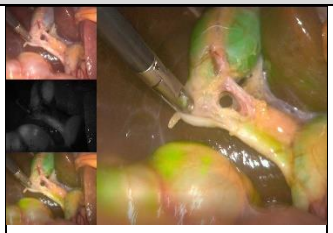	n/a
Time interval	17:47		17:53	**OTC**
CD	Easily identifiable		Easily identifiable	
CHD	Easily identifiable		Easily identifiable	
CBD	Easily identifiable		Easily identifiable	
LHD	Not seen		Not seen	
RHD	Not seen		Not seen	
CA	Not seen		Not seen	

Table 4: NIR-FC clinical trial intraoperative biliary structure results by individual participant. Participant ID, age, indication for surgery, dose of ICG received, time interval from administration to fluorescent assessment and surgeon assessment of extrahepatic biliary structure fluorescent detection shown. Abbreviations: y – years; CD – cystic duct; CHD – common hepatic duct; CBD common bile duct; LHD left hepatic duct; right hepatic duct; CA – cystic artery; n/a - not available; OTC – on table cholangiogram.

ICG Dose	2.5mg	0.25mg/kg		
Target dosing interval	20-40min	20 - 4min	90min – 3 hours	12 – 36 hours
N = 22	8	4	5	5
ICG Dose (mg) (±S.D)	2.5 (±n/a)	21.4 (±1.5)	17.6 (±3.8)	18.5 (±3.5)
Mean Operation length (h:mm) (±S.D)	1:17 (±0:50)	0:59 (±0:27)	1:07 (±0:27)	1:07 (±0:25)
Operative length range (h:mm)	0:38 – 2:49	0:24 – 1:18	0:37 – 1:38	0:35 – 1:44
Interval to 1st assessment achieved (h:mm) (±S.D)	0:40 (±0:12)	0:32 (±0:12)	3:01 (±0:41)	19:19 (±2:11)
Interval to 2nd assessment achieved (h:mm) (±S.D)	0:52 (±19)	0:40 (±19)	3:10 (±53)	19:56 (±2:40)
Interval to 3rd assessment achieved (h:mm) (±S.D)	1:05 (±0:27)	0:47 (±0:14)	3:21 (±0:43)	19:40 (±2:17)

Table 5: Time to assessment by dosing regimen subgroup.

Structure Visualisation

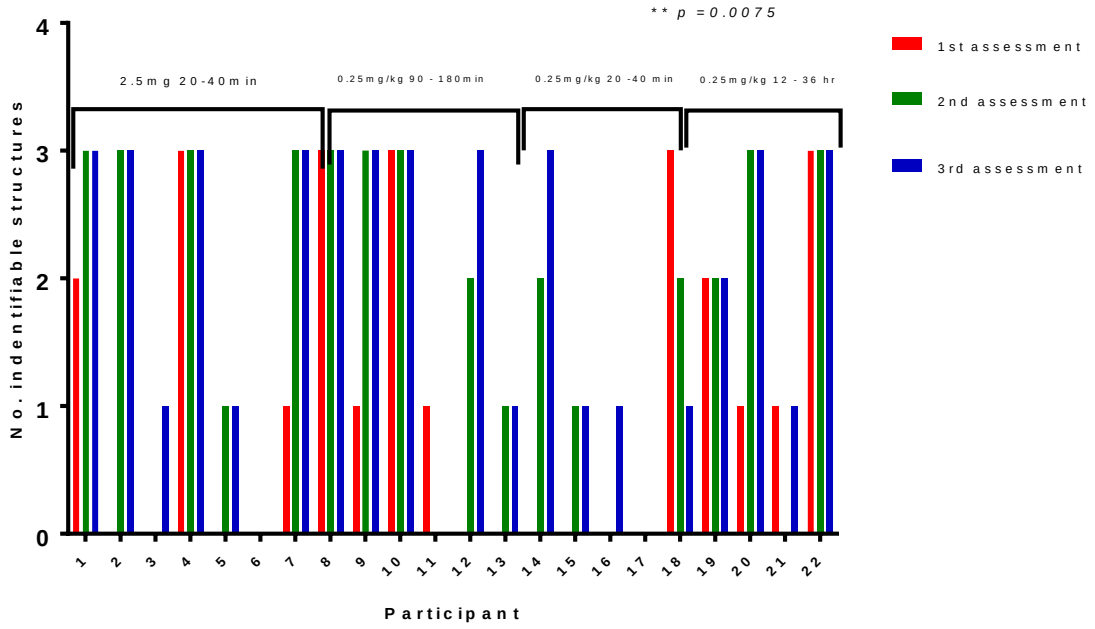

Figure 12: Number of extrahepatic biliary structures (CD, CHD and CBD) graded as clearly identifiable at each assessment point by participant. One-way ANOVA p = 0.007 N = 22

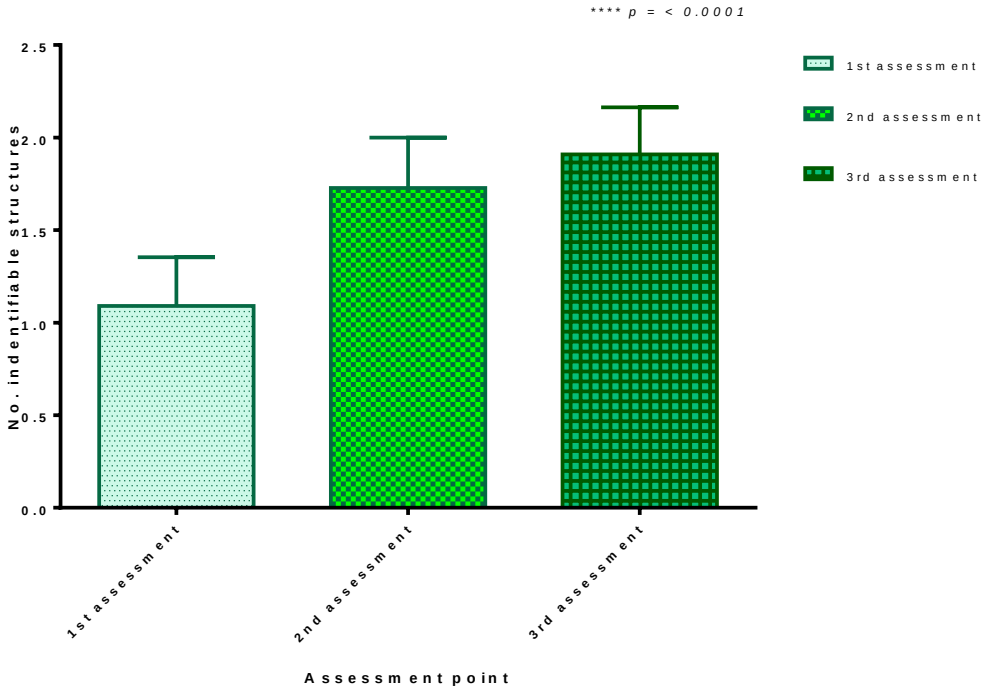

Figure 13: Average number of structures clearly delineated at each assessment point for all dosing intervals combined. Standard error bars shown. One-way ANOVA p = <0.0001 (N = 22)

The number of extrahepatic biliary structures detectable with NIR-FC varied considerably between participants and subgroups. The dosing regimen 2.5mg/kg 20-40 minutes prior to surgery was the least effective (participants 14 to 19 in *Table 4*). The dose of ICG was too high and the interval to allow accumulation in the bile ducts was too short to produce acceptable bile duct mapping. The signal to noise ratio was very low in this subgroup.

In participants who underwent acute index admission laparoscopic cholecystectomy, there was often peri-hilar inflammation and oedema, which might have interfered with the penetrance of NIR-FC and its ability to clearly delineate biliary anatomy - examples shown in *Table 4*, participant ICG010 and ICG012.

On-Table Cholangiogram

Ten participants (48%) required on-table cholangiogram (OTC). All biliary ductal structures were *"clearly identifiable"* with OTC. The addition of OTC identified distal CD stones for one patient, which were not detectable by NIR-FC alone.

Figure 14 compares the number of extrahepatic ductal structures clearly delineated at the third NIHR-FC assessment point to the results of OTC. Paired t-test of mean number of extrahepatic biliary structures clearly identifiable at OTC and the third NIR-FC assessment point found a significant difference of 2.4 structures (95% C.I. -2.37 to - 0.38, $p = 0.01$). OTC was superior to NIR-FC in the ten participants analysed.

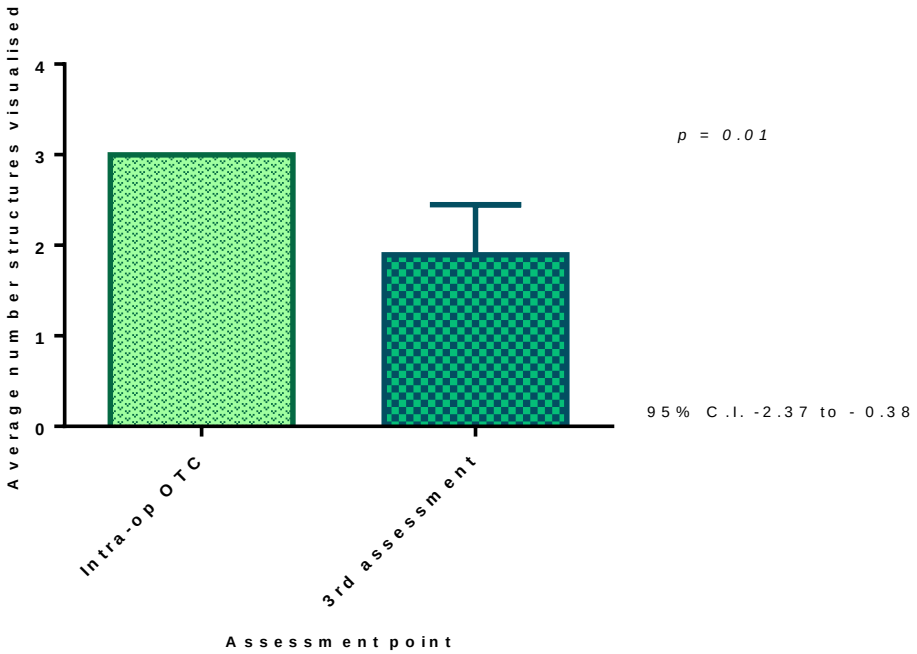

Figure 14: NIR-FC compared to OTC. Number of biliary structures reported as "clearly identifiable" at each assessment point (structures assessed CD, CBD, CHD, LHD and RHD (N = 10).

Factors Adversely Affecting Structure Delineation

Linear regression was performed to ascertain if there was a clear linear relationship between participant factors and fluorescent bile duct mapping. The total numbers of structures identified across the three times points were plotted as a function of participant body mass index (BMI), pre-operative serum CRP, and serum albumin values. The Goodness of fit, r^2 value, was low and the p value not significant. The sample size is likely too small and heterogeneous to make any more meaningful conclusions of the relationship between these factors and trial outcome.

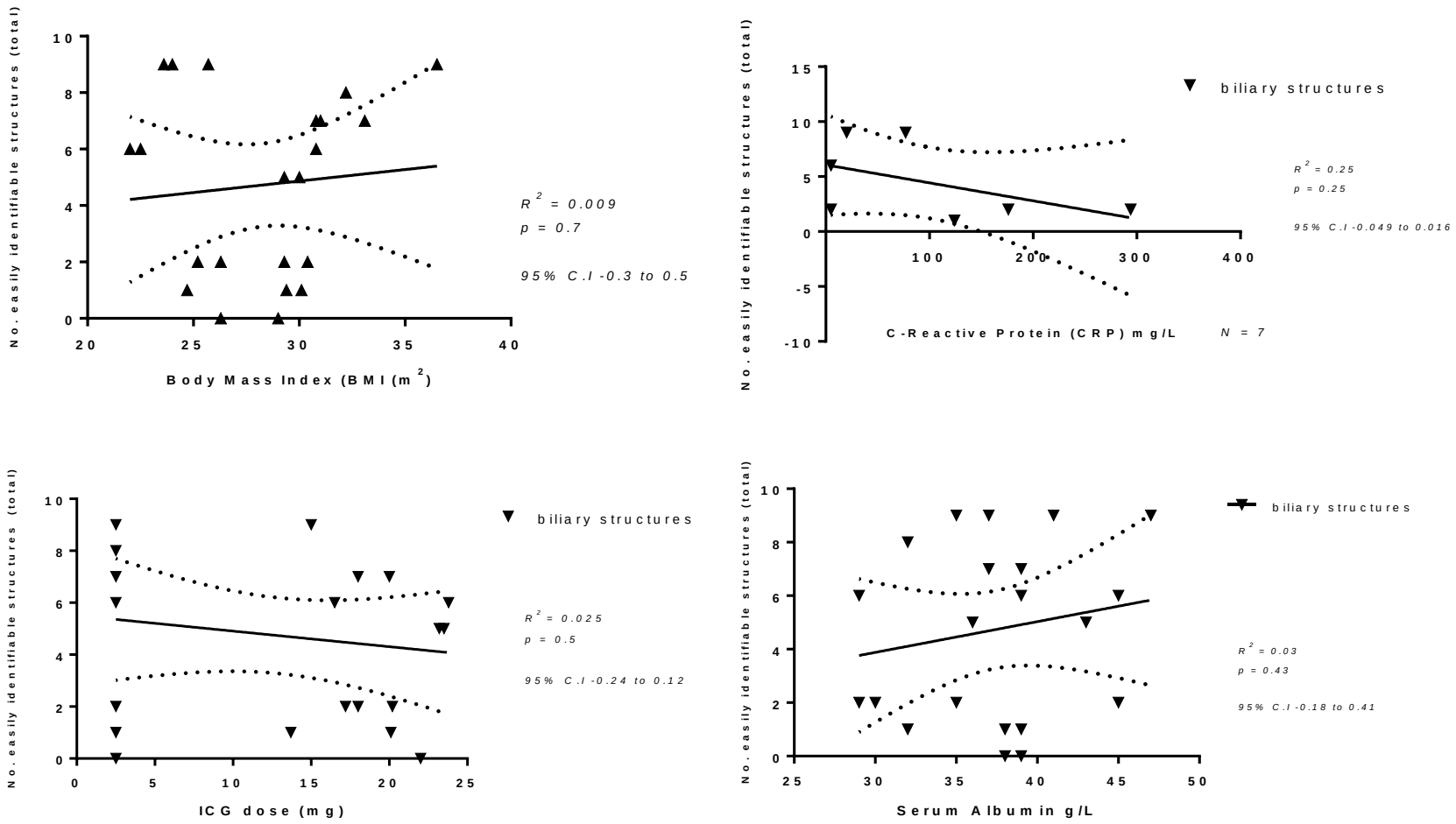

Figure 15: linear regression of participant factors and an average number of extrahepatic biliary structures visualised with NIR-FC. N = 22 for BMI, ICG dose and serum Albumin pre-operatively, N = 7 for pre-operative CRP value. All p values not significant

Optimum Dosing Interval

Exploration of the dosing intervals found 0.25mg/kg more than 12 hours before surgery to be the optimum regimen. Four participants received this regimen. Participant 20 (*Table 4*) received a weight-adjusted dose of ICG 17 hours prior to surgery. This allowed ICG loaded bile to accumulate in the biliary tree and aid delineation. The bifurcation of the cystic duct and common hepatic duct was clearly identified through the surrounding tissue. This was not seen with other dosing intervals.

Administration of ICG more than 20 hours appears to exceed the optimum window for imaging of bile ducts with NIR-FC. Participant 19 and 21 (*Table 4*) received ICG more than 20 hours before surgery and their NIR-FC signal was weak. Participant 19 shows limited accumulation of ICG in the biliary system and poor fluorescent signal was obtained. This may be individual participant specific or a detectable trend in the group. The surgeon satisfaction questionnaire also concluded 0.25mg/kg 12 to 36 hours prior to surgery was the optimum dosing regimen.

Operative Length

The mean operative procedure length, defined as duration from introduction of umbilical port to closure of laparoscopic port sites, is shown in *Table 5*. The heterogeneity of the subgroups and the wide range of operative times has skewed the data and precludes meaningful statistical analysis at interim and final review.

Secondary Review

Two consultant hepatobiliary surgeons at LTHT reviewed the anonymised NIR-FC videos and OTC for the first 21 trial participants. The reviewers used the same semi-quantifiable scale to quantify the number of biliary structures clearly delineated with the addition of NIR-FC bile duct mapping.

There was considerable variance between the initial NIR-FC intraoperative assessment and the secondary review result, and a degree of variance between the two assessors. *Figure 16* compares the number of structures defined as easily identifiable intraoperatively at each assessment point against the score provided by the reviewing surgeons.

The secondary reviewers consistently reported less structures as *"easily identifiable"* with NIR-FC compared to the intraoperative result at all three of the assessment points (*p value = < 0.0001, 0.003 and 0.009 respectively*). The exact cause of this variance is uncertain; however, it may be attributed to the lack of white light visual information provided. The reviewers were only shown short edited NIR-FC videos and they specifically assessed if the structures were clearly delineated in NIR-FC mode only. The reviewers were more strongly influenced by the noise to signal ratio created by strongly background liver fluorescence with some of the dosing regimens.

The intraoperative assessment and the secondary review confirmed OTC was superior to NIR-FC for the detection of biliary structures. OTC was performed on 10 occasions and for every participant the reviewers confirmed the intraoperative grading, deeming the key biliary structures as *"easily identifiable" (p = 0.01).*

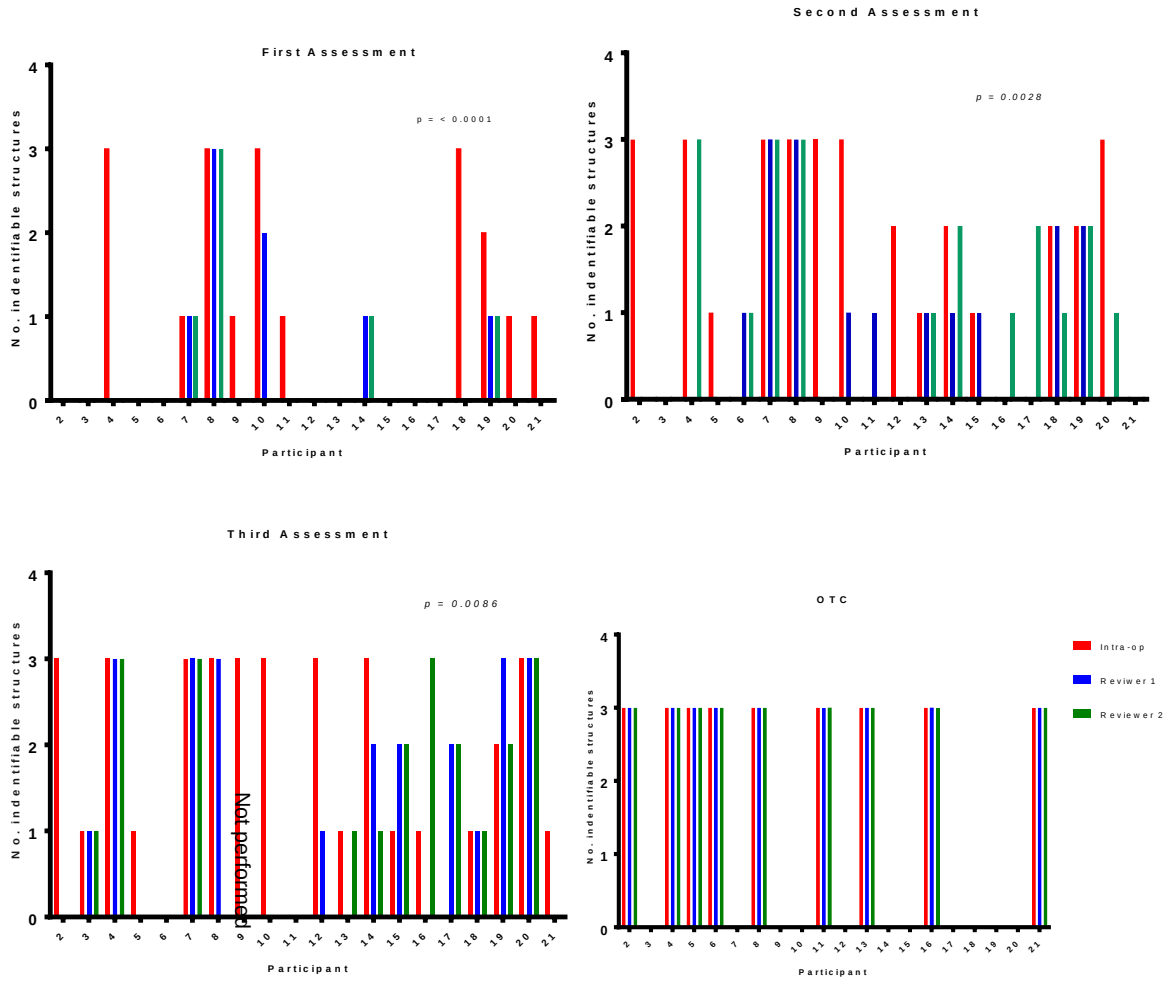

Figure 16: Secondary review by assessment point on individual participant level. The number of structures classified as "easily identifiable" (CD, CBD, and CHD). One-way ANOVA analysis of variance performed. N = 21.

Interim Analysis

Surgeon Satisfaction

After each case, participating surgeons completed a Likert score of their experience using the NIR-FC technique. They found the Novadaq Pinpoint® Near Infrared Laparoscopic System easy to use and adequate for the procedure, the option *"strongly agree"* or *"agree"* was selected for all cases appraised.

Table 6 shows the response to each question by dosing subgroup. The individual subgroups are small and differing in size, therefore calculation of percentage of total and statistical analysis cannot be performed. However, the addition of ICG was considered to aid identification of extrahepatic biliary structures with greatest certainty at a dose of 0.25mg/kg more than 12 hours before surgery. It was also the only regimen felt to make "the surgical procedure easier" and to increase surgeon "confidence in biliary structure identification" in all cases.

It was reassuring to see that background liver fluorescence produced with ICG was not felt to hinder the operative procedure. At the short dosing interval, surgeons could use a proprietary feature of the Novadaq® NIR laparoscopic system, the CSF mode, to artificially colour and semi-quantify areas of maximal fluorescence demonstrated in *Table 4*, to delineate structures from background. The prolonged dosing interval (0.25mg/kg 12 to 36 hours prior to surgery) did not require the CSF mode owing to reduction in background hepatic fluorescence.

NIR-FC was not felt to produce comparable results to OTC or be able to replace OTC at any of the dosing regimens explored. Free text data from surgeons clarified the reason for this; NIR-FC could not identify intraductal stones or demonstrate free flow of contrast into the duodenum in the same manner as OTC.

N = 21	2.5mg	0.25mg/kg		
		20- 40min	90 -180 min	12 – 36 hr
	8	4	5	4
The addition of ICG aided the identification of extrahepatic biliary structures during laparoscopic cholecystectomy	3 (37.5%)	2 (50%)	3 (60%)	4 (100%)
The background liver fluorescence produced with ICG hindered the operative procedure	0 (0%)	0 (0%)	1 (20%)	0 (0%)
The addition of ICG made the surgical procedure easier and increased my confidence in biliary structure identification	2 (25%)	0 (0%)	1 (20%)	4 (100%)
NIR cholangiography provided comparable results to standard radiological OTC	1 (12.5%)	0 (0%)	0 (0%)	0 (0%)
In the future, NIR cholangiography could replace standard radiological OTC in my operative practice	0 (0%)	0 (0%)	1 (20%)	0 (0%)
Using ICG could help to reduce intraoperative complications including bile duct injuries	7 (87.5%)	2 (50%)	2 (40%)	3 (75%)
ICG should be reserved for technically difficult and/or acute laparoscopic cholecystectomies only	0 (0%)	0 (0%)	0 (0%)	0 (0%)
I am keen to use ICG in laparoscopic cholecystectomy surgery again	8 (100%)	4 (100%)	5 (100%)	4 (100%)

Table 6: Participating surgeon NIR-FC laparoscopic cholecystectomy operative feedback results. Number of "strongly agree" or "agree" responses given to each question and as percentage of total.

Final Analysis

The interim analysis defined 0.25mg/kg of ICG 12 – 36 hours prior to surgery as the optimum dosing regimen. Therefore, this regimen was assessed in more detail at final analysis. Following recruitment of the final participant (participant 22) the feasibility, optimum dose and safety of the intervention were assessed.

Safety

Participants received trial specific follow up at 30 days post operation. There were no Serious Unexpected Serious Adverse Reaction (SUSARS) reported. There were two Serious Adverse Events (SAEs) observed. Causality was assessed promptly, and neither were deemed related to the trial specific intervention. One participant returned to theatre on post-operative day 3 and was found to have a slow bleeding ooze in the gallbladder fossa, and one participant was re-admitted to investigate the possibility of pulmonary embolism, which was excluded with CT pulmonary angiography (CTPA) in the weeks following surgery.

Specifically, in relation to the secondary safety endpoints of the trial, there were no bile duct injuries, no incidences of vascular injury and no intraoperative conversions to open cholecystectomy. The sample size was too small to draw any further conclusions or perform statistical analysis on SAE causation.

The minor post-operative adverse events were expected complications of umbilical port-site infection reported in two participants. The surgical site infection responded to oral antibiotics and no further intervention was required for both participants.

The inclusion criteria for the trial were adequate for the purposes of recruitment (

Figure 11). Only 28 individuals screened were ineligible to participate (15.9%). Of these, 26 were excluded due to pre-existing medical conditions, most commonly renal dysfunction, and hyperthyroidism. One individual was excluded as they lacked capacity to consent and one individual had limited understanding of English and we lacked facilities to translate trial documents. Only 23 (13.1%) of those approached declined to participate in the trial, further details of reason for this decision were not captured.

The greatest barrier to recruitment was the availability of the NIR equipment and research staff able to facilitate the trial intervention in theatre and the number of participating surgeons. Seventy-seven (43.8%) of eligible individuals screened were excluded because they were undergoing surgery under the care of a surgeon not participating in the trial. Only 5 Hepatobiliary consultant surgeons at Leeds participated in the trial, limiting the number of cases that could be recruited during the study period. Also, LTHT has only one NIR laparoscopic system and this is shared with several surgical specialties limiting access to the equipment needed to perform the surgery.

The trial was able to achieve the target dosing interval for each regimen. The average time taken from administration of ICG to introduction of the umbilical port was 32 minutes for the 2.5mg given 20 to 40 minutes beforehand group; 29 minutes for the 0.25mg/kg 20 to 40 minutes subgroup; 2 hours and 55 minutes for 0.25mg/kg 90 to 180 minutes subgroup, and 19 hours 34 minutes for the 0.25mg/kg 12 to 36 hours prior to start of surgery subgroup. The 90 to 180-minutes dosing subgroup was the most difficult interval to coordinate. It was extremely difficult to accommodate delays in theatre lists and ensure the ICG was administered at the correct time to ensure the target interval was achieved.

Optimum Dosing Regimen

A composite score of the average number of extrahepatic structures considered easily identifiable at the first and third assessment time points was generated to compare the dosing intervals. The standard deviation was also calculated *Figure 17.* The optimum dosing regimen was ascertained at 0.25mg/kg 12 to 26 hours prior to laparoscopic cholecystectomy.

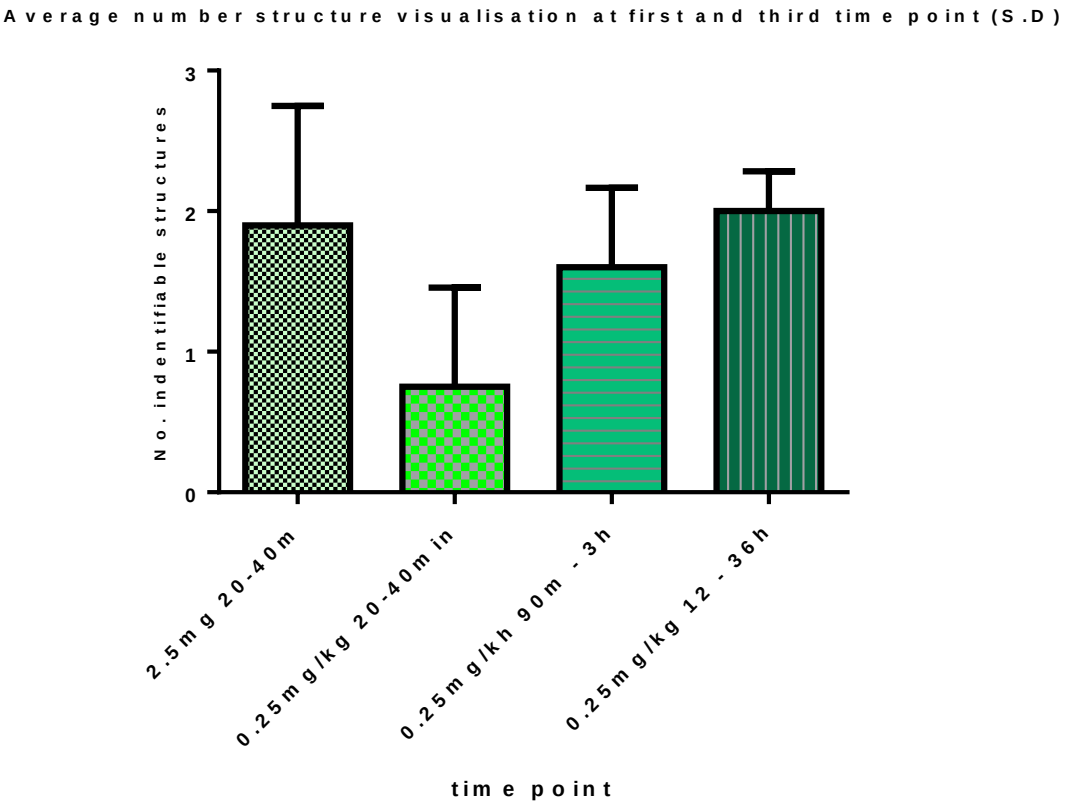

Figure 17: the average total number of extrahepatic biliary structures visible at the first and third assessment point for participants allocated to each of the dosing interval subgroups with standard deviation error bars. One Way ANOVA p = 0.02. N = 22.

Trial Closure

The trial endpoint was defined as the LVLS. This was performed on 31st December 2018. The trial closed to recruitment on 22nd January 2019. The Declaration of End of Study (Declaration of End of Study non-CTIMP v1.3, August 2014) was submitted to the REC North East on 28th February 2019.

2.4 DISCUSSION

Limitations of NIR-FC

Iatrogenic Gallbladder Perforation

When the gallbladder was opened during laparoscopic cholecystectomy, the spillage of bile contaminated the operative field with ICG loaded bile. This is demonstrated in participant 11 (*Table 4*), and prevented delineation of any biliary structures with NIR-FC. This is a limitation of NIR-FC technology not discussed in the previously published literature.

Tissue Penetrance with Peri-Hilar Inflammation

This trial did not fully explore NIR-FC in the acute setting. Index admission laparoscopic cholecystectomy is the gold standard treatment, but there is significant variance across centres, and with presenting complaint. These patients often have significant peri-hilar inflammation with dense adhesions and oedema. The depth of tissue penetrance with NIR-FC is limited and may be insufficient to overcome the inflammatory tissue seen in emergency hepatobiliary surgery. Participants 5 and 6 in *Table 4* demonstrate the dense adhesions that make this surgery technically more challenging.

The necessary planning required to administer ICG the day prior to surgery precluded enrolment of many emergency admission patients into the prolonged dosing sub-group, despite this being deemed the most effective at interim analysis. Currently, LTHT does not have “hot” cholecystectomy operating lists. The availability of these theatre lists, as seen in other hospitals, may have allowed operative planning and recruitment of patients admitted acutely with biliary pathology.

The dosing regimen of 0.25mg/kg more than 12 hours prior to surgery is likely to be the most effective for delineation of biliary structures. This allows sufficient time for the ICG to accumulate in bile and increases the signal to noise ratio – there is reduced or absent liver

fluorescence at this dosing interval. It also allows the operation to be performed with the fluorescent overlay mode and does not require the artificial coloration mode (CSF mode) to delineate structures. Only five participants were enrolled into this subgroup and there was variability in the timing of the dose. For the participant who received their dose more than 18 hours prior to surgery, the fluorescent signal was weak. This may relate to individual participant factors, for example gallbladder/sphincter dysfunction allowing rapid transit of ICG loaded bile into the duodenum or confirm a generalisable finding of the maximum dosing interval for NIR-FC. The subgroup is too small to perform meaning statistical analysis of time of administration and biliary structure identification by means of logistical regression modelling. Further to this, structure identification may be impaired by Sphincter of Oddi dysfunction and or previous ERCP therapy. This data was not captured for trial participants but is likely to have affected retention of ICG loaded bile in the biliary system and therefore operative fluorescent signal detected.

The results of this feasibility study contrast previously published studies of NIR-FC in laparoscopic cholecystectomy. The majority of previously published trials have used a standardised dose of 2.5mg ICG immediately pre-operatively. Our experience of NIR-FC is that this dose is inadequate to consistently saturate the bile with ICG and allow NIR assisted bile duct mapping in the elective setting.

This concurs with *Zarrinpar et al's* conclusion of the optimum ICG dose but challenges the timing of its administration. A dose of 0.25mg/kg is within the maximum safe dose of ICG permitted and appears to allow ICG to accumulate in the extrahepatic bile ducts more consistently. However, *Zarrinpar et al* concluded 45 minutes was an acceptable dosing interval(123). In our experience, this was the least effective interval. Intravenous administration of 0.25mg/kg of ICG on average 32 minutes prior to assessment had very poor signal to noise ratio and visualisation of the bile ducts was hindered by limited ICG accumulation in the ducts and strong background liver fluorescence. A prolonged pre-

operative dosing interval, possibly 12 to 18 hours, appears to increase signal to noise ratio with low background liver fluorescence and demonstrates the greatest tissue penetrance.

Overall, participating surgeons were satisfied with the image quality of the Novadaq® NIR laparoscopic system and found it easy to use. However, the unanimous opinion was that NIR-FC was inferior to standard OTC and could not replace radiological assessment of the bile ducts intraoperatively. In cases were OTC was performed, NIR-FC was inferior in its ability to delineate extrahepatic bile duct structures. The prolonged dosing interval (0.25mg/kg 12 to 36 hours before surgery) was the only subgroup where surgeons felt NIR-FC increased their confidence in structure identification in all cases performed.

There is also considerable variance in the interpretation of NIR-FC results not seen with radiological OTC. The secondary review of intraoperative NIR-FC videos at the interim analysis showed a significant difference of opinion between the intraoperative assessment of structure visualisation and to some degree between the two reviewers. Overall, at secondary review NIR-FC was felt to be less effective at delineating biliary anatomy. The reviewers agreed that the prolonged dosing interval (0.25mg/kg 12 to 36 hours prior to surgery) was likely to be the most effective. To confirm this hypothesis, the sample size needs to be increased and the ICG should be administered less than 18 hours prior to the start of surgery.

NIR-FC may be considered a useful adjunct to standard care in laparoscopic cholecystectomy. It has been proven safe and feasible to explore the optimum dosing regimen in a mixed patient population in a tertiary referral hepatobiliary unit. However, as yet, we have not conclusively proved NIR-FC is effective in delineating biliary structures or in reducing serious intraoperative complications. Compared to OTC, NIR-FC appears inferior, so the additional cost of the technology and burden of ICG administration may not be cost-effective in the longer term.

In the future, a dedicated trial of NIR-FC in the acute setting is needed. This trial would need specific eligibility criteria to identify patients with acute cholecystitis and likely peri-hilar inflammation. This may include elevated CRP and deranged LFTs on admission blood tests,

treatment with IV antibiotics, and radiological evidence of acute cholecystitis on ultrasound scan. This trial would need a much larger sample size to analyse the effect of NIR-FC on operative outcomes.

The trial conducted was underpowered to determine the effect of NIR-FC on iatrogenic bile duct injury. The highest level of evidence remains a randomised controlled trial of an intervention. Bile duct injury is a rare but serious complication of cholecystectomy. If we assumed a conservative bile duct injury rate is 0.4% with laparoscopic cholecystectomy, and 75% reduction bile duct injury rate as the dichotomous endpoint in the study population, with an equal 1:1 randomisation to control and intervention arms, and with a two-sided 5% level of significance and 80% power, a sample size of 8696 participants would be require. If we were to settle for comparing a single study cohort against the published literature incidence, negating the need for a control arm, and assuming a literature bile duct injury rate of 0.4% and study population rate of 0.2%, we would still need to recruit 6505 patients for a two-sided 5% level of significance and 80% power to confirm the efficacy of NIR-FC in reducing iatrogenic bile duct injuries(222). A trial of this magnitude would be extremely costly and time-consuming to conduct. It is also unfeasible to conduct a trial of this size in a single centre and would require collaboration with multiple centres.

This single centre, phase IIa, feasibility study has shown that NIR-FC is feasible and safe. The dosing regimen optimisation aim of this study successful identified 0.25mg/kg of ICG administered intravenously 12 to 36 hours prior to surgery as the optimum regimen to delineated extrahepatic biliary anatomy. This regimen was favoured by the operating surgeons and yielded identification of a greater number of biliary structures compared to the shorter dosing intervals. NIR-FC appears inferior to OTC in patients who undergo radiological intraoperative bile duct mapping. Further exploration of NIR-FC in the acute index admission laparoscopic cholecystectomy setting is required. These are the most technically challenging cases and would benefit the most from a real-time dynamic method of performing intraoperative bile duct mapping.

3. CHAPTER THREE

EXPLORATION OF EMI-137 AS AN IMAGING AGENT IN 2D AND 3D MODELS OF COLORECTAL CANCER

Name: Gemma Armstrong
Student No: 201073014

3.2 AIMS AND OBJECTIVES

1. To confirm the spectral properties of EMI-137 at various concentration dilutions.
2. To explore a novel c-Met targeted fluorescent molecule (EMI-137) to detect primary colon cancer and metastases.
    a. To determine the colorectal cancer cell line with highest c-Met protein expression
    b. To confirm the c-Met receptor specificity of EMI-137 by means of mRNA silencing in a selected colorectal cancer cell line.
    c. To compare EMI-137 as an optical imaging agent against standard indirect immunofluorescence.
3. To develop an animal model of colorectal cancer.
    a. To assess the specific binding of EMI-137 in an animal model of colorectal cancer and explore the renal excretion of the compound.
4. To assess c-Met expression by methods of immunohistochemistry in anonymised donor colorectal cancer tissue.
5. To map and quantify c-Met expression in tissue microarrays from a defined colorectal cancer population.

3.3 MATERIALS AND METHODS

EMI-137 Supply

The investigational medical product EMI-137 was kindly supplied by our research collaborators at Edinburgh Molecular Imaging Ltd, Nine Edinburgh Bioquarter, 9 Little France Road, Edinburgh, UK. EMI-137 was supplied as a blue dry powder in individual vials. It was stored at 4°C in a temperature controlled and monitored refrigerator and shielded from light.

EMI-137 Spectral Properties Assessment

The photophysical properties of EMI-137 were confirmed using the NanoDrop 3300 UV-Vis spectrophotometer. A serial dilution of EMI-137 was prepared with Dulbecco's Phosphate-Buffered Saline (DPBS). The concentrations ranged from 20,000nm to 1,000nm and were shielded from light. A single 1µL drop of EMI-137 was loaded into the nanodrop and excited with the white light emitting diode (LED) (excitation maxima 460 to 650nm). Results were normalised to a phosphate buffer control solution. This ascertained the peak absorbance wavelength for EMI-137 across the range of concentrations.

3.3.1 *In Vitro* 2D Model of Colorectal Cancer

3.3.1.1 Western Blotting

Mammalian Cell Lines

Several CRC cell lines were strategically selected for evaluated to find a c-Met in CRC representative cell line. The colorectal adenocarcinoma cell lines were selected for expected high expression of c-Met protein with the aim of identifying a single cell line for further research and development of an *in vivo* xenograft mouse model. Breast adenocarcinoma MCF-7 was used as a predicted low expressing adenocarcinoma line, whilst HFFF-2 was used as a non-cancerous normal human fibroblast control cell line. c-Met expression by HFFF-2 was

expected to be low because c-Met is normally expressed by cells of epithelial origin. HGF secretion is restricted to cells of mesenchymal origin, such as fibroblasts. The immortal murine fibroblast cell line 3T3, was used to confirm the selectively of the antibody for human c-Met prior to commencing any murine xenograft work.

Primary Cell Culture

All cell lines were obtained from European Collection of Authenticated Cell Cultures (ECACC) (Salisbury, England) and cultured in the appropriate medium enriched with 10% (v/v) Foetal Bovine Serum (FBS) (Sigma-Aldrich, Dorset, UK; Cat. No. F7524) and incubated at a constant temperature of 37°C with 5% carbon dioxide. Regular passage of the cell lines was performed in a class II laboratory cabinet as per usual laboratory technique to maintain viability. Cell lines routinely tested for mycoplasma infection.

Human colon adenocarcinoma cells lines, SW480, HCT-116, HT-29 and Caco-2 cells were cultured in Roswell Park Memorial Institute (RPMI) 1640 Medium + GlutaMAX™-I (Gibco® by Life Technologies™, Paisley, UK; Cat. No. 11875093). The human colon adenocarcinoma LoVo cell line was cultured in F-12 Nutrient Mixture + GlutaMAX™-I Medium (Gibco® by Life Technologies™, Cat No: 31331-028). The human breast adenocarcinoma Michigan Cancer Foundation-7 (MCF-7), the Human Foetal Foreskin Fibroblast HFFF-2, and the mouse embryonic fibroblast 3T3 cell line were cultured in Dulbecco's Modified Eagles Medium (DMEM) (1X) + GlutaMAX™-I (Gibco® by Life Technologies™, Paisley, UK; Cat No. 10569010).

Protein Extraction and Quantification

The selected cell lines were grown to a confluent state. The media was removed, and the cells washed in ice cold Dulbecco's Phosphate-Buffered Saline (DPBS) (1X), (Gibco® by Life Technologies™; Cat. no. 14190094) solution before 4ml of protein lysate buffer was added for 10 minutes and maintained at 4°C. The protein lysate buffer was prepared from equal quantities of radio-immunoprecipitation assay (RIPA) buffer (100mM Tris HCL pH 7.4; 300mM NaCl; 10% NP40 and diH_2O) and complete protease inhibitor cocktail tablets. The cells were scraped from the flask, and the supernatant prepared for storage at -80℃.

The protein concentration was determined using the BIO-RAD *DC* colorimetric assay kit with Bovine Albumin Serum (BSA) as the known protein standard. Serial dilutions of BSA control and BSA with protein lysate were prepared and the optical density (OD) read at 620nm on a fluorescence microplate reader. The standard was used to construct a standard curve in Microsoft Excel 2013.

Protein Gel Electrophoresis and Transblotting

Standardised volumes of protein lysate dissolved in loading buffer and diH_2O were loaded into individual wells of a protein gel. Proteins were resolved by electrophoresis at 180 volts for 1 hour 45 minutes. Equal quantities of two western protein standards were used as a molecular marker. The resolved proteins were then transferred to an activated PVDF membrane with an appropriate transfer buffer solution. All reagents and equipment are described in *Table 7*. The membrane was blocked in 5% and 1% skimmed milk solution.

The membrane was then probed for the primary antibody with a Horseradish Peroxidase (HRP) enzyme conjugated secondary immunoglobulin. Anti-β Actin and anti-α-Tubulin were used to probe for the loading control. All concentrations described were achieved by diluting

the antibody in 1% skimmed milk solution in TBST (mixture of DPBS, tris-buffered saline and Tween-20%).

Membrane Imaging

The PVDF membrane was imaged using the Gel Doc™ XR+ Gel Documentation System (Bio-Rad Laboratories, Inc; Hertfordshire, UK). Immunoreactive protein bands with HRP-conjugated substrate were detected by application of ECL; West Femto high sensitivity chemiluminescence substrate was used to detect the c-Met protein and West Pico was used to detect the loading control (

Table 8).

Relative Quantification of Western Blot Bands

The image processing program ImageJ (Rasband, W.S., ImageJ, U. S. National Institutes of Health, Bethesda, Maryland, USA) was used to analyse the Western Blot images. To quantify the bands, the mean gray value was calculated for the protein band, the loading control band, and a neighbouring negative control band for each cell line. The pixel density was inverted, and the net value of the band compared to its matched control was calculated. This allowed the relative ratio of each band to be determined as previously described by *Davarinejad et al*(223).

Product	Full Product Name	Supplier/Manufacturer	Product Code
Protease Inhibitor	complete protease inhibitor cocktail tablets	Roche diagnostics GmbH Ltd.	Cat No: 11697498001
Colorimetric protein assay kit	DC Protein Assay Reagents Package 1. DC™ Protein Assay Reagent A (SDS) alkaline copper tartrate 2. DC™ Protein Assay Reagent B (SDS) Folin reagent 3. DC™ Protein Assay Reagent S (SDS) surfactant solution	Bio-Rad Laboratories, Inc.	Cat No: 5000111
Fluorescence Microplate Reader	Mithras LB 940 Multimode Microplate Reader with MikroWin 2010 v5.21	Berthold Technologies GmbH & Co. KG	n/a
Loading control	NuPAGE™ Sample Buffer (4X)	Invitrogen™ - Thermo Fisher Scientific Inc	Cat No: NP0007
Protein Gel	NuPAGE™ 12% Bis-Tris Protein Gels, 1.0 mm, 10-well	Invitrogen™ - Thermo Fisher Scientific Inc	Cat No: NP0341BOX
Running Buffer	NuPAGE™ MOPS SDS Running Buffer (20X)	Invitrogen™ - Thermo Fisher Scientific Inc	Cat No: NP0001
Transfer Buffer	NuPAGE® Transfer Buffer (20X)	Invitrogen™ - Thermo Fisher Scientific Inc	Cat No: NP00061
Western standard marker 1	SeeBlue™ Plus2 Pre-stained Protein Standard	Invitrogen™ - Thermo Fisher Scientific Inc	Cat No: LC5925
Western standard marker 2	MagicMark™ XP Western Protein Standard	Invitrogen™ - Thermo Fisher Scientific Inc	Cat No: LC5602

PVDF Membrane	Polyvinyl Difluoride (PVDF) Transfer Membrane, 0.45 µm, 26.5 cm x 3.75 m	Thermo Fisher Scientific Inc	Cat No: 88518
Milk powder	Marvel Dried Skimmed Milk Powder 340g	Premier Foods Group Ltd	n/a
chemiluminescence substrate (ECL)	1. SuperSignal™ West Femto Maximum Sensitivity Substrate	Thermo Fisher Scientific Inc	Cat No: 34095
	2. SuperSignal™ West Pico PLUS Chemiluminescent Substrate	Thermo Fisher Scientific Inc	Cat No: 34580
Gel Imaging system	Molecular Imager® Gel Doc™ XR+ System with Image Lab™ Software	Bio-Rad Laboratories, Inc	Cat No: 1708195

Table 7: Western Blot equipment and reagents

Antibody	Origin	Product code	Commercial Source	Dilution	Incubation time	Temperature
Recombinant anti c-Met	Rabbit monoclonal	ab51067	Abcam Plc	1:1000	Overnight	4℃
Anti-Rabbit Horseradish peroxidase (HRP) immunoglobulin	Goat Polyclonal	P0448	Dako - Agilent Technologies Ltd	1:2000	60 minutes	RT
Anti-Mouse Horseradish peroxidase (HRP) immunoglobulin	Rabbit Polyclonal	P0260	Dako - Agilent Technologies Ltd	1:2000	30 minutes	RT
Alpha (α) tubulin	Mouse monoclonal	T516	Sigma Aldrich	1:20,000	60 minutes	RT

Table 8: Western Blot Antibodies. Abbreviations: RT - room temperature. HRP - Horseradish peroxidase

3.3.1.2 Temporary silencing of c-Met mRNA transcription

Temporary messenger RNA (mRNA) suppression was used to confirm expression of c-Met by the HT-29 cells line and that EMI-137 specifically binds to the c-Met transmembrane protein present. EMI-137 was compared against the same anti c-Met recombinant monoclonal antibody used in the western blot described in 3.3.1.1 with an immunofluorescent (IF) specific secondary antibody for protein localisation.

Immediately upon delivery, the concentration of SiRNA was verified. The concentrated SiRNA sample was briefly centrifuged and re-suspended in RNAse-free water (ThermoFisher Scientific Inc., Cat: AM7001) to achieve a concentration of 20µM. The sample was then mixed via continuous agitation at RT for 30 minutes. The concentration of RNA was confirmed using the NanoDrop 3300 UV-Vis spectrophotometer at an excitation maxima wavelength of 260nm. A total of three repeat sample analyses, each at 1µL were performed to confirm an average SiRNA concentration of 1uM =13.3ng/µL.

Transfection of cells

HT-29 cell lines were grown to 80% to 90% confluence in RPMI media supplemented with 10% FBS v/v. Sterile microscope glass cover slips (22mm x 22mm) were prepared in 6-well flat bottom cell culture plates (Corning Costar Inc., New York, USA; Cat. No. 3516) seeded to a density of $1.2x10^6$/well. The cells were allowed to settle overnight before transfection.

Short interfering Ribonucleic Acid (SiRNA) was used to temporarily silence c-Met mRNA transcription and c-Met protein expression in HT-29 cells. Cells were allowed to settle overnight and were then transfected with a pooled c-Met SiRNA (*Table 9*) or a pooled non-targeted SiRNA control (siGENOME Non-Targeting SiRNA Pool #1; (Dharmacon Inc., Lafayette, CO, USA). Cat No: D-001206-13-05) using an appropriate transfection reagent (DharmaFECT Transfection Reagent #1; Cat No: T-2001-01 (Dharmacon Inc., Lafayette, CO, USA). The SiRNA was diluted to the desired concentration in RNAse-free water and RPMI cell

culture media. At 24 hours, an additional 2mL of complete cell media enriched with 10% v/v FBS was added to each well to reduce the potential cell toxicity effect.

When ready, the cells were fixed by incubation with 4% w/v Paraformaldehyde (PFA) for 10 minutes. Blocking was performed by incubation with 0.5% w/v skimmed milk solution for 5 minutes at room temperature. Localisation of the protein of interest was performed by either direct or indirect labelling methods described in detail below. Between steps, the slides were thoroughly washed with an appropriate quantity of DPBS. The control slides were prepared by incubating HT-29 cells in RPMI complete cell media for 72 hours in identical controlled conditions. The slides were then treated with the imaging agent as described.

	SiRNA component	Target Sequence
1.	SiGENOME SMARTpool SiRNA D-003156-09	GAAGAUCAGUUUCCUAAUU
2.	SiGENOME SMARTpool SiRNA D-003156-10	CCAGAGACAUGUAUGAUAA
3.	SiGENOME SMARTpool SiRNA D-003156-11	GAACAGAAUCACUGACAUA
4.	SiGENOME SMARTpool SiRNA D-003156-12	GAAACUGUAUGCUGGAUGA

Table 9: Composition of Dharmacon siGENOME Human MET (4233) SiRNA SMARTpool 5 nmol (Dharmacon Inc., Lafayette, CO, USA). Cat No: M-003156-02-0005).

Indirect c-Met Protein Expression Detection

To localise the c-Met protein via indirect labelling methods, selected slides were incubated with 100µL/well of the c-Met antibody described in

Table 8 at a concentration of 1: 200 prepared in 0.5% w/v skimmed solution for 1 hour, followed by 100µL/well of 1:300 Goat anti-Mouse IgG (H+L) Cross-Adsorbed Secondary Antibody, Alexa Fluor 488 (ThermoFisher Scientific Inc Cat: A-11001) prepared in 0.5% w/v skimmed milk solution for 30 minutes at RT in the dark. To exclude non-specific secondary antibody binding, a negative control slide was treated with the fluorescent secondary antibody only.

Imaging

Slides were mounted on Superfrost Plus Adhesion glass microscope slides (25 x75 x10 mm) (ThermoFisher Scientific Inc, Cat: J1800AMNT) with ProLong Diamond Antifade with DAPI (4′,6-diamidino-2-phenylindole) mountant (ThermoFisher Scientific Inc Cat: P36962) and cured overnight at RT. Imaging was performed at x63 and x40 magnification under oil immersion using the Zeiss Axioimager fluorescent microscope (Carl Zeiss, Hertfordshire, UK). c-Met protein was imaged with the FITC (fluorescein isothiocyanate) fluorescent light channel. Nuclear staining was performed with the DAPI channel light filter.

The Advanced Microscopy Group (AMG) EVOS™ FL Imaging System inverted fluorescent microscope using the DAPI and Cy5 filters (Life Technologies, Loughborough, UK) at x40 magnification was used to image EMI-137 stained slides. The DAPI filter confirmed nuclear staining. Direct staining of the protein of interest with EMI-137 was performed with the Cy5 filter (excitation 628±40nm and emission 692±40nm). The images were analysed and an overlay image created where necessary using ImageJ (Rasband, W.S., ImageJ, U. S. National Institutes of Health, Bethesda, Maryland, USA) software. This determined location of staining relative to the cell nucleus and confirmed c-Met protein staining in the cell membrane.

Optimisation of SiRNA Concentration

To determine the lowest concentration of c-Met targeted SiRNA required to produce detectable c-Met protein suppression with immunofluorescent microscopy with the fewest off-target effects, HT-29 cells were transfected with SiRNA at a concentration of either 25nM, 37.5nM or 50nM and incubated in controlled conditions for 72 hours.

Optimisation of EMI-137 Concentration

The optimum concentration of EMI-137 to detect c-Met protein expression in HT-29 cells was determined. HT-29 cells grown to confluence on sterile glass cover slips for 72 hours as described above. A serial dilution of EMI-137 diluted in DPBS was prepared to yield final concentrations of 1000nM, 500nM, 250nM, 125.nM, and 62.5nM. Each plate was then incubated with 100µL/well of EMI-137 for one hour at RT in the dark. Untreated HT-29 cells stored in DPBS until imaged were used as negative control.

EMI-137 Specificity for c-Met

To determine the utility of EMI-137 as a molecular targeting agent in CRC, the expression of c-Met protein was investigated using temporary mRNA silencing in HT-29 as a representative CRC cell line. HT-29 cells were transfected with a range of concentrations of c-Met SiRNA or the non-targeted SiRNA control (05nM, 15nM or 25nM) and treated with a fixed concentration of EMI-137 (500nM) or the anti c-Met combination described above. The concentration of EMI-137 and SiRNA used was defined by previous experimental results described above.

HT-29 cells were cultured and transfected with pooled c-Met SiRNA or untargeted SiRNA at a concentration of 5nM, 15nM or 25nM. The prepared cover slips were then probed with the monoclonal c-Met antibody and FITC tagged fluorescent secondary antibody or with 100µL/well of 500nM of EMI-137 for 1 hour.

3.3.2 3D Animal Model of Colorectal Cancer

Experiments were conducted at a dedicated animal research facility at the University of Leeds under Home Office Project License Number 40/3291 held by Dr. L Coletta. The experiment was conducted under the supervision of Dr. Nikki Ingham (Home office personal license no. 40/9070) and Mr. Tom Maisey. Experiments were conducted in accordance with the Animals (Scientific Procedures) Act 1986 (ASPA). The ASPA incorporates the European Directive 2010/63/EU on the protection of animals used for scientific purposes.

The murine models were developed to analyse EMI-137 excretion and bioaccumulation in live tissue. The xenograft was used to analyse c-Met protein expression and EMI-137 binding to tumour expressed c-Met in a 3D model of colorectal cancer.

Xenograft Preparation

Low passage number HT-29 human colorectal cells were grown to a confluent state (70% to 80% confluence) in complete RPMI media with FBS 10% (v/v) supplementation. The HT-29 cells were washed, typsinised and then re-suspended in serum-free RPMI media to yield a final concentration of $1x10^7$ HT-29 cells per ml in accordance with standard laboratory procedures.

Twelve female BALB/c nude athymic mice were purchased Charles River UK, Ltd (Margate, UK) and raised in protected conditions. When the mice were six weeks old, twelve individual mice of 20g in weight were selected for experimentation. The mice received a subcutaneous injection of $1x10^6$ HT-29 cells in a volume of 100µL of media into the right flank without anaesthesia. The xenograft tumour was allowed to develop for 14 days and achieved a maximum diameter of 10mm.

EMI-137 Administration

The athymic mice were restrained and injected with 0.18mg/kg of EMI-137 reconstituted in 100µL of sterile DPBS via the tail vein. The control mice received 100µL of sterile DPBS intravenously only.

Biodistribution Visualisation

At each of the specified time points (1 hour, 4 hours and 6 hours post-injection of EMI-137) the female BALB/C nude athymic mice were anaesthetised by inhalation of vaporised Isoflurane and immediately humanly sacrificed. The mice were dissected and solid organs - heart, liver, lungs, spleen, brain, and kidneys, and tumour xenografts were retrieved and orientated for imaging using IVIS Spectrum *In-Vivo* Imaging System (PerkinElmer Inc. Seer Green, Buckinghamshire, UK). Image acquisition settings were standardised for all 12 animal specimens.

Tissue Preparation

The mouse organs were immediately individually preserved in 4% PFA. A sample of the xenograft from each animal was also snap-frozen with the aid of dry ice. The sample was embedded in Optimal Cutting Temperature (OCT) compound (Bright Cryo-M-Bed Embedding Compound, Bright Instrument Company Ltd, Cambridgeshire, UK) and frozen with the aid of dry ice. Samples were stored at -80°C in a HTA approved facility for future use.

Fluorescent Microscopy

Ten-micron (10µm) thickness slices of frozen xenograft tissue were sectioned using the Leica GeoSystems CM3050 S cryostat (Leica Geosystems Holdings AG; St. Gallen, Switzerland) in preparation for imaging by fluorescent laser scanning microscopy. Xenograft tissue was sectioned at -45°C and renal tissue at -28°C. Tissue slices were mounted on to Superfrost Plus Adhesion glass microscope slides (25 x75 x10 mm) using ProLong Diamond Antifade with DAPI mountant with a glass coverslip. Slides were shielded from light and allowed to cure at room temperature overnight.

Tissue Imaging

The tissue was imaged using the Nikon Eclipse Ti inverted microscope mounted on Nikon A1R Confocal Laser Scanning Microscope (Nikon Instruments UK Ltd; Kingston-Upon-Thames, Surrey, UK) at x60 magnification with Apo-oil immersion. Image acquisition settings were standardised for the tissue type. EMI-137 staining was detected with Cy5 laser filter settings and nucleus localisation was performed with DAPI laser filter settings. An image overlay of both channel filters was created.

3.4 *IN-VITRO* RESULTS

3.4.1 Spectral properties of EMI-137

The peak absorbance was detected at 650nm wavelength across the sample range. This confirmed Cy5 nature of the fluorescent peptide coupled to the c-Met peptide and guided filter selection for fluorescent microscopy (*Figure 18*).

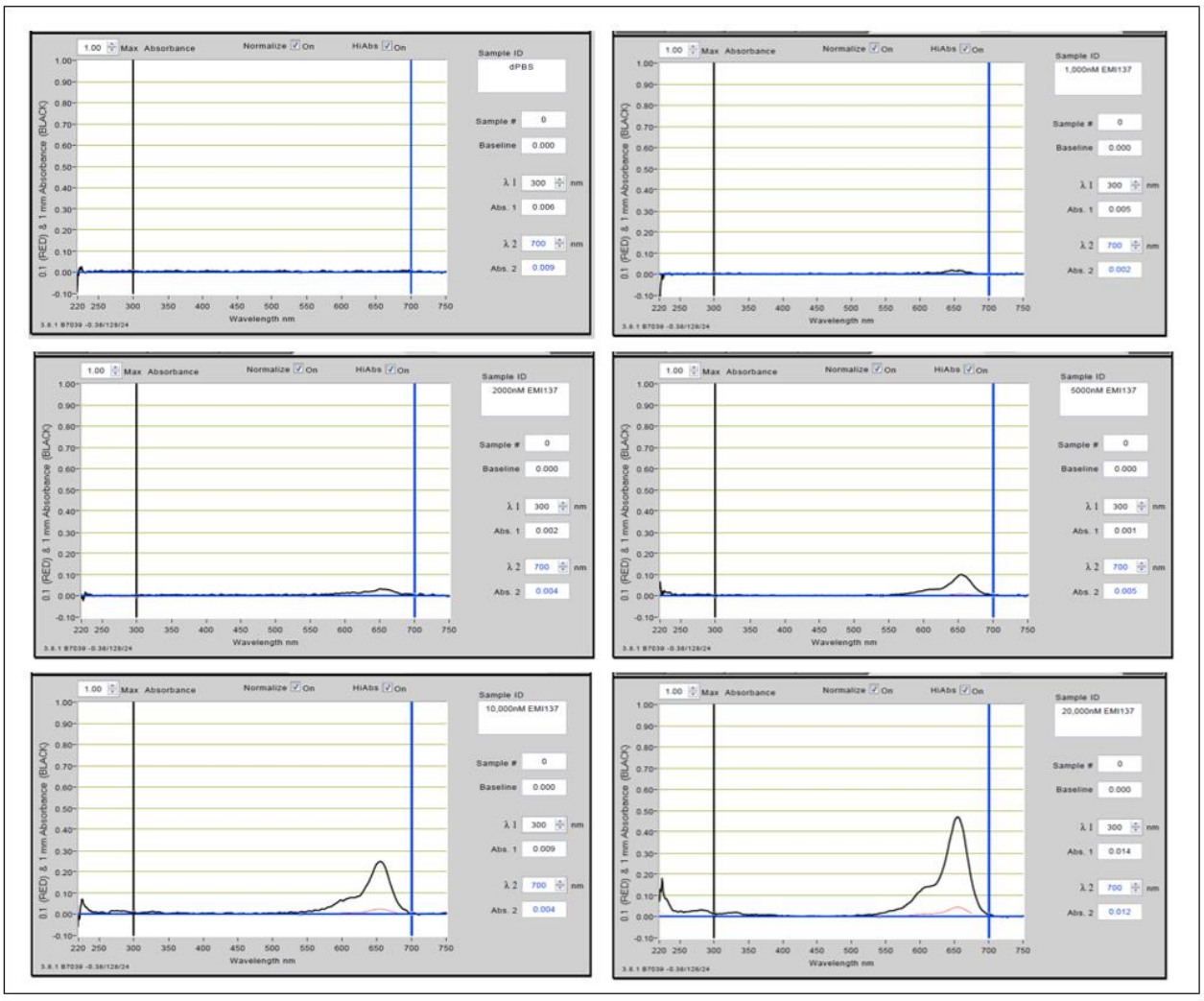

Figure 18: EMI-137 peak absorbance at variable concentrations (20,000nm to 1,000nm) and DPBS control. Left to right; top row DPBS and 1000 NM. Middle row 2000nM and 5000nM. Bottom row 10,000nM and 20,000nM.

Assessment of spectral properties of EMI-137 confirmed the excitation and emission wavelength as described in the Investigator's Brochure from EM Imaging Ltd and in *Burggraaf et al's* research(218,220) (excitation 653nm and emission at 675nm). As expected, there was an increase in detectable absorbance signal with an increase in concentration of EMI-137. It also confirmed there was a consistently detectable signal from EMI-137 at the likely predicted concentrations required for *in vitro* clinical research in primary tissue culture and in a murine model of CRC.

3.4.2 C-Met Protein Expression Quantification by Western Blot

Western Blot Protein Quantification

The average relative protein concentration for each cell line was calculated with BSA as the known standard. The gradient of the straight line was calculated to yield an R^2 value of 0.9959 (*Table 10* and

Figure 19).

	CELL LINE							
RUN	**HT-29**	**CACO-2**	**LOVO**	**SW480**	**HCT-116**	**MCF-7**	**HFFF-2**	**3T3**
1	0.271	0.128	0.106	0.257	0.206	0.133	0.143	0.137
2	0.296	0.135	0.117	0.264	0.215	0	0.14	0.16
3	0.302	0.145	0.113	0.251	0.221	0.149	0.133	0.135
AVERAGE (AU)	**0.290**	**0.136**	**0.112**	**0.257**	**0.214**	**0.141**	**0.139**	**0.144**

Table 10: Western Blot Protein Quantification with BSA Standard

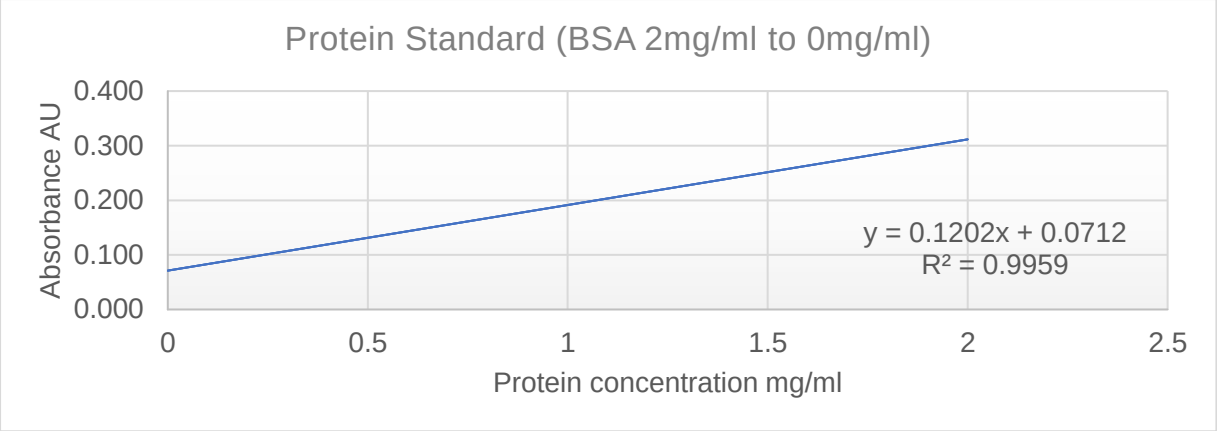

Figure 19: Western Blot BSA Standard Curve

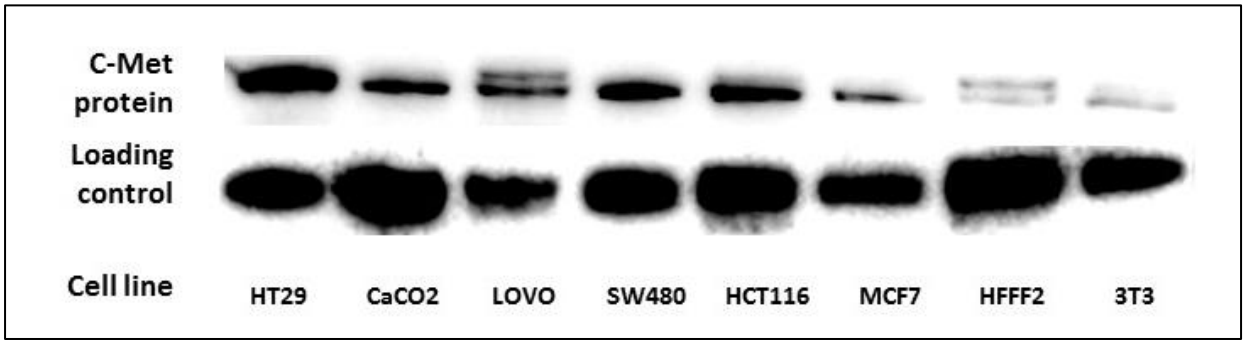

Figure 20: Western Blot –detection of c-Met protein expression with a mouse monoclonal anti C-Met antibody (1:1000) at 190-220kDa and alpha tubulin loading control.

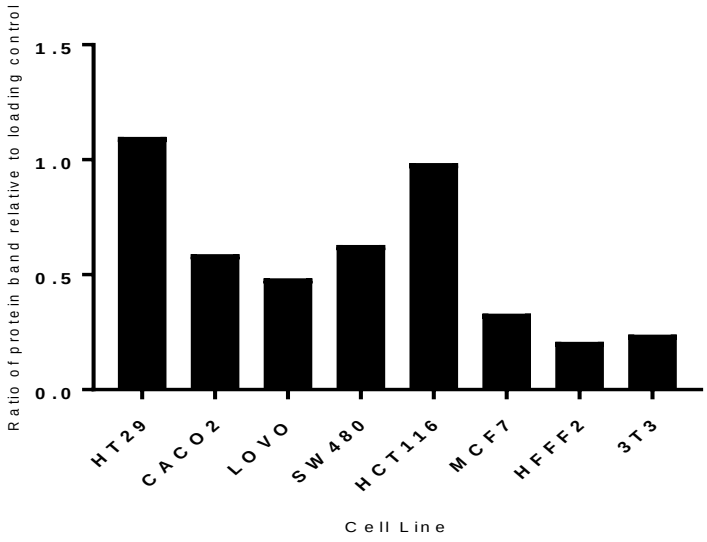

Figure 21: Relative quantification of c-Met protein band density relative to matched loading control.

Protein expression in the selected cell lines was investigated by western blotting. A protein band of 190-210kDa corresponding to the c-Met protein was identified (

Figure 20) when imaged with high sensitivity chemiluminescence substrate. Equal protein loading was confirmed by probing the PVDF membrane with α-tubulin antibody and imaging with chemiluminescence substrate.

Visual inspection of the image obtained, and relative quantification of the band density compared to the loading control, identified HT-29 as the cell line consistently expressing high levels of c-met protein detectable by means of western blot analysis. This was followed by the colorectal cancer cell lines HCT-116 and SW-480. MCF-7 was confirmed as a low expressing human cancer cell (*Figure 20* and *Figure 21*). This correlates with previously published data of c-Met expression in CRC cell lines by *Zeng et al*(204).

3.4.3 c-Met Silencing with Short Interfering RNA

c-Met mRNA Transcription Silencing

HT-29 cells transfected with pooled c-Met specific SiRNA for 72 hours showed markedly reduced c-Met protein expression relative to the untreated positive control and to the matched pooled non-targeted control with immunofluorescent microscopy (*Figure 22*). The resulting image was similar with all concentrations of c-Met SiRNA used. This suggests that 25nM of c-Met SiRNA is the maximum required concentration to temporary silence c-Met mRNA transcription at 72 hours post transfection under these experimental conditions and there is no additional benefit using a higher concentration of c-Met SiRNA.

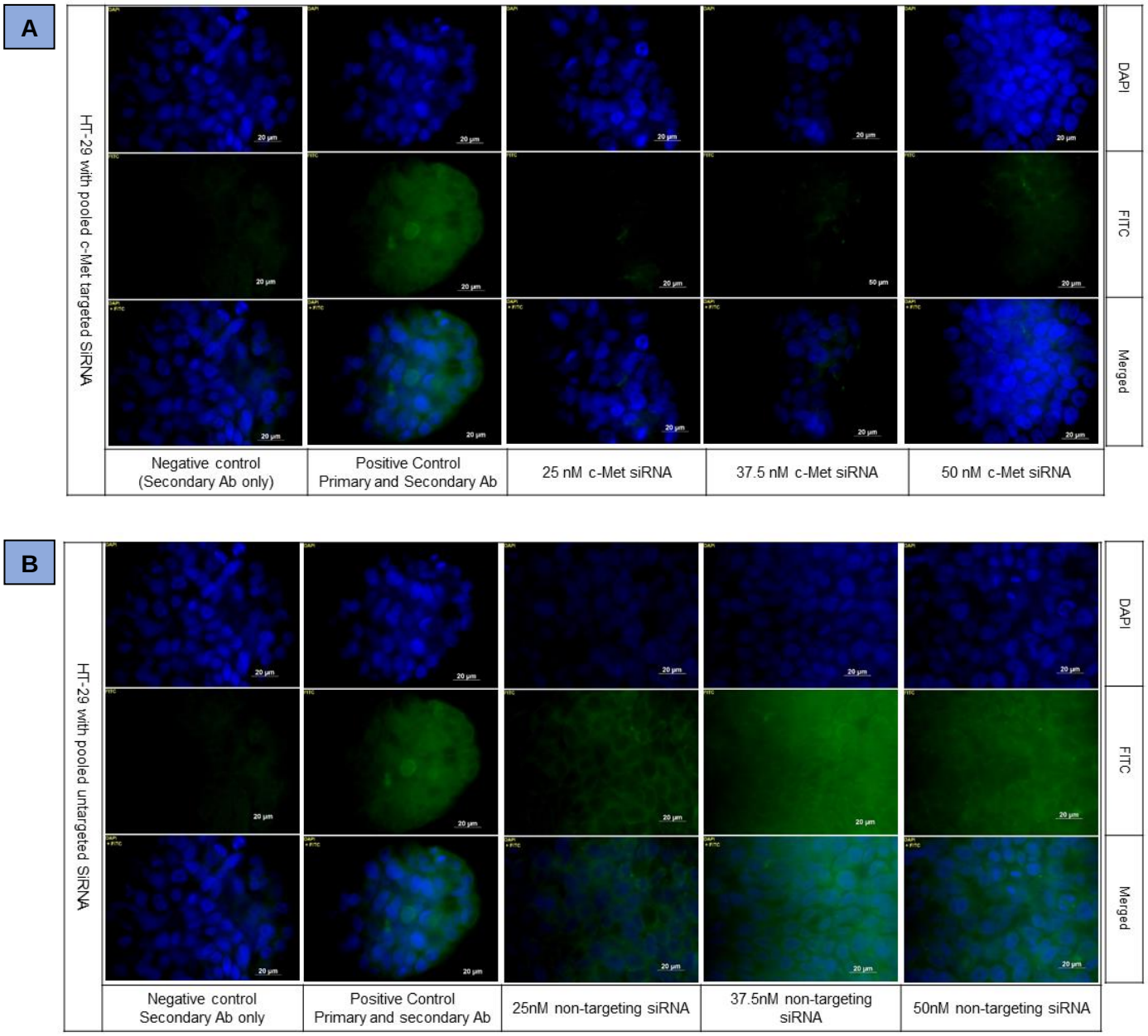

Figure 22: HT-29 cells at variable concentrations of SiRNA. A) Targeted to c-Met SiRNA and B) pooled matched untargeted SiRNA. Imaged at x63 magnification using the Zeiss Axioimager fluorescent microscope. Top row shows DAPI nuclear staining. Middle row shows membrane staining with 1:200 monoclonal rabbit recombinant anti c-Met as primary antibody and 1:300 Goat anti-Mouse IgG (H+L) Cross-Adsorbed Secondary Antibody - Alexa Fluor 488 in the FITC channel. Bottom row shows the merged composite image of DAPI nuclear staining and FITC membrane staining.

Optimisation of EMI-137 Concentration

A concentration of 500nM EMI-137 was confirmed as the optimum concentration for fluorescent microscopy imaging of c-Met. This concentration provided consistent bright fluorescent detection of the transmembrane c-Met protein at standardised image acquisition settings. Relative to control, a concentration of 62.5nM and 125nM of EMI-137 demonstrated little to no detectable fluorescence, whilst 1000nM demonstrated a degree of non-specific binding and excessive fluorescent signal that was prohibitive to accurate delineation of structures *(Figure 23).*

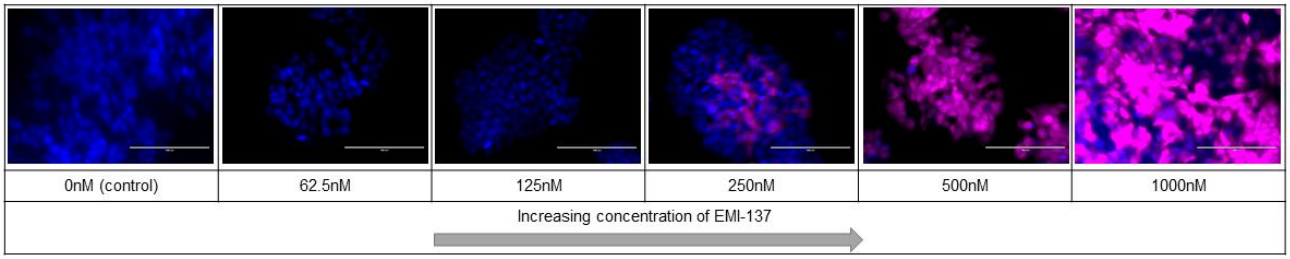

Figure 23: *HT-29 incubated with variable concentrations of EMI-137 for 1 hour. Imaged at x40 magnification on the EVOS inverted fluorescent microscope with standardised image acquisition settings. Merged DAPI and Cy5 filter images.*

3.4.4 EMI-137 Specificity for c-Met

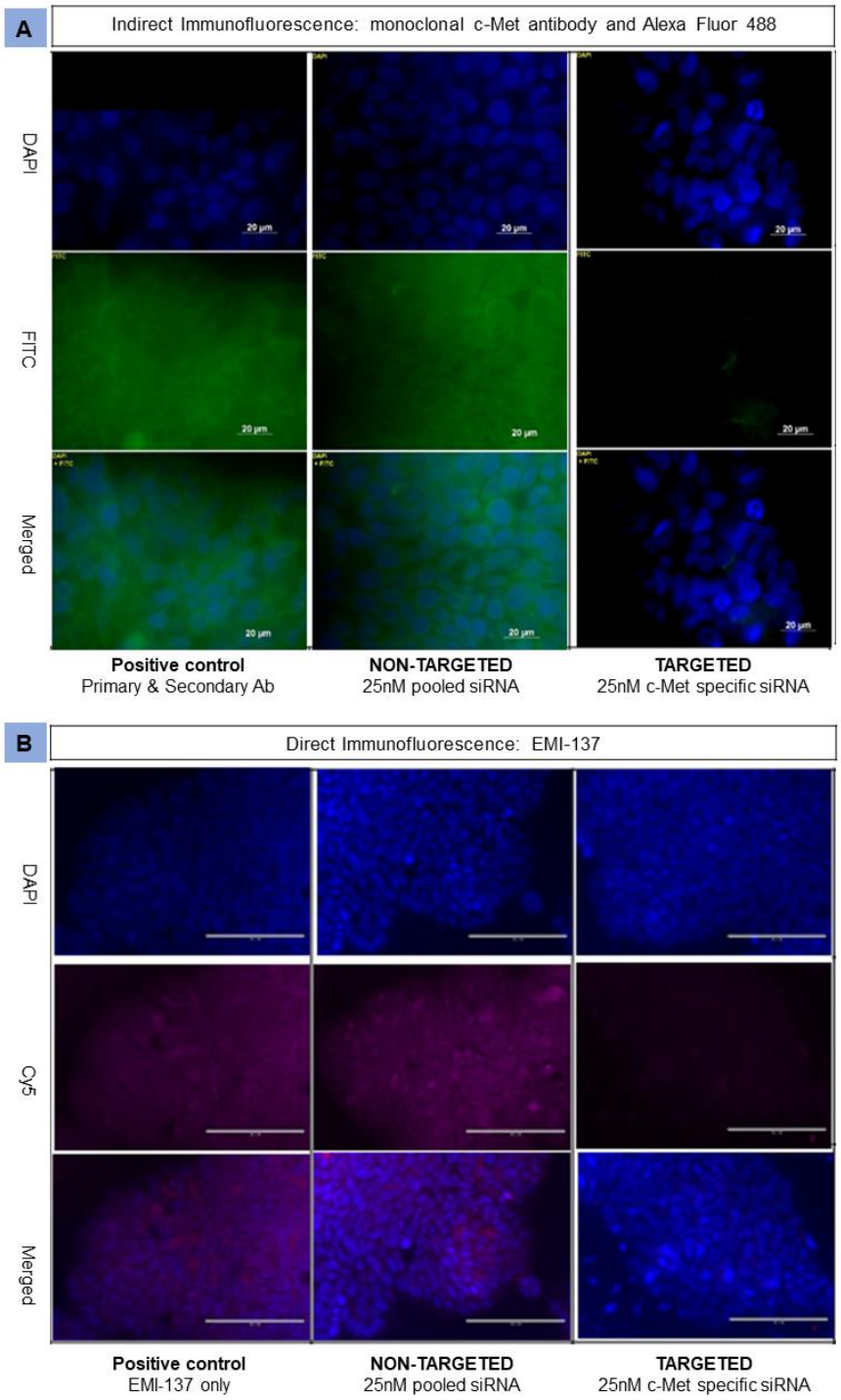

Figure 24: HT-29 incubated with 25nm of pooled c-Met targeted SiRNA and untargeted SiRNA. C-Met protein located with a) 1:200 monoclonal c-Met antibody and 1:300 Alexa Fluor 488 fluorescent secondary antibody. Zeiss fluorescent microscope at x40 magnification. b) HT-29 incubated with 500nM EMI-137 and imaged using the EVOS inverted fluorescent microscope at x40 magnification.

The specificity of EMI-137 for the c-Met transmembrane protein in HT-29 cells was confirmed via temporary c-Met mRNA transcription suppression. HT-29 cells were transfected with pooled c-Met targeted SiRNA for 72 hours at a concentration of 5nM, 15nM, or 25nM or with untargeted SiRNA of a matched concentration. C-Met protein expression was detected by direct or indirect labelling with the novel fluorophore EMI-137 or with anti c-Met primary antibody and a FITC conjugated fluorescent secondary antibody respectively.

The positive control images in

Figure 24 show identical cell membrane binding with the two fluorescent combinations (a and b). This confirms EMI-137 is selective for the human c-Met protein expressed by HT-29 cells and comparable to the monoclonal antibody and fluorescent secondary.

The untargeted SiRNA treated HT-29 cells showed near identical morphology to their matched positive control, confirming the mode of action of the untargeted SiRNA and the continued c-Met protein expression by these cells. EMI-137 appears to give a brighter fluorescent signal at a concentration of 500nM when compared to the antibody combination and showed marginally less non-specific background binding. A concentration above 500nM is prohibitive to fluorescent imaging of HT-29 c-met expression.

3.5 ANIMAL MODEL RESULTS

Mouse Model Organ Fluorescent Imaging

A suitably sized tumour developed on the flank in 11 of the 12 female athymic mice selected. Owing to their lack of bladder control and therefore inability to store and concentrate urine, blue urine discoloration was not observed if the mice.

Figure 25 shows the fluorescent signal of each organ dissected from the mice at one, four and six hours post intravenous administration of EMI-137. The kidneys and xenograft showed high fluorescent signal relative to the control and other organs.

The lack of fluorescence in control animals excluded this being the result of auto-fluorescence only. From the pre-clinical data supplied by EM Imaging Ltd we expected renal excretion of EMI-137 and therefore the high renal signal was to be expected. At 6 hours post administration, kidneys from treated mice showed very low fluorescent signal, whereas the xenograft remained bright. The reducing renal signal relative to kidney indicates EMI-137 is specific and shows prolonged binding to the human c-Met protein, whereas kidney immunofluorescence represented excretory flow only. With increasing duration from injection, there was increased xenograft signal relative to kidney. The lack of signal in the other mouse organs confirmed EMI-137 specificity for human c-Met protein.

Immunofluorescence

Fresh frozen tissue from selected control and EMI-137 treated animals was imaged with standardised fluorescent imaging settings at x60 magnification. The composite images show bright membranous and cytoplasmic fluorescent signal at the expected wavelength of EMI-137 excitation/emission, relative to the DPBS-treated negative control *(*

Figure 26). There was maximal fluorescence in the xenograft tissue between one- and four-hours post-administration, with an overall reduction in signal at six hours post administration.

This likely demonstrated clearance of the EMI-137 compound from the tissue and circulation. *Figure 25* shows continued mouse kidney fluorescence at 6 hours post-administration, indicating there was ongoing renal excretion of EMI-137 by the mice at this time-point.

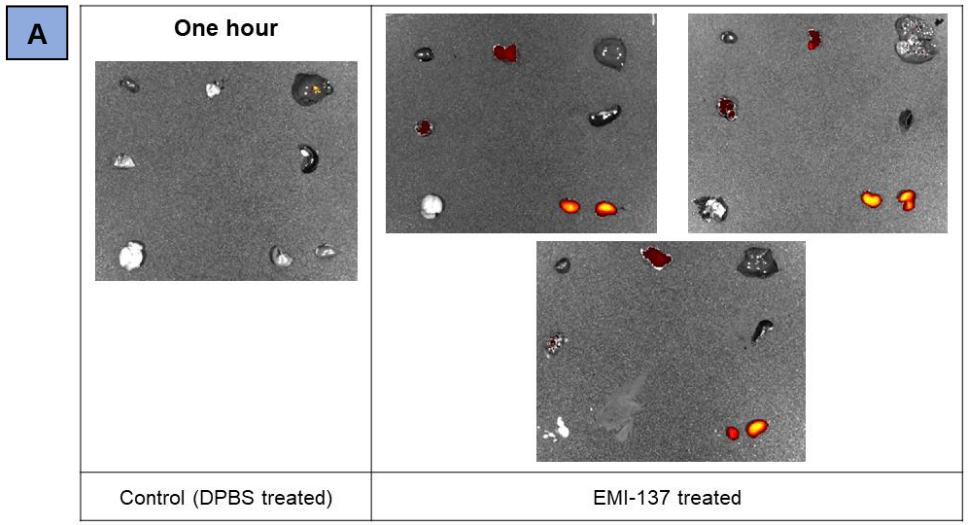

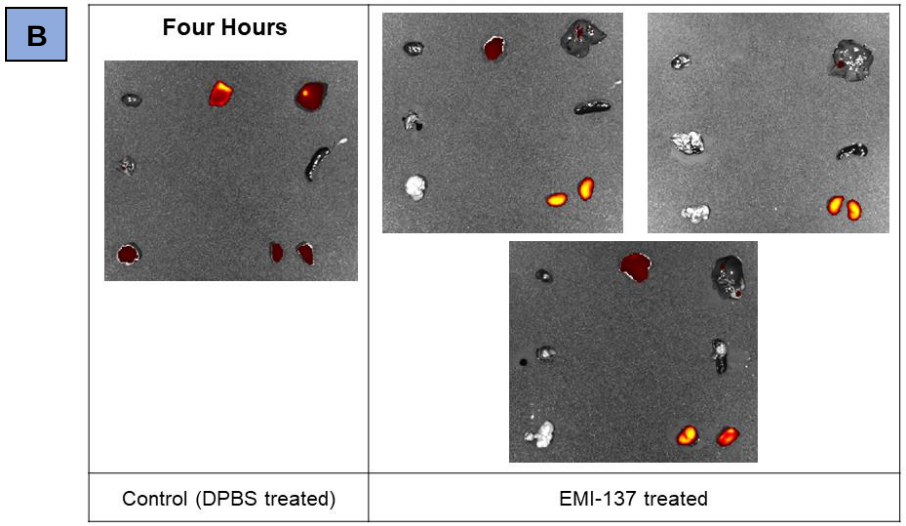

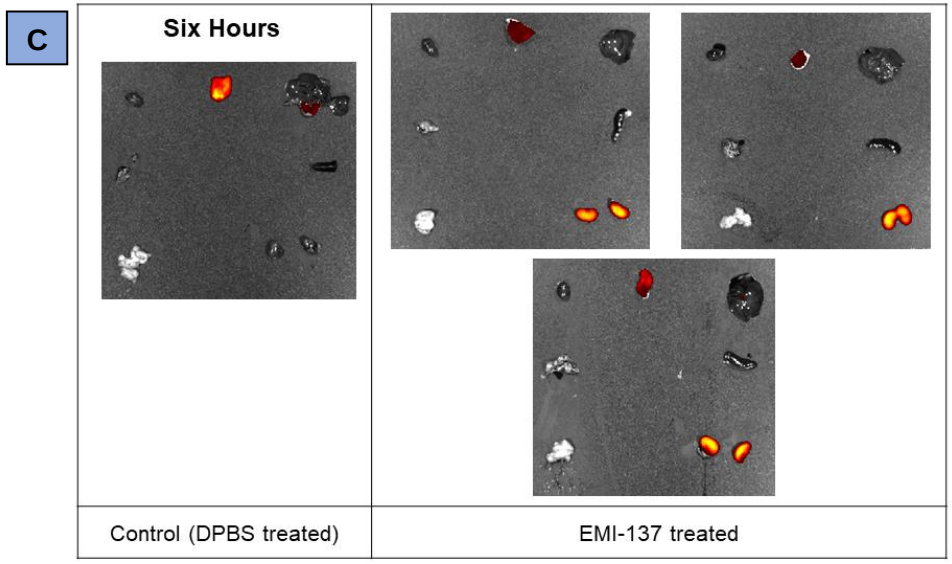

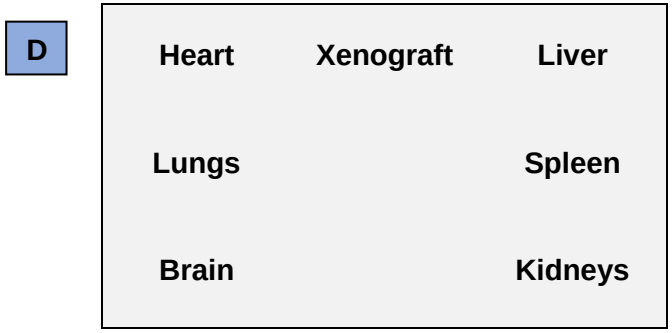

Figure 25: Dissected organs from each mouse. PBS control versus treated with 0.18mg/kg EMI-137 at each time point. Clockwise from top left A) One-hour post administration B) Four hours post administration and C) Six hours post administration. d) Organ lay-out index map. Imaged using the IVIS Spectrum In-Vivo Imaging System.

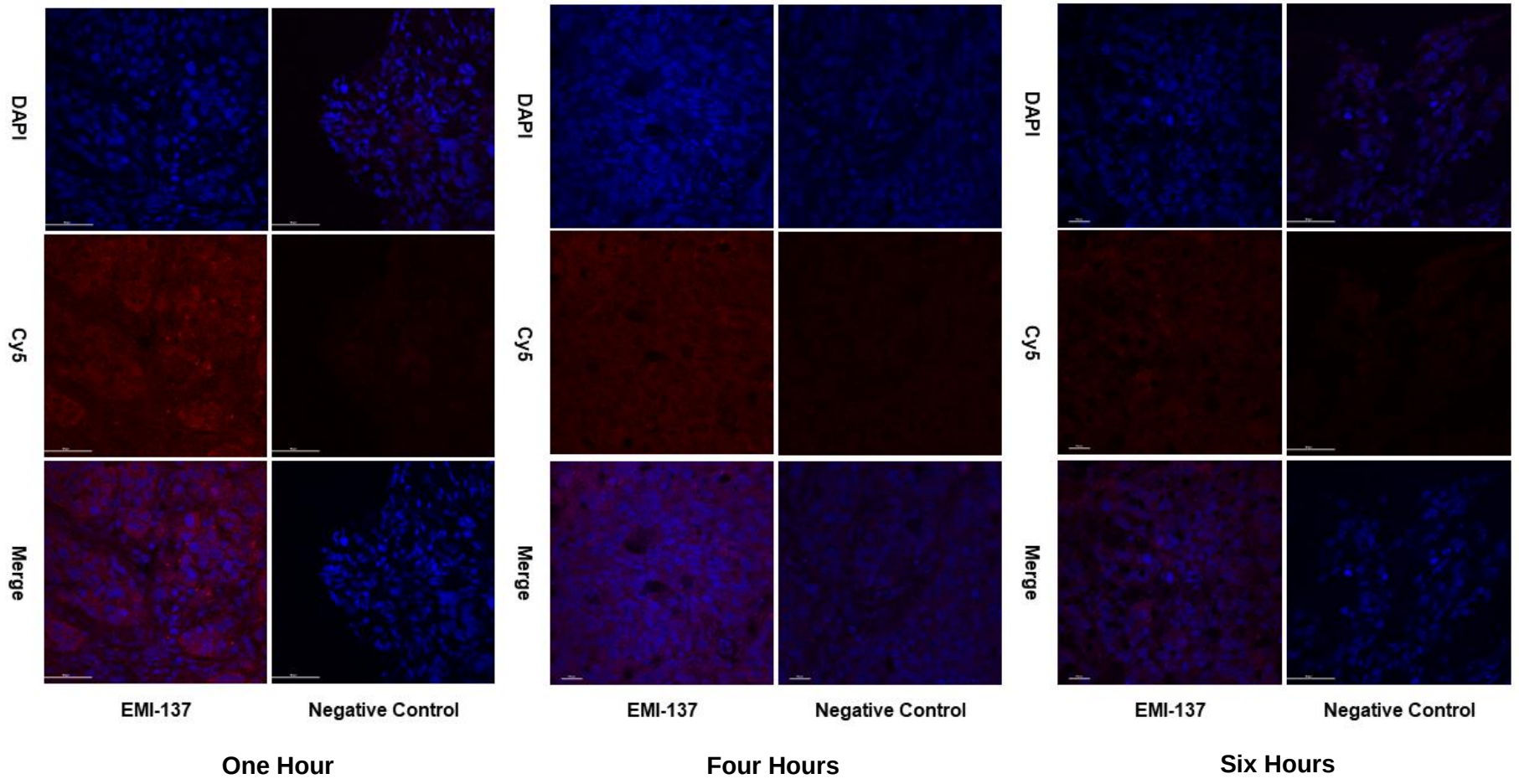

Figure 26: HT-29 colorectal cancer xenograft from BALB/C nude mice imaged at various time points post IV administration of 0.18mg/kg EMI-137. Imaged with Nikon Eclipse Ti inverted microscope mounted on Nikon A1R Confocal Laser Scanning Microscope at x60 magnification

3.6 DISCUSSION

Colonic cancer is a leading cause of cancer related death in the UK and around the world(140). Current methods of detecting pre-operative tumour stage and lymph node status are imprecise and this makes planning the radicality of surgery difficult(166,224). The c-Met targeted peptide, EMI-137, is a novel potential solution to this problem. *Burggraaf et al* have demonstrated EMI-137 shows high affinity for the c-Met receptor and can significantly increase the polyp yield in high risk patients with the addition of fluorescence guided colonoscopy(218). The aim of this pre-clinical work was to assess c-Met expression in colorectal cancer and explore the ability of EMI-137 to detect and visualise c-Met protein expression.

2D model of c-Met Expression in CRC

With Western blot, I identified a colorectal cell line that consistently overexpressed c-Met protein - the well differentiated cell line, HT-29. I was then able to use HT-29 cells to model colorectal cancer for further analysis. Temporary silencing of c-Met mRNA transcription in HT-29 confirmed that EMI-137 has high specificity for colorectal cancer c-Met receptors and could be imaged with fluorescent microscopy.

The optimum concentration of c-Met SiRNA to achieve detectable c-Met mRNA transcription suppression in a monolayer of HT-29 cells was determined as 25nM. Above 25nM there was no further reduction in signal, but the potential for off-target effects was higher. The HT-29 cells treated with the control pooled non-targeting SiRNA continued to show high detectable levels of c-Met expression regardless of SiRNA concentration. The optimum concentration of EMI-137 for c-Met protein imaging was also determined as 500nM.

By conducting these experiments, I was able to optimise conditions to compare direct immunofluorescence with EMI-137 against the standard two-step indirect immunofluorescence method.

This research confirms that the HT-29 cell line expresses high concentrations of c-Met protein and EMI-137 is selective for the human c-Met protein expressed by HT-29 cells. The results appear to show EMI-137 is comparable to the commercially available c-Met monoclonal antibody.

3D Murine Model of CRC

The xenograft models of colorectal cancer developed in female nude athymic mice showed that EMI-137 was uptaken preferentially by binding to high c-Met expressing HT-29 cells *in vivo*. The xenograft showed high fluorescent signal relative to other mouse organs and the DPBS treated control. The strong kidney fluorescent signal confirmed the rapid renal excretion of EMI-137. The signal detected in the control tissue probably represents a degree of autofluorescence from the highly vascularised liver tissue due to the automatic settings of IVIS microscope which could not be optimised further.

Similar results were also found in immunofluorescent imaging of fresh frozen samples of EMI-137 and DPBS treated mouse kidney and xenograft. The differing pattern of fluorescent signal seen between the two tissue types and the control may represent membrane binding and/or internalisation of the EMI-137 probe by the c-Met expressing xenograft, whilst the renal tissue is likely to represent tubular clearance only.

Limitations

Primary tissue culture produces a homogenous monolayer of identical cells. They have equal access to nutrients and demonstrate similar cell-to-cell adhesions properties. Although 2D culture is extremely useful in clinical research, it has its limitations and does not fully replicate the tumour micro-environment. The HT-29 cell line used is a low grade, well differentiated line. This might not replicate the typical nature of colorectal cancer encountered in clinical practice.

It also contradicts the findings of multiple previous studies which have found c-Met expression is directly related to tumour advanced stage and is a prognostic indicator of advanced disease and vascular invasion(204,206,207).

I have compared direct and indirect immunofluorescence with SiRNA silencing techniques in section **Error! Reference source not found.** and section 3.4.3. These techniques are not always directly comparable and should be interpreted with caution. For greater understanding and accuracy, I would have explored the propriety c-Met peptide and fluorescent tag developed by EM Imaging Ltd separately and compared the results to the combined peptide and the indirect immunofluorescence. Exploration of the fluorescent tag coupled to an untargeted peptide would have been extremely useful. However, these components have not been made available to the research group at Leeds and only the combined molecule could be evaluated.

Mouse xenografts are a 3D model and therefore can demonstrate the altered cellular metabolism and protein expression in response to variable access to oxygen and vital nutrients we see with human *in vivo* colorectal cancer. Colorectal tumours are highly heterocellular systems composed of cells of epithelial, mesenchymal, and lymphoid origin. However, this xenograft was composed of a single cell type. HT-29 cells form a well differentiated adenocarcinoma model of colorectal cancer. This homocellular malignant proliferation model may not accurately represent the heterogeneous nature of a colorectal tumour *in vivo*.

The immunohistochemistry performed on the FFT samples confirms the technique has been optimised and c-Met can consistently be detected in human colonic tissue samples, even after long periods of storage at -80°c. However, the small number of FFT samples available and lack of information regarding the tumour stage and pre-morbid patient state limits the wider interpretation of the IHC performed.

This pre-clinical research using 2D and 3D models has confirmed c-Met is a feasible target in colorectal cancer fluorescent guided imaging. I have established consistently high levels of c-Met expression in HT-29 cells with western blot and was able to confirm that EMI-137 shows high specificity for the human c-Met receptor in colorectal cancer with immunofluorescence. The animal xenograft model of colorectal cancer further confirmed that EMI-137 is highly specific for human c-Met and can be imaged with our IVIS imaging system.

The next stage of this research was to define c-Met expression in a large sample of human colorectal cancer tissue via immunohistochemistry and to progress to a small phase IIa clinical trial of EMI-137 in laparoscopic colorectal cancer surgery.

4. CHAPTER FOUR

C-MET PROTEIN EXPRESSION QUANTIFICATION IN A COLORECTAL CANCER POPULATION: FFPE TISSUE FROM THE MRC CLASICC CLINICAL TRIAL

4.1 AIMS & OBJECTIVES

i. To optimise the method of quantification of c-Met expression in colorectal and normal tissue with immunohistochemistry.

ii. To correlate c-Met IHC expression scores with final pathological stage (TNM v5.0) in CLASICC cohort.

iii. To explore c-Met as diagnostic biomarker of colorectal cancer (CRC)

   a. To develop and utilise a semi-quantifiable grading system to examine the average c-met protein expression in human CRC tissue relative to matched normal control tissue

   b. To determine the sensitivity and specificity of c-Met as a diagnostic marker of CRC.

   c. To determine the IHC cut-off threshold for c-Met as a diagnostic marker of CRC.

   d. To determine the Area Under Curve and predictive likelihood of c-Met as a diagnostic marker in CRC.

4.2 METHODS

The antibody used (Rabbit monoclonal anti c-Met antibody (ref: ab51067) Abcam Plc) had been validated in mouse and human tissue for IHC and immunofluorescence. The antibody was used at dilution concentration of 1:250 throughout. Reagent batch numbers and timings were recorded for each run of IHC performed and stored securely in the trial specific laboratory folder. The method was optimised and validated in control fresh frozen tissue obtained from the Leeds Multidisciplinary Research Tissue Bank prior to undertaking the CLASICC tissue c-Met quantification process.

Control Samples

Fresh Frozen Tissue (FFT) samples of colonic tumour, normal tissue and colonic adenomas (polyps) were obtained from two anonymised patients (c0007 and c0008). The tissue was obtained from the Leeds Multidisciplinary Research Tissue Bank (RTB) held under active project license from Prof D Jayne and with support of laboratory RTB manager S Perry.

Analysis of these samples explored c-Met expression in early and pre-cancerous lesions as compared to the late cancerous lesions obtained in the trial. It also assessed the impact of formalin fixation on background staining and possible auto-fluorescence on imaging results obtained.

Control Slide Preparation

The tissue was embedded in Optimal Cutting Temperature Compound (OCT) and snap frozen. Samples had been stored at -80°C in a HTA approved facility at the University of Leeds, UK. Ten-micron (10µm) thickness sections of frozen tissue were produced using the Leica GeoSystems CM3050 S cryostat (Leica Geosystems Holdings AG; St. Gallen, Switzerland) at -28°C. Sections were mounted on to Superfrost Plus Adhesion glass microscope slides (Thermo Fisher Scientific, Altrincham, UK) and returned to -80°C. Immediately prior to use, the slides were slowly defrosted at RT for 30 minutes and rehydrated in PDS solution.

CLASICC Tissue Samples

The Medical Research Council (MRC) CLASICC randomised controlled trial was a superiority, parallel group, randomised controlled trial of laparoscopic assisted versus conventional open surgery in the treatment of colorectal cancer (Trial Number ISRCTN74883561). CLASICC recruited 794 patients from 27 UK centres undergoing CRC surgical resection surgery between 1996 and 2002. Consent was obtained from participating patients for biopsies of

normal colonic epithelium and CRC to be stored for future research. The study aimed to compare completeness of oncological resection, peri-operative mortality, patient-reported quality of life outcome measures and long term survival between the two surgical approaches(152,153,155). Final pathological staging of the resected CRC specimen was reported according to the contemporary American Joint Committee on Cancer (AJCC) TNM Classification of Malignant Tumours, Fifth Edition (1997)(225).

CLASICC Tissue Microarray (TMA) Preparation

Formalin Fixed Paraffin Embedded (FFPE) colorectal cancer and matched normal colorectal mucosa tissue core samples deemed most representative at Hematoxylin and Eosin (H&E) staining, provided by a representative sample of 280 patients recruited in to the CLASICC trial, were incorporated in to seven anonymised Tissue Microarrays (TMA) (Ethics London-Dulwich Committee - 12/LO/1327, approval granted in 2012) by S Yeluri previously. Each TMA contained three 0.6mm core tumour samples and three matched normal tissue samples from each of the 280 participants. Control normal tissue archival samples of placenta, ovary, prostate, kidney, epididymis, liver, gallbladder, stomach, oesophagus, pancreas, small bowel, lung and muscle held within the University of Leeds archive were incorporated into the TMA margins for comparative and orientation purposes. Comprehensive TMA block indexes were produced and stored securely at the University of Leeds and utilised during sample analysis.

CLASICC Slide Preparation

Five-micron sections from the TMA blocks were prepared with the Leica RM2235 Manual Rotary Microtome (Leica Microsystems (UK) Ltd, Milton Keynes, UK), mounted on SuperFrost AdhesivePlus glass slides with the aid of a thermostatic water bath maintained at a constant temperature of 47°c and dehydrated overnight in a drying cabinet. To ensure resistance to mechanical manipulation, slides were heated at 78°c for 10 minutes on the Leica HI1220

flattening table (Leica Microsystems (UK) Ltd, Milton Keynes, UK) and allowed to cool at RT. The prepared slides were then de-paraffinised in xylene and 99.8% v/v ethanol and rehydrated in water according to laboratory SOP in preparation for specific antibody probing and imaging.

4.2.1 Immunohistochemistry

Antigen Retrieval

The FFPE CLASICC trial TMA tissue required antigen retrieval prior to immunohistochemical processing. The fresh frozen control tissue from the RTB did not require this step. Heat induced antigen retrieval was performed by placing the slides into citric acid buffer solution adjusted to pH6.2, and into a microwave for 10 minutes at 900W. The slides were allowed to cool at RT then washed for 5 minutes in running cold water.

c-Met Expression Immunohistochemistry

The monoclonal recombinant anti-Met (c-Met) antibody ([EP1454Y], Abcam PLC, Cambridge, UK) concentration and protein detection conditions were optimised with human appendix and tonsil tissue obtained from stored samples held on behalf of the research group in accordance with Human Tissue Act (HTA) guidance prior to conducting the experiments described below (data not shown).

Slides were incubated with 1:250 Recombinant Anti-Met (c-Met) primary antibody [EP1454Y] for one hour at room temperature in a humidified chamber. Next, a rabbit specific labeled Horseradish Peroxidase (HRP) immunoenzymatic antigen detection system was used for protein detection and chromogenic visualisation. Slides were incubated with 100µL of HRP containing Equilibrate SignalStain® Boost IHC Detection Reagent (Cell Signalling Technology Inc, Leiden, The Netherlands. Cat: 8114S) as the secondary antibody for 30 minutes in a humidified chamber. Slides were repeatedly washed in TBS solution. Enzymatic chromogenic

detection was performed with the SignalStain® 3,3'-diaminobenzidine (DAB) Substrate Kit (Cell Signalling Technology Inc, Leiden, The Netherlands. Cat: #8059S). Slides were incubated with 100µL of the prepared chromogen reagent for 10 minutes in a humidified chamber at RT. Development of brown tissue colouration was observed. In between each incubation step, the slides were washed repeatedly in a pre-prepared dilute tris-buffered saline (TBS) solution.

A control slide of tissue was prepared in an identical manner except for incubation with the primary anti-c-Met antibody. The control slide was used to exclude background staining or oxidation.

Counterstaining

Counterstaining was performed according to local laboratory protocol. Prepared tissue slides were incubated with Meyer's Hematoxylin solution (Sigma-Aldrich Scientific Inc., Cat: H9627-25G) for 60 seconds and washed under running tap water before incubation with Scott's tap water (laboratory stock reagent). Slides were dehydrated in gradient concentrations of ethanol and cleaned in xylene, then mounted on to glass cover slides with DePeX Mounting Medium for histology and allowed to cure overnight at RT.

Imaging

CLASICC Tissue Imaging

The CLASICC slides were imaged at x40 magnification and digitalised with the Leica BioSystems Aperio AT2 whole slide scanner (Leica Microsystems Ltd, Milton Keynes, UK) and proprietary microscopic imaging platform software by Mr. M Hale in the Virtual Pathology team within the Division of Pathology and Data Analytics at the Leeds Institute of Medical Research at St. James's. Slide images were uploaded to the virtual pathology website portal

(https://www.virtualpathology.leeds.ac.uk/). The slides were viewed with Aperio ImageScope v12.4.0.5043 (Leica BioSystems Pathology Imaging Ltd, Milton Keynes, UK).

RTB Control Tissue Imaging

Bright-field microscopy imaging of prepared slides was performed using the Nikon Eclipse MicroscopyU E1000 automated microscope (Nikon Instruments Inc., New York, USA) at x20 magnification.

4.2.2 c-Met Expression Scoring

A semi-quantified scale used to score CRC biomarker expression developed by J. Tiernan within the research group in 2014(226),(227) was adapted and applied to score the c-Met expression in the CLASICC tissue samples. The system utilised previously established and validated protein expression grading systems(228–231). c-Met protein immunopositivity in epithelial cell membranes from each tissue core was scored. The intensity of the chromogenic reaction was quantified with a numerical scale between 0 and 3 (0 = no detectable expression, 1 = mild expression, 2 = moderate expression and 3 = strong expression). The distribution of membranous c-Met immunopositivity was determined by calculating the percentage of tumour or normal epithelial cells deemed positive as a percentage of all of the tumour/normal epithelial cells in the core total area. For tumour cores, non-cancerous tissue was excluded from the analysis. The intensity and distribution scores generated were multiplied to provide a compound c-Met expression score, with a maximum score of 15 (*Equation 1)*.

The intensity and distribution measurements were done in triplicates for each tissue sample. Cores with insufficient mucosal (epithelial) tissue, for example core samples lost through processing, were discounted. In total, 263 tumour and 253 normal epithelium core triplicates (or pairs if single core not assessable) were suitable for analysis and 242 matched tumour-normal tissue paired samples (86.43% of pairs) were included in the final analysis.

$$\boldsymbol{Total\ c-Met\ expression\ score = \ intensity \times distribution}$$

Equation 1: Equation to calculate total c-Met expression scores of TMA specimens

The scoring criteria was appraised and approved by several colleagues with experience of IHC and grading IHC immunopositivity at consensus meeting prior to initiating the scoring process. Representative examples of c-Met expression at each distribution score (0 to 5) and intensity score (0 to 3) were approved by the group and available for reference throughout the scoring process.

Statistical Analysis

Microsoft Excel and GraphPad Prism 7 (GraphPad V7.04 Software, Inc., California, USA) were used for all data handling and statistical analyses. A D'Agostino-Pearson test was performed to determine the normality and skewness of the data. This confirmed the data was not from a normal Gaussian distribution and guided the selection of non-parametric statistical tests.

A Wilcoxon matched-pairs signed-rank test was used to compare the median rank between the two matched TMA populations, tumour and normal tissue. The Interquartile Range (IQR), and two- tailed p value is reported. A statistical significance threshold *of* $p = <0.05$ was applied. The Wilcoxon matched-pairs signed-rank estimate of the 95% confidence interval (95% C.I) of the ranked median population score for both tissue types and the median difference bound by the IQR is also quoted. This method used binominal probabilities to predict the 95% C.I around the median and is therefore asymmetrical around the median value provided(232). The likelihood ratio, an alternative measure of diagnostic accuracy, is also quoted. In clinical practice, a likelihood ratio of 2 increases the probability of the disease or condition being present by around 15% compared to a negative result(233). A Spearman test assessed the correlation in the matched pair results and provided an overall R value. To account for

uncertainty in the data caused by missing core samples pairs, a sensitivity analysis assuming the highest c-Met expression (compound score 15) for all missing data fields was performed.

To determine the relationship between the final pathological stage (AJCC TNM v5.0) and the c-Met expression observed with IHC, the median c-Met IHC expression for tumour, normal and the difference between the values (tumour minus normal score), for each Tumour (pT) and Nodal stage (pN) (TNM v5.0) was calculated. The Spearman rank correlation between the pT stage, pN stage and difference between tumour and normal tissue score and TMA c-Met expression score was obtained. A Chi-Squared test of trend analysed the relationship between pT stage and pN stage median tumour c-Met IHC expression score to generate a *p value* to determine significance.

A Receiver Operating Characteristic curve (ROC curve) was plotted to determine the diagnostic capability of c-Met protein as a biomarker of CRC and potential intraoperative differentiator of normal from malignant colonic tissue. The sensitivity of c-Met as a predictive CRC biomarker (true positive) rate was plotted as a function of the specificity (true negative) and used to calculate varying decision cut-off thresholds and the relevant 95% C.I. The Area Under Curve (AUC) was calculated to numerically quantify the diagnostic capability of c-Met in discriminating malignant from normal colorectal tissue.

4.3 RESULTS

Method Optimisation

Control RTB Tissue

C-Met expression in fresh frozen tissue samples from two donor patients were analysed with IHC. The three tissue types (normal, tumour and pre-malignant polyp) all showed areas of high levels of c-Met expression relative to negative (untreated) control tissue *(*

Figure 27). These results were used to confirm the required antibody protocol described below and exclude background non-specific chromogenic staining inference. The results also guided the development of the c-Met grading system described. The CLASICC participant samples were compared to the fresh frozen tissue samples. The comparison excluded interference in the IHC results observed by the formalin fixation process.

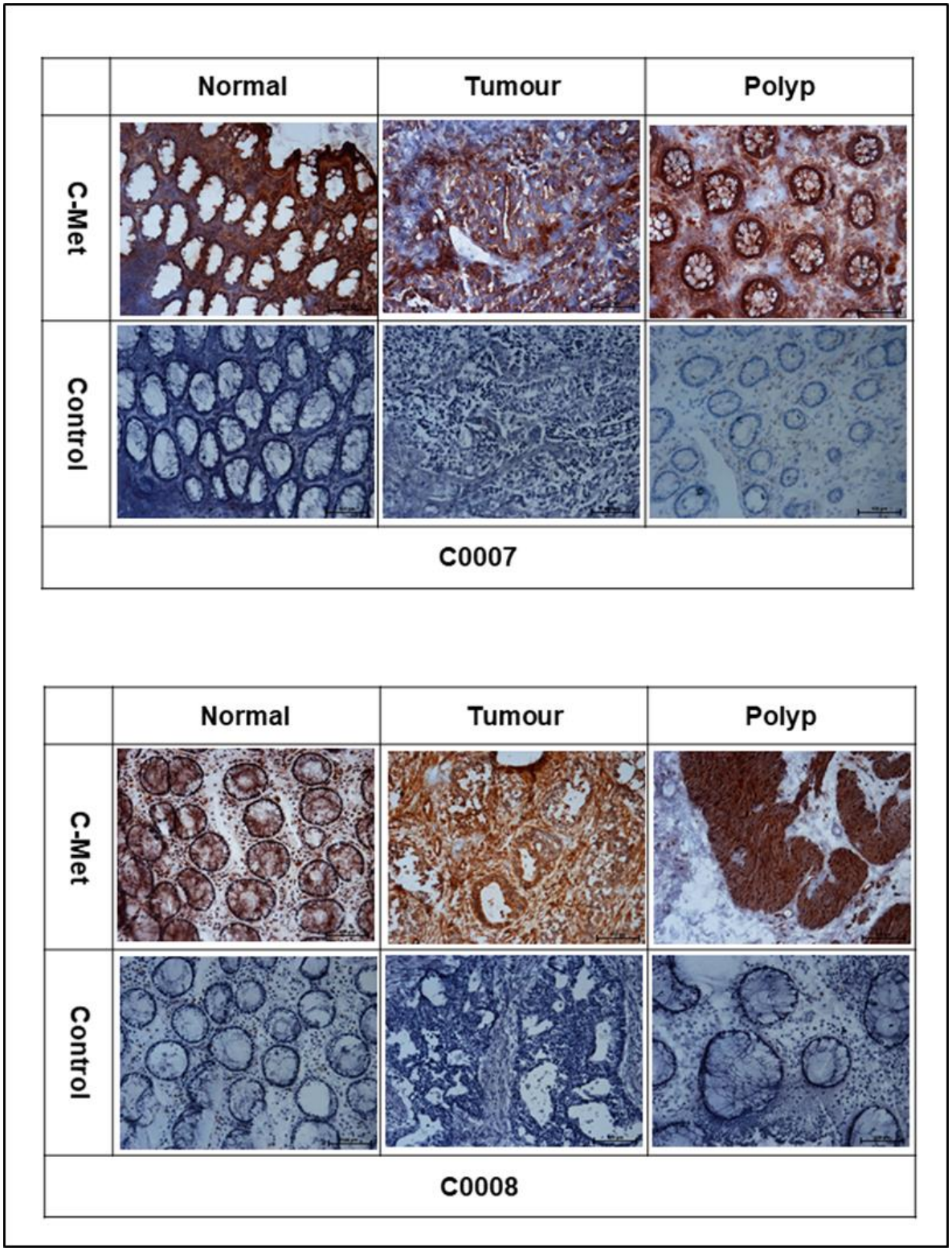

Figure 27: IHC optimisation results. Fresh frozen colorectal malignant, normal and polyp tissue from two donor patients. Immunohistochemistry analysis of c-Met protein expression (antibody concentration 1;250) relative to matched negative control tissue. Imaged at x20 magnification with Nikon Eclipse MicroscopyU E1000 automated microscope.

CLASICC Population Demographics

The key demographic and clinicopathological characteristics of the CLASICC trial 280 patient cohort incorporated in to the TMA blocks is described in

Table 11 (adapted from Tiernan et al (2014), Guillou et al (2005) and Jayne et al (2005)(152,153,227)*).* Forty-six (46/560; 8.2%) individual tissue samples were deemed ungradable (18/280 tumour and 28/280 normal tissue samples). There was an expected pT3 (TNM v5.0) predominance in the population, with a mean age of 68.9 years.

Characteristic	Number of cases (%) *N = 280*
Age range: 33 - 93 years Mean age: 68.9 years	
Gender	
Male	144 (51.4%)
Female	136 (48.6%)
pT stage	
1	10 (3.6%)
2	54 (19.3%)
3	161 (57.5%)
4	52 (18.6%)
Unknown	3 (1.1%)

Table 11: Key clinical and pathological features of CLASICC patient cohort. Adapted from Jayne et al (2007) and Guillou et al (2005) (152,153)

CLASICC c-Met Expression

The c-Met immunopositivity of epithelial cells varied considerably throughout the normal and tumour tissue population; examples of very low and low expression were observed in both populations as shown in *Figure 28*.

The D'Agostino & Pearson normality test confirmed the populations were not sampled from a normal distribution and a non-parametric test was required; skewness -0.6 and 0.3 and kurtosis -1.1 and -1.3 for tumour and normal tissue respectively (*p = <0.0001)*.

Variable c-Met levels detected with chromogenic techniques were observed across the matched specimens. CRC cancers frequently demonstrated stronger c-Met protein expression as compared to normal tissue. High expression was defined as an overall c-Met expression intensity score of 15 and was found in 30.80% (81/263) of CRC samples as compared to 12.25% (31/253) in normal tissue samples *(p<0.0001)*. No detectable c-Met expression with a composite c-Met expression score of 0 was found in 7.90% (20/253) of normal colorectal tissue samples versus 3.42% (9/263) in matched tumours *(p<0.0001).* Representative examples of c-Met expression are shown in *Figure 28* and *Figure 29*.

Wilcoxon matched-pairs signed-rank test showed a significant difference between the median expression scores of normal colonic epithelium and colon cancer. Median c-Met IHC expression scores of 12.0 (95% C.I 10.0 to 13.0; IQR 6.0 to 15.0) and 6.0 (95% C.I 5.0 to 7.5; IQR 2.7 to 12.0) for tumour and normal tissue respectively. The sum of signal rank W score was -133 (*p = <0.0001).* The median differential expression score (tumour – normal) was 2.3 (95%C.I 1.0 to 3.5 and IQR -0.25 to 7.7; *p = <0.0001*) (*Figure 30).*

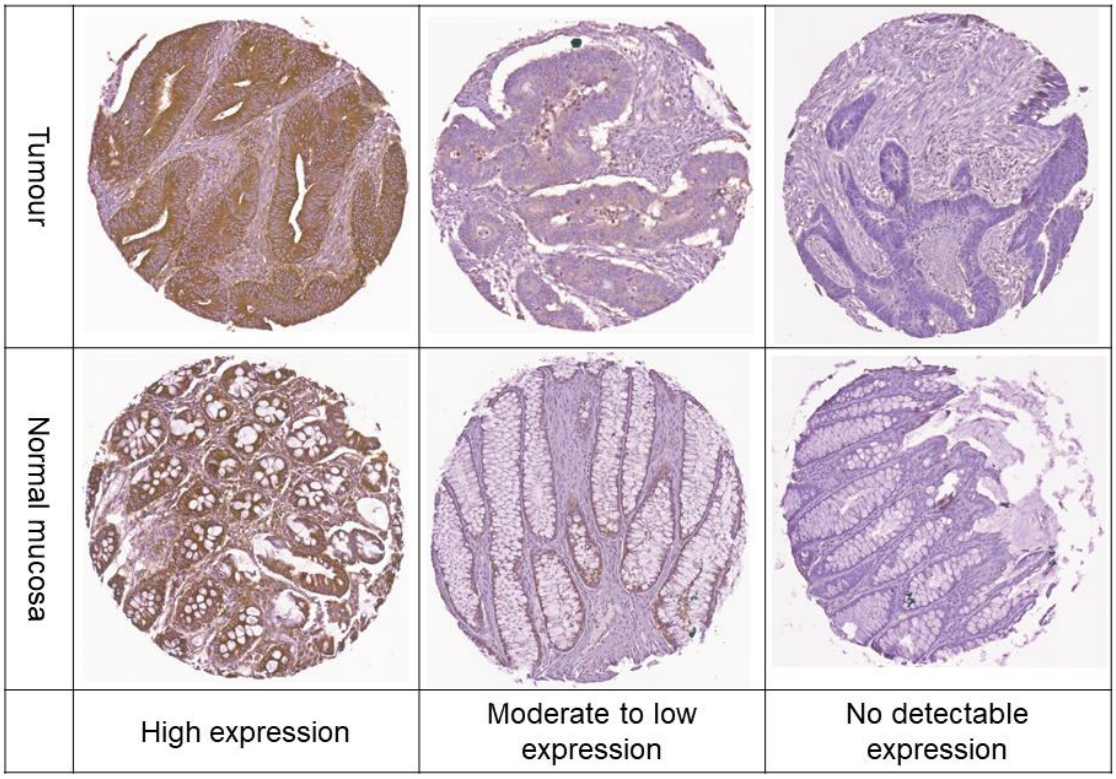

Figure 28: Representative examples of TMA c-Met immunohistochemical chromogenic visualisation.

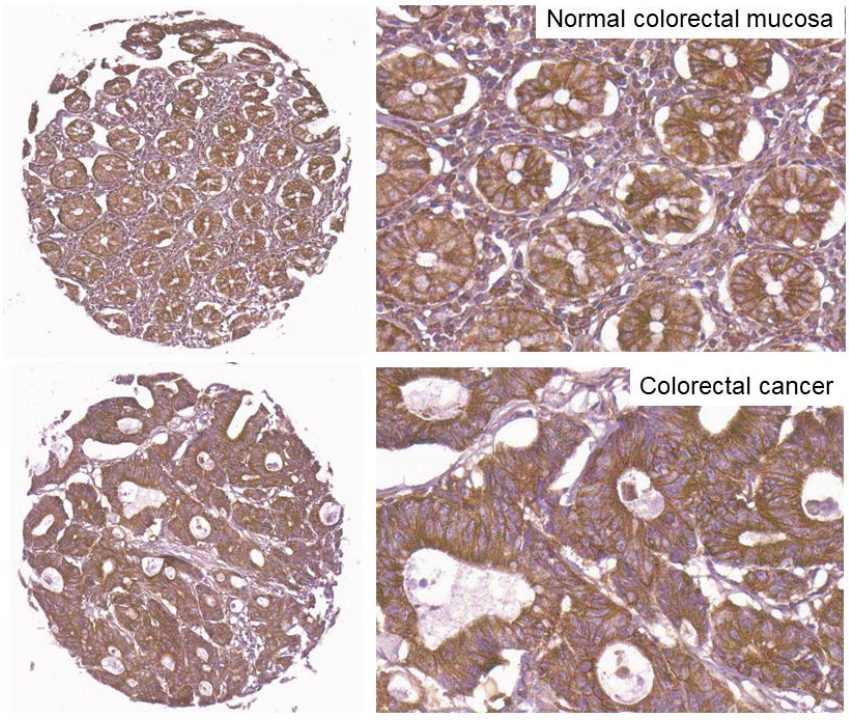

Figure 29: Example of high c-Met expression in normal and colorectal cancer tissue at x13 and x40 magnification.

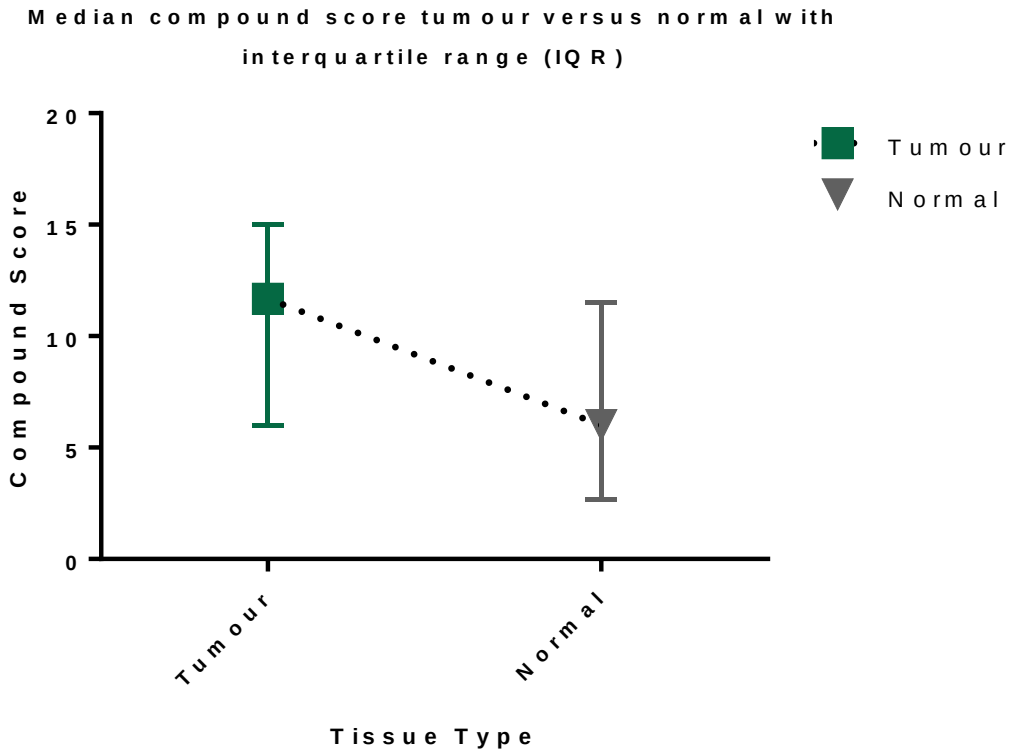

	Tumour	Normal	Difference
Number of pairs	242		
Minimum	0.0	0.0	-14.0
25% Percentile	6.0	2.8	-0.25
Median	12.0	6.00	2.3
75% Percentile	15.0	12	7.7
Maximum	15.0	15.0	15.0
Wilcoxon Matched Pairs Signed Rank Test			
p value (two tailed)	*< 0.0001*	*< 0.0001*	
95% C.I of median difference			1.0 to 3.5
IQR median difference			-0.3 to 7.7
Sum of signed ranks (W)	15397		
Sum of positive rank	22274		
Sum of negative rank	-6877		

Figure 30: Summary of statistical analysis of TMA c-Met expression by IHC tumour versus normal tissue. CLASICC TMA c-Met expression median score and interquartile range. Median difference Tumour – normal tissue 2.33 (95%C.I 1.0 to 3.5).

Correlation Tumour & Normal Tissue Score

The correlation between normal and tumour tissue c-Met expression was statistically significant but yielded a weak overall association between the matched samples; Spearman R value 0.3 (95% C.I 0.2 to 0.4; *p = < 0.0001).* We cannot assume a linear relationship between normal and tumour tissue expression. There was a potential for a strong detectable noise to signal ratio with c-Met as the target for intraoperative optical imaging and differentiation of tissue types.

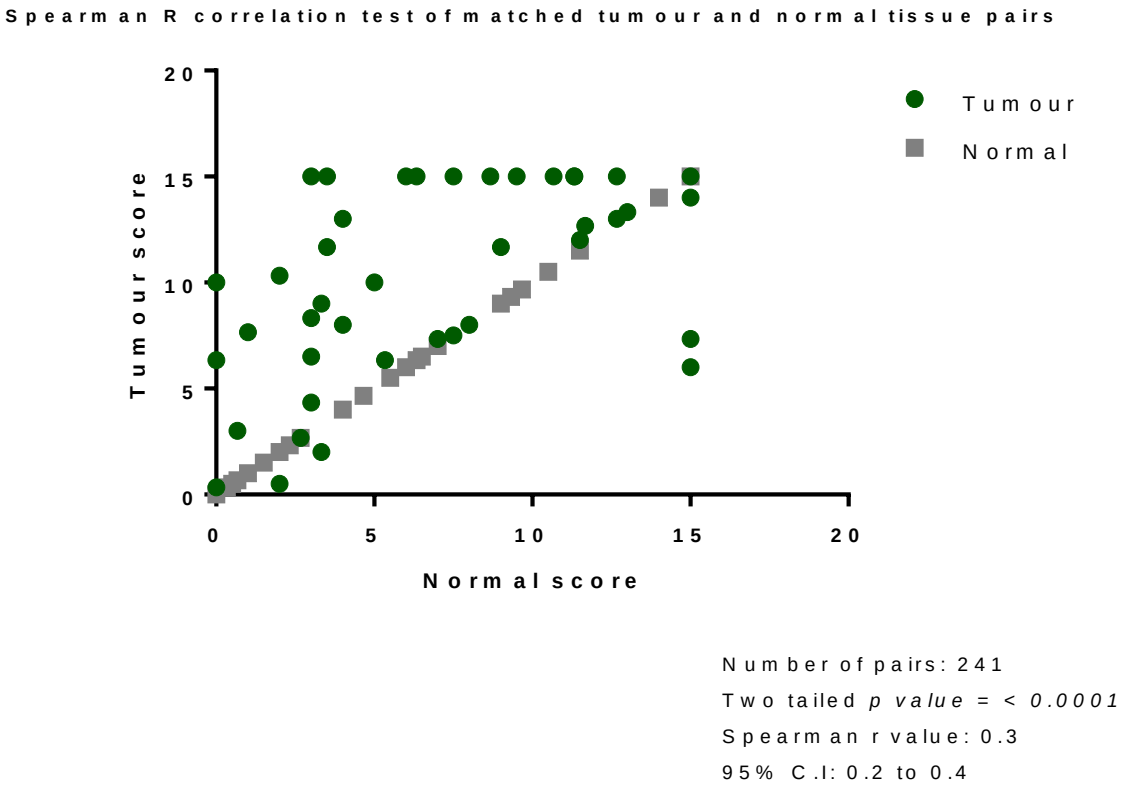

Figure 31: Spearman correlation of c-Met expression. Intensity of tumour tissue plotted as function of matched normal tissue from CLASICC trial participants. N = 241 pairs.

Correlation with TNM stage

T stage	*N*	Median tumour c-Met IHC expression score	S.D	IQR
1	9 (3.5%)	13.3	3.2	4.0
2	51 (20.0%)	11.0	5.8	13.0
3	149 (58.5%)	11.7	4.9	9.0
4	46 (18%)	13.0	5.2	8.0
P value	*0.2*			
N Stage				
0	146 (57.3%)	11.5	5.2	9
1	67 (26.3%)	11.5	5.0	9
2	42 (16.4%)	13.3	5.1	8
P value	*0.2*			
Total	*255 (91.1%)*			

Table 12: Median tumour sample c-Met immunohistochemistry expression score of CLASICC TMA by final pathological Tumour (pT) and Nodal (pN) stage (TNM v5.0) with percentage of total, standard deviation and interquartile range shown, 255/280 TMA tumour samples were suitable for assessment and had TNM stage data available for correlation.

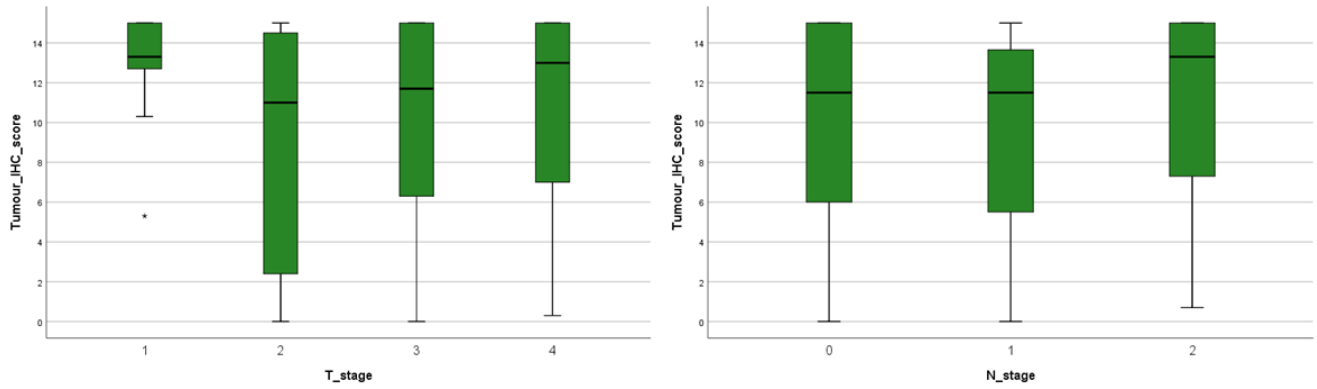

Figure 32: Box and whisker plot of CLASICC TMA median tumour c-Met IHC expression score by tumour (pT) and node (pN) stage with IQR and range shown.

pT stage	*Tumour IHC average*	*Normal IHC average*	*Difference (tumour-normal)*
R	0.04	0.13	-0.14
95% C.I of R	-0.08 to 0.2	0.004 to 0.3	-0.3 to -0.01
P value	*0.5*	*0.04*	*0.03*

Table 13: Final tumour (pT) pathological stage (TNM v5.0) and Spearman correlation with Median c-Met immunohistochemistry expression score of CLASICC TMA with difference between tumour and normal tissue expression score. N = 255 pairs.

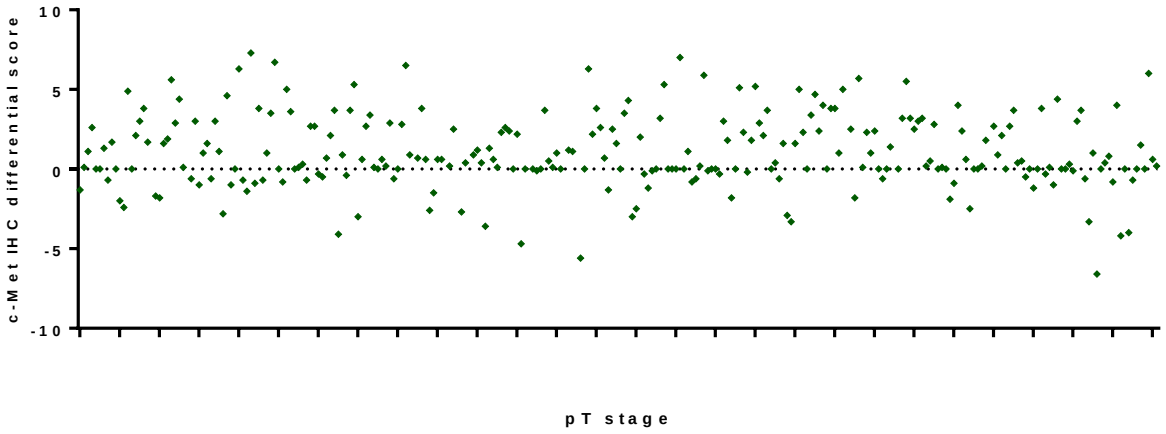

Figure 33: Spearman rank correlation of p stage (ranked from pT1 to pT4) and difference between tumour and normal c-Met IHC expression score in CLASICC TMA cohort samples. Correlation coefficient R -0.14 (p = 0.03). N = 255 pairs.

N Stage	*Tumour IHC average*	*Normal IHC average*	*Difference (tumour-normal)*
R	0.05	0.14	-0.11
95% C.I of R	-0.08 to 0.17	0.01 to 0.3	-0.2 to 0.02
P value	*0.5*	*0.03*	*0.09*

Table 14: Final lymph node (pN) pathological stage (TNM v5.0) and Spearman correlation with Median c-Met immunohistochemistry expression score of CLASICC TMA with difference between tumour and normal tissue expression score.

The final pathological TNM (v5.0) stage and intact TMA triplicates suitable for scoring were available for 255 patients (91.1%) from the CLASICC cohort. Forty-four percent of pT1 (4/9 44.4%) tumour samples had an average tumour IHC c-Met expression score of 15, compared to 24% (13/53) of pT2, 31.4% (49/156) of pT3, and 28.6% of pT4 (Chi Squared test of trend *p = 0.09)*.

The median tumour c-Met IHC expression score was higher for pT1 and pT4 tumours, 13.3 and 13.0 respectively (*Table 12*), although the trend was not statistically significant *(p = 0.2). Figure 32* shows the wide spread of data with a broad IQR observed at each tumour stage.

Spearman rank correlation confirmed there was no evidence of a monotonic relationship between the pT or pN stage and the normal tissue c-Met expression score or the difference between tumour and normal tissue IHC c-Met expression score in the CLASICC cohort (*Table 13* and *Table 14*). The correlation coefficient R is very close to the neutral zero value for pT stage and pN stage, -0.14 *(p = 0.03)* and -0.11 *(p = 0.09)* respectively. *Figure 33* is a visual representation of the spread of data for pT stage and differential c-Met expression score. There does not appear to be any trend in the data or evidence of a relationship between tumour stage and c-Met expression observed with IHC. The *p value* for pT stage and pN stage and median tumour IHC score did not reach statistical significance, *p = 0.5* and *0.5* respectively, so no further conclusions about this relationship can be drawn.

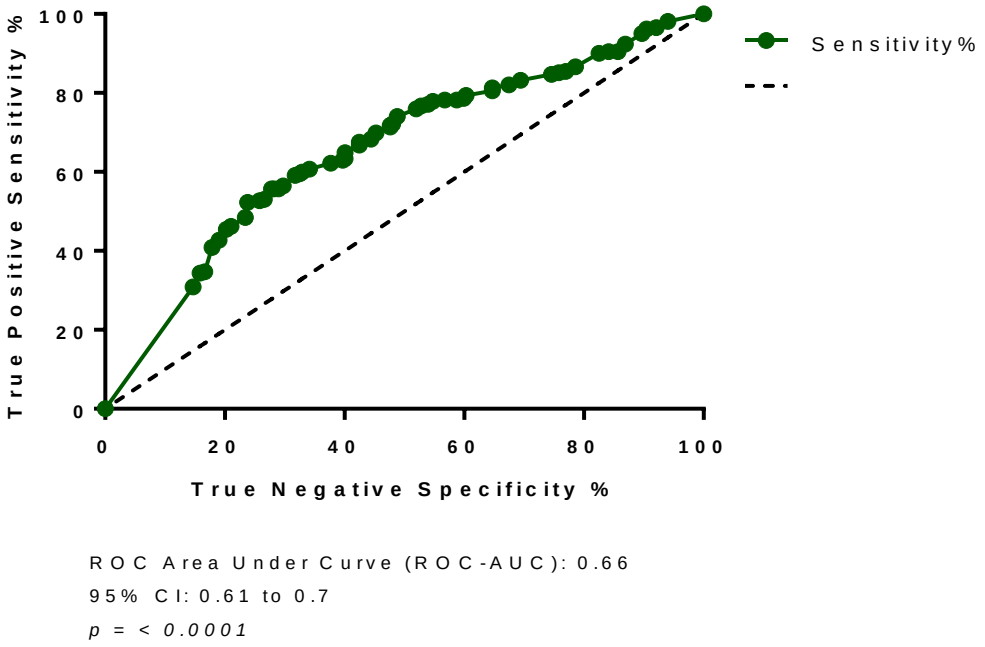

Figure 34: Receiver Operating Characteristic (ROC) curve and Area under Curve (AUC) for c-Met. Sensitivity plotted as function of specificity at various decision thresholds for c-Met as a diagnostic biomarker in colorectal cancer detection.

Receiver Operating Characteristic (ROC) Curve

The Receiver Operating Characteristics (ROC) curve of the sensitivity and specificity of c-Met IHC expression at various thresholds for the diagnosis of CRC is shown in *Figure 34*. The ROC-AUC score yielded an overall predictive probability likelihood of 0.66 (CI: 0.61 to 0.7; *p = <0.0001)*. The 95% C.I indicates the results from the CLASICC study population are likely very close to the actual population diagnostic accuracy value.

A total c-Met expression score of ≥14.5 yielded a high sensitivity of 85.3% (C.I. 80.3% to 89.5%), but there was a substantial trade-off with specificity of only 30.9% (C.I. 25.4% to 36.9%), with a likelihood ratio of 2.1. A combined score of the total sensitivity and specificity from each cut-off generated by the ROC curve was also calculated. This determined the

greatest sensitivity and specificity ratio for c-Met as a CRC detection marker. An overall cut-off expression score of ≥11.6 yielded the greatest combined true positive and true negative rate with a sensitivity for CRC of 55.7% (95% C.I 49.5% to 61.8%) and specificity rate of 71.8% (95% C.I 65.8% to 77.3%); likelihood ratio 2.0. The highest likelihood ratio, 2.3 was observed with a c-Met expression score of ≥13.2; sensitivity 40.8% (95% C.I 34.8% to 47.1%) and specificity 82.1% (95% C.I 76.9% to 86.7%).

Sensitivity Analysis

The sensitivity analysis assumed the highest level of c-Met expression for all missing data (compound score 15). This again confirmed a significant difference in median score between the matched tissue samples, 12.3 (IQR 7.6– 15.0) and 10.0 (IQR 6.0 – 13.3) respectively, with a median difference of 1.0 (IQR -2.0 to 5.0; 95% C.I 0.33 to 1.67; $p = <0.0001$). Similarly, the ROC-AUC analysis showed an AUC value of 0.6 (95% C.I 0.55 to 0.64; $p = < 0.0001$). However, assumed intense c-Met immunopositivity (expression score ≥14.5) yielded a slightly lower CRC predictive value specificity of 78.5% (95% C.I 73.1% to 83.2%) and sensitivity of 33.9% (95% C.I 28.4% to 39.9%), likelihood ratio 1.2.

4.4 DISCUSSION

Oncogenic activation of the transmembrane c-Met protein has been reported to induce multiple intracellular changes leading to the development and progression of cancers(197,200,207,234,235). Overexpression of c-Met has been reported in several gastrointestinal malignancies, including colorectal cancer(236). Previous studies have identified the overexpression of c-Met in CRC as a predictor of poor prognosis and poor overall and progression-free survival(203).

I quantified the expression of c-Met protein using IHC in matched tumour and normal epithelial tissue samples from participants involved in the MRC CLASICC trial. This analysis of TMA tissue from matched tumour and normal tissue samples confirmed the median c-Met protein expression score in a large population of UK colorectal cancer patients who underwent surgery between July 1996 and July 2002. With the adapted grading system applied, I demonstrated that total c-Met transmembrane protein expression was significantly increased relative to matched normal tissue *(p = <0.0001).* The median expression score was significantly higher in tumour compared to normal colorectal tissue, 12.0 and 6.0 respectively. There was poor correlation between normal and tumour tissue and a non-linear relationship (*Figure 31*). This suggests there is potential for a high signal to noise ratio between tumour and normal tissue if c-Met is used as an intra-operative tumour and metastatic lymph node detection agent.

The ROC curve and AUC confirm c-Met could be a potential biomarker for CRC detection. In practice, a score of 12 or over, composed of maximal intensity score (intensity graded as 3 high) in over 60% of epithelial-type cells yields the greatest combined specificity and sensitivity for the detection of colorectal cancer, 76.2% and 52.3% respectively. A total score of 15, composed of maximal expression intensity in more than 80% of cells is highly sensitive, 85.3% but there is a significant trade-off with specificity of only 30.9%. At this threshold the false negative rate is low, but at the expense of a high false positive rate. The likelihood ratio at this decision threshold was 2.1. This translates to the presence of a c-Met expression score ≥14.5 increasing the likelihood of colorectal cancer by little more than 15%.

Overall, 96.6% of all tumour cores analysed demonstrated detectable c-Met expression at IHC. These results correlate with previous research that has shown c-Met is upregulated and overexpressed in gastrointestinal cancers (206,237,238). *Esfahani et al* confirmed c-Met positivity in 81% of 163 CRC samples analysed using a TMA and IHC techniques and concluded there was no statistically significant trend in c-Met expression levels and tumour stage(221).

IHC assessment of protein expression in TMA tissue allowed rapid quantification of c-Met levels in a systematic manner. It required a relatively small amount of tissue from the precious and finite CLASICC tissue resource and the permanency of prepared slides allowed review of results to confirm accuracy and fidelity.

Assessment of colorectal cancer tissue samples from small observational studies, such as *Gayyed et al*, found a strong positive correlation between c-Met expression levels and clinical pathological characteristics(239). However, my analysis of c-Met expression in CRC TMA samples obtained within the rigors of a large randomised controlled trial discredit this. I did not find any evidence of a monotonic relationship between pT or pN stage and differential c-Met expression scores at IHC in the samples analysed. The c-Met protein is consistently overexpressed in CRC relative to matched normal tissue and c-Met has the potential to be a useful tissue biomarker but its expression does not correlate with disease stage (*Figure 33, Table 13 and Table 14*). This work suggests c-met is present at all stages of disease in variable quantities. Fluorescent detection of c-Met may aid intra-operative navigation for both early and advanced tumours at laparoscopic resection surgery.

Limitations

There are limitations to this experiment and the subsequent inferences of the efficacy of c-Met as potential biomarker of CRC in laparoscopic resection surgery with EMI-137. The TMA tissue samples were obtained from the “most representative” area of tissue in the tumour and normal tissue provided by individual participants. The exact location of the sample was not provided. The samples are most likely a mix of central and peripheral tissue. The tumour microenvironment is highly heterogeneous and hypoxia upregulates expression of c-Met protein(202). Central tumour samples obtained from areas of reduced oxygen delivery could potentially show an increase in c-Met expression relative to peripheral samples from areas of tumour with adequate oxygenation.

Immunohistochemistry only allows a semi-quantitative assessment of protein expression. The grading system applied was at risk of subjectivity bias and there were a limited number of scoring combinations possible. An alternative method, such as real-time quantitative polymerase chain reaction (q-PCR), would have provided continuous numeric data of c-Met DNA transcription and may have been a more objective measure.

The data supports the results of smaller studies and is the largest cohort of patients samples obtained within the confines of an RCT. *Tiernan et al* confirmed the potential of Carcinoembryonic Antigen (CEA) as a biomarker in CRC and used a very similar scoring method to this study(228). They identified increased CEA expression in CRC tissue when compared to corresponding normal tissue. c-Met expression levels in my study were inferior to CEA, but it outperformed the other common cancer biomarkers explored by Tiernan *et al*: Epidermal Growth Factor Receptor (EGFR), Folate Receptor Alpha (FRα) and Tumour-Associated Glycoprotein 72 (TAG-72)). Previous research suggested a possible link between c-Met amplification and resistance to EGFR inhibitors in metastatic CRC(213,214). A possible area of further research would include co-expression of c-Met and EGFR and the crosstalk between these signalling pathways in CRC.

The investigational medical product, EMI-137, explored during this thesis is known to be internalised in the presence of the ligand HGF(221). In trial participants, with endogenous HGF present, I expected the EMI-137 to bind to the tumour and lymph node surface c-Met receptor and be internalised. This is likely to increase the overall fluorescence and c-Met targeted detection. To date, the intensity of fluorescence and depth of tissue penetrance of EMI-137 has not been clearly defined. For EMI-137 to function as an intraoperative imaging agent, it must bind to the transmembrane receptor and the fluorescent tag must be excited by the appropriate wavelength of light. Therefore, the c-Met receptor must not only be accessible to the EMI-137 molecule but also in a relatively superficial or peripheral location to allow excitation of the Cy5 fluorescent tag and detection of the light emitted. The density,

accessibility and location of the c-Met protein is important for the diagnostic yield of EMI-137 in intraoperative colon cancer mapping and will be explored in a phase IIa trial.

Immunohistochemical analysis of c-Met expression in human tissue samples showed a significant differential expression between matched normal colonic epithelium and colorectal cancer. Malignant tissue consistently overexpressed c-Met protein, relative to normal tissue. EMI-137 is a c-Met targeted peptide coupled to an inert fluorophore. The presence of endogenous HGF may increase the internalisation of the imaging molecule and facilitate clear fluorescent tumour and lymph node localisation. These pre-clinical results indicated c-Met was overexpressed by CRC tissue relative to background, although results did not correlate with disease stage, there was sufficient evidence of a potential therapeutic advantages to warrant exploration of EMI-137 in the intraoperative setting for the resection of colonic cancer and regional metastatic lymph nodes during laparoscopic surgery.

5 CHAPTER FIVE

EMI-137 AS AN OPTICAL IMAGING AGENT IN COLON CANCER: A PHASE IIA CLINICAL TRIAL

Name: Gemma Armstrong

Student No: 201073014

5.1 AIMS AND OBJECTIVES

Primary Objectives

The purpose of this study was to investigate the ability of EMI-137 to produce visible fluorescence of colon cancer during laparoscopic surgery. We hypothesised that colon cancer and/or metastatic lymph nodes would preferentially uptake the EMI-137 marker due to overexpression and/or upregulation of the c-Met receptor and this would allow intraoperative localisation of the primary cancer and diseased lymph nodes.

The pre-clinical research conducted and described in Chapters 2 and 3 supported the hypothesis that c-Met was a suitable imaging target in colon cancer and that EMI-137 showed the required sensitivity and specificity for human c-Met to facilitate intraoperative delineation of colonic tumours and metastatic lymph nodes.

The primary aim of this trial was to investigate the ability of EMI-137 to produce visible fluorescence of colon cancer during laparoscopic surgery.

Secondary Objectives

1) To investigate the ability of EMI-137 to produce visible fluorescence in regional lymph nodes draining the colon cancer.
2) To investigate the concordance of visible fluorescence in colon cancer with histopathological stage and c-MET expression in resected specimens.
3) To investigate the concordance of visible fluorescence in cancer draining lymph nodes with histopathological evidence of metastasis.
4) To explore the tumour (signal) to background (noise) fluorescence
5) Investigation of the safety profile of EMI-137

6) Exploration of systemic, operative, and patient factors, which adversely affect EMI-137 fluorescence detection of colon cancer.

7) Study of *in vivo* imaging compared to *ex vivo* fluorescent detection.

5.2 CLINICAL TRIAL METHODS

The clinical feasibility study of EMI-137 in laparoscopic colonic resections was an early phase clinical trial. It explored the feasibility of EMI-137 as an intraoperative imaging agent in patients undergoing laparoscopic colonic cancer surgery at LTHT.

5.2.1 Trial Design

This trial was designed as an unblinded, non-randomised, phase IIa feasibility study. The trial was conducted at the single site, St James' University Hospital in Leeds, with support from the University of Leeds. The eligibility criteria are defined in *Table 15.*

The primary aim of the study was to investigate the ability of the novel c-Met targeted fluorescent imaging agent, EMI-137, to produce visible fluorescence in colon cancer during laparoscopic surgery. The planned secondary endpoints included exploration of fluorescence in metastatic lymph nodes, dose optimisation, safety, and feasibility outcome measures.

The intraoperative image obtained with EMI-137 and the ability to detect metastatic lymph nodes will be compared to the final pathological stage (TNMv8.0) as the gold standard.

Regulatory Approval

Ethical approval was granted by the Yorkshire and Humber Leeds West Research and Ethics Committee (Y&H REC) (Ref 17/YH/0263) on 27th October 2017. Regulatory approval was

granted by MHRA under The Medicines for Human Use (Clinical Trials) regulations 2004.S.I 2004/131 (Ref 16767/0294/001-0001) 29th August 2017.

Local approval from Leeds Teaching Hospital Trust (LTHT) clinical directorate of Abdominal Medicine and Surgery (AMS) was obtained prior to commencing participant recruitment and active data collection. The trial was conducted in accordance with all quality assurance and ethical best practice guidelines and there were robust systems in place for reporting of any protocol breaches or adverse events to the trial sponsor, the University of Leeds, and the regulatory authorities. LTHT Surgical Clinical Trials Unit (CTU) supported the trial and were actively involved in participant screening, recruitment, and data collection for the duration of the trial.

Substantial Amendments

Introduction of the Union for International Cancer Control TNM v8 classification system Tumour Node Metastasis (TNM) v8.0 classification system on 1st January 2018 at LTHT necessitated a substantial amendment to the trial protocol. Regulatory approval was granted for this prior to trial commencement by REC and MHRA on 5th January and 10th January 2018 respectively.

The Investigator Brochure (IB) and Investigational Medicinal Product Dossier (IMPD) were updated twice by the Industrial Partner and drug supplier (EM Imaging Ltd) to incorporate batch re-test results and new safety information discovered. This facilitated shelf-life extension of the EMI-137 batch supplied to LTHT. MHRA approved the first substantial amendment to these supporting documents in March 2018 and in March 2019.

Non-Substantial Amendments

Non-substantial amendments to the protocol was approved locally by the University Leeds/LTHT Quality Assurance (QA) team:

1. Incorporated a change to external pharmacovigilance reporting processes. This was approved on 14th February 2018.
2. The expected recruitment period was extended by a further six months. This was approved on 4th September 2018.
3. The expected recruitment period was extended by a further six months. This was approved on 15th February 2019.

Participants

The trial recruited 10 participants with a diagnosis of colon cancer at the single LTHT site – St James' University Hospital. The first participant was enrolled into the trial on 14th February 2018.

5.2.2 Eligibility Criteria

The eligibility criteria are listed in *Table 15.*

Inclusion criteria	Exclusion criteria
• Age ≥18 years. • Patients with a diagnosis of colonic cancer (the disease can be of any radiological TNM stage and be located anywhere from the caecum up to but not including the rectosigmoid junction) • Patients with or without distant visceral or lymphatic metastatic disease. • Patients with synchronous colon cancers or polyps can participate. • American Society of Anaesthesiologists (ASA) classification ≤3. • Normal hepatic and renal function (eGFR ≥60 mls/min/1.73m^2) and bilirubin within institutional limits and/or ALT ≤2.5x upper limit of institutional normal value) on serum laboratory blood tests performed ≤30 days prior to EMI-137 administration. • Female participants who are surgically sterile (documented bilateral oophorectomy and/or hysterectomy), post-menopausal (cessation of menses for more than 1 year), or pre-menopausal with two negative urine pregnancy tests performed within 24 hours of administration of EMI-137 Injection. • Pre-menopausal female participants of child-bearing potential who agree to	• Patients who are participating in another intra-operative fluorescence study or have participated in another fluorescence study within 3 months of the planned surgical procedure. • Received an investigational medicinal product at any dose within 28 days of planned EMI-137 administration • Patients with pre-existing inflammatory bowel disease. • Patients who have undergone neoadjuvant chemotherapy to treat the colon cancer. • Patients with impaired renal function (eGFR <60 mls/min/1.73m^2). • Patients with impaired liver function (Bilirubin above institutional limits and/or ALT >2.5x upper limit of normal). • Pregnant and breastfeeding woman. • Pre-menopausal woman planning to become pregnant within 90 days of receiving EMI-137; or pre-menopausal woman of child-bearing potential who refuse to use two forms of contraception for at least 90 days after receiving EMI-137 • Male patients with a currently pregnant partner or male patients who are planning to conceive a pregnancy with a

employ two method of contraception (as defined in eligibility criteria section 8.2) during the study period and for 90 days after EMI-137 administration. • Male participants with a non-pregnant female partner. Male participants with a pre-menopausal partner of child-bearing potential who agree to use two forms of contraception (as defined in section 8.2) during the study period and for at least 90 days after receiving EMI-137. (The only permissible exception would be if the participant had undergone documented bilateral orchidectomy or their female partner is post-menopausal (cessation menses >1 year) or has undergone documented bilateral oophorectomy and/or hysterectomy).	female partner within 90 days of receiving EMI-137; or male participants who refuse to use two forms of contraception as defined in section 8.2 for at least 90 days after receiving EMI-137 with their female partner of child-bearing potential. • Poorly controlled or serious medical or psychiatric illness that, in the investigator's opinion, is likely to interfere with participation and/or compliance in this clinical trial. • Previous adverse reaction to fluorescent agents

Table 15: Eligibility Criteria for Intraoperative Imaging of Colon Cancer using a Fluorescent peptide (EMI-137) against the c-Met receptor feasibility study

Screening and Recruitment

Potential participants were identified thorough the LTHT Colorectal Cancer Multi-Disciplinary Team (MDT) Meeting, the LTHT theatre booking platform, or during outpatient clinic appointments. All participant eligibility screening and recruitment was performed by the clinical research fellow and the participating consultant surgeons, with support from the LTHT Surgical Research Unit (SRU).

Screened participants deemed to me*et al*l the eligibility criteria were approached to participate either in face-to-face interactions or over the telephone. All participants were provided written information in the form of a Participant Information Sheet (PIS) and given verbal information

about the trial at least 24 hours prior to involvement. All potential participants were given the opportunity to ask questions and provided with the name and contact details of a delegated member of the research team if they wished to discuss their involvement further at a later date. All members of the research team were experienced in gaining consent for a clinical trial and had valid GCP training. It was stressed to all potential participants that their involvement was voluntary, they could withdraw at any time, and refusal to participate would not adversely affect the care they received in any way. No incentives to participate were offered to participants.

Patients wishing to participate in the clinical trial were asked to sign a trial specific patient consent form prior to receive EMI-137 and undergoing surgery. Their usual General Practitioner (GP) was also informed of their trial involvement. Patients were assigned a unique trial participant number and baseline preoperative demographics were collected including age, gender, Body Mass Index (BMI), pre-operative blood test results, imaging results, comorbidities and previous surgical history via a paper preoperative Case Report Form (CRF).

5.2.3 Trial Intervention

Fluorescent Laparoscope Equipment and Training

The laparoscope used in this trial was a standard blue light Karl Storz® (KS) fluorescent endoscopy system (Karl Storz Endoscopy (UK) Ltd., Slough, Berkshire, UK) with a propriety detachable red-light camera head filter that was selected for intraoperative imaging with the fluorophore EMI-137. The Clinical Research Fellow and EM Imaging Ltd worked closely with KS Research and Innovation (R&I) team in Germany to develop a laparoscopic system suitable for use with EMI-137 during the trial development stage. The excitation filter in the light source transmitted light from 620 nm to 656 nm, whilst the emission filter transmitted light from 663 nm to 738 nm. This was appropriate for the photo-physical properties of EMI-137 with peak excitation (λmax ex) of 648 nm.

The operating surgeons, Research Fellow, and key members of the theatre clinical team received thorough training from UK based Karl Storz Ltd (Rotherham UK) representatives on safe operation of the fluorescent laparoscope in theatre. An equipment manual was always available and the company representative could be contacted during office hours for technical advice. The representatives were also present in theatre during the early cases should technical support have been required.

Figure 35: Karl Storz® D -Light Fluorescent laparoscopic system (left) and the prototype detachable camera head filter supplied by Karl Storz® Research & Innovation department (right).

Investigational Medical Product (EMI-137)

The Investigational Medical Product (IMP) was supplied by the industrial partner, Edinburgh Molecular Imaging Ltd (EM Imaging Ltd, Edinburgh, UK) to the clinical site, LTHT, with trial specific labels attached which conformed to the Directive 2001/20/EC and Medicines for Human Use (Clinical Trials) Regulation. The IMP was supplied as a dark blue dry powder and was stored in a temperature monitored and controlled refrigerator (between 2$^{\circ C}$ and 8$^{\circ C}$) and shielded from light prior to reconstitution and administration.

Participants received a single weight-adjusted intravenous bolus of EMI-137 (maximum dose 0.13mg/kg) 1 to 3 hours prior to the planned start of their surgical procedure.

Surgical Procedure

The surgical procedure was completed as per surgeon usual technique. Participation in the trial did not require any deviation from the accepted surgical technique of laparoscopic colonic resection. All surgical interventions were performed by consultant colorectal surgeons at LTHT.

Intraoperative Assessment

The KS fluorescent endoscopy system was used to perform the intraoperative fluorescent assessment for all cases. After establishment of a pneumoperitoneum and any required mobilisation/adhesion division, the endoscope was switched to fluorescent mode and an assessment of the fluorescent signal achieved with EMI-137 was performed by the operating surgeon. The fluorescent signal detected in the tumour, any regional lymph nodes, or any suspected or confirmed intra-abdominal metastases was assessed. Any fluorescent nodes were marked with a surgical clip to allow correlation with final pathology nodal status assessment. The signal to noise ratio was also appraised. The fluorescence was graded using

a semi-quantifiable scale and the opinion of the operating surgeon was considered as part of the evaluation process. The assessment was made in relation to the background fluorescence (signal to noise ratio). Data was directly entered into the CRF in the operating theatre by the trial research fellow.

Follow-up

All trial participants received a single trial-specific follow-up 2 to 3 weeks following discharge from hospital. The purpose of this visit was for the assessment of any post-operative complications, including adverse events specifically related to the administration of EMI-137. This follow-up appointment usually coincided with routine postoperative follow-up to minimise participant inconvenience. After this visit, all trial involvement ceased, and no further data was collected from participants.

Data Management

The majority of trial data was captured on trial specific paper CRFs. Digital media data including intraoperative videos and resected specimen photographs were also collected. All data collected was stored securely on-site at LTHT in paper form, and where necessary on an LTHT recoverable network drive. At the trial endpoint all data was sent to be securely archived for 15 years. After this date, data will be destroyed confidentially and in adherence to data protection regulations.

Trial Oversight and Quality Assurance

Due to the size and design of the trial, it did not require a dedicated trial steering committee or trial monitoring group. Instead, the trial was overseen and monitored by the LTHT/University of Leeds Quality Assurance (QA) team. As per the data management plan, the trial was

inspected at regular intervals by the QA team. All CRFs were checked against the original source data for completeness and accuracy. Any discrepancies were queried and rectified.

Progress reports were submitted at six monthly intervals to the trial sponsor.

Regular progress and development meetings were held with EM Imaging Ltd and Karl Storz Research and Innovation team in Germany to analyse the early results and discuss potential methods of optimisation.

Trial Closure

Trial recruitment ceased on 29th July 2019. The trial closed on 28th August 2019 following the last visit of the last subject as per the schedule of visits and approved trial design. An end of notification and end of trial report was submitted to Y&H REC, MHRA and to EM Imaging Ltd in due course.

5.2.4 Radiology Assessment

Dr. Damian J. Tolan (Consultant Gastrointestinal Radiologist) at LTHT performed all trial specific radiology assessments. The pre-operative abdominal and pelvic CT scans were reviewed according to the criteria outlined in the radiology appendix of the protocol and radiology CRF, and any suspected malignant nodes were marked on a Modified Japanese staging subgroups diagram. The Union for International Cancer Control TNM v8 classification system(149) was used to predict pre-operative radiological stage.

5.2.5 Histopathology Assessment

Dr. Nick P West, Associate Professor in Molecular & Digital Pathology, and Honorary Consultant in Gastrointestinal Pathology at LTHT, performed the trial specific histopathological assessments. Participants in the trial consented to the retrieval and storage of tissue for

purposes of research as part of the standard trial consent process. Tissue was collected and stored in accordance with the approved trial protocol version and the University of Leeds/LTHT histopathology trial specific laboratory SOP. The Union for International Cancer Control TNM v8 classification system(240) as used for final tumour grade classification.

The whole fresh tumour specimen was photographed with labels identifying the anterior and posterior surface, the tumour, and the vascular high tie. Any lymph nodes that were suspected to contain metastatic tumour deposits during surgery were clearly marked. Trial specimen photographs were stored securely in individual NHS patient electronic records and anonymised copies were transferred to a secure recoverable University of Leeds network drive for research purposes and future long-term archiving.

The trial participant tumour specimens were prepared as per standard local policy. They were fixed in formalin and the non-peritonealised surfaces were painted with India Ink. The tumour was sliced into 3-4mm slices and all lymph nodes present were mapped according to the Modified Japanese staging subgroups diagram *(Figure 36).* The distance from the tumour and the presence of tumour deposits was also recorded. All preoperative radiological and intraoperative fluorescent results obtained were compared to the TNM v8 grade as the gold standard.

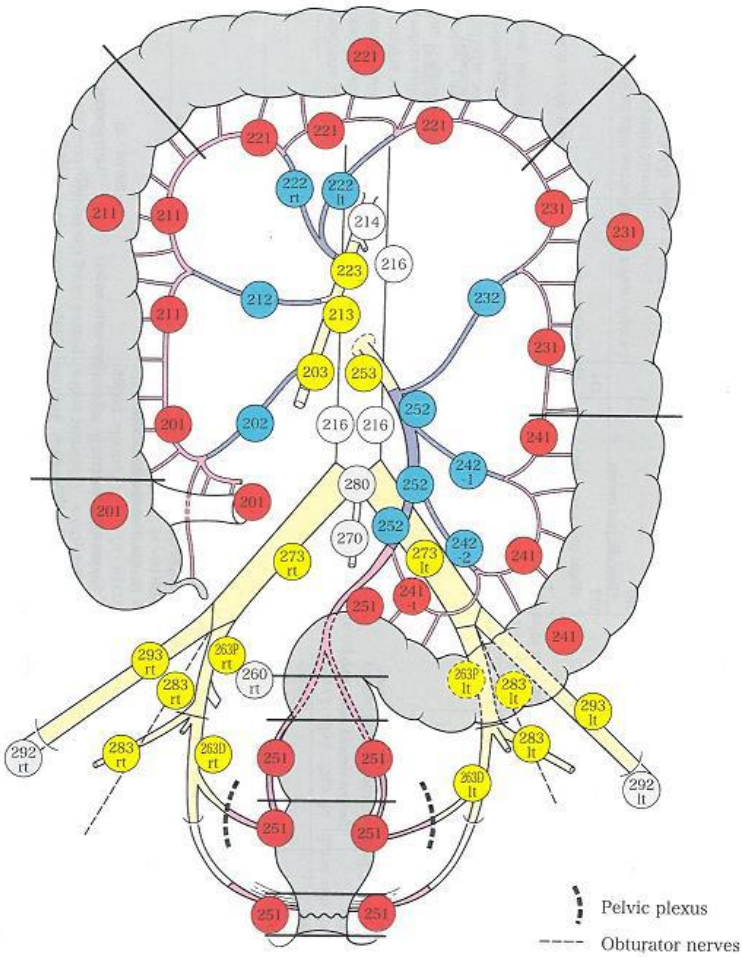

Figure 36: Modified Japanese colorectal lymph node staging subgroups diagram - Pericolic, D1 lymph nodes (red); Intermediate D2 lymph nodes (blue); Main, D3, lymph nodes (yellow). Adapted from GLiSten trial protocol(172) *with N.P West and D.J Tolan.*

H&E Staining

Counterstaining with Hematoxylin and Eosin (H&E) was performed as part of standard care by laboratory staff in the LTHT department of histopathology as per departmental SOP. Slide images were digitalised and uploaded to the secure virtual pathology portal (Virtual Pathology Image Viewer 0.3.02, Section of Pathology and Tumour Biology, Leeds Institute of Medical Research, University of Leeds, 2019) and made available to the research team for the duration of the trial.

Immunohistochemistry

FFPE Tissue from Trial Participants

FFPE tissue blocks of tumour (x2), normal colonic tissue, and positive lymph node tissue where available from each trial participant and transferred from LTHT pathology department to a HTA approved storage facility at the University of Leeds as per the trial specific laboratory agreement. For consistency, the IHC method described in *Chapter 4* was applied to trial participant FFPE tissue blocks. The antibody used (Rabbit monoclonal anti c-Met antibody (ref: ab51067) Abcam Plc) had been validated in mouse and human tissue for IHC and immunofluorescence.

Imaging

Bright-field microscopy imaging of IHC stained and prepared slides was performed using the Nikon Eclipse MicroscopyU E1000 automated microscope (Nikon Instruments Inc., New York, USA) at x20 magnification. A representative image from each sample was captured for review purposes.

Statistical Analysis

The analysis of the intraoperative results was mainly descriptive. Microsoft Excel and GraphPad Prism 7 (GraphPad V7.04 Software, Inc., California, USA) was used for statistical analysis. The frequency, mean, range and standard deviation were calculated. Wilcoxon matched-pairs signed rank test was used to assess the accuracy of pre-op radiology CT (cT and pT) to predict final pathological tumour stage and lymph node status (cN and pN). Spearman correlation was applied to assess the relationship between intraoperative fluorescence signal (isofluorescent to background or mildly fluorescent) and participant

demographic factors and final pathological stage (TNM v8.0 pT stage and pN stage). The Spearman R coefficient value (R) and the *p value* are quoted.

5.3 CLINICAL TRIAL RESULTS

5.3.1 Participants

Recruitment and Screening

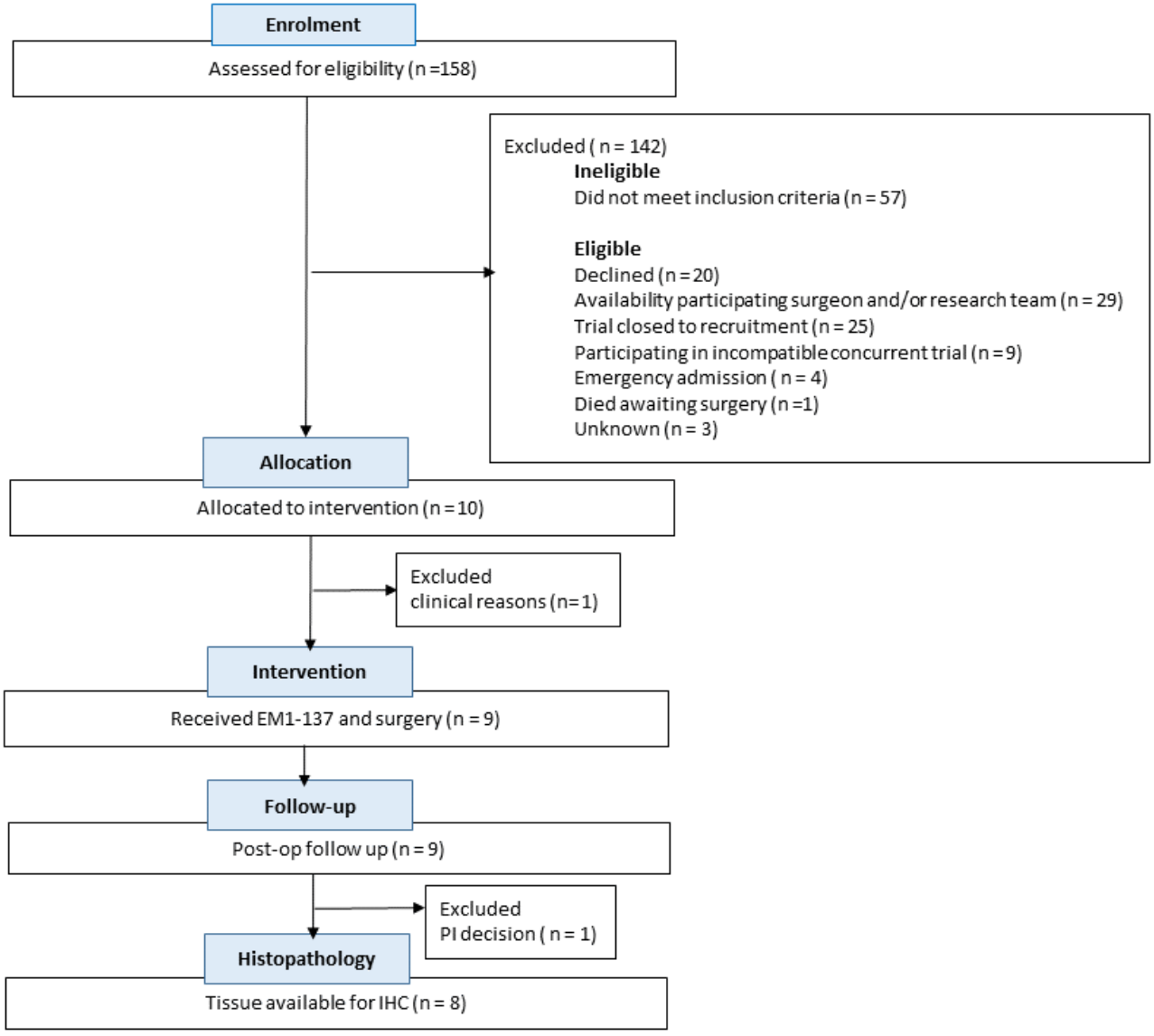

Figure 37: EMI-137 in laparoscopic colonic resections consort diagram

(Abbreviations: PI principal investigator; IHC Immunohistochemistry)

Figure 37 shows the total number of patients screened, treatment allocation, and participants followed up to trial completion. Thirty-six percent (57/158) of all patients screened did not meet the eligibility criteria. This is relatively high for a clinical trial and relates to the strict eligibility criteria of the trial. This was a phase IIa trial of EMI-137 with limited safety data provided from small healthy volunteer studies, which limited inclusion of participants with impaired hepatorenal function(218,220). CRC is a disease of advanced age, trial participation required normal hepatorenal function which tends to decline with age *(Table 15).* Only 12.7% of patients screened declined to participate showing the trial was acceptable to the majority of patients approached. A major barrier to recruitment was availability of research staff and/or the necessary trial equipment (29/142; 20.4%). As an internally funded study with limited trained personnel

Recruitment Timeline

The first patient was recruited to the trial on 14th February 2018 with a total of 10 patients recruited. The last patient underwent fluorescent guided surgery on 29th July 2019. The last visit of the last subject was conducted on 28th August 2019.

Participant Demographics

Table 16 shows the baseline demographics of the nine participants enrolled into the trial who underwent trial specific laparoscopic colonic resection surgery with the addition of EMI-137.

(N = 9)		*Mean average*	*S.D*
Age (years)		72	± 3.9
Gender M: F	4: 5		
Body Mass Index (m^2)		26.5	± 4.1
ASA grade			
1	1		
2	4		
3	4		
Co-morbidities			
Cardiovascular disease Yes: No	6: 3		
Peripheral vascular disease Yes: No	0: 9		
Respiratory disease Yes: No	3: 6		
Diabetes Yes: No	0: 9		
Pre-op colonoscopy			
Tumour location			
Ascending colon	2		
Transverse colon	1		
Hepatic flexure	1		
Descending colon	1		
Sigmoid colon	4		
Tumour morphology			
Polypoidal	2		
Semi annular	1		
Circumferential (annular)	6		
Colorimetric tattoo applied	9: 0		

Table 16: Summary of participant baseline demographics

Participant Summary

Participant ID	Gender M/F	Age (y)	BMI (m^2)	ASA grade	Tumour location	Operation performed	Interval to assessment (hh: mm)	pT stage	Tumour fluorescence	Max tumour ⌀ (mm)	pN stage	Lymph node fluorescence
EM001	F	75	24.8	2	Ascending colon	Right hemicolectomy	02:31	pT3	Isofluorescent to background	80	pN0	None
EM002	M	76	22.7	3	Sigmoid colon	High anterior resection	01:36	pT3	Isofluorescent to background	25	pN0	None
EM003	F	67	23.0	1	Descending colon	Left hemicolectomy	01:40	pT3	Mildly fluorescent	15	pN1b	None
EM004	M	77	31.5	3	Sigmoid colon	High anterior resection	01:15	pT2	Mildly fluorescent	35	pN1a	None
EM005	M	73	19.8	3	Hepatic flexure	Left hemicolectomy	01:50	pT4b	Isofluorescent to background	38	pN2a	None
EM007	F	70	30.5	2	Sigmoid colon	Left hemicolectomy	01:09	pT3	Isofluorescent to background	17	pN1c	None
EM008	M	67	28	2	Ascending colon	Right hemicolectomy	01:55	pT3	Isofluorescent to background	55	pN0	None
EM009	F	68	27.3	2	Sigmoid colon	Robotic anterior resection	01:49	pT1	Mildly fluorescent	28	pN0	None
EM010	M	71	30.8	3	Transverse colon	Extended right hemicolectomy	02:14	pT3	Mildly fluorescent	15	pN1b	None

Table 17: Key characteristics of trial participants. Abbreviations: pT pathological Tumour stage; pN pathological node stage; M male; F Female; m^2 metre^2: y years; ASA American Society of Anesthesiologists Grade.

N.B pN stage pN1c indicates there are no regional lymph nodes are positive but there are tumour deposits in the subserosa, mesentery or non-peritonealised pericolic or perirectal/mesorectal tissues.

5.3.2 Intra-Operative Results

Primary Tumour Fluorescence

The primary tumour was considered mildly fluorescent (relative to background) in 44% (4/9) of participants and isofluorescent to background in the remaining 5 participants (56%) (*Table 17*). Representative operative images are shown. The most promising results were observed in participant EM009 (*Figure 38*). This 68-year-old female had a pT1 sigmoid tumour and in fluorescent light assessment there was distinct delineation of the tumour relative to background signal.

(n = 9)	Frequency *n*	Mean	± S.D
EMI-137 dose received			
0.13mg/kg	8		
0.09mg/kg	1		
Dose volume administered (mg)		9.5	± 1.4
Dosing interval (hh:mm)		01:46	± 00:17
Tumour fluorescence			
Highly fluorescence to background	0		
Mild fluorescent to background	4		
Isofluorescent to background	5		
Lymph node fluorescence			
Presence of fluorescence in LN Yes: No	0 : 9		
Surgical procedure performed			
Right hemicolectomy	2		
Extended right hemicolectomy	1		
Left hemicolectomy	3		
High anterior resection	3		
Laparoscopic length of procedure (hh:mm)		02:30	00:47
Curative resection performed? Yes: No	9 : 0		
Serious intra-operative complications? Yes: No	0 : 9		

Table 18: Summary of intraoperative results. (Abbreviations: hh: mm Hour: minute)

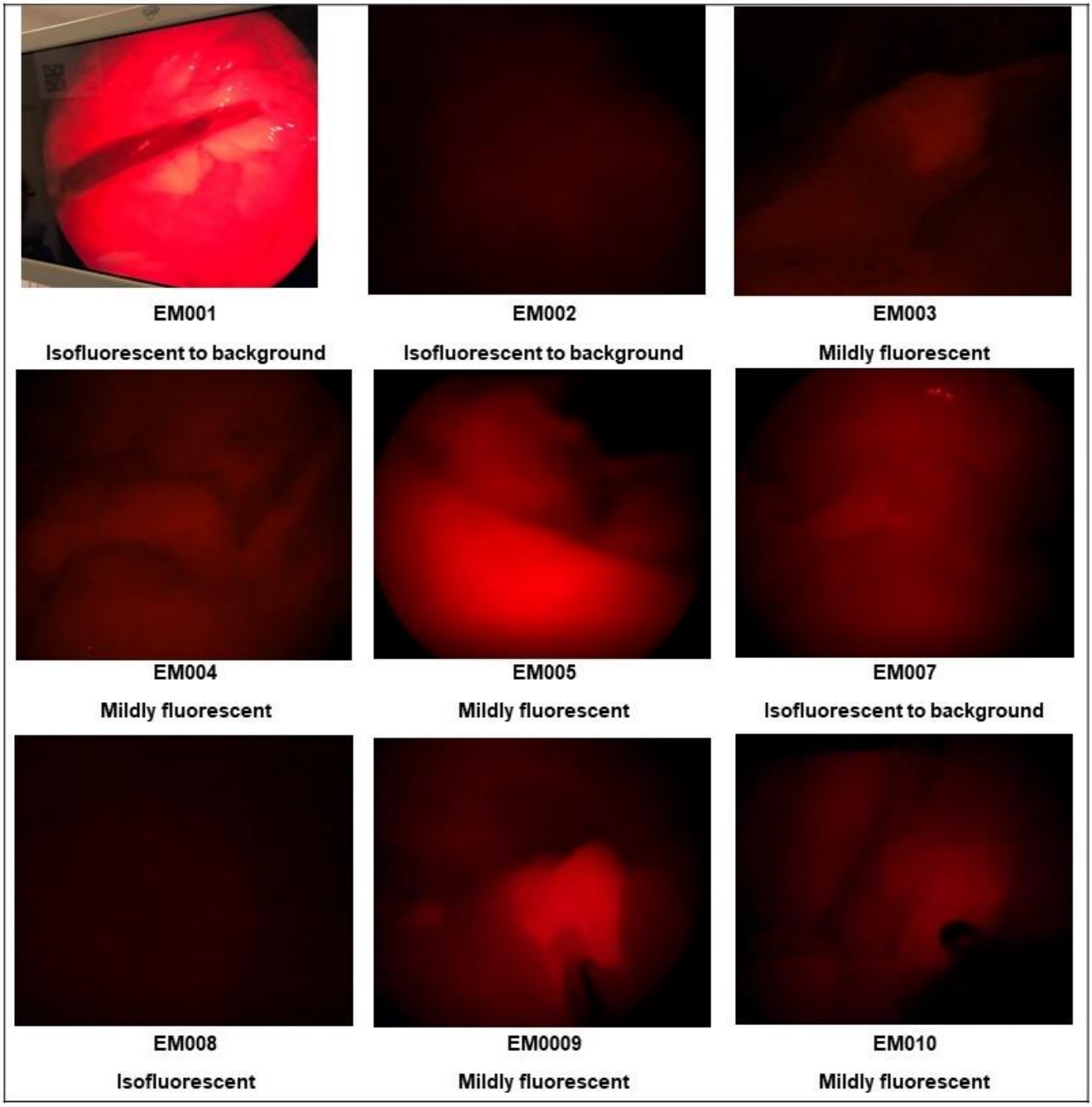

Figure 38: fluorescent assessment operative still image from each participant

Safety

EMI-137 was well tolerated by trial participants. There were no Suspected Unexpected Serious Adverse Reactions (SUSARs) arising from, or possibly related to the administration of EMI-137. Eight Expected Adverse Events (AEs), or known expected complications of major abdominal surgery, were recorded (*Table 19*).

Expected Adverse Events (AEs)	
Respiratory	
Hospital acquired pneumonia	2
Gastrointestinal	
Constipation	1
Prolonged ileus	2
Biochemical: deranged liver function tests	1
Cutaneous	
Phlebitis at cannula site	1
Genito-urinary	
Urinary tract infection	1
Total	**8**
Unexpected Adverse Event	
Mechanical fall at home	1
Total events	**9**
Serious Adverse Events (SAE)	
Neurological	
Vasovagal syncope episode	1
Suspected Unexpected Serious Adverse Reactions (SUSARs)	
None	0

Table 19: Summary of adverse events reported

Protocol Adherence

There were two protocol deviations reported.

Participant ID	Deviation	Reason	Outcome
EM003	Fresh frozen tumour samples not obtained for long-term storage and potential future translation research.	Patient safety. Tumour was too small to safety take tissue for storage and ensure adequate tissue for standard NHS histopathology assessment.	No fresh tumour stored. Normal colon tissue stored.
EM006	Withdrawn from trial after consent obtained.	Patient safety. A lack of high dependency post-operative beds at the clinical site, LTHT meant surgery was cancelled on the day. Surgery was urgently rescheduled but the research team could not support the new date.	Participant was withdrawn from the trial. Underwent standard care surgery without EMI-137.

Table 20: Protocol deviations reported during trial active phase.

Subject ID	*T stage*		*N stage*	
	Radiology (c)	*Pathology (p)*	*Radiology (c)*	*Pathology (p)*
EM001	T4a	pT3	N1c	pN0
EM002	T3	pT3	N0	pN0
EM003	T3	pT3	N1a	pN1b
EM004	T2	pT2	N0	pN1a
EM005	T4a	pT4b	N0	pN2a
EM007	T3	pT3	N1a	pN1c
EM008	T3	pT3	N1b	N0
EM009	Tx	pT1	N0	pN0
EM010	T3	pT3	N1	pN1b

Table 21: Comparison of pre-operative radiological (CT) TNM v8.0 staging and final pathological grade for each subject.

Radiology Accuracy

Pre-operative radiological CT scan assessment (cT and cN stage) correctly predicted the final pathological pT stage and pN status in 67% and 22% of subjects respectively. The correlation between CT radiological and final pathological TMN v8.0 was poor and did not reach statistical significance. Wilcoxon matched-pairs signed rank test of cT and pT stage and cN and pN stage gave a $p = > 0.99$ value for both comparisons. The accuracy of CT for predicting nodal (cN) stage was particularly poor overall and reflects previously published data relating to the role of CT in pre-operative colon cancer staging(166,224).

Participant Factors and Influence on Intraoperative Fluorescent Signal

Spearman correlation was performed to try and ascertain the relationship between peri-operative trial participant characteristics and intraoperative fluorescent signal detected with EMI-137. The data did not show a strong monotonic relationship between participant age, BMI, gender, ASA grade or tumour location (right versus left sided lesions) or interval from EMI-137 administration to assessment of fluorescence, and the *p value* was not significant (*Table 22*). These results are from a small observation study. No further inference on the relationship between these patient demographic factors and fluorescent signal detected with EMI-137 can be made.

Participant Factor	Coefficient R	P value
Age (years)	-0.13	0.44
Gender	-0.35	0.33
BMI (m2)	0.43	0.29
ASA grade	-0.05	0.22
Tumour location (right>left)	0.36	0.43
Assessment interval (minutes)	*-0.09*	*0.56*

Table 22: *Spearman correlation of intraoperative tumour fluorescent signal versus participant peri-operative characteristics, p value not significant.*

5.3.3 Histopathology Results

Immunohistochemistry results for each participant are shown below (*page 193 to 200*) and the summary of final pathological stage results are shown in *Table 23* below.

Tumour tissue from all participants demonstrated moderate to high c-Met immunopositivity across the samples (8/8) and six (6/8) matched normal mucosa samples were strongly positive for c-Met expression. All four of the participant tumour samples deemed mildly fluorescent at intraoperative assessment showed strong c-Met immunopositivity with IHC.

Five participants (5/9, 56%) showed lymph node involvement at final histopathological assessment (mean total lymph node yield 24.3 ± 10.7; range 5 – 38 and involved node range 1 to 4). Eight malignant nodes, from four participants were examined with IHC. All nodes showed moderate to high c-Met immunopositivity. Participant 005 had three involved lymph nodes, one of which was identified as highly suspicious for malignancy intra-operatively during white light assessment, but no fluorescent nodes with EMI-137 were observed.

(N = 9)		Mean ± S.D	Range
Tumour differentiation			
Well/moderate	9		
Poor	0		
Tumour histological sub-type			
Adenocarcinoma	8		
Adenocarcinoma variant - mucinous	1		
Max tumour diameter (mm)		34.2 ± 20.3	15 - 80
Max distance tumour extends beyond muscularis propria (mm) (≥pT3) *(n = 7)*		2.5 ± 2.3	1 - 7
Plane of excision			
Mesocolic	5		
Intramesocolic	4		
Muscularis Propria	0		
Complete resection at all margin achieved?			
R0 (yes)	9		
R1 (no)	0		
Tumour T stage*			
pT1	1		
pT2	1		
pT3	6		
pT4a	0		
pT4b	1		
Distance to circumferential margin (mm)		25.4 ± 27.4	2.5 – 75
Lymph node yield		24.3 ± 10.7	5 – 38
Total number lymph nodes involved			
0	5		
1	1		
2	1		
3	1		
4	1		
Tumour N stage*			
pN0	4		
pN1a	1		
pN1b	2		
pN1c	1		
pN2a	1		
pN2b	0		
Apical node involvement			
Yes	0		
No	9		
Size largest malignant node (mm) *(n = 4)*		7.0 ± 1.2	6 – 9
Deepest level of venous invasion			
None	6		
Intramural	0		
Extramural	3		
Deepest level of lymphatic invasion			
None	4		
Intramural	0		
Extramural	5		
Deepest level of perineural invasion			
None	7		
Intramural	0		
Extramural	2		
Histologically confirmed distant metastatic disease Yes: No	0: 9		
*Tumour M stage**			
M0	9		
M1 a/b/c	0		

Table 23: Summary of subject histology results. Abbreviations: S.D standard deviation. * in accordance with TNM v8.0.

EM002

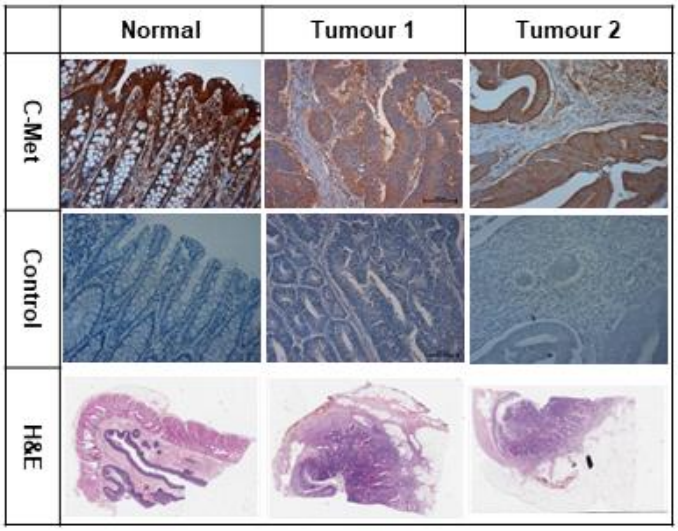

Fresh Specimen Photographs

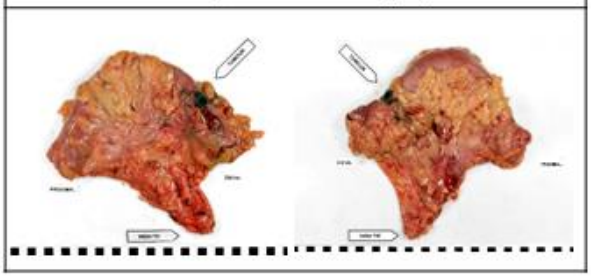

Formalin Fixed Specimen Photographs

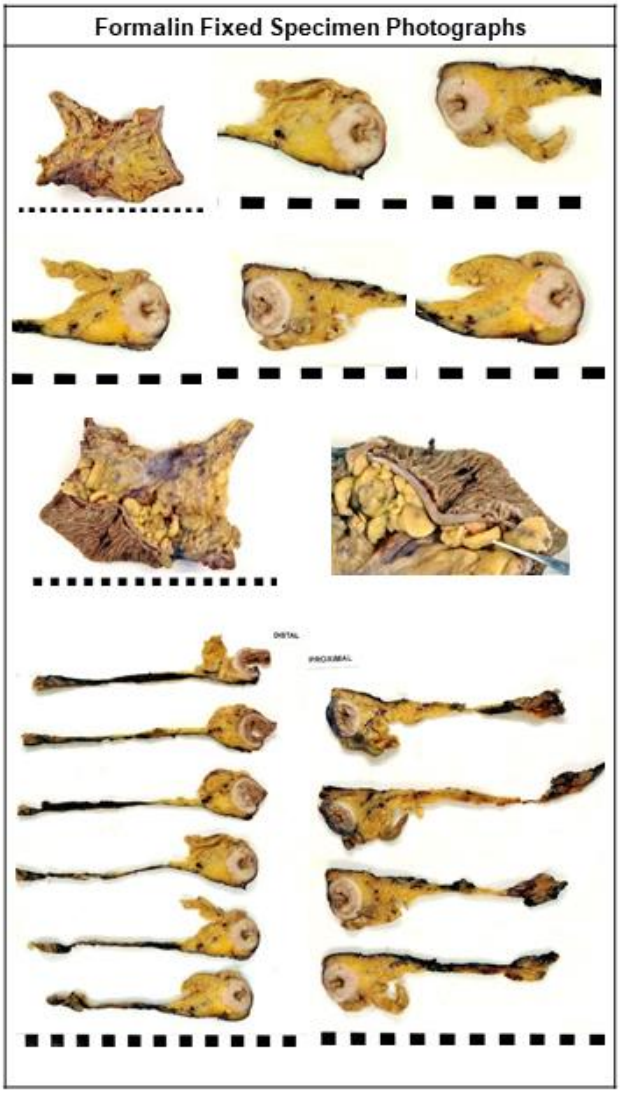

EM002	
Age (years)	76
Gender	Male
Tumour location	Sigmoid colon
Maximum tumour diameter (mm)	25
Pathological stage	pT3 N0 (0/19) M0 R0 V0
Plane of excision	Mesocolic
Histological sub-type	Adenocarcinoma
Differentiation	We///moderately differentiated
Tumour fluorescence	Isofluorescent to background
Lymph Node fluorescence	None
Interval to assessment (hh:mm)	01:36

EM003

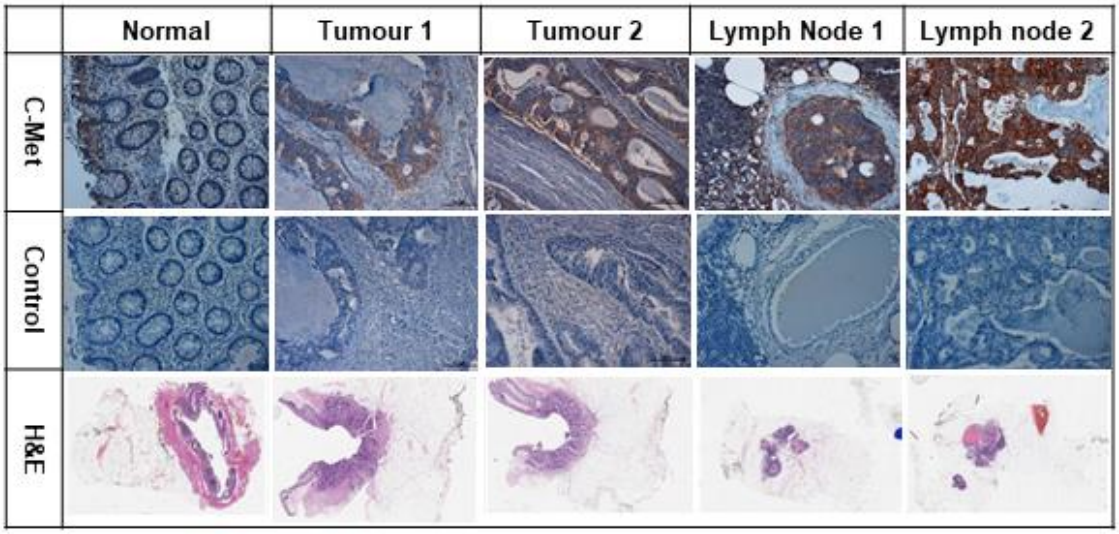

Fresh Specimen Photographs

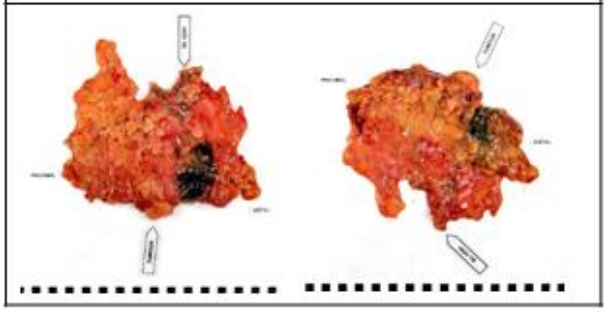

Formalin Fixed Specimen Photographs

EM003	
Age (years)	67
Gender	Female
Tumour location	Descending colon
Maximum tumour diameter (mm)	15
Pathological stage	pT3 N1b (2/14) M0 R0 V0
Plane of excision	Mesocolic
Histological sub-type	Adenocarcinoma
Differentiation	Well/moderately differentiated
Tumour fluorescence	Mildly fluorescent
Lymph node fluorescence	None
Interval to assessment (hh:mm)	01:40

Name: Gemma Armstrong

Student No: 201073014

EM004

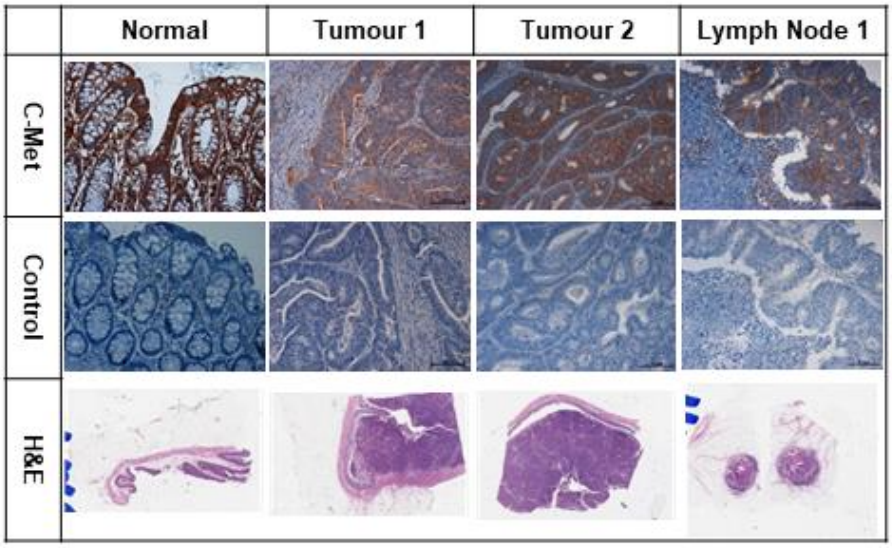

Fresh Specimen Photographs

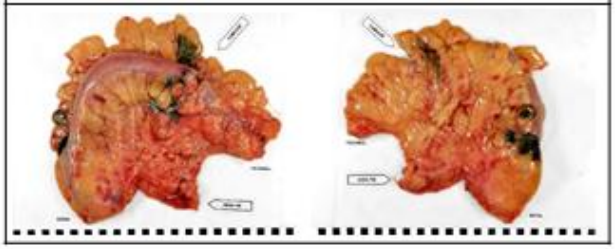

Formalin Fixed Specimen Photographs

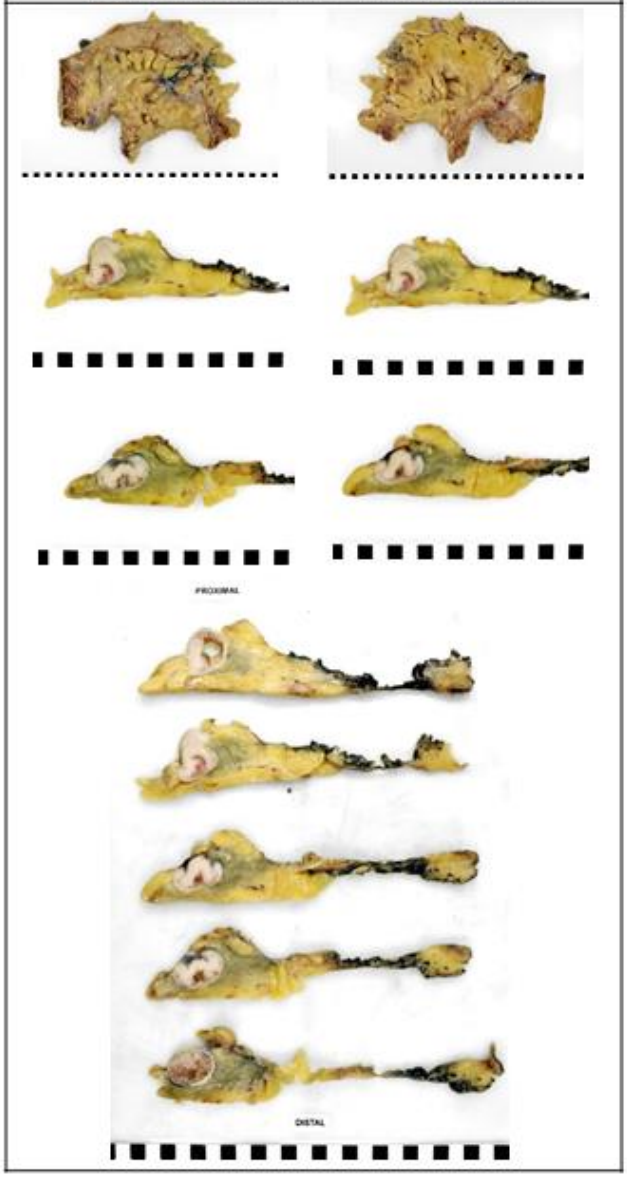

EM004	
Age (years)	77
Gender	Male
Tumour location	Sigmoid colon
Maximum tumour diameter (mm)	35
Pathological stage	pT2 N1a (1/21) M0 R0 V0
Plane of excision	Intramesenteric
Histological sub-type	Adenocarcinoma
Differentiation	Well/moderately differentiated
Tumour fluorescence	Mildy to background
Lymph node fluorescence	None
Interval to assessment (hh:mm)	01:15

EM005

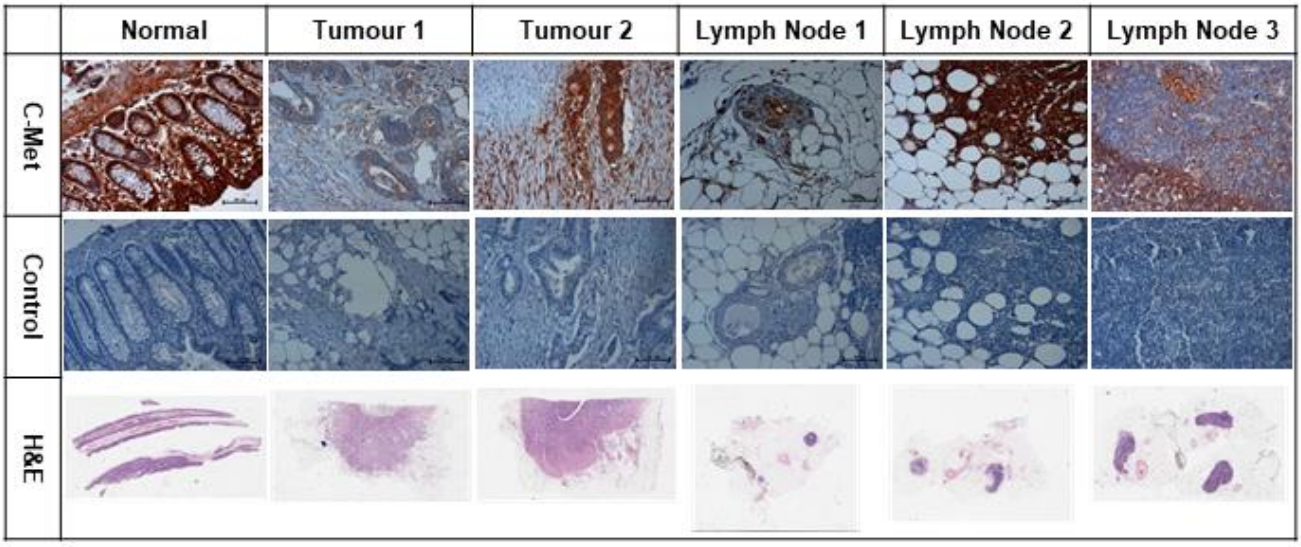

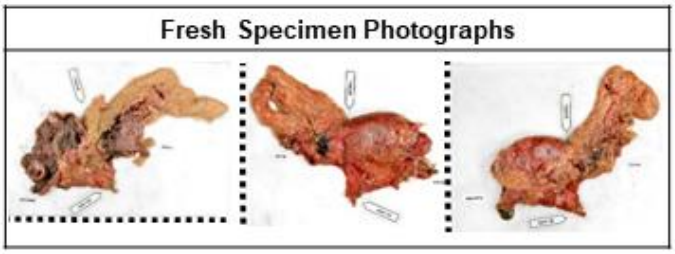

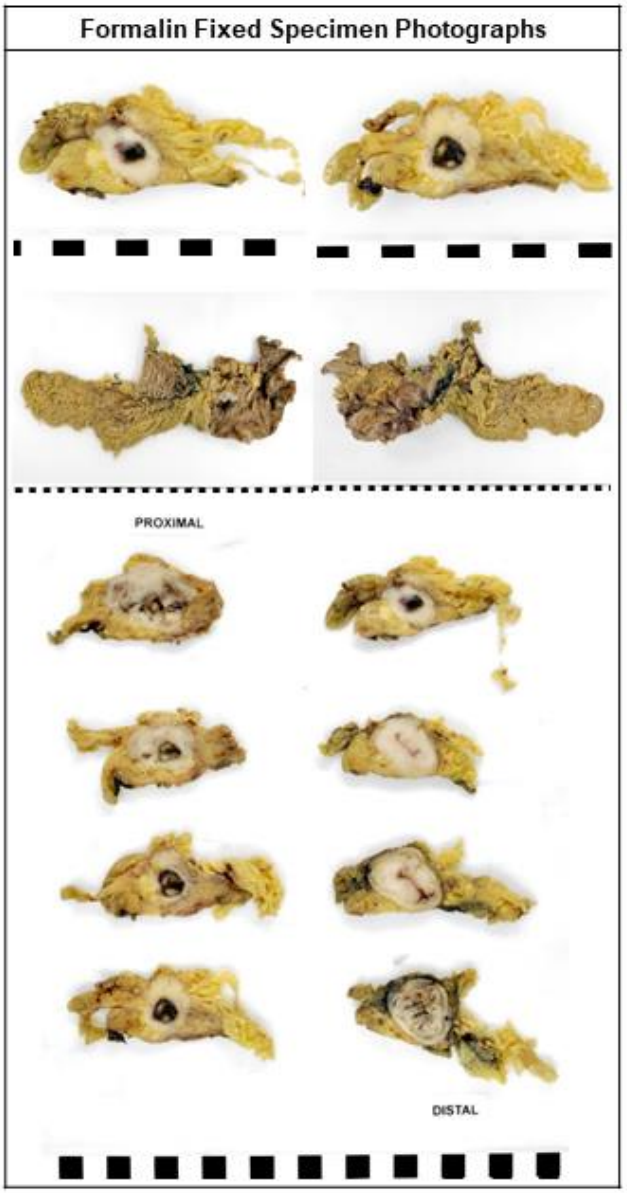

EM005	
Age (years)	73
Gender	Male
Tumour location	Hepatic flexure
Maximum tumour diameter (mm)	38
Pathological stage	pT4b N2a (4/28) M0 R0 V1
Plane of excision	Mesocolic
Histological sub-type	Adenocarcinoma
Differentiation	Well/moderately differentiated
Tumour fluorescence	Isofluorescent to background
Lymph node fluorescence	None
Interval to assessment (hh:mm)	01:50

EM007

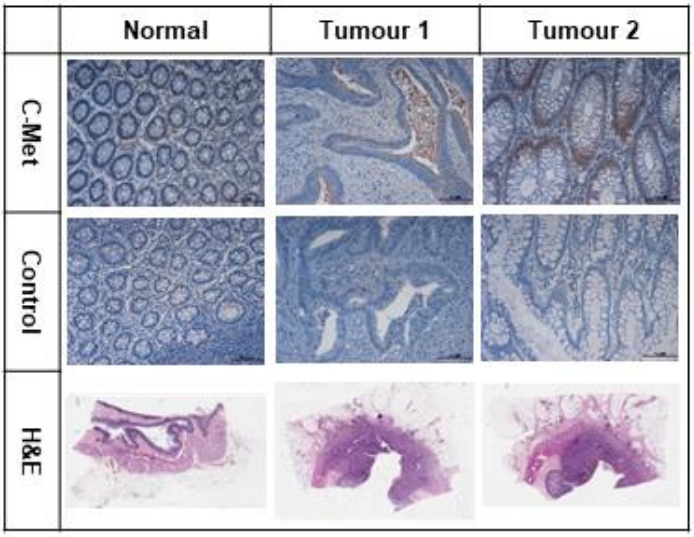

Fresh Specimen Photographs

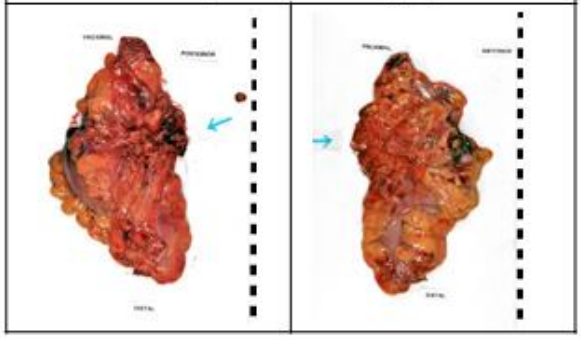

Formalin Fixed Specimen Photographs

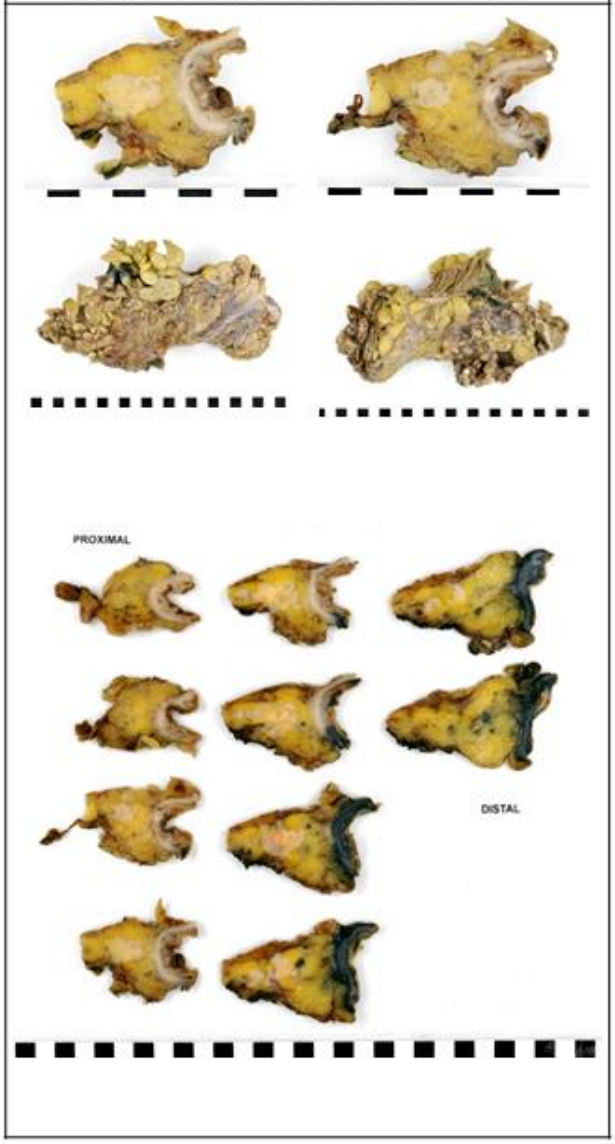

EM007	
Age (years)	70
Gender	Female
Tumour location	Sigmoid colon
Maximum tumour diameter (mm)	17
Pathological stage	pT3 N1c (0/35) M0 R0 V1
Plane of excision	Mesocolic
Histological sub-type	Adenocarcinoma
Differentiation	Well/moderately differentiated
Tumour fluorescence	Isofluorescent to background
Lymph node fluorescence	None
Interval to assessment (hh:mm)	01:09

EM008

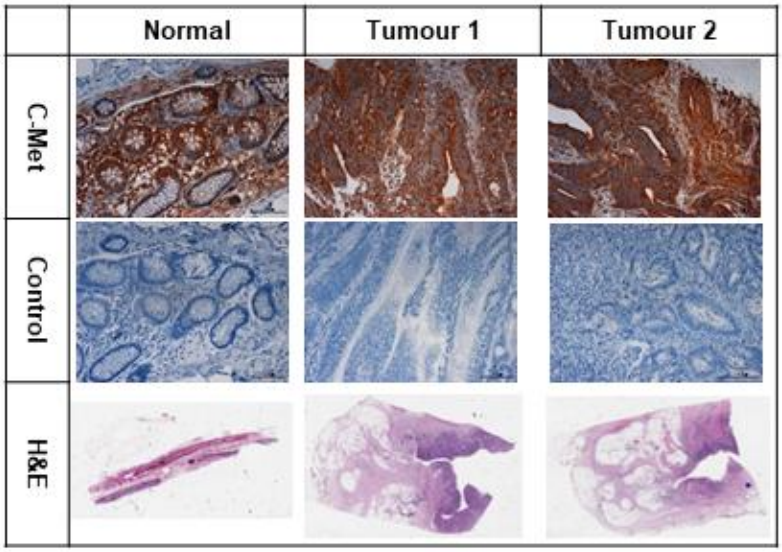

Fresh Specimen Photographs

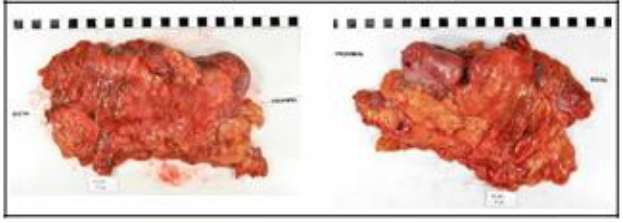

EM008	
Age (years)	67
Gender	Male
Tumour location	Ascending colon
Maximum tumour diameter (mm)	55
Pathological stage	pT3 N0 (0/38) M0 R0 V0
Plane of excision	Intramesenteric
Histological sub-type	Adenocarcinoma
Differentiation	Well/moderately differentiated
Tumour fluorescence	Isofluorescent to background
Lymph node fluorescence	None
Interval to assessment (hh:mm)	01:55

Formalin Fixed Specimen Photographs

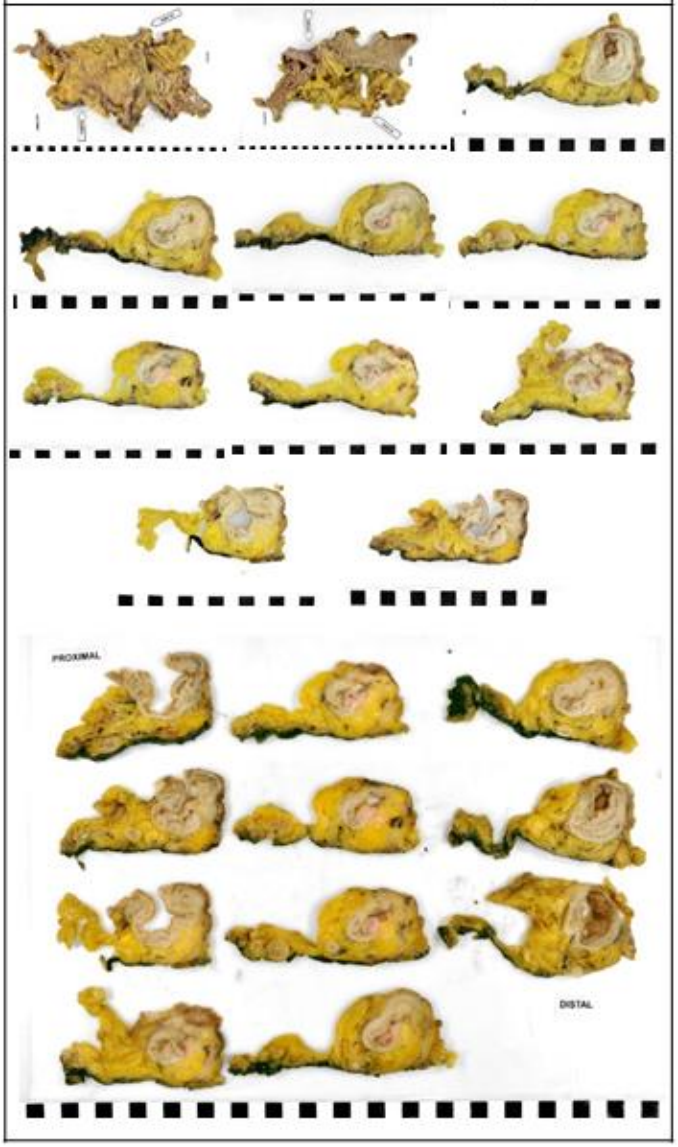

EM009

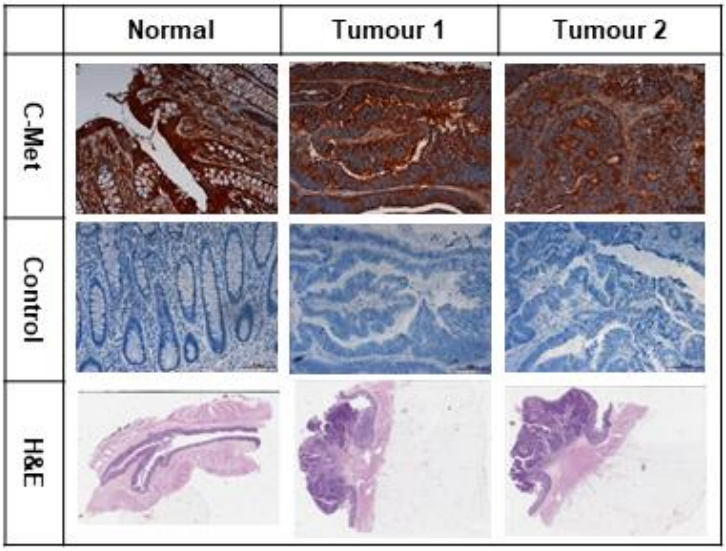

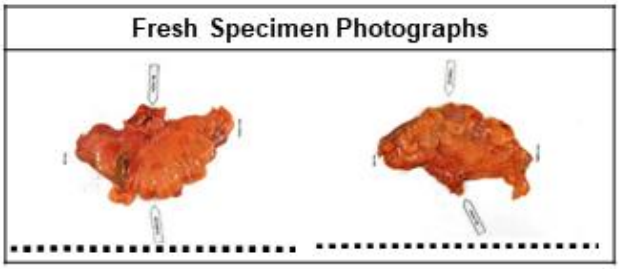

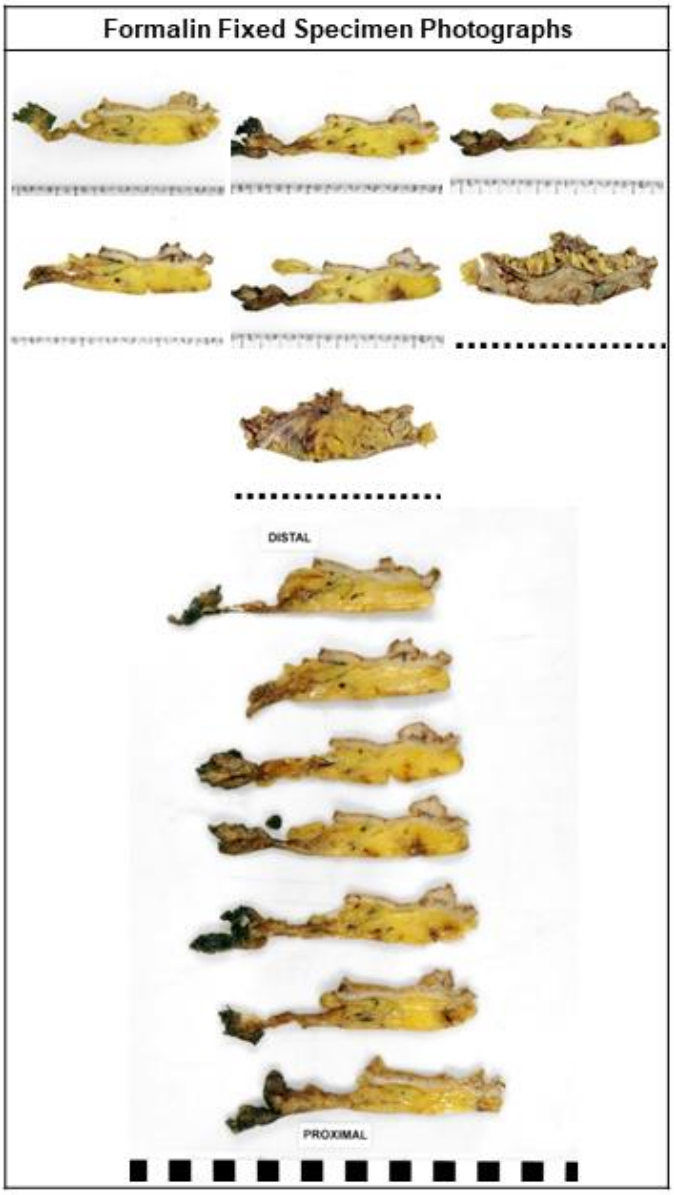

EM009	
Age (years)	68
Gender	Female
Tumour location	Sigmoid colon
Maximum tumour diameter (mm)	28
Pathological stage	pT1 N0 (0/5) M0 R0 V0
Plane of excision	Intramesenteric
Histological sub-type	Adenocarcinoma
Differentiation	Well/moderately differentiated
Tumour fluorescence	Mildly fluorescent
Lymph node fluorescence	None
Interval to assessment (hh:mm)	01:49

EM010

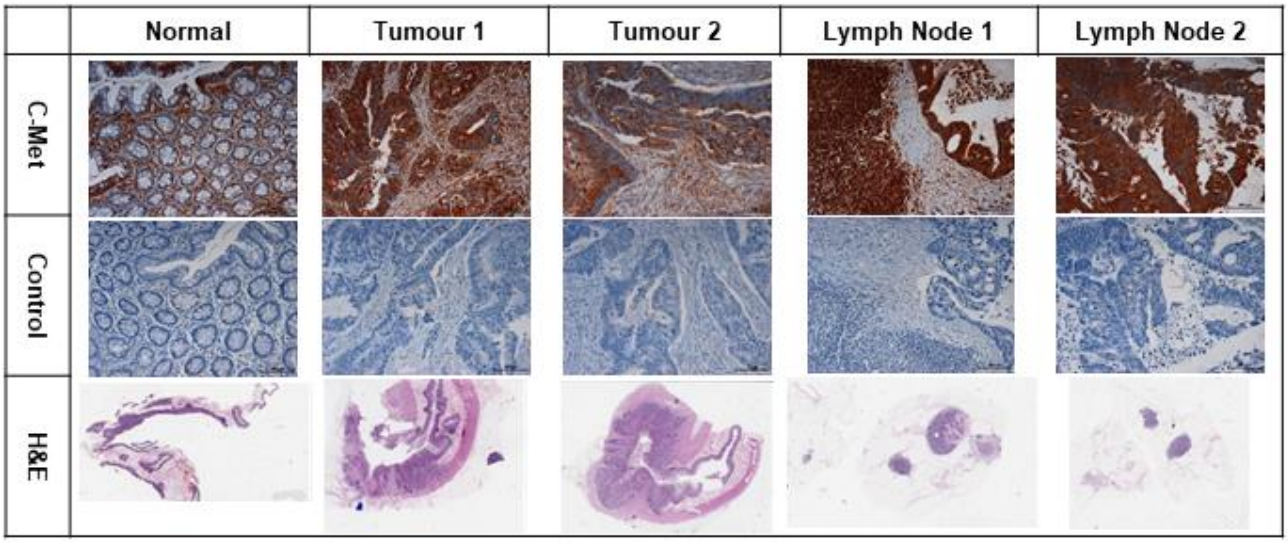

Fresh Specimen Photographs

Formalin Fixed Specimen Photographs

EM010	
Age (years)	71
Gender	Male
Tumour location	Transverse colon
Maximum tumour diameter (mm)	15
Pathological stage	pT3 N1b (3/21) M0 R0 V1
Plane of excision	Intramesenteric
Histological sub-type	Adenocarcinoma
Differentiation	Well/moderately differentiated
Tumour fluorescence	Mildly fluorescent
Lymph node fluorescence	None
Interval to assessment (hh:mm)	02:14

5.4 DISCUSSION

EMI-137 was safe and well tolerated by all nine participants. No Serious Adverse Events (SAEs) directly related to the administration of EMI-137 were recorded (*Table 19*). The trial intervention was also acceptable to patients with a relatively few declining to participate *(Figure 37).*

However, EMI-137 guided fluorescent surgery failed to produce consistent detectable tumour and metastatic lymph node fluorescence. The tumour was deemed mildly fluorescent in less than half of all cases and the tumour was isofluorescent to background in five of the nine enrolled participants (*Figure 38*). A strong monotonic relationship between any single participant factor and adverse fluorescent detection could not be identified in this patient cohort.

My preliminary results support the safety data described by *Burggraaf et al* in their study of EMI-137 (previously known as GE-137) in colonoscopy, where volunteers in both placebo and treatment arms (*n=31*) reported only mild unrelated AEs (commonly headache or somnolence) and no SAEs or SUSURS(218).. *Burggraaf et al* calculated the background clearance half-life of EMI137 as 2.5 hours. Within the confines of a pragmatic surgical trial, I was able to achieve a mean average assessment interval of 1 hour and 46 minutes. I expected this to have been sufficient to produce sufficient signal to noise ratio (tumour relative to background signal). I did not identify any correlation between tumour fluorescent signal and interval to assessment(218).

My efficacy data does not support *Burggraaf et al's* previously published conclusions of EMI-137 as a highly specific diagnostic imaging agent in colorectal cancer(218). They found EMI-137 fluorescence was detectable in all colorectal adenomas (47/47) and 78% (33/42) hyperplastic polyps with a prototype fluorescence colonoscope compatible with EMI-137 excitation. A significant difference with our study is the depth of penetrance of fluorescent light required. Colonic tumours are intraluminal lesions, and most participants in my trial were stage

T3 or less and by definition had not breeched the colon serosa. *Burggraaf et al* used an endoluminal technique (colonoscopy) to visualise the lesions of interest, the photons of light exciting and emitted from the bound EMI-137 had minimal biological tissue to diffuse through and there would have been significantly less scattering of light(218). It is estimated at the edge of the NIR window at around 600nm the depth of penetrance in biological tissue is only 1 to 3mm(241). In our trial, the tumour was imaged intracorporeally, but extraluminally. The additional serosa, mesentery and omental tissue layers are likely to have impeded visualisation in this setting.

Schweiger et al's analysis of colorectal cancer and pulmonary metastases identified c-Met expression as being significantly higher at the invasive margin as compared to central tumour areas(205). They also found median tumour and metastases c-Met expression scores at IHC were closely correlated in only 21% (7/33) of cases. This demonstrates c-Met expression may vary considerably throughout a single tumour or metastases and between the primary tumour and the related secondary metastases. The participant tissue analysed in this trial showed significant c-Met expression variance between individuals and between primary tumour and lymph node metastases. This supports the findings of *Schweiger et al* and previous research examining c-Met expression in colorectal cancer liver metastases(205,221).

Limitations

The study population was small (9 participants) and highly heterogenous. This limits the ability to draw any firm conclusions on the efficacy of EMI-137 in the detection of colon cancer or factors that adversely affect visualisation with the fluorophore. The Snap-on filter was manufactured and optimised by Karl Storz® Ltd R&I department for use with a standard D-Light laparoscopic system. The addition of the filter added another refractive layer and reduced the transmission of light. Attaching the filter to the camera head was also time-consuming and

cumbersome. Ideally, the filter would have been built into the laparoscope, to reduce the refraction of light and improve usability. At the exploratory trial phase this was not feasible. There is an option to explore this with EM Imaging Ltd and Karl Storz® Ltd in future.

6 CHAPTER SIX

6.1 CONCLUSION

In this PhD project, I aimed to explore and evaluate two fluorescent imaging agents for the purposes of dynamic intraoperative visualisation in laparoscopic surgery. With the advent of commercially available fluorescent laparoscopy systems and multiple compatible fluorophores, exploration of their utility and clinical benefit was needed. The potential to clearly, in real-time, delineate biliary anatomy and colonic tumour margins and lymph node spread with fluorescent compounds and a dedicated light source aimed to aid the decision-making process and allow individualised surgery tailored to the anatomy and disease characteristics.

To achieve my aims, I divided my research in to three distinct sections. Firstly, I explored and optimised the technique of Near Infrared Fluorescent Cholangiography (NIR-FC) with the untargeted fluorophore ICG in an early phase clinical trial. Then, I conducted extensive pre-clinical research in 2D and 3D models of colorectal cancer to evaluate c-Met as a potential diagnostic biomarker and imaging target. I also assessed the specificity of EMI-137, a novel c-Met targeted peptide for human c-Met and the biodistribution of EMI-137 in a murine model of colorectal cancer. This culminated in the exploration of EMI-137 as a diagnostic imaging agent during colon cancer resection surgery in a phase IIa clinical trial.

Through my research I found NIR-FC in laparoscopic cholecystectomy surgery to be a feasible intraoperative intervention; it was well-tolerated by patients and gained high surgeon satisfaction scores. I was able to demonstrate improved extra-hepatic structure visualisation achieved with a longer ICG dosing interval; this is contrary to several previously published studies. The exploration of NIR-FC in both the acute and elective laparoscopic setting also highlighted several limitations of NIR-FC not widely described; namely limited depth of fluorescent tissue penetrance in peri-hilar inflammation and spillage of bile saturating the field with ICG and limiting delineation of structures. If I were to perform this study again, I would have undertaken a dedicated sub-study of NIR-FC in the index admission (emergency) laparoscopic cholecystectomy setting. This would be of higher research value and would have allowed greater comparison between the two distinct patient populations. It would have

facilitated exploration of fluorescent bile duct mapping in the setting of dense peri-hilar inflammation and tissue oedema.

The role of ICG and several other untargeted fluorophores have been explored previously in the surgical setting. The advent of novel, targeted peptides, such as the c-Met protein targeted EMI-137, appeared to be a new era in fluorescence guided laparoscopic surgery. I thoroughly investigated c-Met protein expression in pre-clinical models of CRC. By immunohistochemical appraisal of c-Met expression in a large representative sample of tissue from the CLASICC clinical trial, I confirmed tumour tissue consistently expressed higher levels of c-Met protein relative to matched normal mucosa tissue *(Figure 30)*. Levels of detectable c-Met expression did not correlate with disease pT or pN stage. The median expression scores were variable, but significantly higher in tumour tissue relative to normal background mucosa at all stages of disease. It therefore appeared that c-Met had potential as an imaging target for fluorescent guided resection of colonic tumours irrespective of tumour stage. Although c-Met was possibly inferior to CEA as a CRC biomarker(228), c-Met did show superior diagnostic accuracy compared to several targets evaluated by other groups. The significant differential expression indicated that c-Met was a suitable biomarker in colorectal cancer for further evaluation and a potential imaging target. C-met expression also did not appear to correlate with disease stage, this justified the inclusion of patients of all suspected Tumour stage in the exploratory trial of EMI-137 as an intraoperative fluorescent biomarker in colon cancer surgery.

Pre-operative staging of colon cancer is imprecise and this makes planning the radicality of surgery difficult. The early phase IIa trial of EMI-137 as a diagnostic imaging agent showed that EMI-137 was safe and well tolerated, and the trial design applied was feasible to explore the trial end points. Intravenous administration of EMI-137 and diagnostic laparoscopy with the adapted Karl Storz® fluorescent laparoscope produced detectable fluorescence in all of the nine study participants. The colon tumour was deemed mildly fluorescent by the operating surgeon in 4/9 (44%) and isofluorescent to background in the remaining 5/9 (56%) of cases. The addition of EMI-137 did not delineate any regional lymph nodes in the patient cohort.

The cohort was very small and heterogenous so limited conclusions about patient or tumour factors that adversely affected visualisation can be made. There was a possible inverse relationship between tumour pT stage, number of lymph nodes involved and size of largest malignant node; as the colon cancer stage progressed the fluorescence decreased. *Takeuchi et al* showed the greatest incremental increase in c-Met mRNA expression between stage T1 and T2 compared to T3 and T4, indicating a role for high c-Met expression in early invasiveness and local colorectal cancer progression(208). Our sub-group analysis of the CLASICC trial TMA population did not support this, and there was no correlation between pT stage and differential c-Met expression score observed at IHC in a large RCT cohort (*Table 13, Table 14 and Figure 33*). Immunohistochemical analysis of c-Met expression in the eight tissue specimens available from the EMI-137 clinical trial cohort also showed that the variable intra-operative fluorescent results observed cannot be attributed to pre-operative participant factors.

Future research should focus on optimisation of the fluorescent laparoscopy hardware used with EMI-137 and increasing the signal to noise ratio observed intraoperatively. Another area of research could include exploration of co-expression of c-Met with other defined biomarkers of colorectal cancer. Small studies have described a synergic relationship between c-Met and EGFR in colorectal cancer proliferation(242) and high c-Met expression and resistance to anti-EGFR biologic agents. A fluorescent biomarker targeted to c-Met and a marker such as EGFR, may provide greater fluorescent diagnostic sensitivity and specificity.

REFERENCES

1. Sauer M, Hofkens J, Enderlein J. Handbook of Fluorescence Spectroscopy and Imaging. 1st ed. Handbook of Fluorescence Spectroscopy and Imaging. Weinheim, Germany: Wiley-VCH Verlag & Co. KGaA; 2011. 1–29 p.

2. ThermoFisher Scientific Inc. Fluorescence Fundamentals [Internet]. Fluorescence Fundamentals. 2017 [cited 2018 May 18]. Available from: https://www.thermofisher.com/uk/en/home/references/molecular-probes-the-handbook/introduction-to-fluorescence-techniques.html

3. Würth C, Grabolle M, Pauli J, et al. Relative and absolute determination of fluorescence quantum yields of transparent samples. Nat Protoc [Internet]. 2013 Jul 18 [cited 2018 May 18];8(8):1535–50. Available from: http://www.nature.com/doifinder/10.1038/nprot.2013.087

4. Jablonski A. Efficiency of Anti-Stokes Fluorescence in Dyes. Nature [Internet]. 1933 [cited 2018 Jan 12];131:839–40. Available from: https://www.nature.com/articles/131839b0.pdf

5. Davidson M. Molecular Expressions Microscopy Primer: Fluorescence - Jablonski Diagram - Interactive Tutorial [Internet]. 2017 [cited 2018 Apr 24]. Available from: http://micro.magnet.fsu.edu/primer/java/jablonski/lightandcolor/index.html

6. Weissleder R. A clearer vision for in vivo imaging. Nat Biotechnol [Internet]. 2001 [cited 2018 May 25];19(4):316–7. Available from: https://www.nature.com/articles/nbt0401_316.pdf

7. National Center for Biotechnology Information. Compound Summary for CID 11967809 - Indocyanine Green [Internet]. PubChem Compound Database; CID=11967809. 2017 [cited 2018 May 14]. Available from: https://pubchem.ncbi.nlm.nih.gov/compound/indocyanine_green#section=Top

8. Burchell H, Fox I, Wood EH. Symposium on Indocyanine Green and Its Clinical Applications. In: Proceedings of the Staff Meetings of the Mayo Clinic [Internet]. Rochester; 1960 [cited 2018 May 14]. p. 729–43. Available from: http://www.mayoclinicproceedings.org/pb/assets/raw/Health Advance/journals/jmcp/jmcp_la_89_8_2_2.pdf

9. Desmettre T, Devoisselle JM, Mordon S. Fluorescence properties and metabolic features of indocyanine green (ICG) as related to angiography. Surv Ophthalmol.

2000;45(1):15–27.

10. Ott P. Hepatic Elimination of Indocyanine Green with Special Reference to Distribution Kinetics and the Influence of Plasma Protein Binding. Pharmacol Toxicol. 1998;83(Suppl 11):5–48.

11. ICG-PULSION®. Summary Product Characteristics. 2013.

12. Muckle TJ. Plasma proteins binding of indocyanine green. Biochem Med [Internet]. 1976;15(1):17–21. Available from: http://www.ncbi.nlm.nih.gov/pubmed/942422

13. Yoneya S, Saito T, Komatsu Y, Koyama I, Takahashi K, Duvoll-Young J. Binding properties of indocyanine green in human blood. Invest Ophthalmol Vis Sci. 1998;39(7):1286–90.

14. Cherrick G, Stein S, Leevy C. Indocyanine green: observations on its physical properties, plasma decay, and hepatic extraction. J Clin Invest. 1960;39(4):592–600.

15. Mordon S, Devoisselle JM, Soulie-Begu S, Desmettre T. Indocyanine Green: Physicochemical Factors Affecting Its Fluorescence in Vivo. Microvasc Res [Internet]. 1998 [cited 2018 May 17];55(2):146–52. Available from: https://ac.els-cdn.com/S0026286298920684/1-s2.0-S0026286298920684-main.pdf?_tid=2fb5fd0e-7498-4cbc-9f27-1f08206cff27&acdnat=1526552350_f2dc45e974ea25d061a925a978052e19

16. Shinohara H, Tanaka A, et al; Direct measurement of hepatic indocyanine green clearance with near-infrared spectroscopy: Separate evaluation of uptake and removal. Hepatology [Internet]. 1996;23(1):137–44. Available from: http://linkinghub.elsevier.com/retrieve/pii/S0270913996000122

17. Alander JT, Kaartinen I, Laakso A, Pätilä T, Spillmann T, Tuchin VV., et al. A Review of indocyanine green fluorescent imaging in surgery. J Biomed Imaging. 2012;2012(940585).

18. Huang L, Vore M. Multidrug Resistance P-Glycoprotein 2 Is Essential for the Biliary Excretion of Indocyanine. Drug Metab Dispos. 2001;29(5):634–7.

19. Wheeler H 0, Cranston WI, Meltzer JI, Bradley SE. Hepatic Uptake and Biliary Excretion of Indocyanine Green in the Dog. Proc Soc Exp Biol Med [Internet]. 1958 [cited 2018 May 14];99(1):11–4. Available from: http://journals.sagepub.com/doi/pdf/10.3181/00379727-99-24229

20. Ketterer S, Weigand B. Hepatic uptake and biliary excretion of Indocyanine green and

its use in estimation of hepatic blood flow in dogs ’. Am J Physio. 1960;199(3):481–4.

21. Gurfinkel M, Thompson AB, Ralston W, Troy TL, Moore AL, Moore TA, et al. Pharmacokinetics of ICG and HPPH-car for the detection of normal and tumor tissue using fluorescence, near-infrared reflectance imaging: a case study. Photochem Photobiol [Internet]. 2000;72(1):94–102. Available from: http://www.ncbi.nlm.nih.gov/pubmed/10911733

22. Alacam B, Yazici B, Intes X, Chance B. Extended Kalman filtering for the modeling and analysis of ICG pharmacokinetics in cancerous tumors using NIR optical methods. IEEE Trans Biomed Eng. 2006;53(10):1861–71.

23. Dietrich CG, Götze O, Geier A. Molecular changes in hepatic metabolism and transport in cirrhosis and their functional importance. World J Gastroenterol [Internet]. 2016 [cited 2018 May 17];22(1):72–88. Available from: http://www.ncbi.nlm.nih.gov/pubmed/26755861

24. Ohkubo H, Musha H, Okuda K. Effects of Caloric Restriction on the Kinetics of Indocyanine Green in Patients with Liver Diseases and in the Rat. [cited 2018 May 14]; Available from: https://link.springer.com/content/pdf/10.1007%2FBF01263102.pdf

25. Landsman ML, Kwant G, Mook GA, Zijlstra WG. Light-absorbing properties, stability, and spectral stabilization of indocyanine green. J Appl Physiol [Internet]. 1976 Apr [cited 2018 May 16];40(4):575–83. Available from: http://www.ncbi.nlm.nih.gov/pubmed/776922

26. Björnsson OG, Murphy R, Chadwick VS. Physicochemical studies of indocyanine green (ICG): absorbance/concentration relationship, pH tolerance and assay precision in various solvents. Experientia [Internet]. 1982 [cited 2018 May 16];38(12):1441–2. Available from: https://link.springer.com/content/pdf/10.1007%2FBF01955757.pdf

27. Philip R, Penzkofer A, Biiumler W, Szeimies RM, Abels C. Absorption and fluorescence spectroscopic investigation of indocyanine green. J Photochem Photobio [Internet]. 1996 [cited 2018 May 15];96:137–48. Available from: https://ac.els-cdn.com/101060309504292X/1-s2.0-101060309504292X-main.pdf?_tid=0e3a27f0-4cbe-4f08-b33a-7aad9d6218a3&acdnat=1526372403_31c15371658614954224bc186aaf29f6

28. Benson R, Kues H. Fluorescence properties of indocyanine green as related to angiography. Phys Med Biol [Internet]. 1978 [cited 2018 May 15];23(1):159–63. Available from: http://iopscience.iop.org/article/10.1088/0031-9155/23/1/017/pdf

29. Reinhart MB, Huntington CR, Blair LJ, Heniford BT, Augenstein VA. Indocyanine Green: Historical Context, Current Applications, and Future Considerations. Surg Innov [Internet]. 2016;23(2):166–75. Available from: http://sri.sagepub.com/cgi/doi/10.1177/1553350615604053

30. Benya R, Quintana J, Brundage B. Adverse reactions to indocyanine green: a case report and a review of the literature. Cathet Cardiovasc Diagn [Internet]. 1989;17(4):231–3. Available from: http://www.ncbi.nlm.nih.gov/pubmed/2670244

31. Rudolf H, Göretzlehner G, Brügmann E, Töwe J, Rudolf K. Assessment of liver function using indocyanine green (Ujoviridin) during normal pregnancy, during labor and in puerperium. Zentralbl Gynakol [Internet]. 1977 [cited 2018 May 14];99(25):1548–53. Available from: http://www.ncbi.nlm.nih.gov/pubmed/610236

32. Diagnostic Green GmBH. Indocyanine Green (Verdye) 5mg/ml Injection: Information for the User. 2016.

33. Stolik S, Delgado JA, Pérez A, Anasagasti L. Measurement of the penetration depths of red and near infrared light in human ″ex vivo″ tissues. J Photochem Photobiol B. 2000;57(2–3):90–3.

34. Imamura H, Sano K, Sugawara Y, Kokudo N, Makuuchi M. Assessment of hepatic reserve for indication of hepatic resection: Decision tree incorporating indocyanine green test. J Hepatobiliary Pancreat Surg. 2005;12(1):16–22.

35. Greco E, Nanji S, Bromberg IL, Shah S, Wei AC, Moulton CA, et al. Predictors of peri-opertative morbidity and liver dysfunction after hepatic resection in patients with chronic liver disease. HPB. 2011;13(8):559–65.

36. Levesque E, Martin E, Dudau D, Lim C, Dhonneur G, Azoulay D. Current use and perspective of indocyanine green clearance in liver diseases. Anaesthesia, Crit care pain Med [Internet]. 2016;35(1):49–57. Available from: http://www.sciencedirect.com/science/article/pii/S2352556815001083

37. Hatzinger M, Kwon ST, Langbein S, Kamp S, Häcker A, Alken P. Hans Christian Jacobaeus: Inventor of Human Laparoscopy and Thoracoscopy. J Endourol [Internet]. 2006 Nov 4 [cited 2020 Apr 3];20(11):848–50. Available from: http://www.liebertpub.com/doi/10.1089/end.2006.20.848

38. Bhattacharya K. Kurt Semm: A laparoscopic crusader. J Minim Access Surg. 2007 Jan;3(1):35–6.

39. Reynolds W, Jr. The first laparoscopic cholecystectomy. JSLS [Internet]. 2001 [cited 2019 Mar 3];5(1):89–94. Available from: http://www.ncbi.nlm.nih.gov/pubmed/11304004

40. Ishizawa T, Tamura S, Masuda K, Aoki T, Hasegawa K, Imamura H, et al. Intraoperative Fluorescent Cholangiography Using Indocyanine Green: A Biliary Road Map for Safe Surgery. J Am Coll Surg. 2009;208(1):1–4.

41. Kudo H, Ishizawa T, Tani K, Harada N, Ichida A, Shimizu A, et al. Visualization of subcapsular hepatic malignancy by indocyanine-green fluorescence imaging during laparoscopic hepatectomy. Surg Endosc Other Interv Tech. 2014;28(8):2504–8.

42. Morita Y, Sakaguchi T, Unno N, Shibasaki Y, Suzuki A, Fukumoto K, et al. Detection of hepatocellular carcinomas with near-infrared fluorescence imaging using indocyanine green: Its usefulness and limitation. Int J Clin Oncol. 2013;18(2):232–41.

43. Morita K, Ishizawa T, Tani K, Harada N, Shimizu A, Yamamoto S, et al. Application of indocyanine green-fluorescence imaging to full-thickness cholecystectomy. Asian J Endosc Surg. 2014;7(2):193–5.

44. Gossedge G, Vallance A, Jayne D. Diverse applications for near infra-red intraoperative imaging. Color Dis. 2015;17(Suppl 3):7–11.

45. Handgraaf HJM, Boogerd LSF, Höppener DJ, Peloso A, Sibinga Mulder BG, Hoogstins CES, et al. Long-term follow-up after near-infrared fluorescence-guided resection of colorectal liver metastases: A retrospective multicenter analysis. Eur J Surg Oncol [Internet]. 2017 Aug 1 [cited 2018 May 14];43(8):1463–71. Available from: http://www.ncbi.nlm.nih.gov/pubmed/28528189

46. Giuliano AE, Ballman K, Mccall L, Beitsch P, Whitworth PW, Blumencranz P, et al. Locoregional Recurrence After Sentinel Lymph Node Dissection With or Without Axillary Dissection in Patients with Sentinel Lymph Node Metastases: Long-Term Follow-Up from the American College of Surgeons Oncology Group (Alliance) ACOSOG Z0011 Randomized Trial. Ann Surg [Internet]. 2016 [cited 2018 May 17];264(3):413–20. Available from: https://www.ncbi.nlm.nih.gov/pmc/articles/PMC5070540/pdf/nihms-821701.pdf

47. Giuliano AE, KK H, Ballman K, Beitsch P. Axillary dissection vs no axillary dissection in women with invasive breast cancer and sentinel node metastasis. Jama [Internet]. 2011;305(6):569–575. Available from: http://mauriciolema.webhost4life.com/rolmm/files/Z0011.pdf

48. National Institute for Health and Care Excellence [NICE]. Early and locally advanced breast cancer: diagnosis and treatment [Internet]. 2009 [cited 2018 Jul 5]. Available from: https://www.nice.org.uk/guidance/cg80/resources/early-and-locally-advanced-breast-cancer-diagnosis-and-treatment-pdf-975682170565

49. Cox CE, Pendas S, Cox JM, Joseph E, Shons AR, Yeatman T, et al. Guidelines for sentinel node biopsy and lymphatic mapping of patients with breast cancer. Ann Surg [Internet]. 1998;227(5):645–51; discussion 651-3. Available from: http://www.pubmedcentral.nih.gov/articlerender.fcgi?artid=1191339&tool=pmcentrez&rendertype=abstract

50. Lyman GH, Giuliano AE, Somerfield MR, Benson AB, Bodurka DC, Burstein HJ, et al. American Society of Clinical Oncology guideline recommendations for sentinel lymph node biopsy in early-stage breast cancer. J Clin Oncol. 2005;23(30):7703–20.

51. Vokach-Brodsky L, Jeffrey SS, Lemmens HJ, Brock-Utne JG. Isosulfan blue affects pulse oximetry. Anesthesiology [Internet]. 2000;93(4):1002–3. Available from: http://www.ncbi.nlm.nih.gov/pubmed/11020754

52. Thevarajah S, Huston TL, Simmons RM. A comparison of the adverse reactions associated with isosulfan blue versus methylene blue dye in sentinel lymph node biopsy for breast cancer. Am J Surg [Internet]. 2005 [cited 2018 Jul 5];189(2):236–9. Available from: https://ac.els-cdn.com/S0002961004005252/1-s2.0-S0002961004005252-main.pdf?_tid=4cbf33e9-dfac-451f-8389-79d14904fb8a&acdnat=1530792126_4242cc26f02c3b011c238acd2f576a74

53. Reyes F, Noelck M, Valentino C, Grasso-Lebeau L, Lang J. Complications of Methylene Blue Dye in Breast Surgery: Case Reports and Review of the Literature. J Cancer [Internet]. 2011 [cited 2018 Jul 5];2(2):20–5. Available from: http://www.jcancer.org

54. Motomura K, Inaji H, Komoike Y, Kasugai T, Noguchi S, Koyama H. Sentinel node biopsy guided by indocyanine green dye in breast cancer patients. Jpn J Clin Oncol [Internet]. 1999 Dec [cited 2018 Jul 5];29(12):604–7. Available from: http://www.ncbi.nlm.nih.gov/pubmed/10721942

55. Guo J, Yang H, Wang S, Cao Y, Liu M, Xie F, et al. Comparison of sentinel lymph node biopsy guided by indocyanine green, blue dye, and their combination in breast cancer patients: a prospective cohort study. World J Surg Oncol [Internet]. 2017 [cited 2018 Jul 5];15(196):doi: 10.1186/s12957-017-1264-7. Available from: https://www.ncbi.nlm.nih.gov/pmc/articles/PMC5667473/pdf/12957_2017_Article_1264.pdf

56. Wishart GC, Loh S-W, Jones L, Benson JR. A feasibility study (ICG-10) of indocyanine green (ICG) fluorescence mapping for sentinel lymph node detection in early breast cancer. Eur J Surg Oncol [Internet]. 2012;38(8):651–6. Available from: http://www.ncbi.nlm.nih.gov/pubmed/22704050

57. Royal College of Obstetricians and Gyanecologists [RCOG]. Sentinel lymph node biopsy in endometrial cancer; Scentific Impact Factor Paper No. 51. Vol. 51, RCOG. 2016.

58. Ballester M, Rouzier R, Daraï E, Dubernard G, Mathevet P, Ballester M, et al. Detection rate and diagnostic accuracy of sentinel-node biopsy in early stage endometrial cancer: a prospective multicentre study (SENTI-ENDO). Lancet Oncol [Internet]. 2011 [cited 2018 Jul 5];12(5):469–76. Available from: https://www.thelancet.com/pdfs/journals/lanonc/PIIS1470-2045(11)70070-5.pdf

59. Papadia A, Mohr S, Imboden S, Lanz S, Bolla D, Mueller MD. Laparoscopic Indocyanine Green Sentinel Lymph Node Mapping in Pregnant Cervical Cancer Patients. J Minim Invasive Gynecol. 2016;23(2):270–3.

60. ASGBI/ACPGBI, Anastomotic Leakage Working Group. Prevention, Diagnosis and Management of Colorectal Anastomotic Leakage [Internet]. Postgrad Med J. 2016. Available from: www.sign.ac.uk/guidelines/fulltext/67/section1.html

61. Jafari M, et al. Perfusion Assessment in Laparoscopic Left-Sided / Anterior Resection (PILLAR II): A Multi-Institutional Study. J Am Coll Surg [Internet]. 2015;220(1):82-92.e1. Available from: http://dx.doi.org/10.1016/j.jamcollsurg.2014.09.015

62. Stamos MJ, Wexner S. A Study Assessing Perfusion Outcomes With PINPOINT® Near Infrared Fluorescence Imaging in Low Anterior Resection (PILLAR III); ClinicalTrials.gov Identifier: NCT02205307 [Internet]. NIH U.S National Library of Medicine: ClinicalTrials.gov. 2020 [cited 2021 Mar 13]. Available from: https://clinicaltrials.gov/ct2/show/study/NCT02205307

63. National Institute for Health and Care Excellence (NICE). Costing statement: Gallstone disease Implementing the NICE guideline on gallstone disease (CG188) Putting NICE guidance into practice [Internet]. Manchester; 2014 [cited 2018 Jan 12]. Available from: https://www.nice.org.uk/guidance/cg188/resources/costing-statement-pdf-193298365

64. Halldestam I, Enell EL, Kullman E, Borch K. Development of symptoms and complications in individuals with asymptomatic gallstones. Br J Surg. 2004;91(6):734–8.

65. Strasberg SM. Acute Calculous Cholecystitis. N Engl J Med. 2008;359(3):325–325.

66. Carey MC. Pathogenesis of gallstones. Recent Prog Med [Internet]. 1992 [cited 2018 May 18];83(7–8):379–91. Available from: http://www.ncbi.nlm.nih.gov/pubmed/1529152

67. Tazuma S. Epidemiology, pathogenesis, and classification of biliary stones (common bile duct and intrahepatic). Best Pr Res Clin Gastroenterol [Internet]. 2006 [cited 2018 May 18];20(6):1075–83. Available from: https://www.sciencedirect.com/science/article/pii/S1521691806000710?via%3Dihub

68. Smith AL, Stewart L, Fine R, Pellegrini CA, Way LW. Gallstone disease. The clinical manifestations of infectious stones. Arch Surg [Internet]. 1989 May [cited 2018 May 18];124(5):629–33. Available from: http://www.ncbi.nlm.nih.gov/pubmed/2712705

69. Lynch JP, Metz DC, Maurer KJ, Carey MC, Fox JG. Roles of Infection, Inflammation, and the Immune System in Cholesterol Gallstone Formation. Gastroenterology [Internet]. 2009 [cited 2018 May 19];136(2):425–40. Available from: https://ac.els-cdn.com/S0016508508021872/1-s2.0-S0016508508021872-main.pdf?_tid=6caafa07-917f-43de-92f0-59165a086768&acdnat=1526727582_241c6e743c8c1ce5872a77f055b20646

70. University JH. Gallstone Disease: Symptoms and Clinical Features [Internet]. gastroenterology and hepatology/pancreas_biliary_tract/gallstone_disease. 2013 [cited 2018 May 19]. Available from: https://www.hopkinsmedicine.org/gastroenterology_hepatology/_pdfs/pancreas_biliary_tract/gallstone_disease.pdf

71. Demehri FR, Alam HB. Evidence-Based Management of Common Gallstone-Related Emergencies. J Intensive Care Med [Internet]. 2016 [cited 2018 May 19];31(1):3–13. Available from: http://journals.sagepub.com/doi/pdf/10.1177/0885066614554192

72. Peters JH, Ellison EC, Innes JT, Liss JL, Nichols KE, Lomano JM, et al. Safety and Efficacy of Laparoscopic Cholecystectomy: A Prospective Analysis of 100 Initial Patients. Ann Surg [Internet]. 1991 [cited 2018 Jan 12];213(1):3–12. Available from: https://www.ncbi.nlm.nih.gov/pmc/articles/PMC1358303/pdf/annsurg00155-0013.pdf

73. Soper J, et al. Laparoscopic cholecystectomy. Arch Surg. 1992;127:917–23.

74. Mühe E. Long-Term Follow-Up after Laparoscopic Cholecystectomy. Endoscopy [Internet]. 1992;24(09):754–8. Available from: http://www.thieme-connect.de/DOI/DOI?10.1055/s-2007-1009119

75. Richardson MC, Bell G, Fullarton GM. Incidence and nature of bile duct injuries following laparoscopic cholecystectomy: An audit of 5913 cases. Br J Surg. 1996;83(10):1356–60.

76. Peters JH, Krailadsiri W, Incarbone R, Bremner CG, Froes E, Ireland AP, et al. Reasons for conversion from laparoscopic to open cholecystectomy in an urban teaching hospital. Am J Surg. 1994;168(6):555–9.

77. Sutton A, Vohra RS, Hollyman M, Marriott PJ, Buja A, Alderson D, et al. Cost-effectiveness of emergency versus delayed laparoscopic cholecystectomy for acute gallbladder pathology. Br J Surg [Internet]. 2017;104(1):98–107. Available from: http://doi.wiley.com/10.1002/bjs.10317

78. Kum C, et al. Laparoscopic cholecystectomy for acute cholecystitis: is it really safe? World J Surg [Internet]. 1996;20(1):43–8; discussion 48-9. Available from: http://www.ncbi.nlm.nih.gov/pubmed/8588411

79. Gurusamy K, et al. Meta-analysis of randomized controlled trials on the safety and effectiveness of early versus delayed laparoscopic cholecystectomy for acute cholecystitis. Br J Surg. 2010;97(2):141–50.

80. de Mestral C, Rotstein OD, Laupacis A, Hoch JS, Zagorski B, Nathens AB. A population-based analysis of the clinical course of 10,304 patients with acute cholecystitis, discharged without cholecystectomy. J Trauma Acute Care Surg [Internet]. 2013 Jan [cited 2018 May 19];74(1):26–31. Available from: http://www.ncbi.nlm.nih.gov/pubmed/23271073

81. Young AL, et al. Index admission laparoscopic cholecystectomy for patients with acute biliary symptoms: Results from a specialist centre. HPB. 2010;12(4):270–6.

82. Vohra RS, Pasquali S, Kirkham AJ, Marriott P, Johnstone M, Spreadborough P, et al. Population-based cohort study of outcomes following cholecystectomy for benign gallbladder diseases. Br J Surg. 2016;103(12):1704–15.

83. Tan CHM, Pang TCY, Woon WWL, Low JK, Junnarkar SP. Analysis of actual healthcare costs of early versus interval cholecystectomy in acute cholecystitis. J Hepatobiliary Pancreat Sci [Internet]. 2015;22(3):237–43. Available from: http://doi.wiley.com/10.1002/jhbp.196

84. Pepingco L, Eslick GD, Cox MR. The acute surgical unit as a novel model of care for patients presenting with acute cholecystitis. Med J Aust. 2012;196(8):509–11.

85. de Reuver P., et al. Litigation after Laparoscopic Cholecystectomy: An Evaluation of the Dutch Arbitration System for Medical Malpractice. J Am Coll Surg. 2008;206(2):328–34.

86. Alkhaffaf B, Decadt B. 15 years of litigation following laparoscopic cholecystectomy in England. Ann Surg. 2010;251(4):682–5.

87. Flum DR, Cheadle A, Prela C, Dellinger EP, Chan L. Bile duct injury during cholecystectomy and survival in medicare beneficiaries. JAMA. 2003;290(16):2168–73.

88. Roy PG, Soonawalla ZF, Grant HW. Medicolegal costs of bile duct injuries incurred during laparoscopic cholecystectomy. HPB [Internet]. 2009 [cited 2018 May 19];11:130–4. Available from: https://www.ncbi.nlm.nih.gov/pmc/articles/PMC2697871/pdf/hpb0011-0130.pdf

89. McLean TR. Risk management observations from litigation involving laparoscopic cholecystectomy. Arch Surg. 2006;141(7):643–8; discussion 648.

90. Landman MP, Feurer ID, Moore DE, Zaydfudim V, Pinson CW. The long-term effect of bile duct injuries on health-related quality of life: A meta-analysis. Hpb [Internet]. 2013;15(4):252–9. Available from: http://dx.doi.org/10.1111/j.1477-2574.2012.00586.x

91. Strasberg S, Hertl M, Soper N. An analysis of the problem of biliary injury during laparoscopic cholecystectomy. J Am Coll Surg. 1995;180(1):101–25.

92. McMahon AJ, Fullarton G, Baxter JN, O'Dwyer PJ. Bile duct injury and bile leakage in laparoscopic cholecystectomy. Br J Surg. 1995;82(3):307–13.

93. Deziel DJ, Millikan KW, Economou SG, Doolas A, Ko ST, Airan MC. Complications of laparoscopic cholecystectomy: A national survey of 4,292 hospitals and an analysis of 77,604 cases. Am J Surg. 1993;165(1):9–14.

94. Nuzzo G, Giuliante F, Giovannini I, et al. Bile duct injury during laparoscopic cholecystectomy. Arch Surg. 2005;140(10):986–92.

95. Waage A, Nilsson M. Iatrogenic Bile Duct Injury: A Population-Based Study of 152 776 Cholecystectomies in the Swedish Inpatient Registry. Arch Surg. 2006;141(12):1207–13.

96. Krähenbühl L, Sclabas G, Wente MN, Schäfer M, Schlumpf R, Büchler MW. Incidence, Risk Factors, and Prevention of Biliary Tract Injuries during Laparoscopic Cholecystectomy in Switzerland. World J Surg [Internet]. 2001 [cited 2018 Feb 9];25(10):1325–30. Available from:

https://link.springer.com/content/pdf/10.1007%2Fs00268-001-0118-0.pdf

97. Buanes T, Mjåland O, Waage A, Langeggen H, Holmboe J. A population-based survey of biliary surgery in Norway Relationship between patient volume and quality of surgical treatment. Surg Endosc [Internet]. 1998 [cited 2018 Feb 9];12(6):852–5. Available from: https://link.springer.com/content/pdf/10.1007/s004649900728.pdf

98. Stewart L, Way LW. Bile Duct Injuries During Laparoscopic Cholecystectomy. Arch Surg [Internet]. 1995 Oct 1 [cited 2018 May 19];130(10):1123. Available from: http://archsurg.jamanetwork.com/article.aspx?doi=10.1001/archsurg.1995.01430100101019

99. Sheffield KM, Riall TS, Han Y, Kuo Y-F, Townsend CM, Goodwin JS. Association Between Cholecystectomy With vs Without Intraoperative Cholangiography and Risk of Common Duct Injury. JAMA. 2013;310(8):812–20.

100. Sarli L, Pietra N, Sansebastiano G, Cattaneo G, Costi R, Grattarola M, et al. Reduced Postoperative Morbidity after Elective Laparoscopic Cholecystectomy: Stratified Matched Case-Control Study. World J Surg [Internet]. 1997 [cited 2018 Feb 9];21(8):872–9. Available from: https://link.springer.com/content/pdf/10.1007%2Fs002689900320.pdf

101. Joseph M, Phillips MR, Farrell TM, Rupp CC. Single Incision Laparoscopic Cholecystectomy Is Associated With a Higher Bile Duct Injury Rate. Ann Surg [Internet]. 2012 Jul [cited 2018 Feb 9];256(1):1–6. Available from: http://www.ncbi.nlm.nih.gov/pubmed/22664556

102. Andrews S. Does concentration of surgical expertise improve outcomes for laparoscopic cholecystectomy? 9 year audit cycle. Surgeon [Internet]. 2013;11(6):309–12. Available from: http://dx.doi.org/10.1016/j.surge.2013.06.005

103. Boddy AP, Bennett JMH, Ranka S, Rhodes M. Who should perform laparoscopic cholecystectomy? A 10-year audit. Surg Endosc Other Interv Tech. 2007;21(9):1492–7.

104. Halbert C, Pagkratis S, Yang J, Meng Z, Altieri MS, Parikh P, et al. Beyond the learning curve: incidence of bile duct injuries following laparoscopic cholecystectomy normalize to open in the modern era. Surg Endosc. 2016;30(6):2239–43.

105. Wauben LSGL, Goossens RHM, van Eijk DJ, Lange JF. Evaluation of protocol uniformity concerning laparoscopic cholecystectomy in The Netherlands. World J Surg. 2008;32(4):613–20.

106. Buddingh KT, Nieuwenhuijs VB. The Critical View of Safety and Routine Intraoperative Cholangiography Complement Each Other as Safety Measures During Cholecystectomy. J Gastrointest Surg. 2011;15(6):1069–70.

107. Eikermann M, Siegel R, Broeders I, Dziri C, Fingerhut A, Gutt C, et al. Prevention and treatment of bile duct injuries during laparoscopic cholecystectomy: The clinical practice guidelines of the European Association for Endoscopic Surgery (EAES). Surg Endosc. 2012;26(11):3003–39.

108. Jamal KN, Smith H, Ratnasingham K, Siddiqui MR, McLachlan G, Belgaumkar AP. Meta-analysis of the diagnostic accuracy of laparoscopic ultrasonography and intraoperative cholangiography in detection of common bile duct stones. Ann R Coll Surg Engl. 2016;98(4):244–9.

109. Kumar A, Kumar U, Munghate A, Bawa A. Role of routine intraoperative cholangiography during laparoscopic cholecystectomy. Surg Endosc [Internet]. 2015;29(9):2837–40. Available from: http://dx.doi.org/10.1007/s00464-014-4002-z

110. Sajid MS, Leaver C, Haider Z, Worthington T, Karanjia N, Singh KK. Routine on-table cholangiography during cholecystectomy: a systematic review. Ann R Coll Surg Engl [Internet]. 2012 Sep [cited 2018 Feb 11];94(6):375–80. Available from: http://www.ncbi.nlm.nih.gov/pubmed/22943325

111. Flum D, Dellinger E, Cheadle A, Chan L, Koepsell T. Intraoperative Cholangiography and During Cholecystectomy. JAMA. 2003;289(13):1639–44.

112. Fletcher DR, Hobbs MS, Tan P, Valinsky LJ, Hockey RL, Pikora TJ, et al. Complications of cholecystectomy: risks of the laparoscopic approach and protective effects of operative cholangiography: a population-based study. Ann Surg. 1999;229:449–57.

113. Ludwig K, Bernhardt J, Steffen H, Lorenz D. Contribution of intraoperative cholangiography to incidence and outcome of common bile duct injuries during laparoscopic cholecystectomy. Surg Endosc. 2002;16(7):1098–104.

114. Sicklick JK, Camp MS, Lillemoe KD, Melton GB, Yeo CJ, Campbell KA, et al. Surgical Management of Bile Duct Injuries Sustained During Laparoscopic Cholecystectomy Perioperative Results in 200 Patients. Ann Surg [Internet]. 2005 [cited 2018 Feb 11];241(5):786–95. Available from: https://www.ncbi.nlm.nih.gov/pmc/articles/PMC1357133/pdf/20050500s00012p786.pdf

115. Sanjay P, Kulli C, Polignano FM, Tait IS. Optimal surgical technique, use of intra-

operative cholangiography (IOC), and management of acute gallbladder disease: the results of a nation-wide survey in the UK and Ireland. Ann R Coll Surg Engl. 2010;92(4):302–6.

116. Ragulin-Coyne E, Witkowski E, Chau Z, et al. Is Routine Intraoperative Cholangiogram Necessary in the Twenty-First Century? A National View. J Gastrointest Surg. 2013;17(3):434–42.

117. Buddingh KT, Hofker HS, Ten Cate Hoedemaker HO, Van Dam GM, Ploeg RJ, Nieuwenhuijs VB. Safety measures during cholecystectomy: Results of a nationwide survey. World J Surg. 2011;35(6):1235–41.

118. Sheen AJ, Asthana S, Al-Mukhtar A, Attia M, Toogood GJ. Preoperative determinants of common bile duct stones during laparoscopic cholecystectomy. Int J Clin Pr. 2008;62(11):1715–9.

119. Khan OA, Balaji S, Branagan G, Bennett DH, Davies N. Randomized clinical trial of routine on-table cholangiography during laparoscopic cholecystectomy. Br J Surg. 2011;98(3):362–7.

120. Figueiredo JL, Siegel C, Nahrendorf M, Weissleder R. Intraoperative near-infrared fluorescent cholangiography (nirfc) in mouse models of bile duct injury. World J Surg. 2010;34(2):336–43.

121. Ishizawa T, Bandai Y, Kokudo N. Fluorescent Cholangiography Using Indocyanine Green for Laparoscopic Cholecystectomy: An Initial Experience. Arch Surg. 2009;144(4):381–2.

122. Ishizawa T, Bandai Y, Ijichi M, Kaneko J, Hasegawa K, Kokudo N. Fluorescent cholangiography illuminating the biliary tree during laparoscopic cholecystectomy. Br J Surg. 2010;97(9):1369–77.

123. Zarrinpar A, Dutson EP, Mobley C, Busuttil RW, Lewis CE, Tillou A, et al. Intraoperative Laparoscopic Near-Infrared Fluorescence Cholangiography to Facilitate Anatomical Identification: When to Give Indocyanine Green and How Much. Surg Innov [Internet]. 2016;23(4):360–5. Available from: http://sri.sagepub.com/cgi/doi/10.1177/1553350616637671

124. Verbeek FPR, Schaafsma BE, Tummers QRJG, Van Der Vorst JR, Van Der Made WJ, Baeten CIM, et al. Optimization of near-infrared fluorescence cholangiography for open and laparoscopic surgery. Surg Endosc Other Interv Tech. 2014;28(4):1076–82.

125. Lifestyles Team NHS Digital.; Statistics on Obesity, Physical Activity and Diet. NHS Digital. 2020.

126. Osayi SN, Wendling MR, Drosdeck JM, Chaudhry UI, Perry KA, Noria SF, et al. Near-infrared fluorescent cholangiography facilitates identification of biliary anatomy during laparoscopic cholecystectomy. Surg Endosc. 2015;29(2):368–75.

127. Kono Y, Ishizawa T, Tani K, Harada N, Kaneko J, Saiura A, et al. Techniques of Fluorescence Cholangiography During Laparoscopic Cholecystectomy for Better Delineation of the Bile Duct Anatomy. Medicine (Baltimore) [Internet]. 2015;94(25):e1005. Available from: http://content.wkhealth.com/linkback/openurl?sid=WKPTLP:landingpage&an=00005792-201506040-00014

128. Tagaya N, Shimoda M, Kato M, Nakagawa A, Abe A, Iwasaki Y, et al. Intraoperative exploration of biliary anatomy using fluorescence imaging of indocyanine green in experimental and clinical cholecystectomies. J Hepatobiliary Pancreat Sci. 2010;17(5):595–600.

129. Jewell EL, Huang JJ, Abu-Rustum NR, Gardner GJ, Brown CL, Sonoda Y, et al. Detection of sentinel lymph nodes in minimally invasive surgery using indocyanine green and near-infrared fluorescence imaging for uterine and cervical malignancies. Gynecol Oncol [Internet]. 2014;133(2):274–7. Available from: http://dx.doi.org/10.1016/j.ygyno.2014.02.028

130. Zroback C, Chow G, Meneghetti A, Warnock G, Meloche M, Chiu CJ, et al. Fluorescent cholangiography in laparoscopic cholecystectomy: The initial Canadian experience. Am J Surg [Internet]. 2016;211(5):933–7. Available from: http://dx.doi.org/10.1016/j.amjsurg.2016.01.013

131. Buchs NC, Pugin F, Azagury DE, Jung M, Volonte F, Hagen ME, et al. Real-time near-infrared fluorescent cholangiography could shorten operative time during robotic single-site cholecystectomy. Surg Endosc Other Interv Tech. 2013;27(10):3897–901.

132. Boni L, et al. Clinical applications of indocyanine green (ICG) enhanced fluorescence in laparoscopic surgery. Surg Endosc [Internet]. 2015;29(7):2046–55. Available from: http://www.pubmedcentral.nih.gov/articlerender.fcgi?artid=4471386&tool=pmcentrez&rendertype=abstract

133. Schols RM, Bouvy ND, Masclee AAM, Van Dam RM, Dejong CHC, Stassen LPS. Fluorescence cholangiography during laparoscopic cholecystectomy: A feasibility study

on early biliary tract delineation. Surg Endosc Other Interv Tech. 2013;27(5):1530–6.

134. Daskalaki D, Fernandes E, Wang X, Bianco FM, Elli EF, Ayloo S, et al. Indocyanine green (ICG) fluorescent cholangiography during robotic cholecystectomy: results of 184 consecutive cases in a single institution. Surg Innov [Internet]. 2014;21(6):615–21. Available from: http://sri.sagepub.com/content/21/6/615.full.pdf

135. Spinoglio G, Priora F, Bianchi P Pietro, Lucido FS, Licciardello A, Maglione V, et al. Real-time near-infrared (NIR) fluorescent cholangiography in single-site robotic cholecystectomy (SSRC): A single-institutional prospective study. Surg Endosc Other Interv Tech. 2013;27(6):2156–62.

136. Igami T, Nojiri M, Shinohara K, Ebata T, Yokoyama Y, Sugawara G, et al. Clinical value and pitfalls of fluorescent cholangiography during single-incision laparoscopic cholecystectomy. Surg Today. 2016;46(12):1–8.

137. Ishizawa T, Kaneko J, Inoue Y, Takemura N, Seyama Y, Aoki T, et al. Application of fluorescent cholangiography to single-incision laparoscopic cholecystectomy. Surg Endosc Other Interv Tech. 2011;25(8):2631–6.

138. Ishizawa T, Bandai Y, Harada N, Muraoka A, Ijichi M, Kusaka K, et al. Indocyanine green-fluorescent imaging of hepatocellular carcinoma during laparoscopic hepatectomy: An initial experience. Asian J Endosc Surg [Internet]. 2010 Feb 1 [cited 2018 Mar 18];3(1):42–5. Available from: http://doi.wiley.com/10.1111/j.1758-5910.2009.00025.x

139. Cancer Research UK. Bowel cancer incidence statistics [Internet]. 2018 [cited 2019 Dec 7]. Available from: https://www.cancerresearchuk.org/health-professional/cancer-statistics/statistics-by-cancer-type/bowel-cancer/incidence

140. Cancer Research UK. Bowel cancer statistics | Cancer Research UK [Internet]. Bowel cancer statistics. 2016 [cited 2018 Mar 18]. Available from: http://www.cancerresearchuk.org/health-professional/cancer-statistics/statistics-by-cancer-type/bowel-cancer

141. National Cancer Intelligence Network. Colorectal cancer survival by stage [Internet]. 2009. Available from: http://www.ncin.org.uk/publications/data_briefings/colorectal_cancer_survival_by_stage

142. Hohenberger W, Weber K, Matzel K, Papadopoulos T, Merkel S. Standardized surgery for colonic cancer: Complete mesocolic excision and central ligation - Technical notes

and outcome. Color Dis. 2009;11(4):354–64.

143. Yun HR, Lee LJ, Park JH, Cho YK, Cho YB, Lee WY, et al. Local recurrence after curative resection in patients with colon and rectal cancers. Int J Color Dis [Internet]. 2008 [cited 2018 Jan 28];23(11):1081–7. Available from: https://link.springer.com/content/pdf/10.1007%2Fs00384-008-0530-0.pdf

144. Sjövall A, Granath F, Cedermark B, Glimelius B, Holm T. Loco-regional Recurrence from Colon Cancer: A Population-based Study. Ann Surg Oncol [Internet]. 2007 [cited 2018 Jan 28];14(2):432–440. Available from: https://link.springer.com/content/pdf/10.1245%2Fs10434-006-9243-1.pdf

145. Mansouri D, Mcmillan DC, Crearie C, Morrison DS, Crighton EM, Horgan PG. Temporal trends in mode, site and stage of presentation with the introduction of colorectal cancer screening: a decade of experience from the West of Scotland. B J Cancer [Internet]. 2015 [cited 2018 Apr 5];113(3):556–61. Available from: https://www.nature.com/articles/bjc2015230.pdf

146. Public Health Enngland. New home test kit for bowel cancer screening: what GPs need to know - PHE screening [Internet]. 2017 [cited 2018 Jun 1]. Available from: https://phescreening.blog.gov.uk/2017/08/04/new-home-test-kit-for-bowel-cancer-screening-what-gps-need-to-know/

147. Atkin W, Wooldrage K, Parkin M, Kralj-Hans I, Macrae E, Shah U, et al. Long-term effects of once-only flexible sigmoidoscopy screening after 17 years of follow-up: the UK Flexible Sigmoidoscopy Screening randomised controlled trial. Lancet [Internet]. 2017 [cited 2018 Jun 1];389(10076):1299–1311. Available from: https://www.thelancet.com/pdfs/journals/lancet/PIIS0140-6736(17)30396-3.pdf

148. Logan RFA, Patnick J, Nickerson C, Coleman L, Rutter MD, Wagner C Von. Outcomes of the Bowel Cancer Screening Programme (BCSP) in England after the first 1 million tests. Gut [Internet]. 2012 [cited 2018 Jan 29];61:1439–46. Available from: http://gut.bmj.com/content/gutjnl/61/10/1439.full.pdf

149. Loughrey M, Quirke P, Shepherd NAN, Hospital GR. G049 Dataset for histopathological reporting of colorectal cancer. Royal College of Pathologists.,. 2017.

150. Liska D, Stocchi L, Karagkounis G, Elagili F, Dietz DW, Kalady MF, et al. Incidence, Patterns, and Predictors of Locoregional Recurrence in Colon Cancer. Ann Surg Oncol. 2017;24(4):1093–9.

151. Phillips EH, Franklin M, Carroll BJ, et al; Laparoscopic colectomy. Ann Surg.

1992;216(6):703–7.

152. Guillou PJ, Quirke P, Thorpe H, et al; Short-term endpoints of conventional versus laparoscopic-assisted surgery in patients with colorectal cancer (MRC CLASICC trial): Multicentre, randomised controlled trial. Lancet. 2005;365(9472):1718–26.

153. Jayne DG, Guillou PJ, Thorpe H, et al; Randomized trial of laparoscopic-assisted resection of colorectal carcinoma: 3-Year results of the UK MRC CLASICC trial group. J Clin Oncol. 2007;25(21):3061–8.

154. Abraham NS, Young JM, Solomon MJ. Meta-analysis of short-term outcomes after laparoscopic resection for colorectal cancer. Br J Surg. 2004;91(9):1111–24.

155. Jayne DG, Thorpe HC, Copeland J, et al; Five-year follow-up of the Medical Research Council CLASICC trial of laparoscopically assisted versus open surgery for colorectal cancer. BJS. 2010;97(11):1638–45.

156. The COlon cancer Laparoscopic or Open Resection Study Group. Laparoscopic surgery versus open surgery for colon cancer short-term outcomes of a randomised trial. Lancet Oncol [Internet]. 2005 [cited 2018 Jan 29];6(7):477–84. Available from: http://oncology.thelancet.com

157. Heald RJ, Husband EM, Ryall RDH. The mesorectum in rectal cancer surgery-the clue to pelvic recurrence? Br J Surg. 1982;69(10):613–6.

158. Heald RJ, Moran BJ, Ryall RD, Sexton R, MacFarlane JK. Rectal cancer: the Basingstoke experience of total mesorectal excision, 1978-1997. Arch Surg [Internet]. 1998 [cited 2018 Apr 5];133(8):894–9. Available from: http://www.ncbi.nlm.nih.gov/pubmed/9711965

159. Willaert W, Ceelen W. Extent of surgery in cancer of the colon: Is more better? World J Gastroenterol. 2015;21(1):132–8.

160. Søndenaa K, Quirke P, Hohenberger W, Sugihara K, Kobayashi H, Kessler H, et al. The rationale behind complete mesocolic excision (CME) and a central vascular ligation for colon cancer in open and laparoscopic surgery Proceedings of a consensus conference. Int J Color Dis [Internet]. 2014 [cited 2018 Apr 5];29(4):419–28. Available from: https://link.springer.com/content/pdf/10.1007%2Fs00384-013-1818-2.pdf

161. Bertelsen CA, Neuenschwander AU, Jansen JE, Wilhelmsen M, Kirkegaard-Klitbo A, Tenma JR, et al. Disease-free survival after complete mesocolic excision compared with conventional colon cancer surgery: a retrospective, population-based study.

Lancet Oncol [Internet]. 2014 [cited 2018 Apr 5];16(2):161–8. Available from: http://dx.doi.org/10.1016/

162. Boyle J, Braun M, Eaves E, Hill J, Kuryba A, Roe A, et al. National Bowel Cancer Audit Annual Report 2017 V2.0 [Internet]. London; 2017 [cited 2018 Apr 5]. Available from: https://www.hqip.org.uk/public/cms/253/625/19/1021/NBOCA-annual-report-2017-Final_v2correction.pdf?realName=oSMuCg.pdf&v=0

163. Acuna SA, Elmi M, Shah PS, Coburn NG, Quereshy FA, Quereshy FayezQuereshy FA. Preoperative localization of colorectal cancer: a systematic review and meta-analysis. Surg Endosc [Internet]. 2017;31(6):2366–79. Available from: https://link.springer.com/content/pdf/10.1007%2Fs00464-016-5236-8.pdf

164. Reynolds IS, Majeed • M H, Soric • I, Whelan • M, Deasy • J, Mcnamara • D A. Endoscopic tattooing to aid tumour localisation in colon cancer: the need for standardisation. Ir J Med Sci [Internet]. 2017 [cited 2019 Mar 1];186(1):75–80. Available from: https://link.springer.com/content/pdf/10.1007%2Fs11845-016-1502-y.pdf

165. Conaghan PJ, Maxwell-Armstrong CA, Garrioch M V., Hong L, Acheson AG. Leaving a mark: the frequency and accuracy of tattooing prior to laparoscopic colorectal surgery. Color Dis [Internet]. 2011 Oct [cited 2018 Dec 17];13(10):1184–7. Available from: http://www.ncbi.nlm.nih.gov/pubmed/20860715

166. Foxtrot Collaborative Group. Feasibility of preoperative chemotherapy for locally advanced, operable colon cancer: the pilot phase of a randomised controlled trial. Lancet Oncol [Internet]. 2012 [cited 2018 Jan 29];13(13):1152–60. Available from: http://dx.doi.org/10.1016/

167. Rollvén E, Abraham-Nordling M, Holm T, Blomqvist L. Assessment and diagnostic accuracy of lymph node status to predict stage III colon cancer using computed tomography. Cancer Imaging [Internet]. 2017 [cited 2018 Jul 11];3(1):doi: 10.1186/s40644-016-0104-2. Available from: http://www.ncbi.nlm.nih.gov/pubmed/28103922

168. Bertagnolli M, Miedema B, Redston M, Dowell J, Niedzwiecki D, Fleshman J, et al. Sentinel Node Staging of Resectable Colon Cancer Results of a Multicenter Study. Ann Surg [Internet]. 2004 [cited 2019 Apr 8];240(4):624–30. Available from: https://www.ncbi.nlm.nih.gov/pmc/articles/PMC1356464/pdf/20041000s00008p624.pdf

169. Redston M, Compton CC, Miedema BW, Niedzwiecki D, Dowell JM, Jewell SD, et al.

Analysis of micrometastatic disease in sentinel lymph nodes from resectable colon cancer: Results of cancer and leukemia group B trial 80001. J Clin Oncol. 2006;24(6):878–83.

170. Tan KY, Kawamura YJ, Mizokami K, Sasaki J, Tsujinaka S, Maeda T, et al. Distribution of the first metastatic lymph node in colon cancer and its clinical significance. Color Dis. 2010;12(1):44–7.

171. Andrew H, Gossedge G, Croft J, Corrigan N, Brown J, Cahill C, et al. A88: GLiSten: next generation intraoperative lymph node staging for stratified colon cancer surgery: trial update | NCRI Cancer Conference abstracts. In: NCRI Cancer Conference [Internet]. Liverpool; 2015 [cited 2018 Jul 11]. Available from: http://abstracts.ncri.org.uk/abstract/glisten-next-generation-intraoperative-lymph-node-staging-for-stratified-colon-cancer-surgery-trial-update-2/

172. Jayne D, Gossedge G, Cahill R, Taylor GW, Corrigan N, Napp V, et al. GLiSten (Next Generation intraoperative Lymph node staging for Stratified colon cancer surgery - Developmental phase) Protocol. Leeds; 2014.

173. DrugBank Inc. Aminolevulinic acid [Internet]. DrugBank (version 5.1.3). 2019 [cited 2019 Apr 9]. p. Aminolevulinic acid. Available from: https://www.drugbank.ca/drugs/DB00855

174. Nabavi A, Thurm H, Zountsas B, Pietsch T, Lanfermann H, Pichlmeier U, et al. Five-aminolevulinic acid for fluorescence-guided resection of recurrent malignant gliomas: A phase II study. Neurosurgery [Internet]. 2009 Dec;65(6):1070–7. Available from: www.neurosurgery-online.com

175. Hadjipanayis CG, Stummer · Walter. 5-ALA and FDA approval for glioma surgery. J Neurooncol [Internet]. 2019 [cited 2019 Apr 9];141(3):479–86. Available from: https://doi.org/10.1007/s11060-019-03098-y

176. Andrew H, Gossedge G, Croft J, Corrigan N, Brown JM, West N, et al. Next Generation intraoperative Lymph node staging for Stratified colon cancer surgery (GLiSten): a multicentre, multinational feasibility study of fluorescence in predicting lymph node-positive disease. Effic Mech Eval. 2016;3(6):1–122.

177. Hoogstins CES, Tummers QRJG, Gaarenstroom KN, De Kroon CD, Trimbos JBMZ, Bosse T, et al. A novel tumor-specific agent for intraoperative near-infrared fluorescence imaging: A translational study in healthy volunteers and patients with ovarian cancer. Clin Cancer Res. 2016;22(12):2929–38.

178. Nakamura T, Teramoto H, Ichihara A. Purification and characterization of a growth factor from rat platelets for mature parenchymal hepatocytes in primary cultures. Proc Natl Acad Sci U S A [Internet]. 1986;83(17):6489–93. Available from: http://www.pubmedcentral.nih.gov/articlerender.fcgi?artid=386529&tool=pmcentrez&rendertype=abstract

179. Nakamura T, Nawa K, Ichihara A. Partial purification and characterization of hepatocyte growth factor from serum of hepatectomized rats. Biochem Biophys Res Commun. 1984;122(3):1450–9.

180. Miyazawa K, Tsubouchi H, Naka D. Molecular Cloning and Sequence Analysis of cDNA for Human Hepatocyte Growth Factor. Biochem Biophys Res Commun. 1989;163(2):967–73.

181. Nakamura T, Nishizawa T, Hagiya M, Seki T, Shimonishi M, Sugimura a, et al. Molecular cloning and expression of human hepatocyte growth factor. Nature. 1989;342(6248):440–3.

182. Gohda E, Tsubouchi H, Nakayama H, Hirono S, Arakaki N, Yamamoto I, et al. Human hepatocyte growth factor in blood of patients with fulminant hepatic failure. Basic aspects. Dig Dis Sci. 1991;36(6):785-90.

183. Stoker M, Perryman M. An epithelial scatter factor released by embryo fibroblasts. J Cell Sci [Internet]. 1985;77(1):209–23. Available from: http://www.ncbi.nlm.nih.gov/pubmed/3841349

184. Stoker M, Gherardi E, Perryman M, Gray J. Scatter factor is a fibroblast-derived modulator of epithelial cell mobility. Nature [Internet]. 1987 [cited 2018 Jun 13];327(6119):239–42. Available from: https://www.nature.com/articles/327239a0.pdf

185. Stoker M. Effect of scatter factor on motility of epithelial cells and fibroblasts. J Cell Physiol [Internet]. 1989;139(3):565–9. Available from: http://www.ncbi.nlm.nih.gov/pubmed/2525565

186. Weidner KM, Behrens J, Vandekerckhove J, Birchmeier W. Scatter factor: Molecular characteristics and effect on the invasiveness of epithelial cells. J Cell Biol. 1990;111(5):2097–108.

187. Naldini L, Weidner KM, Vigna E, Gaudino G, Bardelli A, Ponzetto C, et al. Scatter factor and hepatocyte growth factor are indistinguishable ligands for the MET receptor. EMBO J [Internet]. 1991;10(10):2867–78. Available from: http://www.ncbi.nlm.nih.gov/pubmed/1655405%5Cnhttp://www.pubmedcentral.nih.gov

/articlerender.fcgi?artid=PMC452997

188. Matsumoto K, Nakamura T. Hepatocyte growth factor: Molecular structure and implications for a central role in liver regeneration. J Gastroenterol Hepatol [Internet]. 1991;6(5):509–19. Available from: http://doi.wiley.com/10.1111/j.1440-1746.1991.tb00897.x%5Cnhttp://www.ncbi.nlm.nih.gov/pubmed/1312869

189. Han Z, Wu Y, Wang K, Xiao Y, Cheng Z, Sun X, et al. Analysis of progress and challenges for various patterns of c-MET-targeted molecular imaging: a systematic review. EJNMMI Res. 2017;7(41):doi: 10.1186/s13550-017-0286-z.

190. Donate LE, Gherardi E, Srinivasan N, Sowdhamini R, Aparicio S, Blundell TL. Molecular evolution and domain structure of plasminogen-related growth factors (MGF/SF and HGF1/MSP). Protein Sci. 1994;3:2378–94.

191. Birchmeier C, Gherardi E. Developmental roles of HGF/SF and its receptor, the c-met tyrosine kinase. Trends Cell Biol. 1998;8(10):404–10.

192. Cooper CS, Park M, Blair DG, Tainsky M a, Huebner K, Croce CM, et al. Molecular cloning of a new transforming gene from a chemically transformed human cell line. Nature [Internet]. 1984;311(5981):29–33. Available from: http://europepmc.org/abstract/MED/6590967%5Cnhttp://www.ncbi.nlm.nih.gov/pubmed/6590967

193. Bottaro D, Rubin J, Faletto D, et al. Identification of the hepatocyte growth factor receptor as the c-met proto-oncogene product. Science (80-). 1991;251(4995):802–4.

194. Belen Fajardo-Puerta A, Mato Prado M, Frampton AE, Jiao LR. Gene of the month: HGF. J Clin Pathol [Internet]. 2016 [cited 2019 Apr 28];69(7):575–9. Available from: https://mc.manuscriptcentral.com/jclinpathol

195. Mo H-N, Liu P. Targeting MET in cancer therapy. Chronic Dis Transl Med [Internet]. 2017;3(3):148–53. Available from: http://dx.doi.org/10.1016/j.cdtm.2017.06.002

196. Schmidt C, Bladt F, Goedecke S, Brlnkmann V, Zschiesche W, Sharpet M, et al. Scatter factor / hepatocyte essential for liver development. Nature. 1995;373(6516):699–702.

197. Nakamura T, Sakai K, Nakamura T, Matsumoto K. Hepatocyte growth factor twenty years on: Much more than a growth factor. J Gastroenterol Hepatol [Internet]. 2011;26(Suppl 1):188–202. Available from: http://www.ncbi.nlm.nih.gov/pubmed/21199531

198. Cirri P, Chiarugi P. Cancer-associated-fibroblasts and tumour cells: A diabolic liaison

driving cancer progression. Cancer Metastasis Rev. 2012;31(1–2):195–208.

199. Matsumoto K, Umitsu M, De Silva DM, Roy A, Bottaro DP. Hepatocyte growth factor/MET in cancer progression and biomarker discovery. Cancer Sci. 2017;108(3):296–307.

200. Organ SL, Tsao MS. An overview of the c-MET signaling pathway. Ther Adv Med Oncol. 2011;3(1 suppl):S7-19.

201. Matsumoto K, Nakamura T. Hepatocyte growth factor: molecular structure, roles in liver regeneration, and other biological functions. Crit Rev Oncog [Internet]. 1992 [cited 2018 Apr 5];3(1–2):27–54. Available from: http://www.ncbi.nlm.nih.gov/pubmed/1312869

202. Pennacchietti S, Michieli P, Galluzzo M, et al; Hypoxia promotes invasive growth by transcriptional activation of the met protooncogene. Cancer Cell. 2003;3(4):347–61.

203. Lee SJ, Lee J, Park SH, et al; c-MET Overexpression in Colorectal Cancer: A Poor Prognostic Factor for Survival. Clin Color Cancer. 2018;17(3):165–9.

204. Zeng Z, Weiser MR, D'Alessio M, Grace A, Shia J, Paty PB. Immunoblot analysis of c-Met expression in human colorectal cancer: overexpression is associated with advanced stage cancer. Clin Exp Metastasis. 2004;21(5):409–17.

205. Schweiger T, Starkl V, Glueck O, Glogner C, Traxler D, Jedamzik J, et al. Clinical impact of c-MET expression and mutational status in patients with colorectal cancer lung metastases. Eur J Cardio-thoracic Surg. 2016;49(4):1103–11.

206. Conor A. B, Dunne PD, Bingham V, et al. Transcriptional upregulation of c-MET is associated with invasion and tumor budding in colorectal cancer. Oncotarget. 2016;7(48):78932–45.

207. Liu Y, Yu X, Zou J, et al; Prognostic value of c-Met in colorectal cancer: A meta-analysis. World J Gastroenterol. 2015;21(12):3706–10.

208. Takeuchi H, Bilchik A, Saha S, Turner R, Wiese D, Tanaka M, et al. c-MET Expression Level in Primary Colon Cancer : A Predictor of Tumor Invasion and Lymph Node Metastases c-MET Expression Level in Primary Colon Cancer : A Predictor of Tumor Invasion and Lymph Node Metastases 1. Clin Cancer Res. 2003;9:1480–8.

209. Fearon EF, Vogelstein B. A Genetic Model for Colorectal Tumorigenesis. Cell. 1990;61(5):759–67.

210. Nakayama M, Sakai E, Echizen K, Yamada Y, Oshima H, Han TS, et al. Intestinal cancer progression by mutant p53 through the acquisition of invasiveness associated

with complex glandular formation. Oncogene [Internet]. 2017;36(42):5885–96. Available from: http://dx.doi.org/10.1038/onc.2017.194

211. Vogelstein B, Lane D, Levine AJ. p53: The Most Frequently Altered Gene in Human Cancers. Nature [Internet]. 2010;3(9):6. Available from: http://www.nature.com/articles/35042675

212. Muller PAJ, Trinidad AG, Timpson P, Morton JP, Zanivan S, Van Den Berghe PVE, et al. Mutant p53 enhances MET trafficking and signalling to drive cell scattering and invasion. Oncogene [Internet]. 2013;32(10):1252–65. Available from: http://dx.doi.org/10.1038/onc.2012.148

213. Inno A, Di Salvatore M, Cenci T, Martini M, Orlandi A, Strippoli A, Ferrara AM, Bagalà C, Cassano A, Larocca LM BC. Is there a role for IGF1R and c-MET pathways in resistance to cetuximab in metastatic colorectal cancer? Clin Color Cancer. 2011;10(4):325–32.

214. Giordano G, Remo A, Porras A, Pancione M. Immune resistance and egfr antagonists in colorectal cancer. Cancers (Basel). 2019;11(8).

215. Iveson T, Donehower RC, Davidenko I, Tjulandin S, Deptala A, Harrison M, et al. Rilotumumab in combination with epirubicin, cisplatin, and capecitabine as first-line treatment for gastric or oesophagogastric junction adenocarcinoma: An open-label, dose de-escalation phase 1b study and a double-blind, randomised phase 2 study. Lancet Oncol [Internet]. 2014;15(9):1007–18. Available from: http://dx.doi.org/10.1016/S1470-2045(14)70023-3

216. Catenacci DVT, Tebbutt NC, Davidenko I, Murad AM, Ilson DH, Tjulandin S, et al. Rilotumumab plus epirubicin, cisplatin, and capecitabine as first-line therapy in advanced MET-positive gastric or gastro- oesophageal junction cancer (RILOMET-1): a randomised, double-blind, placebo-controlled, phase 3 trial. Lancet Oncol. 2017;18(11):1467–82.

217. Lee J, Kim ST, Park S, Lee S, Park SH, Park JO, et al. Phase I Trial of Anti-MET Monoclonal Antibody in MET-Overexpressed Refractory Cancer. Clin Colorectal Cancer [Internet]. 2018;17(2):140–6. Available from: https://doi.org/10.1016/j.clcc.2018.01.005

218. Burggraaf J, Kamerling IMC, Gordon PB, Schrier L, de Kam ML, Kales AJ, et al. Detection of colorectal polyps in humans using an intravenously administered fluorescent peptide targeted against c-Met. Nat Med [Internet]. 2015;21(8):955–61.

Available from: http://dx.doi.org/10.1038/nm.3641%5Cnpapers3://publication/doi/10.1038/nm.3641

219. GE Healthcare. c-Met expression in human normal and tumor tissue. 2008.

220. Edinburgh Molecular Imaging Ltd. Edinburgh Molecular Imaging Ltd - Investigator's Brochure for EMI-137. 2017.

221. Esfahani SA, Heidari P, Kim SA, Ogino S, Mahmood U, Athinoula A. Optical Imaging of Mesenchymal Epithelial Transition Factor (MET) for Enhanced Detection and Characterization of Primary and Metastatic Hepatic Tumors. Theranostics [Internet]. 2016 [cited 2018 Mar 14];6(12):2028–38. Available from: http://www.thno.org

222. ClinCalc LLC. Sample Size Calculator [Internet]. ClinCalc LLC. 2019 [cited 2019 Apr 15]. p. Sample Size Calculator. Available from: https://clincalc.com/stats/samplesize.aspx

223. Davarinejad H. Quantifications of Western Blots with ImageJ [Internet]. University of York. 2015 [cited 2018 Jan 25]. Available from: http://www.yorku.ca/yisheng/Internal/Protocols/ImageJ.pdf

224. Dighe S, Swift I, Magill L, Handley K, Gray R, Quirke P, et al. Accuracy of radiological staging in identifying high-risk colon cancer patients suitable for neoadjuvant chemotherapy: A multicentre experience. Color Dis. 2012;14(4):438–44.

225. Sobin LH, Fleming ID. TNM classification of malignant tumors, Fifth edition (1997). Cancer. 1997;80(9):1803–4.

226. Tiernan JP, Ansari I, Hirst NA, Millner PA, Hughes TA, Jayne DG. Intra-operative tumour detection and staging in colorectal cancer surgery. Color Dis. 2012;14(9):510–20.

227. Tiernan JP. Developing a fluorescent, tumour- specific, molecular imaging platform for laparoscopic colorectal cancer surgery. University of Leeds; 2014.

228. Tiernan JP, Perry SL, Verghese ET, et al; Carcinoembryonic antigen is the preferred biomarker for in vivo colorectal cancer targeting. Br J Cancer. 2013;108(3):662–7.

229. Lombardi DP, Geradts J, Foley JF, et al; Loss of KA1 expression in the progression of colorectal cancer. Cancer Res. 1999;59(22):5724–31.

230. Soslow RA, Dannenberg AJ, Rush D, et al; COX-2 is expressed in human pulmonary, colonic, and mammary tumors. Cancer. 2000 Dec;89(12):2637–45.

231. Lyall MS, Dundas SR, Curran S, et al; Profiling markers of prognosis in colorectal cancer. Clin Cancer Res. 2006;12(4):1184–91.

232. Mood A, Graybill F. Nonparameteric Methods. In: Introduction to the Theory of Statistics. 2nd ed. New York: McCraw-Hill; 1963. p. 504–26.

233. McGee S. Simplifying likelihood ratios. J Gen Intern Med. 2002;17(8):647–50.

234. Stuart K a, Riordan SM, Lidder S, Crostella L, Williams R, Skouteris GG. Hepatocyte growth factor/scatter factor-induced intracellular signalling. Int J Exp Pathol [Internet]. 2000;81(1):17–30. Available from: http://www.pubmedcentral.nih.gov/articlerender.fcgi?artid=2517792&tool=pmcentrez&rendertype=abstract

235. Robey RB, Weisz J, Kuemmerle NB, Salzberg AC, Berg A, Brown DG, et al. Metabolic reprogramming and dysregulated metabolism: cause, consequence and/or enabler of environmental carcinogenesis? Carcinogenesis [Internet]. 2015 [cited 2017 Jun 3];36(1):203–31.

236. Rasola A, Fassetta M, De Bacco F, et al; A positive feedback loop between hepatocyte growth factor receptor and b-catenin sustains colorectal cancer cell invasive growth. Oncogene. 2007;26(7):1078–87.

237. Takeuchi H, Bilchik A, Saha S, et al. c-met expression level in primary colon cancer: A predictor of tumor invasion and lymph node metastases. Clin Cancer Res. 2003;9(4):1480–8.

238. Goyal L, Muzumdar MD, Zhu AX. Targeting the HGF/c-MET pathway in hepatocellular carcinoma. Clin Cancer Res. 2013;19(9):2310–8.

239. Gayyed MF, Abd El-Maqsoud NMR, El-Heeny AAEH, et al; c-MET expression in colorectal adenomas and primary carcinomas with its corresponding metastases. J Gastrointest Oncol. 2015;6(6):618–27.

240. Brierley J, Gospodarowicz M, Wittekind C. TNM Classification of Malignant Tumours, Eighth Edition. 8th ed. Union for International Cancer Control (UICC); 2016. 73–77 p.

241. Nioka. S, Wen. S, Zhang. J, et al. Simulation Study of Breast Tissue Hemodynamics During Pressure Perturbation. In: Advances in Experimental Medicine and Biology. vol 556. Boston, MA: Springer International Publishing; 2005. p. 17–22.

242. Liska D, Chen C, Bachleitner-hofmann T, Christensen JG, Weiser MR. HGF rescues colorectal cancer cells from EGFR inhibition via MET activation. Clin Cancer Res.

2012;17(3):472–82.

APPENDIX

MHRA

Regulating Medicines and Medical Devices

MHRA
151 Buckingham Palace Road
London SW1W 9SZ
United Kingdom

mhra.gov.uk

Prof D G Jayne
LEEDS TEACHING HOSPITALS NHS TRUST
LEVEL 7, CLINICAL SCIENCES BUILDING
ST JAMES'S UNIVERSITY HOSPITAL
LEEDS
LS9 7TF
UNITED KINGDOM

29/08/2017

Dear Prof D G Jayne

THE MEDICINES FOR HUMAN USE (CLINICAL TRIALS) REGULATIONS 2004 S.I. 2004/1031

Our Reference:	16767/0234/001-0001
Eudract Number:	2016-003125-22
Product:	EMI-137
Protocol number:	GS16/97090

NOTICE OF ACCEPTANCE OF AMENDED REQUEST

I am writing to inform you that the Licensing Authority accepts your amended request for a clinical trial authorisation (CTA), received on 24/08/2017.

The authorisation is effective from the date of this letter although your trial may be suspended or terminated at any time by the Licensing Authority in accordance with regulation 31. You must notify the Licensing Authority within 90 days of the trial ending.

Finally, you are reminded that a favourable opinion from the Ethics Committee is also required before this trial can proceed; changes made as part of your amended request may need to be notified to the Ethics Committee.

Yours sincerely,

Clinical Trials Unit
MHRA

Medicines and Healthcare Products Regulatory Agency

Figure 39: Medicines and Healthcare Products Regulatory Agency (MHRA) Acceptance of Amendment Letter 29th August 2017

MHRA
151 Buckingham Palace Road
London SW1W 9SZ
United Kingdom

mhra.gov.uk

Prof D G Jayne
LEEDS TEACHING HOSPITALS NHS TRUST
LEVEL 7, CLINICAL SCIENCES BUILDING
ST JAMES'S UNIVERSITY HOSPITAL
LEEDS
LS9 7TF
UNITED KINGDOM

15/03/2018

Dear Prof D G Jayne

THE MEDICINES FOR HUMAN USE (CLINICAL TRIALS) REGULATIONS 2004 S.I. 2004/1031

Our Reference:	16767/0294/001-0004
Eudract Number:	2016-003128-22
Product:	EMI-137
Protocol number:	GS16/87090
Substantial Amendment Code Number:	Version: 4.0
Date: 2018/01/29	

NOTICE OF ACCEPTANCE OF AMENDMENT

I am writing to inform you that the Licensing Authority accepts the proposed amendment to your clinical trial authorisation (CTA), received on 08/02/2018.

For your information:
In future amendment application the sponsor must include a clean copy as well as a tracked changes version of the IB

This amendment may therefore be made.

You are reminded that where it is appropriate, the Ethics Committee should also be notified of amendments.

Yours sincerely,

Clinical Trials Unit
MHRA

Medicines and Healthcare
Products Regulatory Agency

Figure 40: Medicines and Healthcare Products Regulatory Agency (MHRA) Acceptance of Amendment Letter 15th March 2018

Professor David Jayne
Professor of Surgery
University of Leeds & Leeds Teaching Hospital NHS Trust
Clinical Sciences Building
St James' Hospital
Leeds
LS9 7TF

Email: hra.approval@nhs.net

07 November 2017

Dear Professor Jayne

Letter of HRA Approval

Study title:	**Intraoperative imaging of colon cancer using a fluorescent peptide (EMI-137) against the c-Met receptor**
IRAS project ID:	**212190**
EudraCT number:	**2016-003128-22**
Protocol number:	**GS16/87090**
REC reference:	**17/YH/0263**
Sponsor	**University of Leeds**

I am pleased to confirm that **HRA Approval** has been given for the above referenced study, on the basis described in the application form, protocol, supporting documentation and any clarifications noted in this letter.

Participation of NHS Organisations in England

The sponsor should now provide a copy of this letter to all participating NHS organisations in England.

Appendix B provides important information for sponsors and participating NHS organisations in England for arranging and confirming capacity and capability. **Please read *Appendix B* carefully**, in particular the following sections:

- *Participating NHS organisations in England* – this clarifies the types of participating organisations in the study and whether or not all organisations will be undertaking the same activities
- *Confirmation of capacity and capability* - this confirms whether or not each type of participating NHS organisation in England is expected to give formal confirmation of capacity and capability. Where formal confirmation is not expected, the section also provides details on the time limit given to participating organisations to opt out of the study, or request additional time, before their participation is assumed.
- *Allocation of responsibilities and rights are agreed and documented (4.1 of HRA assessment criteria)* - this provides detail on the form of agreement to be used in the study to confirm capacity and capability, where applicable.

Figure 41: Health Research Authority (HRA) Letter of Approval for trial IRAS ID 212190 Intraoperative imaging of colon cancer using a fluorescent peptide (EMI-137) against c-met receptor. Issued 07th November 2017.

NHS
Health Research Authority

Yorkshire & The Humber - Leeds West Research Ethics Committee

Jarrow Business Centre
Rolling Mill Road
Jarrow
NE32 3DT

Tel: 0207 104 8117

Please note: This is the favourable opinion of the REC only and does not allow the amendment to be implemented at NHS sites in England until the outcome of the HRA assessment has been confirmed.

05 January 2018

Professor David Jayne
University of Leeds & Leeds Teaching Hospital NHS Trust
Clinical Sciences Building
St James' Hospital
Leeds
LS9 7TF

Dear Professor Jayne

Study title:	**Intraoperative imaging of colon cancer using a fluorescent peptide (EMI-137) against the c-Met receptor**
REC reference:	**17/YH/0263**
Protocol number:	**GS16/87090**
EudraCT number:	**2016-003128-22**
Amendment number:	**SA1**
Amendment date:	**14 December 2017**
IRAS project ID:	**212190**

The above amendment was reviewed at the meeting of the Sub-Committee held in correspondence.

Summary of amendment

This substantial amendment was submitted due to the radiology and pathology department at the Leeds Teaching Hospital NHS trust using an updated tumour classification system. The site had moved to exclusively using Tumour, Node Metastasis (TNM) Classification of Malignant Tumours 8th edition in 2018. The protocol had been updated to ensure the protocol reflected the current standard practice in the trust and the secondary endpoints so the comparison of the IMP (EMI-137) with standard care could be measured accurately. The protocol had also been updated to provide more detail regarding the planned pathological assessment of specimens. Other minor changes in the protocol had also been made.

Figure 42: Health Research Authority (HRA) approval for substantial amendment to trial IRAS ID 212190 Intraoperative imaging of colon cancer using a fluorescent peptide (EMI-137) against c-met receptor. Issued 05th January 2018.